PAUL SCHERRER INSTITUT

PSI

PSI Scientific Highlights 2012

Cover photo:
Laser expert Marta Divall working on a vacuum chamber for future experiments at SwissFEL.
(Photo: Markus Fischer/PSI)

PSI Scientific Highlights 2012

PSI Scientific Highlights 2012

Published by
Paul Scherrer Institute

Editors
Paul Piwnicki
Trevor Dury

Coordination
Evelyne Gisler

Design and Layout
Christoph Schütz

Photographs
PSI, unless stated otherwise

Printing
Paul Scherrer Institute

Available from
Paul Scherrer Institute
Communications Services
5232 Villigen PSI, Switzerland
Phone +41 56 310 21 11
www.psi.ch

PSI public relations
info@psi.ch

Communications officer
Dagmar Baroke

ISSN 2235-3828

Paul Scherrer Institute, May 2013

Table of contents 3


SINQ

Keeping the balance

Dear Reader,

Seventy percent of the budget! That is what PSI spends on running its Large-Scale Research Facilities, so that users from universities and industry continually have access to world-class instruments at our neutron, muon and synchrotron-light sources.

In 2012, the PSI User Office registered a new record in the number of experiments carried out at our large-scale facilities: almost 2000 experiments were performed by external scientists, corresponding to more than 5500 user visits to the Institute.

However, before scientists pack up their samples and travel to PSI to perform their experiments, they must go through a tough selection process. All submitted proposals are judged on their scientific merit alone, by an international committee, with the result that only the best of them are granted beam time. This procedure ensures the highest possible standards for the experiments performed here.

Over the past few years, we have observed a strong increase in the number of beam-time requests submitted to us, beyond the increase in the number of beamlines we offer. There are a number of reasons for this success: The first reason I would like to mention is the absolutely reliable operation of the facilities, which PSI is constantly improving and expanding. We are proud to offer some of the best experimental stations available anywhere in the world. The second reason, equally decisive, is the outstanding scientific and technical support offered to users by the PSI staff. This is possible because our beamline scientists are committed to maintaining their experimental stations in absolutely first-class condition for external users. To assist in this, we encourage and support these very same scientists, through various measures, to perform their own experiments at their own instrument stations. A further reason for our success is that the on-site location of our specialized laboratories in the fields of energy (both renewable and nuclear), biology and chemistry, as well as our extremely close links with the Swiss universities, are assets that also benefit the users of all of our large-scale facilities.

I do realize that keeping the balance between our own research and user support, while at the same time both collaborating with external scientists as well as, in some cases, competing with them, is a complex procedure, requiring great commitment and public-spiritedness from our staff. It is, however, my deep conviction that this dual strategy is the most promising way of satisfying, in the long-term, the best interests of all parties involved: PSI scientists and PSI users, as well as PSI as an Institution of the ETH Domain and our society at large.

Professor Dr. Joël Mesot
Director, Paul Scherrer Institute

8 SwissFEL – machine project and laser development

Important milestones for the realization of the new SwissFEL facility were reached in 2012. In September, the Swiss Parliament approved the Federal Programme for Education and Research for the 2013 – 2016 period, which includes the mandate for PSI for building SwissFEL. In late December, the budget for Federal building construction was approved, including the funding for the SwissFEL building. The building permit for SwissFEL arrived on 29 January 2013. The project is progressing well. The new SwissFEL facility will open the door to discoveries in many areas of research that cannot be achieved using existing methods. Its unique properties will enable experiments to be carried out at a very high resolution in both time and space. For example, it will be possible to observe the progress of extremely fast chemical and physical processes, including details down to the scale of molecules. This will not only result in a significant increase in knowledge, it will also provide the basis for a range of technical and scientific developments.

The collection of user inputs for the design of the initial set of instruments at the SwissFEL hard X-ray "ARAMIS" undulator beamline started in 2011 with two Scientific Workshops on hard X-Ray instrumentation with SwissFEL. Planning of the design of the experimental stations was continued in 2012 with 5 topical workshops focusing on the different experimental stations (ES): 1) ESA: Multi-purpose pump probe; 2) ESB: Pump-probe crystallography; 3) ESC: Coherent diffraction imaging; 4) Next-frontier SwissFEL Instruments; and 5) SwissFEL Scientific Computing & Data Acquisition. Further workshops on Pump Laser and Sample Mounting were held in November, at which talks by experts from different facilities gave an inspiring view of the existing and planned instrumentation for Pump Laser and Sample Mounting at different FEL and XFEL facilities. More information on these can be found at: http://www.psi.ch/swissfel/swissfel-workshops.

◀ **View along the tunnel of the 250 MeV injector, where technologies are being tested for the first stage of the SwissFEL accelerator.** (Photo: Frank Reiser/PSI)

SwissFEL Machine Project

Marco Pedrozzi, Florian Löhl, Romain Ganther and Hans Braun, *SwissFEL Project, PSI*

SwissFEL activities in 2012 focused on the preparation of the future SwissFEL building site in the Würenlingen forest, the preparation of key technical components for the facility, in close collaboration with partners in industry, and the continuation of beam experiments and component testing in the injector test facility. The Call for Tender for general building construction was issued at the end of May and the contractor chosen at the end of November. Before achieving this, a large amount of work went into the collection of all building requirements and specifications. Since the detailed machine design of SwissFEL was still evolving during 2012, and building specifications are not a common pastime of scientists, this was only possible due to the relentless commitment and patience of the PSI building and infrastructure experts.

Status: SwissFEL Linac

A key component of SwissFEL is its normal conducting linear accelerator based on C-band technology. While C-band technology itself is not new – the SACLA FEL in Japan also uses it – all of the key components of the SwissFEL Linac will be based on new designs, developed mainly in-house at PSI. The goal of this approach is to build the most modern normal conducting accelerator in the world, with a power efficiency around twice as high as in similar facilities elsewhere.
Figure 1 shows the design of a C-band accelerating module of Linac 1. A total of 26 such modules will be installed in the facility. A module consists of the RF source (top) and a Toshiba klystron, which is driven by an IGBT switched modulator (not shown).

A special klystron is being developed for PSI with a design in which the cooling of the collector is separated from the cooling of the body. This allows the collector to be operated at a significantly increased temperature. The cooling water at the collector outlet will have a temperature of around 80 °C and will be used in the PSI energy recovery system. A first prototype of such a klystron will arrive at PSI early in 2013.
The RF pulses, with a frequency of 5.72 GHz, a peak power of up to 50 MW and duration of 3 µs, are guided into a barrel-open-cavity (BOC) type pulse compressor via a wave-guide. In the BOC, which has a quality factor, Q, of around 200,000, the RF pulses are compressed by a factor of four, and the compressed RF pulses are distributed into four 2 m-long accelerating structures.

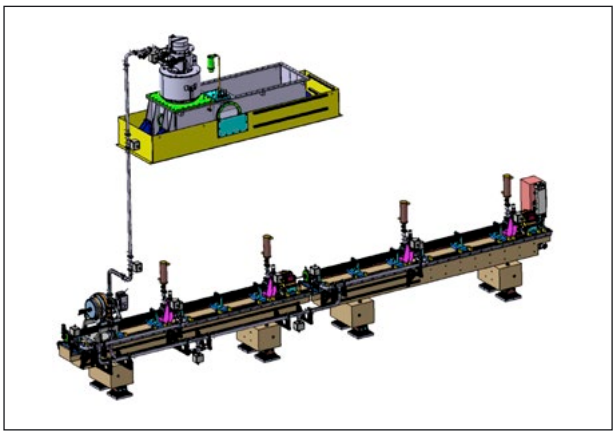

Figure 1: **C-Band accelerating module of Linac 1. A module consists of the RF source (top) and a Toshiba klystron, which is driven by an IGBT switched modulator (not shown).** (Picture courtesy of P. Heimgartner)

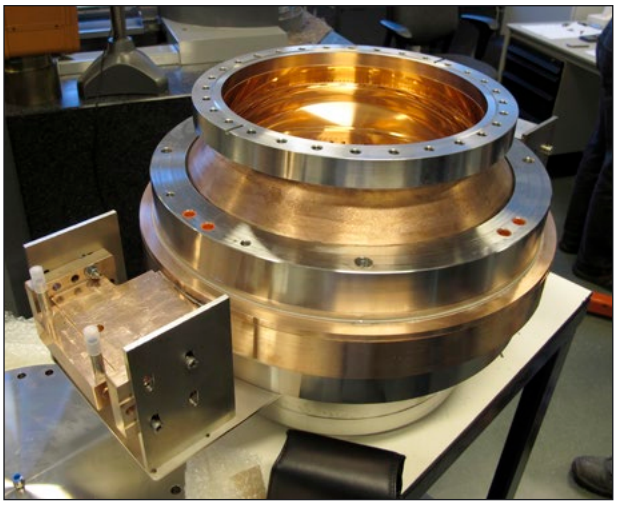

Figure 2: **First prototype of the BOC-type pulse compressor.** (Picture courtesy of R. Zennaro)

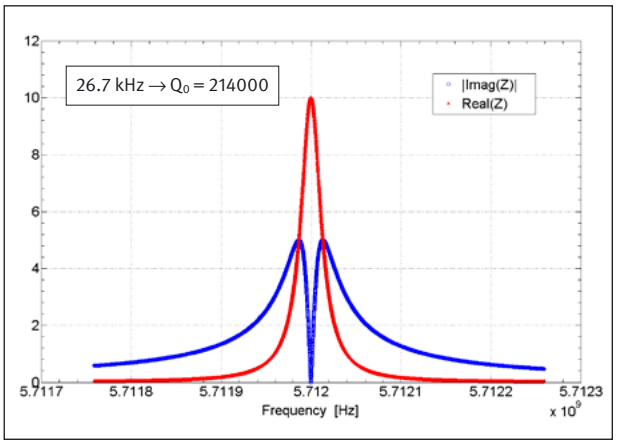

Figure 3: **Characterization of the first BOC prototype in which a quality factor Q > 200,000 was achieved.** (Courtesy of R. Zennaro)

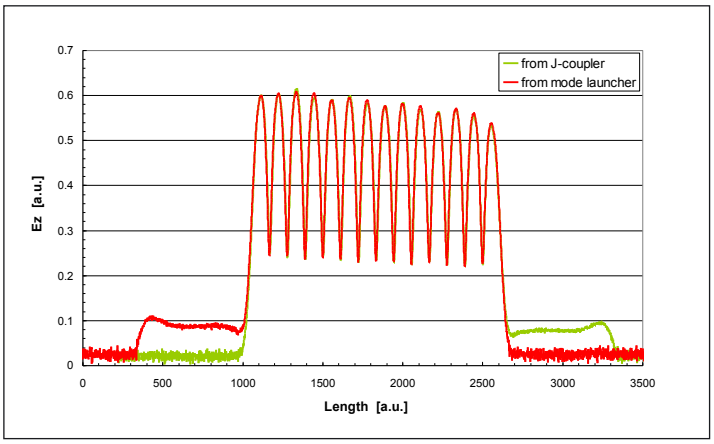

Figure 5: **Electric field profiles for the nominal phase advance of 2π/3 feeding the structure from two different coupler types.** (Courtesy of R. Zennaro)

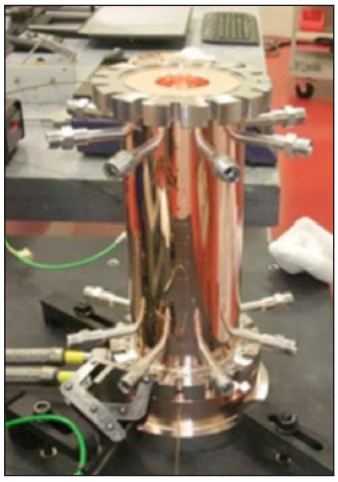

Figure 4: **Short C-band accelerating test structure (IPAC12, THPPC024).**

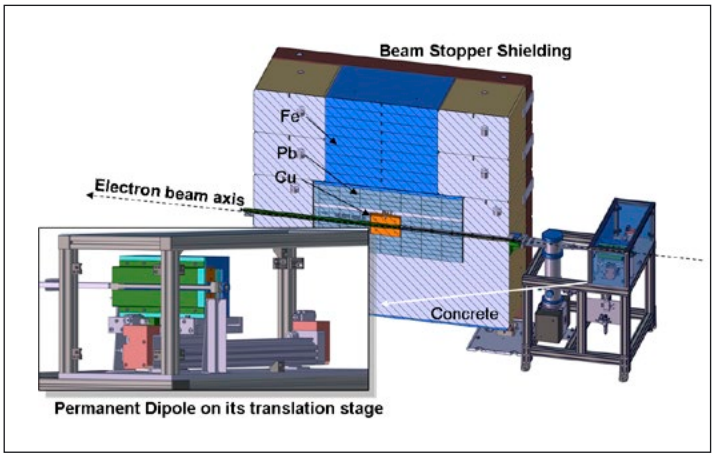

Figure 6: **Beam stopper layout assembly: The 5.8 GeV beam is deflected by 0.7° when the dipole is inserted.** (Picture courtesy of P. Heimgartner)

The nominal accelerating field in each structure is 28 MV/m, yielding an energy gain of 224 MeV per C-band module. This energy gain will be achieved with the klystrons running at 80% of their nominal power specifications, thus leaving a margin for energy management in the Linac and for feedback.

Figure 2 shows a picture of the first BOC prototype manufactured at VDL. Initial RF tests of the BOC gave excellent results, and a quality factor of more than 200,000 could be achieved (see Figure 3). High-power RF tests are currently underway and, when successful, a ramp-up of the series production is foreseen for the year 2013. This is planned to happen in the workshops of PSI's Mechanical Engineering Sciences Division (AMI).

Important progress has also been made in the design and testing of the accelerating structures. Figure 4 shows a picture of a short test structure, consisting of 11 accelerating cells (the final 2 m structures will contain 113 such cells). RF tests have shown excellent field profiles within these test structures (see Figure 5), and excellent results were also obtained in high-power RF tests, with maximum acceleration fields up to 56 MV/m – around twice the field needed for SwissFEL.

A major task for 2013 is building the first 2 m-long structures and qualifying companies for the mass production of the 108 structures needed for SwissFEL.

Status: Undulator and Transfer Line

To protect the undulator segments from electron beam losses which would demagnetize the permanent magnets, a beam stopper system (Figure 6) is foreseen, 10 m upstream of the 1st undulator segment. The design of the system has been completed and procurement has started. In the beam stopper, the beam is deflected horizontally towards the shielding. This deflection is produced by a permanent dipole magnet, which slides transversally and can be moved remotely into the beamline (Figure 6). Using an electromagnet instead of a permanent one would have required more space, as well as a degaussing procedure after each manipulation.

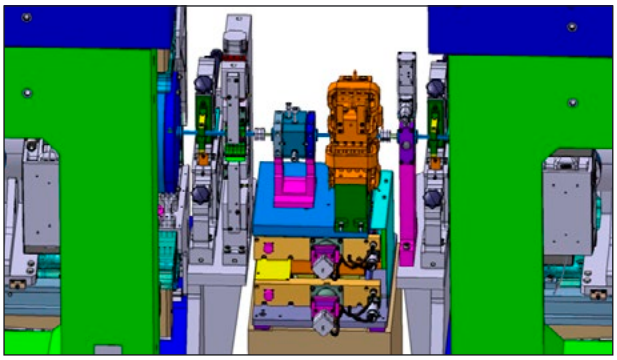

Figure 7: **Inter-segment girder with (from left to right, electron direction): Alignment quadrupole (Q_{Al}); phase shifter; BPM pickup; FODO quadrupole; gate valve and Q_{Al}.**

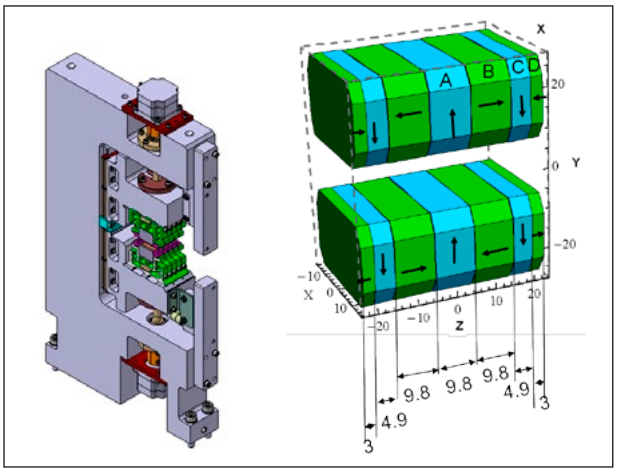

Figure 10: **Phase shifter support with adjustable gap and the corresponding magnet array design.**

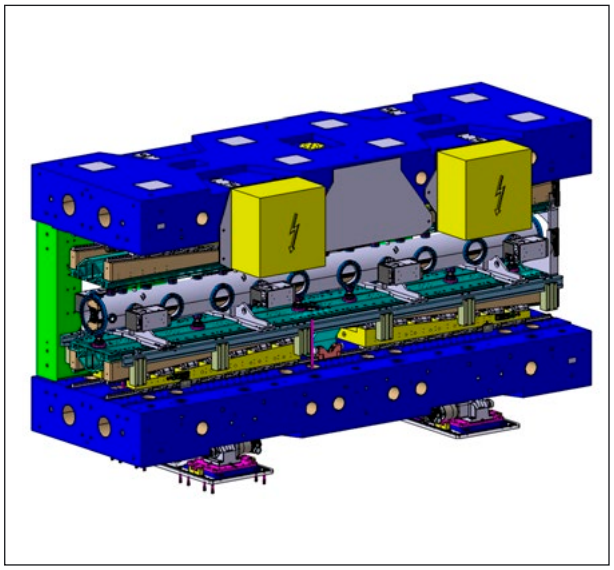

Figure 8: **U15 undulator with in-vacuum magnets and gap adjustment mechanics based on wedge systems.**

The Aramis line has 12 in-vacuum undulator magnets called U15, with a period of λ_U=15 mm (Figure 8). The first prototype of U15 mechanics (Figure 9) has been completed and assembled. The final step of installing permanent magnets and measuring the field will be completed by spring 2013.

The beam trajectory in the Aramis line should not deviate from an ideal straight line by more than a few micrometers. This is achieved by beam-based alignment of the FODO quadrupoles that have motorised X–Y tables (Figure 7). The alignment of each undulator segment on this straight line is made with so-called alignment quadrupoles (Q_{Al}) (Figure 7). Phase shifters (Figure 10) between the undulator segments are used to synchronise the electrons with the phase of the FEL light at the entrance of each undulator segment. By changing the gap of the phase shifter, one can control the phase delay by typically 0.2 degree / µm. The full series of 12 phase shifters, 24 alignment quadrupoles and 20 X–Y positioning tables has already been produced.

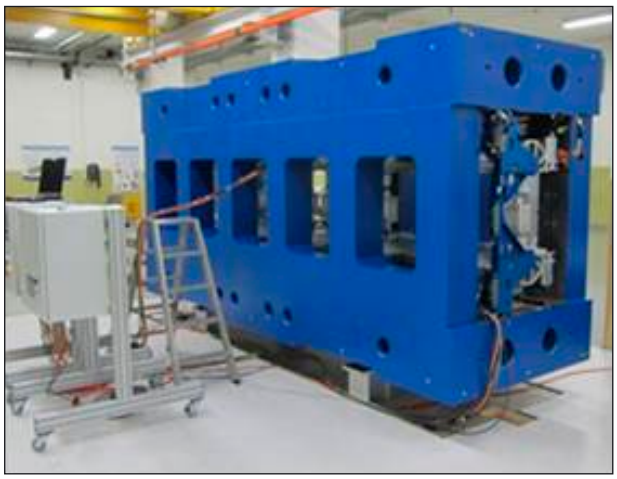

Figure 9: **U15 undulator prototype mechanical support (courtesy of T. Schmidt).**

Record low emittance at the SwissFEL Injector Test Facility

Significant progress was achieved in the past year, during which the injector settings were systematically optimized for maximum brightness of the electron beam (low emittance at high beam current).

The results of this optimization are stable working points for uncompressed electron bunches with minimal emittance dilution.

Bunch charge (pC)	200	10
Normalised projected emittance (nm rad)	~300	~150
Normalised slice emittance (nm rad)	~200	~100

Table 1: **Best emittance values for uncompressed beams.**

At the nominal SwissFEL working point of 200 pC charge, record low emittances were achieved, which are well within SwissFEL specifications. At these conditions, global (projected) emittances below 350 nm rad are now obtained routinely, with best values around 300 nm rad (see Table 1). The free-electron laser-relevant slice emittance, i.e. the emittance measured for individual time slices along the bunch length, is typically below 200 nm rad (see Figure 11), with a record value of 180 nm rad.

Once the influence of the accelerator itself on the beam emittance is minimized, subtle effects of the laser generating the electrons at the cathode (via the photo-electric effect) become accessible to beam optics measurements. In this way, it was possible, for instance by measuring the intrinsic emittance of the photo-emission process, to demonstrate the effect of laser photon energy (or wavelength) on the beam emittance (Figure 12). The measured intrinsic emittance of ~600 nm rad per mm laser spot size (rms) is 30 % smaller than the values assumed so far for the simulations, and indicate the excellent quality of the cathode surface.

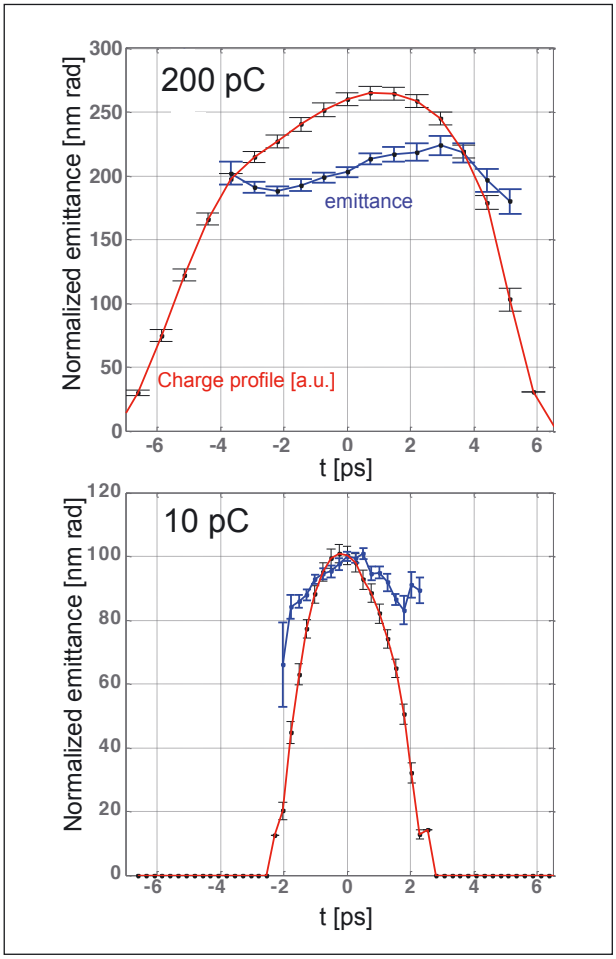

Figure 11: **Typical slice emittance measurement and longitudinal charge distribution along the electron bunch for uncompressed beam (photocathode laser wavelength 260 nm), for two different charge modes.**

To reach the high peak currents necessary to drive a free-electron laser, longitudinal bunch compression is essential. This system will allow for the more uniform compression of the bunch in the magnetic compression chicane. Preliminary studies performed in 2012 easily exceeded a compression factor of 10. The non-linearity of the longitudinal phase space induced by the RF field in the accelerating cavities is clearly visible in Figure 13. This curvature has limited the compression performance so far.

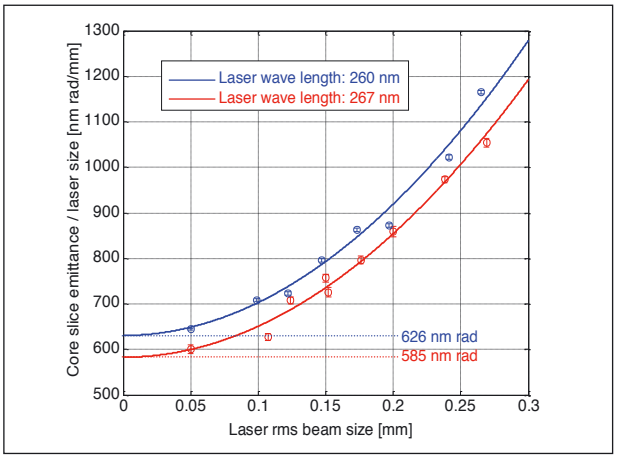

Figure 12: **Core slice emittance versus laser beam size performed at very low charge, to cope with space charge effects.**

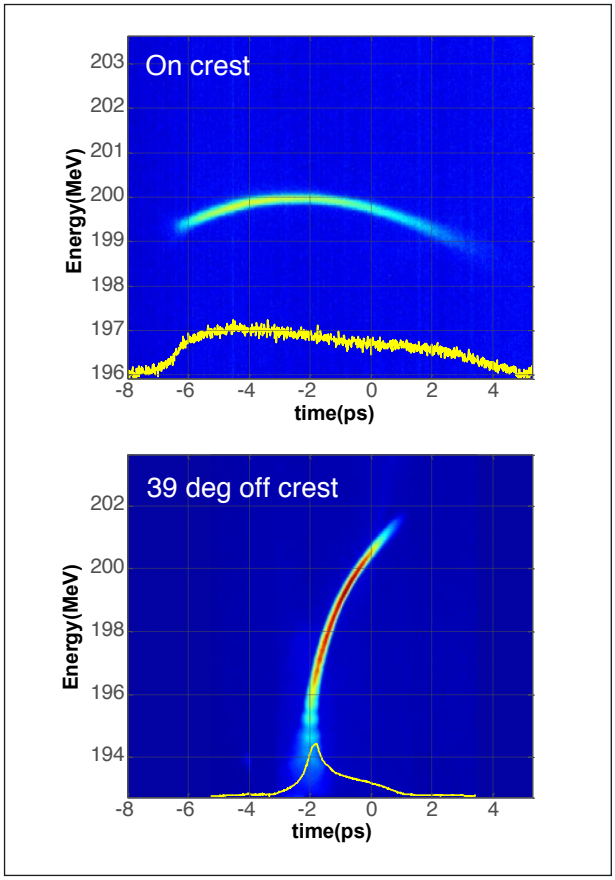

Figure 13: **Longitudinal phase space for uncompressed and compressed beam. In yellow, the projected longitudinal charge profile.**

An intense Terahertz source for SwissFEL

Clemens Ruchert, Carlo Vicario and Christoph Hauri, *SwissFEL, PSI*

Important classes of experiments to be performed at SwissFEL need a laser that will provide a reliable, high-field, single-cycle radiation pulse with a spectrum spanning the full Terahertz Gap (0.1–15 THz). It has been a challenge in the past to produce intense coherent radiation in this frequency range due to the lack of adequate emitters. However, we have recently developed a compact and powerful laser-driven THz source in which the radiation is generated by nonlinear optical rectification of mid-infrared femtosecond laser pulses in organic salt crystals. This delivers single-cycle pulses at record-high peak field strength of 1.5 MV/cm and 0.5 Tesla, and lasts only one optical cycle, paving the way for SwissFEL application.

Background

Terahertz radiation (0.1–15 THz), located between the optical and radio frequency ranges, is suitable for exploring fundamental physical phenomena and driving novel applications in condensed matter physics, biology, surface chemistry and other fields. Ultrashort and intense terahertz pulses are of particular interest in view of the hard X-ray free-electron laser for SwissFEL currently being designed and constructed at PSI, since a series of resonant modes (magnons, phonons, electromagnons) can be coherently excited by THz radiation and tracked by femtosecond X-ray pulses. A high-field terahertz transient provides a novel tool to control and investigate collective motions, since it can be understood as a "cold" stimulus; indeed, the photon energy in the THz range is not more than a few meV, and therefore orders of magnitude lower than the equivalent photon of a conventional laser (e.g. a Ti:sapphire laser, in which $h\nu$=1.6 eV). While the latter significantly heats electronic systems, a terahertz driving field excites only the THz-sensitive port while leaving other degrees of freedom unexcited.

THz emitter development for SwissFEL

It has been a challenge in the past to produce intense coherent radiation in the Terahertz Gap (0.1–15 THz) due to the lack of adequate emitters. Several schemes, based on relativistic electron beams or powerful lasers, have been employed, but none of those fully satisfied the SwissFEL need for a reliable, high-field, single-cycle pulse with a spectrum spanning the full THz Gap. To access significantly higher frequencies, we have recently developed a compact and powerful laser-driven THz source. The radiation is generated by nonlinear optical rectification of mid-infrared femtosecond laser pulses in organic salt crystals such as DAST [1], OH1 [2] and DSTMS [3]. The generation mechanism of THz radiation can be understood as a phase-matched nonlinear $\chi^{(2)}$ process. Different frequency components of the fundamental laser pulse, with relative offset $\Delta\omega$, drive nonlinear emission at frequency $\omega_{THz} = \Delta\omega$ in the organic crystals. The broadband fundamental spectrum and the large phase-matching bandwidth of the organic crystal permit the generation of multi-octave-spanning THz radiation. The difference frequency between components carrying the same absolute phase leads to intrinsically stable carrier-phase pulses, which is essential for the field-sensitive experiments envisaged for SwissFEL. The table-top terahertz source we have developed delivers single-cycle pulses at record-high peak field strength of 1.5 MV/cm and 0.5 Tesla, and lasts only one optical cycle (Figure 1). The high conversion efficiency of one percent provides pulse energies of up to 40 µJ. Most interestingly, our scheme offers the pulse-shaping capability of forming highly asymmetric field shapes, as shown in Figure 1(b), by directly modifying the absolute phase of the pulse. Such asymmetric field shapes open new research opportunities, such as the ultrafast switching of magnetic domains, which our group is currently investigating.

SwissFEL application

For SwissFEL, such Terahertz electrical transients are also required for determining the arrival time and the temporal reconstruction of the femtosecond FEL X-ray pulses. This

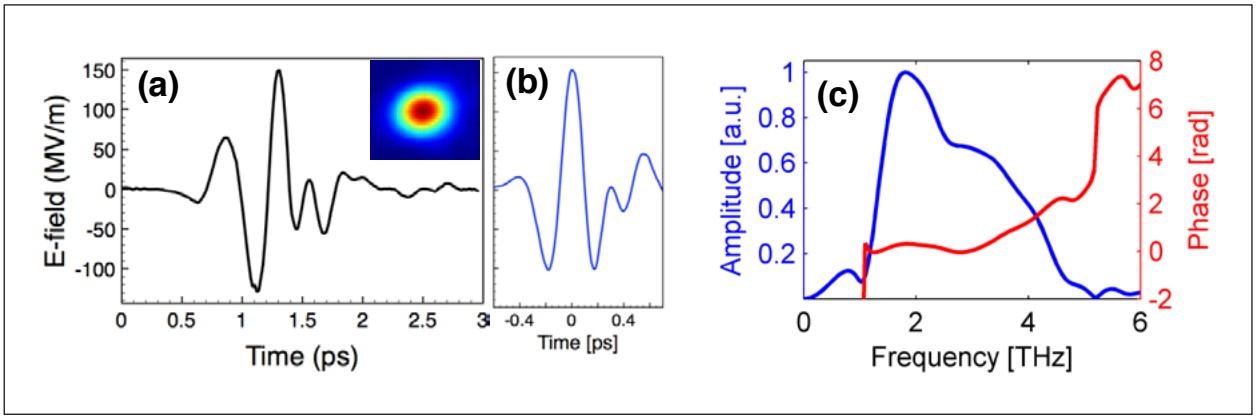

Figure 1: **(a) Single-cycle Terahertz pulse with 150 MV/cm electric field (inset: diffraction limit focus), with (b) the field-shaping capabilities to form highly asymmetric field oscillations; (c) typical spectral amplitude and phase.**

diagnostics method is based on the principle of a conventional streak camera, but using a streaking field at THz frequency. This allows online reconstruction of the femtosecond hard X-ray pulse and measurement of the pulse arrival time with respect to the optical pump laser. The development of a reliable and powerful laser-based THz source is a prerequisite for the realization of such essential online X-ray pulse diagnostics at SwissFEL.

References

[1] C.P. Hauri, C. Ruchert, F. Ardana and C. Vicario, *Strong-field single-cycle THz pulse generated in organic crystal*, Appl. Phys. Lett. **99** 161116 (2011).

[2] C. Ruchert, C. Vicario and C.P. Hauri, *Scaling sub-mm single-cycle transients towards MV/cm fields via optical rectification in organic crystal OH1*, Opt. Lett. **37** 899 (2012).

[3] C. Ruchert, C. Vicario and C. P. Hauri, *Spatio-temporal focusing dynamics of intense supercontinuum THz pulses*, Phys. Rev. Lett. **110** 123902 (2013).

Links

[1] SwissFEL Challenges: http://www.psi.ch/swissfel/scientific-challenges

[2] SwissFEL Research Projects: http://www.psi.ch/swissfel/research-projects

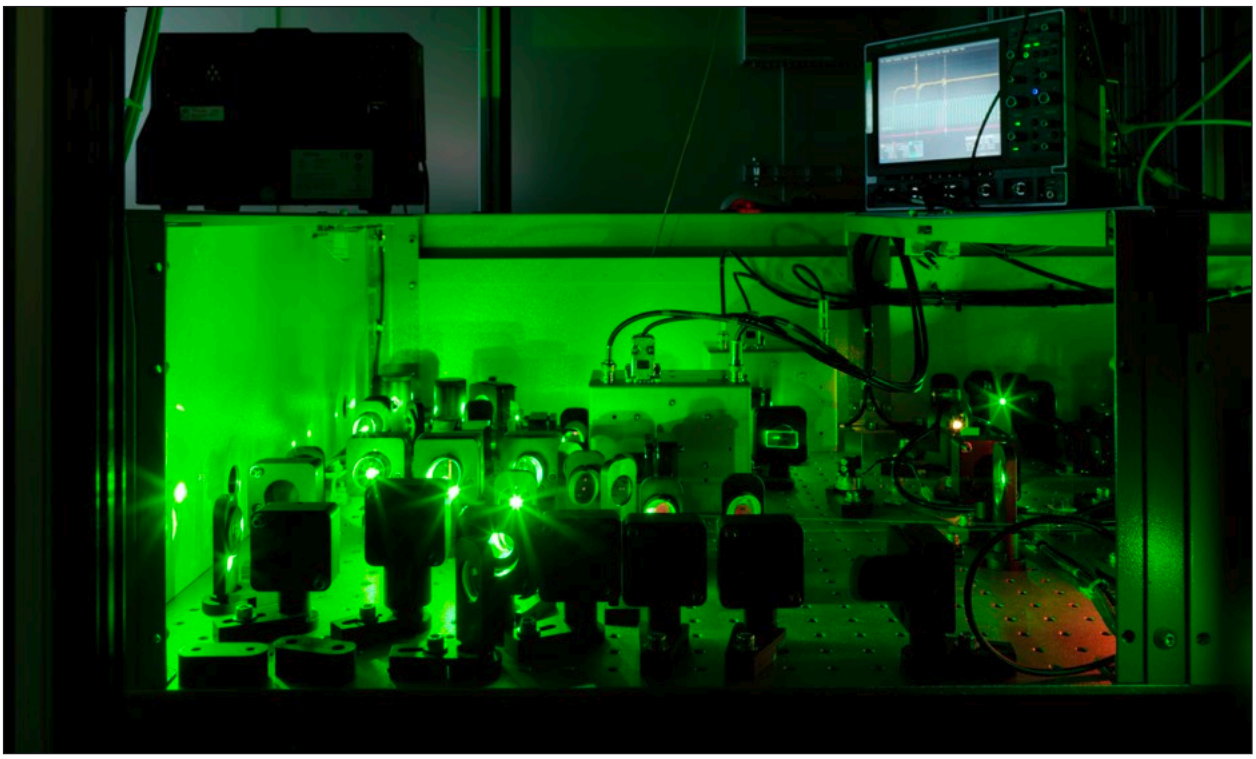

Figure 2: **One of the laser systems being developed for SwissFEL.** (Photo: Scanderbeg Sauer Photography)

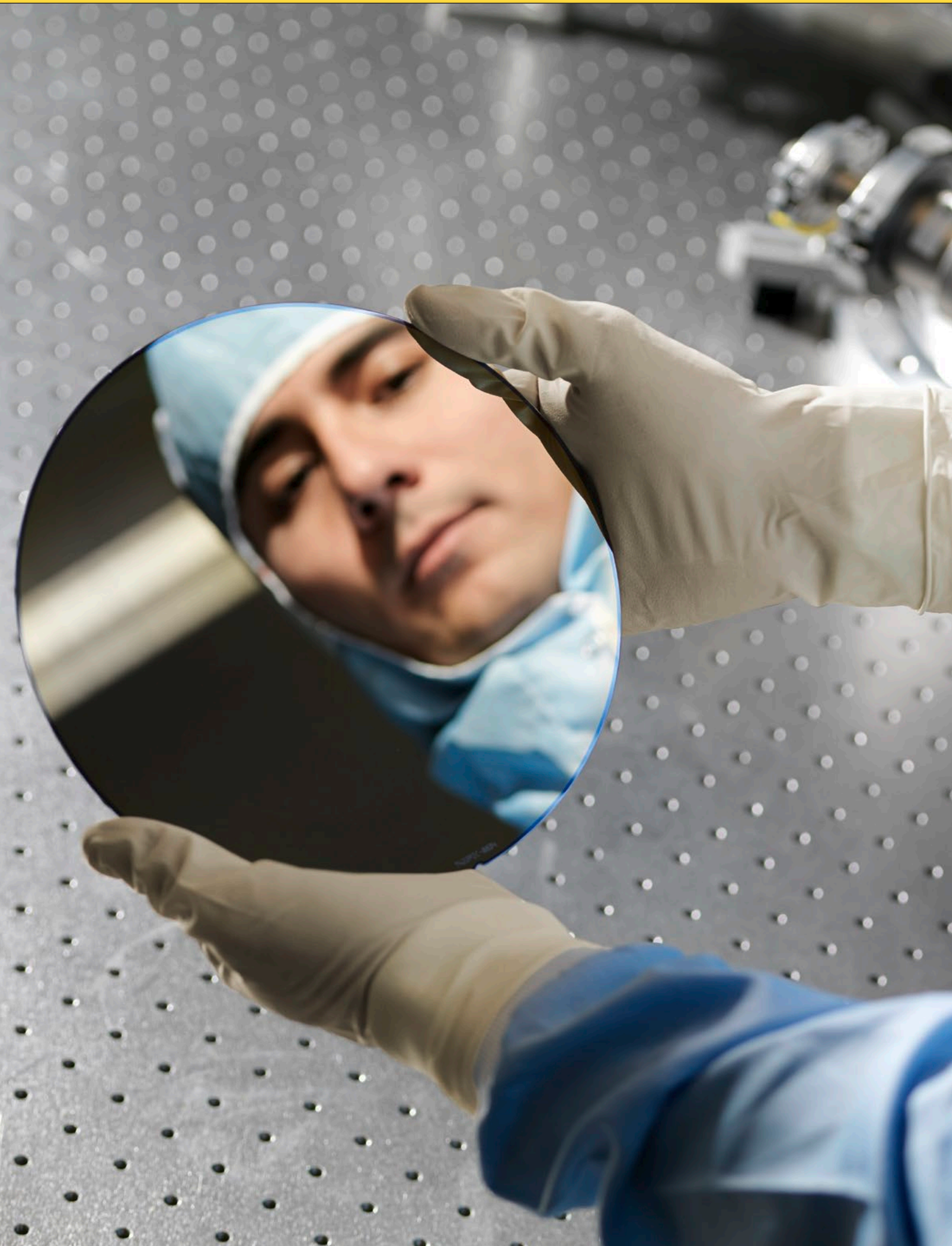

Research focus and highlights 15

The articles on the following pages briefly describe a large variety of scientific topics investigated at PSI in 2012, and include the results of fundamental research as well as the development or improvement of cutting-edge technology. Most of these studies were performed at one of the Institute's large-scale facilities. In the fields of biology and medicine, for example, synchrotron light has been used to gain information about the development of Alzheimer plaques in murine brains. Synchrotron light also provided important insights into G protein-coupled receptors responsible for the transmission of information into a living cell. In the field of solid-state physics, experiments at the SLS showed how some different properties of electrons in a solid are able to separate and move as independent entities, while neutron experiments at SINQ investigated materials in which ferromagnetism and ferroelectricity coexist and are coupled. Apart from their own research, scientists working at the large-scale facilities develop the facilities' experimental stations to meet new requirements of research in many topical fields. One example is the spectroscopic method HEROS, which allows researchers to obtain an insight into fast chemical processes, such as decomposition and synthesis, where questions often arise in connection with research on energy technologies. In materials research, PSI scientists have developed nanometre-sized wires that can be put under strain inside electronic components. This will make it possible to apply the fact that putting certain materials under strain improves their electronic properties, which would result in better performance of electronic devices. Two articles present recent results from the MEGPIE project, in which a liquid-metal target was used at PSI's neutron source SINQ. The insights gained are relevant for possible future accelerator-driven reactor systems that would use nuclear waste to produce energy, at the same time reducing the overall amount of radioactive waste.

◀ **PSI scientist Renato Minamisawa holding a silicon wafer similar to those he used for the development of strained nanowires; see pages 40–41 for details.** (Photo: Scanderbeg Sauer Photography)

The Swiss Light Source – seeing is believing

Johannes Friso van der Veen
Synchrotron Radiation and Nanotechnology Department (SYN), PSI, and Department of Physics, ETH Zürich

The Swiss Light Source (SLS) puts the old adage 'Seeing is believing' into practice. Being one of the world's most brilliant sources of X-rays, the SLS enables researchers to investigate matter on the length scale of nanometres and at time scales down to femtoseconds. Its facilities for X-ray diffraction, imaging and spectroscopy attract researchers from essentially all exact sciences.

The Swiss Light Source (SLS) is a third-generation synchrotron radiation facility of medium electron energy (2.4 GeV), generating electromagnetic radiation at wavelengths ranging from the infrared to the hard X-ray regime (30 keV). The SLS is operated as a user facility with 18 beamlines, open to scientists from Switzerland and abroad. The science areas within the SLS consist of three laboratories: (1) the Laboratory for Condensed Matter Research, (2) the Laboratory for Macromolecules and Bioimaging, and (3) the Laboratory for Catalysis and Sustainable Chemistry. The Laboratory for Micro- and Nanotechnology, which also belongs to the SYN Department, is fully integrated into the activities at the SLS. Major areas of importance in research are: structural biology, biomedical imaging, nanoscale magnetism, properties of correlated electron systems, and pico- and femtosecond X-ray spectroscopy. Internationally highly recognized are the extremely stable source and our R&D programmes in pixel detectors and diffractive X-ray optics.

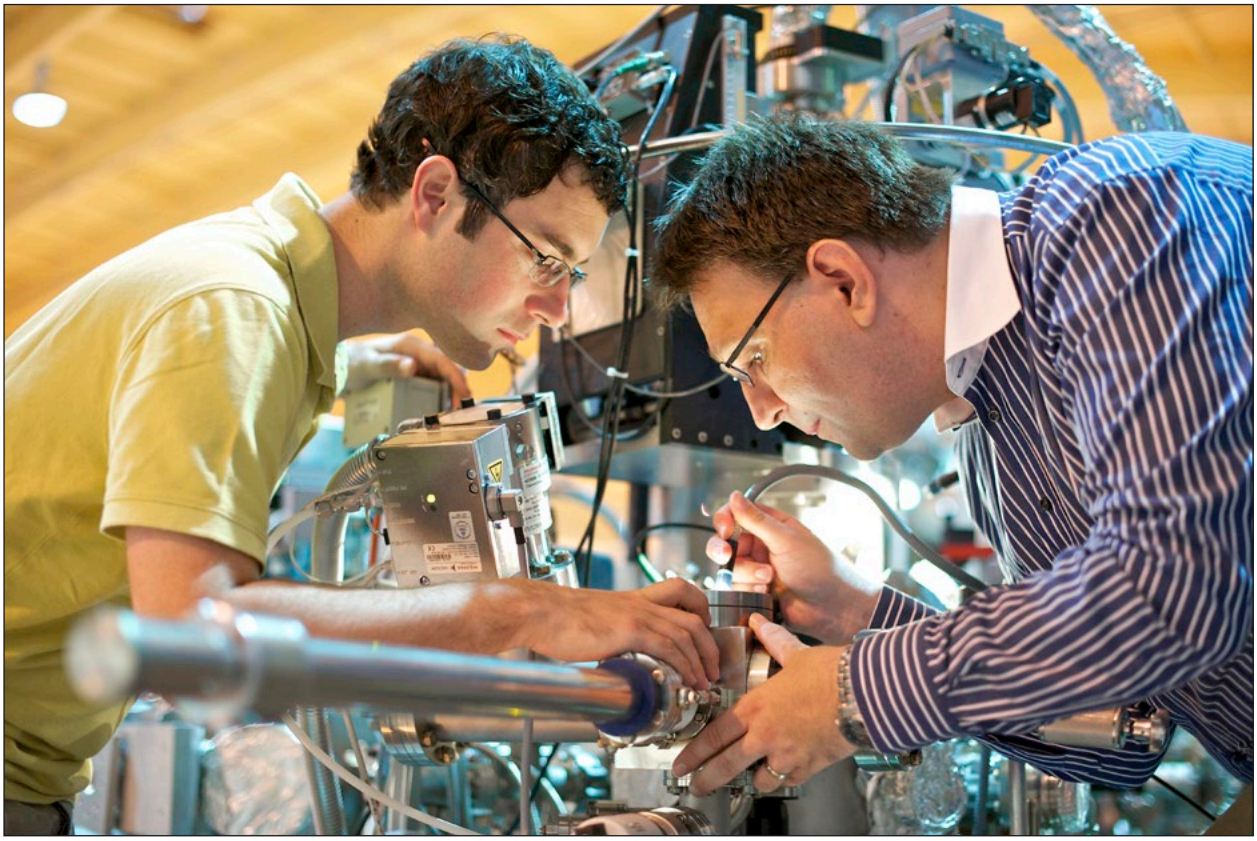

Figure 1: **Scientists Mark Dean (Brookhaven National Laboratory) and Thorsten Schmitt (PSI) at the ADRESS beamline at SLS.** (Photo Markus Fischer/PSI)

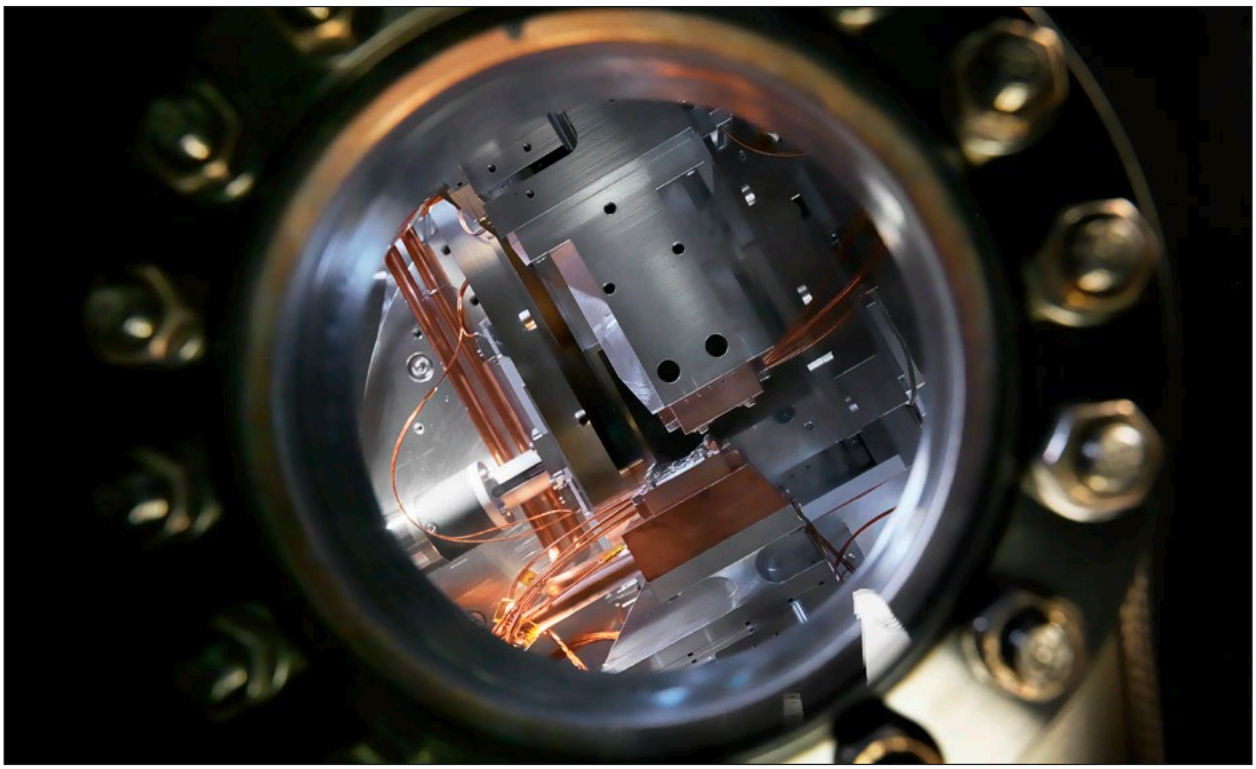

Figure 2: **Monochromator at the new Phoenix beamline at SLS.** (Photo: Scanderbeg Sauer Photography)

The year 2012 has been productive in many respects. In one of the following contributions, T. Schmitt et al. (pp. 22–23) report on resonant inelastic soft X-ray scattering (RIXS) studies of orbital excitations in a spin-chain material [1]. Vacuum ultraviolet ionization measurements of gaseous fuel components (P. Hemberger et al., pp. 24–25) contribute to our understanding of soot formation in combustion engines [2]. The 3D distribution of amyloid plaques in the mouse brain has been visualized by B.R. Pinzer et al. (pp. 18–19), perhaps enabling better diagnosis of Alzheimer's disease [3]. Ultra-high-resolution ptychographic nanotomography has been developed by M. Holler et al. (pp. 20–21) into a general user tool [4]. S. Tsujino et al. (pp. 38–39) have demonstrated plasmon-enhanced electron emission from metallic nanotip arrays, work relevant for X-ray free-electron lasers (XFELs) [5]. Our staff have also successfully conducted measurement campaigns at the XFEL in Stanford, the LCLS. In parallel, SLS is involved in the design of optics and undulators for PSI's own SwissFEL.

Over the years, the SLS has developed innovative X-ray instrumentation, the hybrid pixel detector PILATUS perhaps being the best example. The next generation of pixel detectors (EIGER), having smaller pixel size and faster frame rates, will lead to further breakthroughs in biocrystallography and X-ray imaging. Other examples include X-ray optics such as diffractive grating interferometers and Fresnel zone plates for focusing X-rays to a nanometre spot size. These developments are now finding their way into X-ray free electron lasers, including SwissFEL.

Since 2006, four companies have been spun off from our activities: DECTRIS AG sells the PILATUS detector worldwide; EULITHA AG produces photonic nanostructures using advanced lithography techniques; Expose GmbH provides services in protein crystallography to companies and organisations in the pharmaceutical sector; and Excelsus Structural Solutions offers access to synchrotron-based tools for the structural characterization of organic compounds.

References

[1] J. Schlappa, T. Schmitt et al., Nature **485** 82–85 (2012).
[2] A. Bodi et al., Rev. Sci. Instrum. **83** 083105 (2012).
[3] B.R. Pinzer et al., NeuroImage **61**(4) 1336–1346 (2012).
[4] M. Holler et al., Rev. Sci. Instrum. **83** 123201 (2012).
[5] A. Mustonen, P. Beaud, E. Kirk, T. Feurer and S. Tsujino, *Efficient light coupling for optically excited high-density metallic nanotip arrays*, Scientific Reports **2** 915 (2012).

Links

[1] SLS: http://www.psi.ch/sls/
[2] DECTRIS AG: http://www.dectris.com/
[3] EULITHA AG: http://www.eulitha.com/
[4] Expose GmBH: http://www.psi.ch/industry/spin-off-firmen
[5] Excelsius Structural Solutions: http://www.excels.us/index/pages/id_page.../lang-en/

3D visualization of amyloid plaques in mice could help develop clinical imaging methods

Bernd R. Pinzer[1], Matthias Cacquevel[2], Peter Modregger[1], Thomas Thüring[1] and Marco Stampanoni[1]
[1] *Laboratory for Synchrotron Radiation – Macromolecules and Bioimaging (LSB), PSI*
[2] *Brain Mind Institute, EPFL, Lausanne, Switzerland*

Alzheimer's Disease (AD) is a devastating disorder of the central nervous system that is characterized by a progressive impairment of memory and cognitive function, ultimately leading to dementia. For an early diagnosis, medical imaging techniques could be used to detect specific brain lesions associated with AD, such as amyloid plaques. These micrometre-sized extracellular accumulations of peptides have now been visualized in 3D in the brains of a mouse model of AD. Measuring the global distribution of Aβ plaques in mice could provide a tool for evaluating the specificity of human plaque tracers, and the effect of amyloid-modifying drugs before they go into human trials.

The prevalence of Alzheimer's Disease (AD) is continuously increasing worldwide, with estimates ranging up to 24 million people suffering from dementia today. The numbers are expected to double every 20 years, at least until 2040 [1]. In addition to the individual tragedy that every case represents, a large number of patients results in a significant burden to public health systems. Therefore, considerable research effort is being spent in the search for better diagnosis and treatment of AD.

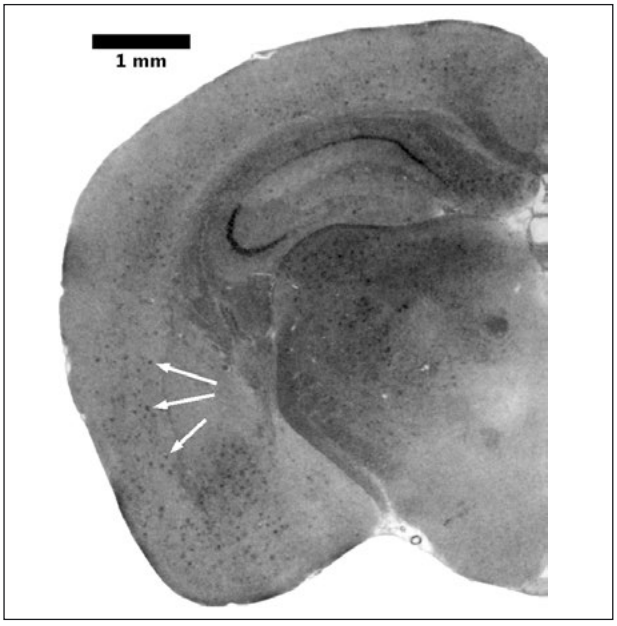

Figure 1: **Reconstructed left hemisphere of a 70-week-old mouse brain. The small spots – some of them are indicated by arrows – were amyloid plaques, identified by comparison with immunohistochemistry.**

The role of amyloid plaques in AD

One particular aspect of AD is the accumulation of small pieces of protein in the brain. This so-called amyloid-beta peptide (Aβ) is produced from a normal membrane protein, but can form small fibrils under pathological conditions. As it accumulates in the brain, it forms micrometre-sized spherical aggregates, known as amyloid plaques. The presence of such plaques is one of the hallmarks distinguishing AD from other kinds of dementia. Apart from their role as a biomarker for the disease, amyloid plaques may also be involved in the death of neurons, via a chain of biochemical reactions known as *amyloid cascade hypothesis* [2]. Although this hypothesis is still under debate, one particular strategy to fight the disease has been to remove the pathogenic form of Aβ from the brain. This strategy of plaque clearance is the aim of several current experimental treatments.

Making the invisible visible with X-ray phase contrast

Due to their small size – on the order of 10 to 40 µm in humans – amyloid plaques are very difficult to visualize. Current clinical imaging methods, such as PET scans, are based on radioactive probes to unravel amyloid plaques in the brains of AD patients. The specificity of the PET signal depends on the affinity of the radioactive probe towards amyloid plaques, which is usually assessed in transgenic mouse models of AD using cumbersome histological methods. X-ray microscopy at a synchrotron source is well known for its excellent resolution, but soft tissue has a

very low contrast when only the traditional absorption properties are considered. The contrast between different types of soft tissue can be enhanced when – instead of absorption – a different interaction mechanism is taken into account. Elastic scattering leads to refraction when the refractive index (i.e. the electron density) in the sample changes spatially, and mapping the refraction angle downstream of the sample allows the distribution of the refractive index within the sample to be reconstructed.

One particularly sensitive and versatile method for measuring the refraction angle is based on a grating interferometer (GI), which is installed at the TOMCAT tomography beamline at the Swiss Light Source SLS [4]. Typical refraction angles are on the order of micro-radians, which translate to lateral offsets on the order of 100 nm after 20 cm propagation downstream of the sample. Such small deviations cannot be directly observed, because the detector pixels are usually much larger. Instead, we determine the refractive lateral shift of the wave front by first producing a well-defined interference pattern (period of 2µm), and second shifting an absorption grating with the same period in front of the detector [5]. With this protocol, a bright-dark pattern is observed in every pixel, depending on the relative positions of the interference pattern and the absorption grating. The properties of a GI – i.e. the combination of high resolution and large field of view – are crucial for visualising brain anatomy as well as certain pathology. Imaging the brain with X-rays is very challenging, because of the tiny differences in soft tissue density between different anatomical regions. To show that GI can resolve amyloid plaques, we used the 5xFAD mouse model [6], which exhibits plaques with similar sizes compared with the ones of humans. One tomographic reconstruction of the refractive index of a wet (excised) mouse brain (70 weeks old) is shown in Figure 1, where structural anomalies in the form of dark spots are clearly visible. A validation with two-photon microscopy proved that these features are indeed amyloid plaques [7].

Automated segmentation yields quantitative analysis

The high quality of the images enabled automated segmentation, yielding quantitative, volumetric measures, such as the classical histological parameter *plaque load*. The 3D nature of the data has the additional advantage that the spatial variation of this important parameter can be extracted – clearly an added value of our method compared to histological evaluation. Even more importantly, knowledge of the full 3D distribution of the plaques gives access to information that would otherwise only be attainable by slicing, followed by histopathological analysis of large areas of the brain. Local

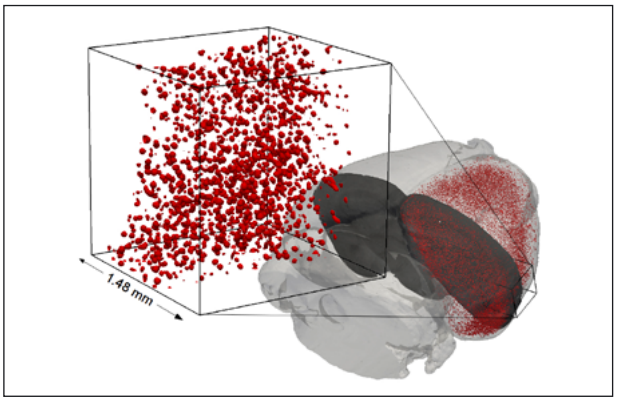

Figure 2: **3D representation of a brain scan of a 70-week-old mouse. The red dots are amyloid plaques, shown throughout the right neocortex. The position of the slice shown in Figure 1 is also indicated.**

plaque density, plaque sizes, mutual separation, etc. are easily accessible, as demonstrated in Figure 2, which shows a visualization of the 3D distribution of plaques (red) within the (manually segmented) neo-cortex.

The future of human tracer development?

The information provided by a DPC scan could be used in the future to accelerate the development of human PET tracers or to evaluate the effectiveness of anti-amyloid drugs. Both these research areas will likely have a large impact on future diagnosis and treatment of AD. Interdisciplinary collaboration involving synchrotron imaging could finally improve significantly the diagnosis and understanding of the disease, fostering the development of drugs to modify the progression of Alzheimer's disease.

References

[1] R. Mayeux and Y. Stern, Cold Spring Harbor Perspectives in Medicine **2**(8) (2012).
[2] J. Hardy and D.J. Selkoe, Science **297** No. 5580 (2002).
[3] S. Oddo et al., Neuron **43**(3) 321–332 (2004).
[4] S.A. McDonald et al., Journal of Synchrotron Radiation, **16**(4) 562–572 (2009).
[5] T. Weitkamp et al., Optics Express **13**(16) 6296–6304 (2005).
[6] H. Oakley et al., Journal of Neuroscience **26**(40) 10129–10140 (2006).
[7] B.R. Pinzer et al., NeuroImage **61**(4) 1336–1346 (2012).

Links

[1] Tomography group at the Swiss Light Source: http://www.psi.ch/sls/tomcat/
[2] The Brain Mind Institute at EPFL: http://bmi.epfl.ch/

High-resolution X-ray tomography at the SLS: Unravelling the nano-structure of cement paste

Mirko Holler, Ana Diaz, Manuel Guizar-Sicairos, Christoph Quitmann, Andreas Menzel, Jörg Raabe and Oliver Bunk, *Synchrotron Radiation and Nanotechnology Department (SYN), PSI;* Pavel Trtik, *Neutron Imaging and Activation Group (NIAG), PSI; Faculty of Civil Engineering, Czech Technical University in Prague, Czech Republic; and Laboratory for Concrete and Construction Chemistry, Empa, Switzerland*

A new instrument for hard X-ray nano-tomography has been developed at PSI. Integrated laser interferometry enables the advanced positioning metrology required for high-resolution imaging of large volumes. The instrument has been applied to a hydrated cement sample in fully saturated conditions. Understanding the 3D structure of cementitious materials at the nanoscale is crucial to improving this ubiquitous material. Our measurements allowed segmentation of individual material phases and quantitative determination of their electron densities, which can be used as input for next-generation material modelling.

The development of more durable cementitious materials has the potential to significantly reduce construction and maintenance costs. To achieve material improvements, information on the 3D structure at the nanoscale is crucial. Knowing the mass density of the individual material phases is needed for modelling of processes occurring in these materials, such as hydration and degradation. The challenge in imaging cementitious materials lies in covering a statistically representative volume element in a native state undisturbed by sample preparation while simultaneously capturing the nanoscale features.

Over the past few years, X-ray ptychographic imaging has been pioneered at PSI. Ptychographic imaging utilises advanced understanding of light wave interference patterns to determine additional image information that is not accessible by classical means, thereby boosting the resolution by orders of magnitude. It involves scanning the sample in two dimensions through a coherent X-ray beam and recording the X-ray diffraction patterns. Using iterative phase-retrieval algorithms, overlapping illuminated areas guide the image reconstruction. To obtain 3D tomographic datasets, 2D ptychographic imaging is repeated with a range of sample orientations that can be computed into a single 3D quantitative model of electron density [1–3]. The achievable image resolution can be orders of magnitude better than both the size of the beam and the scanning step, but requires extremely high positioning accuracy and stability of the sample.

In order to take full advantage of the potential of ptychographic imaging, PSI has developed an X-ray ptychographic tomography instrument with integrated novel positioning metrology [4].

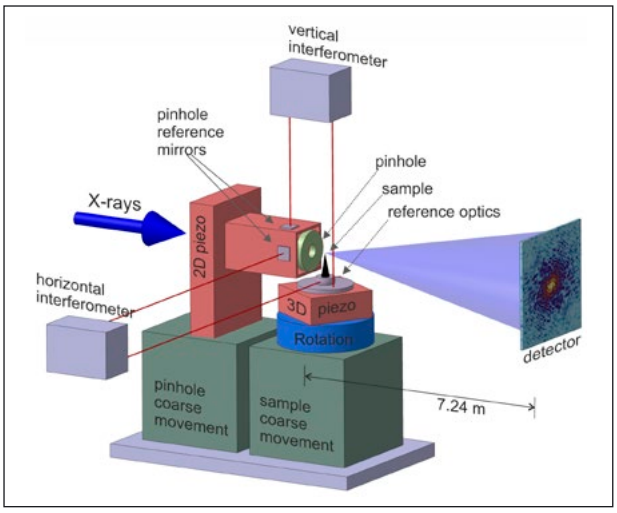

Figure 1: **Schematic of the instrument for nano-tomographic measurements.**

As depicted in Figure 1, a monochromatic X-ray beam, whose size and position are defined by a pinhole or other appropriate optics, illuminates a small sample area and the resulting far-field diffraction pattern is recorded via an area detector. A combination of positioning stages provides translations and rotation of the sample with ranges of millimetres and 370 degrees, combined with a resolution of 0.5 nm and 80 microdegrees. Positioning precision and stability is achieved by the integration of two laser interferometers that measure at any rotation angle the relative position of mirrors mounted close to both the sample and X-ray optics (pat. pend.). Thermal drift is minimized by the design of the interferometer system and mirror placement.

The interferometric resolution is below 1 nm, and in closed-loop operation the combined metrology and positioning system achieves a stability of better than 10 nm standard deviation. Closed-loop operation is not only important for achieving high imaging resolution, but also for the measurement of large sample volumes that require long scan times, where thermal drift of the mechanical system would otherwise accumulate over time and result in image distortion.
Demonstration experiments of this system at the cSAXS beamline at SLS have reached a 2D resolution of 8 nm and a 3D resolution of 36 nm with test objects illuminated by an X-ray beam of approximately 2 µm diameter and a wavelength of 2 Å.

Hydration of alite

The hydration of alite is a critical process in the setting of modern cement, having a strong influence on the material properties. To study this, alite powder was enclosed in a tapering glass capillary and hydrated for about two weeks in sealed conditions. A sample volume of approximately 412,000 µm^3, which is close to the representative volume element of a bulk sample, was then imaged over the course of about 2 days. A non-sequential projection acquisition strategy was utilized in order to avoid artefacts caused by changes in the sample over time [5]. The integrated metrology allows previous measurements of epoxy-impregnated samples [6] to be extended in volume and resolution.
Provision of congruent 3D datasets of both phase and absorption contrast permits the trustworthy, quantitative [3] segmentation of individual material phases, as presented in Figure 2. Major phases identified are calcium-silicate hydrates, calcium hydroxide, unhydrated alite grains and capillary porosity, observed with spatial resolution of about 100 nm. This allows the range of electron density of calcium-silicate hydrates in hydrated cement paste in fully saturated state to be derived. It is foreseen that such datasets, thanks to the combination of wide field of view and high resolution, can be used as statistically significant input for the assessment of mechanical and transport properties.

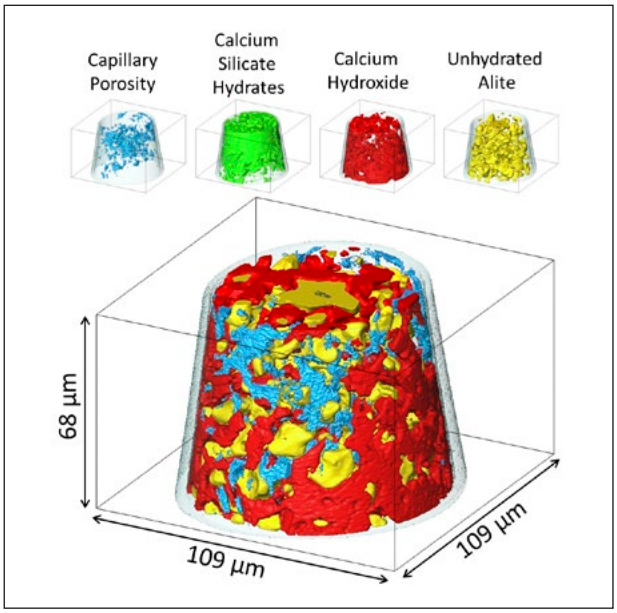

Figure 2: **Surface renderings showing the identified individual major material phases of alite hydration.**

Conclusion and Outlook

This unique instrumental setup allows the measurement of a volume representative of a sample's coarse structure without compromising fidelity. Quantitative density measurements of large sample volumes at high resolution are enabled by the combination of the high resolving power and large penetration depth of hard X-ray ptychography with integrated position metrology.
The setup presented here is a prototype of the OMNY (tOMography Nano crYo) project, which aims to develop a dedicated end-station for ptychographic nano-tomography of cryogenic samples in ultra-high vacuum, to reduce radiation damage. In addition to solid-state physics samples, this will permit the measurement of cryogenically fixed biological specimens, including soft tissue, entire cells, and cellular networks close to their native state.

References

[1] M. Dierolf, A. Menzel, P. Thibault, P. Schneider, C.M. Kewish, R. Wepf, O. Bunk and F. Pfeiffer, Nature **467** (7314), 436 (2010).
[2] M. Guizar-Sicairos, A. Diaz, M. Holler, M.S. Lucas, A. Menzel, R.A. Wepf and O. Bunk, Opt. Exp. **19**(22) 21345 (2011).
[3] A. Diaz, P. Trtik, M. Guizar-Sicairos, A. Menzel, P. Thibault and O. Bunk, Phys. Rev. B **85**(2) 020104 (2012).
[4] M. Holler, J. Raabe, A. Diaz, M. Guizar-Sicairos, C. Quitmann, A. Menzel and O. Bunk, Rev. Sci. Instrum. **83** 073703 (2012).
[5] A. Kaestner, B. Münch, P. Trtik and L. Butler, Opt. Eng. **41** 123201 (2011).
[6] P. Trtik, A. Diaz, M. Guizar-Sicairos, A. Menzel and O. Bunk, Cement & Concrete Composites **36** 71 77 (2013).

Link

[1] Coherent X-ray Scattering Group: http://www.psi.ch/coherent-x-ray-scattering/

Spin-orbital separation in a cuprate spin-chain probed with Resonant Inelastic X-ray Scattering

Thorsten Schmitt[1], Justine Schlappa[1,4], Ke Jin Zhou[1,5], Vladimir N. Strocov[1], Krzysztof Wohlfeld[2], Jeroen van den Brink[2], Martin Mourigal[3] and Henrik M. Rønnow[3]

[1]*Laboratory for Synchrotron Radiation – Condensed Matter (LSC), PSI;* [2] *IFW Dresden, Germany;* [3] *EPFL Lausanne, Switzerland;* [4]*present affiliation: Helmholtz-Zentrum Berlin, Germany;* [5]*present affiliation: Diamond Light Source, UK*

In an orbital excitation, the electron occupation of orbitals that are crystal-field split into different symmetries is changed. The photon-in/photon-out spectroscopy known as Resonant Inelastic X-ray Scattering (RIXS), available at the ADRESS beamline of the SLS, efficiently probes such electronic excitations. We have observed that such an orbital excitation can decay into collective spin and orbital excitations in a spin-chain material, represented by so-called *spinon* and *orbiton* quasi-particles. This establishes that the electronic degree of freedom in a solid can, in general, be split up into its separate spin and orbital degrees of freedom. The implications for future practical applications of this research lie in creating the basis for improving the understanding of the origin of high-temperature superconductivity and the development of quantum computers.

One of the pivotal questions of contemporary condensed matter physics deals with the role of magnetic fluctuations for the pairing interaction in high-temperature superconductors made from two-dimensional cuprate materials. In this context, it is also of fundamental interest to better understand related quasi one-dimensional copper-oxide materials like spin-chain materials and their low-energy excitations. Sr_2CuO_3 is a quasi one-dimensional single-chain compound, which has the nearly ideal properties of a one-dimensional Heisenberg spin-1/2 system. It consists of corner-sharing connected CuO_4-plaquettes with very small interchain interaction, giving the system strong one-dimensional properties. Along the chains, the magnetic interaction through a 180 degree Cu-O-Cu path results in large antiferromagnetic (AF) super-exchange of ca. 0.25 eV. We investigated Sr_2CuO_3 with Cu L_3 edge RIXS at the Advanced Resonant Spectroscopies (ADRESS) beamline [1] of the Swiss Light Source (SLS) at PSI. By varying the photon-momentum transfer, ***q***, the dispersion of collective orbital and spin excitations could be tracked across the majority of the first Brillouin zone for this spin chain. In these measurements, a new spin-orbital separation phenomenon could be observed in a one-dimensional solid, which allows the electronic degree of freedom to be split into its spin and orbital degrees of freedom.

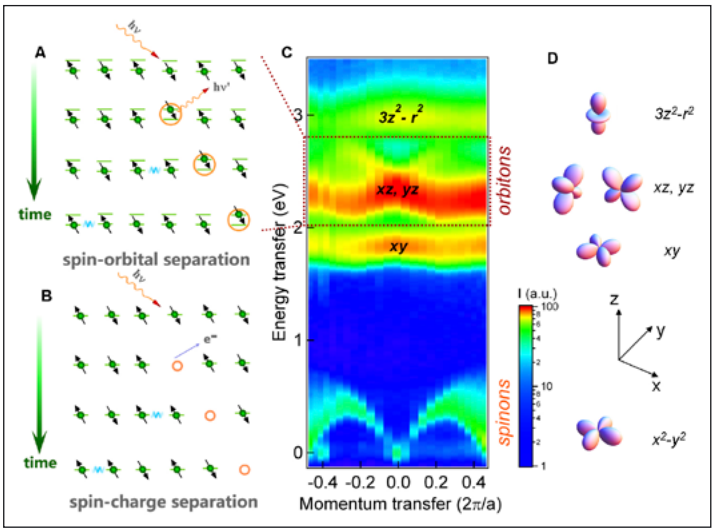

Figure 1: **Schematic illustration of: (A) spin-orbital and (B) spin-charge separation processes observable in RIXS and ARPES, respectively; (C) RIXS intensity map of the dispersing spinon and orbiton excitations vs. photon momentum transfer along the chains and photon energy transfer. The dashed rectangle indicates the part of the spectrum related to the xz orbital excitation for which the spin-orbital separation process is most clearly visible; (D) Symmetry of the involved Cu 3*d* orbitals (adapted from [6]).**

Momentum transfer dependent RIXS

The ADRESS beamline is currently the best facility for this RIXS experimental technique in the soft X-ray energy range, using the Super-Advanced X-ray Emission Spectrometer (SAXES) [2], with a total resolution of better than 120 meV at the Cu L_3 edge. RIXS is a photon-in/photon-out spectroscopic method which measures the energy transfer to the electronic system

between incident and inelastically scattered X-ray photons. The momentum transfer **q = k' - k** (where **k'** and **k** denote the wave vectors of scattered and incident X-ray light, respectively) to the material system can be varied in such an experiment by changing the scattering geometry between incident and detected X-rays. This can be accomplished in the set-up at the ADRESS beamline by rotating the sample as well as the whole instrument, supported by air-cushion devices below the spectrometer platform.

Dispersive spin and orbital excitations

In Figure 1C, we observe, in the Cu L_3 RIXS measurments on Sr_2CuO_3, pronounced strongly momentum-dispersive collective excitations well separated in two energy loss regions. Up to ca. 0.8 eV energy transfer, the RIXS spectrum comes from pure spin excitations. At higher energies, between roughly 1.5 and 3 eV, the spectrum originates from excitations between the orbital ground state 3d $x^2–y^2$ hole symmetry to xy, xz/yz and $3z^2–r^2$ orbital symmetries (see illustration in Figure 1D). The magnetic RIXS data in the low-energy sector, below 0.8 eV, agree very well with recent inelastic neutron scattering (INS) studies on Sr_2CuO_3 that probe the two-spinon (and higher-order) continuum [3]. This confirms that magnetic Cu L_3 RIXS probes the spin dynamical structure factor.

Analyzing the orbital excitations spectrum in detail reveals a distinct dispersion that has never been observed before. To our knowledge, this experiment is the first unambiguous observation of the momentum transfer dispersion of low-energy excitations in the orbital degree of freedom. From all orbital symmetries, the xz excitation in our study has the clearest dispersion, with ca. 0.2 eV. Its spectrum is made up of a lower intense and sharp component with a period π dispersion, as well as a weaker double-structured continuum spectrum above. The fact that the observed orbital dispersion has clear similarities to ARPES spectra of one-dimensional cuprates, showing the separation of the spin- and charge degree of freedom [4], suggests that, in RIXS, it might be possible to detect the separation of spin and orbital degrees of freedom.

Orbiton quasi-particle discovered

Theoretical analysis of this dispersion behaviour with a Kugel-Khomskii model describing the spin-orbital interactions in Sr_2CuO_3 [5] gives solid proof for a previously unobserved novel spin-orbital separation process [6], analogous to the well-known spin-charge separation mechanism occurring when a hole is created in a one-dimensional chain. After initiating an orbital excitation between the copper 3*d* orbitals in RIXS, the created orbiton can propagate through the lattice after having excited a spinon (a domain wall in the AF chain), thereby separating the electron in its orbital and spin degrees of freedom (see schematics in Figure 1A). By this RIXS study, it could thus be shown that the orbital excitations break up into spinons and orbitons that propagate as independent quasi-particles through the spin-chain. Details of this study can be found in [6].

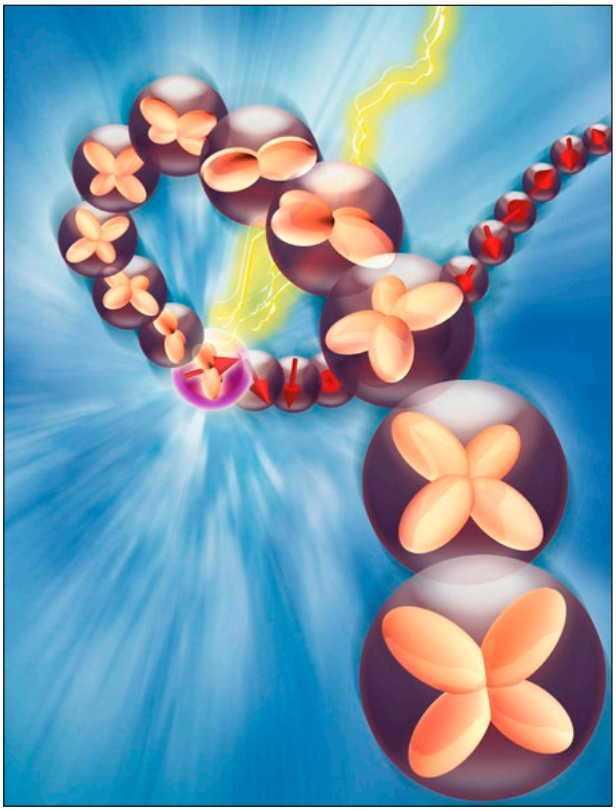

Figure 2: **Artist's view of how an orbital excitation in a spin-chain separates into spinon and orbiton waves.**
(Graphic: David Hilf, Hamburg)

References

[1] V.N. Strocov and J. Synchrotron Rad. **17** 103 (2010).
[2] G. Ghiringhelli et al., Rev. Sci. Instrum. **77** 113108 (2006).
[3] A.C. Walters et al., Nature Physics **5** 867–872 (2009).
[4] C. Kim et al., Phys. Rev. Lett. **77** 4054–4057 (1996).
[5] K. Wohlfeld et al., Phys. Rev. Lett. **107** 147201 (2011).
[6] J. Schlappa, K. Wohlfeld, K.J. Zhou, M. Mourigal, M.W. Haverkort, V.N. Strocov, L. Hozoi, C. Monney, S. Nishimoto, S. Singh, A. Revcolevschi, J.-S. Caux, L. Patthey, H.M. Rønnow, J. van den Brink and T. Schmitt, Nature **485** 82–85 (2012).

Link

[1] ADRESS Beamline: http://www.psi.ch/sls/adress/

Vacuum ultraviolet ionization in combustion science: from pyrolysis to catalysis

Patrick Hemberger and Thomas Gerber, *Combustion Research Laboratory (LVF), PSI;*
Andras Bodi, *Laboratory for Catalysis and Sustainable Chemistry (LSK), PSI*

The formation of carcinogenic polycyclic aromatic hydrocarbons (PAHs) in fuel combustion is still not fully understood. In our experiments, Xylyl radicals and their reaction products (PAH precursors) have been produced in a pyrolysis reactor and studied isomer-selectively using photoelectron spectroscopy. We discuss here the insights this yields into soot formation processes. In a second experiment, the photoelectron photoion coincidence (PEPICO) technique unveils the energetics of urea thermolysis, relevant in diesel engines, namely in exhaust gas aftertreatment to lower toxic NO_x emissions. Our work in both fields aims at understanding fundamental processes, in order to further improve combustion technologies.

About 90% of the global energy consumption is supplied by fuel combustion, of which almost 90% is due to non-renewable fossil fuels. How can we make the most of this energy source? In order to be economical, we have to increase efficiency. In order for combustion to be more benign, we have to mitigate the environmental load of fuel burning. Here we will follow the conversion of fuel into exhaust components and show how vacuum ultraviolet (VUV) photoionization can help us understand the combustion process, soot formation in particular, and the energetics of exhaust gas aftertreatment.

Soot Formation

Xylenes are petrol additives used for their high energy density and octane number. Although the initial stage of xylene decomposition is known to be the formation of a xylyl radical, the combustion chemistry of these additives is mostly unexplored. Radicals are known to produce large polycyclic aromatic hydrocarbons (PAHs), which can coagulate to form soot particles. Since soot lowers the efficiency of combustion engines and is a health hazard, it is an unwanted combustion product. This motivated us to study the combustion chemistry of *ortho*-xylyl radicals on a molecular level [1].

Soft VUV photoionization and the detection of ions and electrons in coincidence permit us to measure mass-selected threshold photoelectron (TPE) spectra at the newly upgraded VUV beamline [2], and provide an isomer-selective tool to study reactive intermediates and combustion products. *O*-xylyl radicals were generated by controlled flash pyrolysis of the 2-methylbenzyl bromide precursor (mass/charge ratio, m/z = 184 and 186) in a molecular beam (blue traces in Figure 1). With increasing temperature, the precursor vanishes from the mass spectrum and several new peaks appear at m/z = 102–106. The reaction products can be disentangled by TPE spectroscopy (red, blue and green boxes, Figure 1). At intermediate temperatures, the precursor reacts to the desired *o*-xylyl radical ***1*** (m/z = 105). At higher temperatures, the radical decomposes by hydrogen atom abstraction (m/z = 104). Modelling the TPE fingerprint identifies the two different reaction products: *o*-xylylene ***2*** and benzocyclobutane ***3***. A minor reaction product is anthracene ***4*** (m/z = 178), which is a PAH. In the first step of the proposed reaction mechanism,

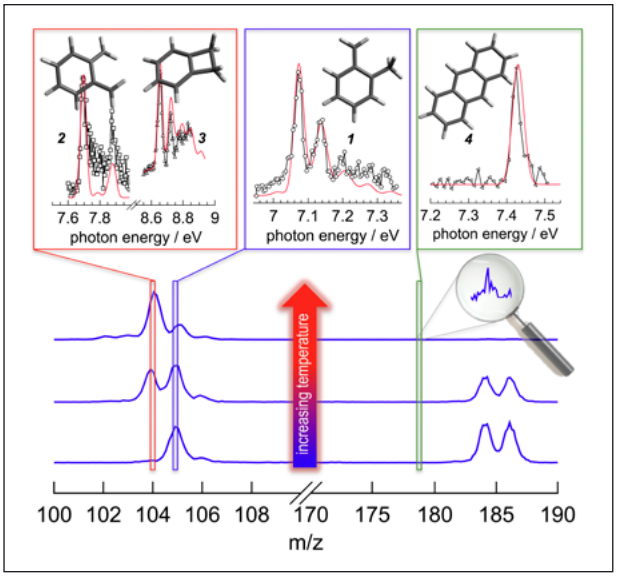

Figure 1: **Mass (blue lines) and TPE (upper boxes) spectra showing the decomposition of *o*-xylyl to *o*-xylylene and benzocyclobutane.**

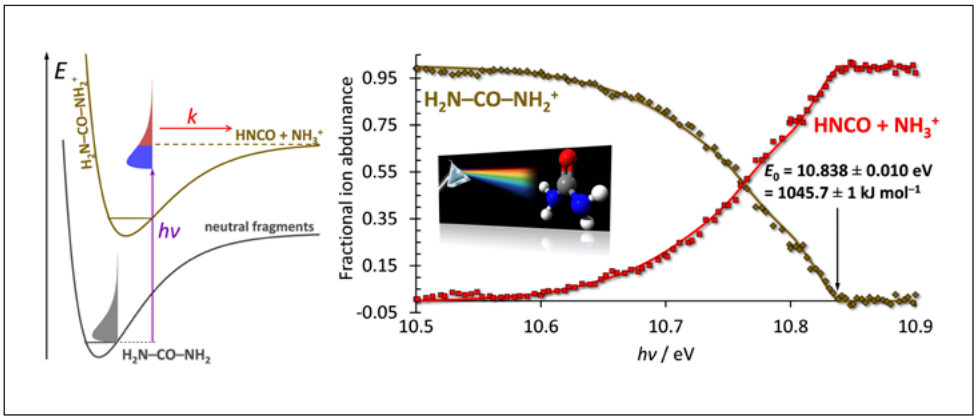

Figure 2: **Potential energy (left) and breakdown diagram (right) for the dissociative photoionization of urea.**

a hydrogen atom is abstracted from the methyl group of the *o*-xylyl radical, leading to *o*-xylylene, which undergoes an intramolecular [2+2] cycloaddition yielding the benzocyclobutane ***3***. A [4+2] cycloaddition of two *o*-xylylene intermediates ***2*** might initiate the creation of the 14-membered anthracene ring system, which is followed by hydrogen and ethylene loss. TPE spectroscopy is thus a versatile tool to disentangle complex chemical reaction mixtures, helping us to understand soot formation processes in combustion engines. In the future, we will also apply this technique to study reaction mechanisms in catalytic reactors as well as in low-pressure flames.

Energetics of exhaust gas aftertreatment

Quickly reaching high flame temperatures in the combustion cycle is a strategy to lower PAH concentrations, but, at the same time, it favours NO_x formation. NO_x emissions can be reduced in selective catalytic reduction (SCR) processes, as studied by the CEG group at PSI [3], by introducing ammonia (NH_3) to the exhaust stream, yielding nitrogen and water in a symproportionation reaction. However, bulk ammonia is dangerous and difficult to handle and is thus synthetized from a harmless precursor, typically urea, in situ. Upon thermolysis, urea releases an ammonia molecule and isocyanic acid (HNCO), which can further be hydrolyzed to ammonia and carbon dioxide. Inconsistencies plague the energetics data on urea thermolysis in the literature. Well-established energetics data on SCR processes may help to find suitable candidates to replace urea, either with more efficient ammonia precursors, e.g. guanidine, or in applications where a urea solution is impractical, e.g. in the extreme cold.

Threshold photoionization in coincidence with photoion mass spectrometry is not only useful to record photoelectron spectra of individual components in a mixture. It can also be used to scan the internal energy of the photoion and establish the energetics of the dissociation processes. The photon energy is scanned, and all the excess energy above the ionization threshold is deposited as internal energy in the photoion. At low photon energies, there is insufficient internal energy to break a chemical bond and the cation cannot fragment. When the photon energy is increased, only hot neutral molecules will initially move above the dissociation threshold (energy diagram in Figure 2). In the absence of an overall barrier to H-transfer to form NH_3, the dissociation will be fast ($k > 10^7\ s^{-1}$), because of the absence of tunnelling [4]. The dissociative photoionization energy then lies precisely at the photon energy, where even the rovibrational ground-state neutrals can dissociate, and the parent ion signal disappears from the mass spectrum. The fractional parent and fragment ion-abundances are plotted in the breakdown diagram, as shown in Figure 2. In urea, the first dissociative photoionization process, $NH_2–CO–NH_2 + h\nu \rightarrow NH_3^+ + HNCO + e^-$, corresponds to the thermolysis of urea, but yields ammonia cation instead of neutral ammonia. Since the ionization energy of ammonia is very well known, this means that the photoionization measurement yields the thermolysis energy of gas phase urea as 62.9 ± 1 kJ mol^{-1} by way of a thermochemical cycle. The difference between our measurement and widely used tabulated values is more than 20 kJ mol^{-1}, which prompted us to revise the urea and isocyanic acid gas phase enthalpies of formation to –235.7 ± 1.4 and –119.2 ± 1.4 kJ mol^{-1} at 298 K [5]. In future experiments, such energetics studies will be applied to combustion intermediates, giving insight into their thermochemical parameters.

References:

[1] P. Hemberger, A. Trevitt and G. da Silva, *in preparation*.
[2] A. Bodi et al., Rev. Sci. Instrum. **83** 083105 (2012).
[3] A.M. Bernhard et al., Catal. Sci. Technol. **3** 942 (2012).
[4] A. Bodi et al., Phys. Chem. Chem. Phys. **14** 16047 (2012).
[5] A. Bodi et al., J. Chem. Thermodyn. **58** 292 (2013).

Links

[1] Combustion Research Laboratory (LVF): http://rag.web.psi.ch
[2] Laboratory for Catalysis and Sustainable Chemistry (LSK): http://www.psi.ch/lsk/lsk
[3] VUV beamline: http://www.psi.ch/sls/vuv/vuv

Topological sector fluctuations in spin ice

Ludovic Jaubert, *Okinawa Institute of Science and Technology, Japan;* Mark Harris, *School of Divinity, University of Edinburgh, Scotland;* Tom Fennell, *Laboratory for Neutron Scattering (LNS), PSI;*
Roger Melko, *Department of Physics and Astronomy, University of Waterloo, Canada;*
Steven Bramwell, *London Centre for Nanotechnology, University College London, UK;*
Peter Holdworth, *Laboratoire de Physique, École Normale Supérieure de Lyon, France*

Frustration, or competition amongst interactions, can be identified in diverse situations including magnetic materials, stellar nuclear matter, protein folding, or social dynamics. In spin systems, it promotes degeneracy by suppressing long-range order, resulting in strongly correlated, fluctuating states that may be described by emergent gauge theories or topological orders. Investigations of a spin ice, $Ho_2Ti_2O_7$, are described here, which have established an experimental connection with the topological character of the spin correlations [1].

Topological order and sectors are concepts of growing interest in condensed matter, but are typically not accessible by experiment [2]. Systems are usually classified by their (broken) symmetries, rather than topology, but objects with topological qualities can be extremely robust to minor perturbations. For example, quantum spin liquids, which have no broken symmetries, may be distinguished by topological ordering, and this could create a material with system-spanning, coherent entanglements with possible application in a topologically protected quantum computer. Distant as this may appear from the work on spin ice described below, this work is a first step in addressing experimentally accessible topological quantities in a spin system.

Frustration exists in a system when all the pairwise interactions cannot be simultaneously minimized [3]. In geometrically frustrated magnets, this effect can be introduced by the appropriate choice of lattice geometry and interactions. It is often associated with connected triangular plaquettes with antiferromagnetic interactions, as spins at the vertices of a single triangle cannot all be antiparallel simultaneously. We are concerned with three-dimensional systems based on the pyrochlore lattice, which is an array of corner-sharing tetrahedra (Figure 1a).

Surprisingly, on this lattice, it is possible for ferromagnetic interactions to be frustrated, as in the spin ice $Ho_2Ti_2O_7$. In this material, a local crystal field anisotropy constrains the spins to point along the body axes of the tetrahedron and they are coupled ferromagnetically. The local ground state has two spins pointing into, and two pointing out of, every single tetrahedron (the coupling is actually dominated by the dipolar interaction). This constraint is degenerate and does not uniquely constrain neighbouring tetrahedra. Instead, it can be used to construct an extensively degenerate manifold of ground states, which is statistically identical to those of the hydrogen bonded network in ice, hence the name spin ice (the 'two-in, two-out' condition is an example of the ice rule, similar to the condition for the satisfaction of bonding around an oxygen atom in ice, which is two covalent and two hydrogen bonds, or 'two-close, two-distant' for the position of the hydrogen atoms relative to the oxygen atom).

The ice-rule spin correlations produce a fascinating state at low temperature – it can be seen that the ice rule is non-divergent, and a perfect ice-rule obeying state will be globally non-divergent, with all spins being members of closed loops. Consequently, the spin configurations can be coarse-grained into a non-divergent field, making a spin ice an example of a Coulomb phase [4]. Exploration of the many ice-rule obeying ground states requires reversal of a loop of spins, or introduction of a local spin flip excitation that breaks the ice rules. These excitations are deconfined fractional quasi-particles carrying magnetic charge – a pair of them is created by a single spin flip and they can hop apart across the lattice. At low temperature, a spin ice is effectively described by a gas of these emergent magnetic monopoles diffusing along the trajectories of the field lines traced by the loops in the spin configurations.

In theory, and in the absence of monopoles, the spin correlations have a topological character. Along a loop, the spins have an alternating in-out, or head-to-tail, configuration (see Figure 1a). A cut through the lattice intersects a particular

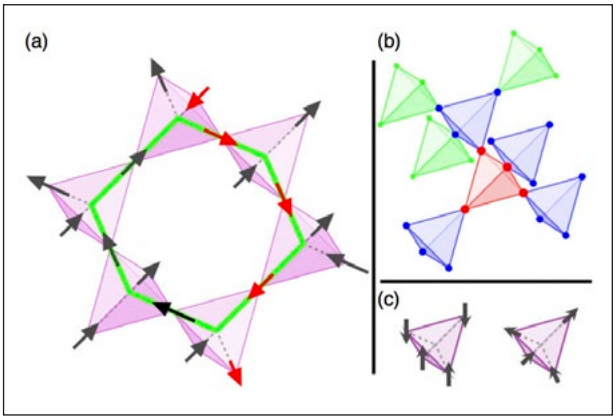

Figure 1: **Fragment of the pyrochlore lattice (a) showing the corner-linking tetrahedrons and ice-rule spin configurations. A short, closed loop is highlighted by green bonds, and a long, winding loop by red spins (the loop is connected by periodic boundary conditions). Huisimi tree of tetrahedrons (b) used for calculating the susceptibility – the connectivity precludes short loops.**

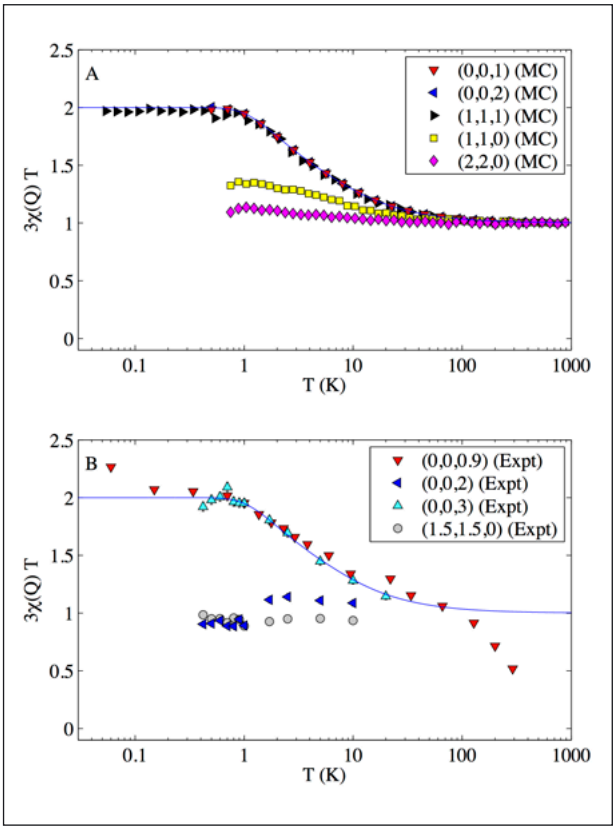

Figure 2: **Numerical simulations of the wave-vector-dependent susceptibility of $Ho_2Ti_2O_7$ compared with the exact result obtained from the Huisimi tree (line) (A). The susceptibility crosses over from a conventional Curie law at high temperature to one dominated by topological sector fluctuations at low temperature, and this effect can be measured at wave vectors of type (0,0,l). Comparison with neutron scattering intensities shows excellent agreement at wave vectors at the zone boundary, but the effect is suppressed at zone-centre wave vectors characteristic of the longest loops (B).**

number of loops, which have a positive or negative magnetization across the cut. The cut is characterized by the sum of these magnetizations – short loops which turn and pass back through the cut contribute zero, while long loops, which wind around the periodic boundaries of the system, make a contribution to the overall magnetization (see Figure 1a). When all loops are closed, any parallel cut will have the same layer magnetization, and the magnetization vector of the system is simply related to the winding vector – the number of long loops which wind through the system boundaries. This winding vector is a topological quantity, and its components define the topological sector. In a spin ice, topological order would correspond to selection of a single sector. On the other hand, fluctuations of the magnetization, measurable by susceptibility, imply a fluctuating population of long loops and a fluctuating topological sector.

A theory for the susceptibility of spin ice was developed using the Huisimi tree (Figure 1b), on which no short loops are possible. The bulk and wave-vector-dependent susceptibilities could be calculated analytically and simulated numerically (Figure 2A), showing that they cross over from a paramagnetic regime described by a Curie Law to a new Curie Law describing the low temperature Coulomb phase, where all fluctuations derive from long loops. It describes the bulk susceptibility remarkably well, but the wave-vector-dependent susceptibility (from neutron scattering experiments, Figure 2B) only at certain wave vectors. In reality the dynamics of a spin ice are due to diffusing monopoles (large-scale tunnelling of loops being generally regarded as impossible) and this could place a temperature-dependent length-scale cut-off on the topological sector description, depending on the defect population. However, the most important part of the comparison is the crossover between Curie laws, when defects are anyway numerous. That this occurs shows that the description of the developing Coulomb phase in terms of a fluctuating topological sector is useful. It appears that the problem may have more to do with a weighting in favour of short loops that is not captured by the theory, since no clear cut-off is detected.

References

[1] L.D.C. Jaubert et al., *Topological-Sector Fluctuations and Curie-Law Crossover in Spin Ice*, Physical Review X **3** 011014 (2013).

[2] S.R. White, *Quantum spin liquids: Tell-tale topology*, Nature Physics **8** 863 (2012).

[3] C. Rüegg, *Frustrated Magnetism: a pinwheel without wind*, Nature Physics **6** 837 (2010).

[4] T. Fennell, P.P. Deen, A.R. Wildes, K. Schmalzl, D. Prabhakaran, A.T. Boothroyd, R.J. Aldus, D.F. Mcmorrow, and S.T. Bramwell, *Magnetic Coulomb phase in the spin ice $Ho_2Ti_2O_7$*, Science **326** 415 (2009).

Visualizing soot and ash distributions in diesel particulate filters using neutron imaging

Christian Gruenzweig, David Mannes, Anders Kaestner, Matthias Vogt, Florian Schmid, Jan Hovind, Peter Vontobel and Eberhard Lehmann, *Spallation Neutron Source Division (ASQ), PSI*

Even though diesel particulate filters (DPFs) are commonly used with diesel engines, it is still difficult to determine the soot distribution within the filter. Neutron tomography provides at present the only possibility for obtaining information about the three-dimensional distributions of soot and ash in a filter monolith. The estimation of the soot distribution in a DPF with neutron imaging is possible because neutrons are highly sensitive to the hydrogen, which is a component of soot. This information is of great interest to the automotive industry, regarding the optimisation of DPFs as well as for validating numerical simulation techniques used in their design and implementation.

Introduction

Particulate filters can nowadays be found in almost all new diesel vehicles. This is a statutory requirement, as the particles in exhaust gas consist mainly of harmful soot and ash, and should not escape into the environment. Inside these filters, the exhaust gases pass through a system of honeycomb-like channels, in which only alternate 'honeycombs' have an exit. Because of this, the exhaust gas has to penetrate into the porous walls between the honeycombs before it can flow any further. Soot and ash particles cannot pass through these pores and are therefore deposited onto the walls. Particle filters can be examined non-destructively using X-ray measurements, but this can only reveal the distribution of ash. For the assessment of soot, neutrons have an advantage over X-rays as they are not only more sensitive to carbon but, more importantly, they have a significantly higher sensitivity to hydrogen when compared with X-rays. Soot thus yields high contrast in the neutron images because it contains small amounts of hydrogen, caused by incompletely burned fuel.

Tomography data of an entire canned DPF

Neutron tomography data of an entire canned diesel particulate filter (DPF) provide spatially resolved information on the local soot and ash distributions. Figure 1 shows a photo of the DPF (a) as well as an overview neutron tomography picture (b), with a pixel size of 150 µm/pixel, giving a three-dimensional volumetric view into the DPF. One can clearly distinguish the monolith with its individual segments and its filter channels. The special feature of this DPF is the additional mounting of an inlet-sided centric mask, which was installed before the last loading phase. This coverage partially blocks the exhaust flow onto the monolith. The diameter of the mounting was chosen such that the central segment is completely protected and its surrounding segments only partially loaded. The outer segments were exposed to the full exhaust stream.

Local soot and ash distributions

Figure 2(a) displays the local loading levels of ash and soot in a vertical section through the middle of the filter.

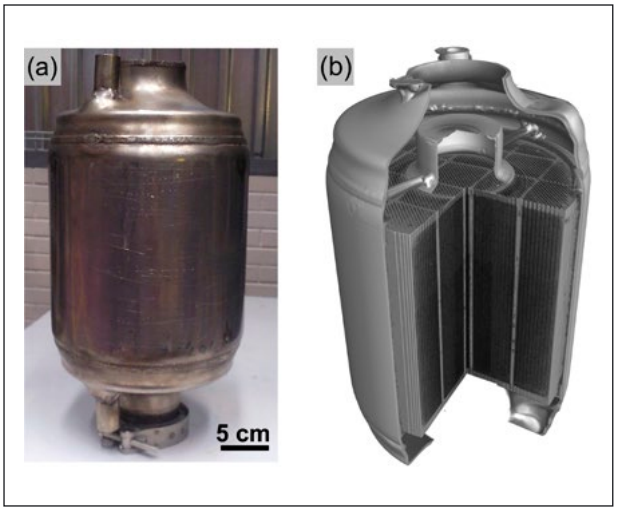

Figure 1: **(a) Photograph of the canned DPF; (b) Neutron tomography data: The steel jacket is no barrier for neutrons and allows the interior to be visualised.**

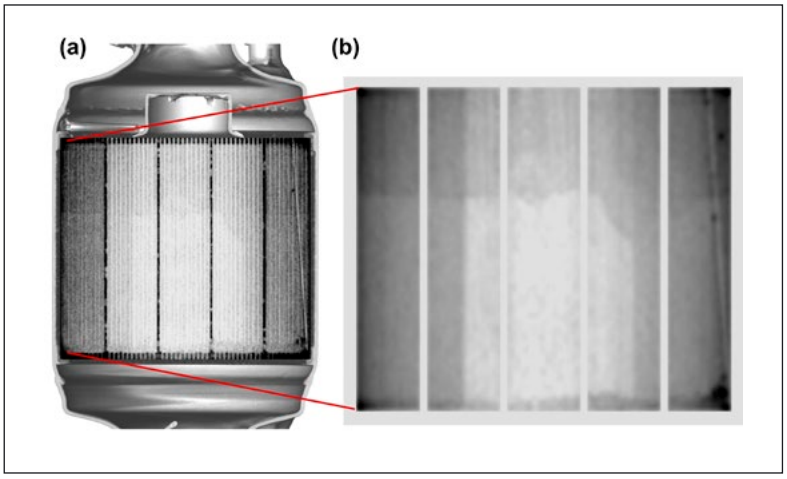

Figure 2: **(a) Vertical, centre section trough the filter; (b) Monolith region. Clearly visible are the two vertical lines as sharp boundaries between loaded and unloaded filters regions. Similarly, a horizontal line is seen in the upper third, which is due to the catalytic zone coating.**

Figure 2(b) shows the loading more clearly. For a better representation of the ash and soot distributions, the image was processed by a Gaussian filter, which eliminated the channel structures. The darker the areas appear, the higher is the loading. Two areas are particularly noticeable: Firstly, a vertically extended region below the coverage running through the whole monolith, which is separated by two clear vertical lines from the rest of the monolith. This area is brighter, meaning there are fewer, or no, soot and ash deposits. Secondly, a horizontally extended region in the upper third of the filter, which is due to a catalytic zone coating. The trend shows that the outer regions experienced more abundant soot loading than expected. Ash residues originating from the two regenerations when the filter was loaded without using the coverage caused the thin layer of deposits in the bottom region.

High-resolution tomography

To obtain detailed information about the ash and soot accumulations along individual filter channels, a high-resolution tomography experiment was performed, with a pixel size of 13.5 µm/pixel. The sample is shown in Figure 3(a) and a three-dimensional representation of the tomography data in Figure 3(b). With the help of the tomography data, different materials – such as the filter material, soot and ash, and even metallic particles – can be segmented. An animation of the high-resolution tomography can be downloaded from [2].

Outlook

The neutron imaging results have created a foundation from which diesel particulate filters can be optimised and developed further. The localization and quantification of soot in DPFs is of great interest for the automotive industry, for answering questions regarding the design and optimization of filters and flow geometries as well as providing the possibility for validating theoretical simulation.

References

[1] C. Grünzweig, D. Mannes, A. Kaestner and M. Vogt, *Visualisation of the soot and ash distribution in diesel particulate filters using neutron imaging*, MTZ Motortechnische Zeitschrift **73**(4) 326–331 (2012).
[2] http://www.youtube.com/watch?v=A4kWCP39t6U

Link

[1] Neutron Imaging and Activation Group: http://www.psi.ch/niag/niag

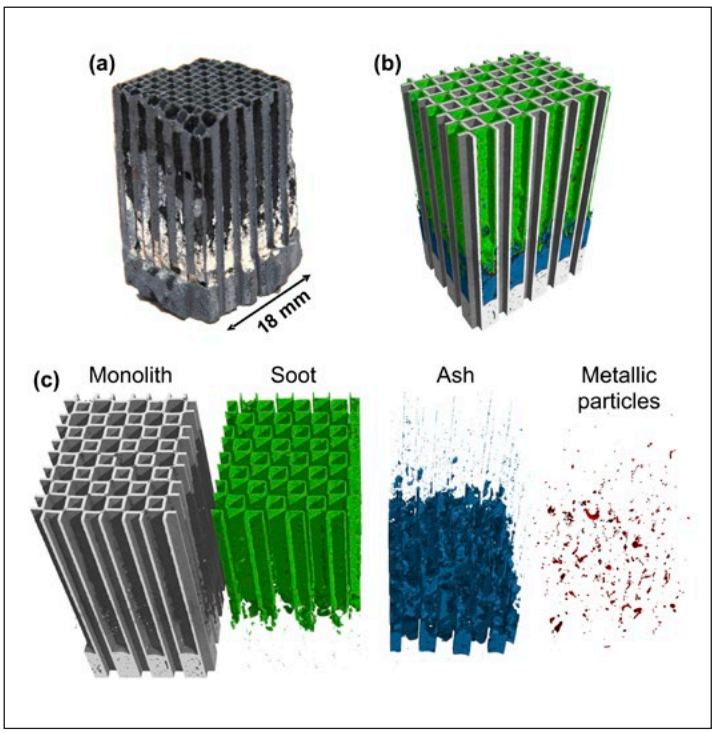

Figure 3: **(a) Photo of the sample – ash residues (light), soot (black); (b) 3D representation of the tomography data; (c) Segmentation of the individual components of the sample.**

Single-molecule magnets – from bulk to thin films

Zaher Salman, Andrea Hofmann, Alex Amato, Elvezio Morenzoni, Thomas Prokscha and Andreas Suter, *Laboratory for Muon Spin Spectroscopy (LMU), PSI;* Matteo Mannini, Luigi Malavolti and Roberta Sessoli, *Dipartimento di Chimica "Ugo Schiff" Università di Firenze & INSTM, Italy*

A promising strategy for encoding information in molecular units is provided by Single-Molecule Magnets (SMMs), chemically identical nanoscale clusters of exchange-coupled ions and associated ligands. The assembly of these systems on surfaces represents a necessary prerequisite for their technological application. However, neither the effect of the surface on the magnetic properties of individual SMMs nor that of reduced dimensionality is well understood. Here, we show that the magnetic properties of a prototypical SMM are dramatically different from its bulk properties when deposited in a thin film on gold.

Single-Molecule Magnets (SMMs) [1] have been used to study quantum tunnelling of magnetization and topological quantum phase interference and may find applications in quantum information processing. In recent years, the assembly of these systems on surfaces and understanding the effects of the surface on their magnetic properties has attracted much attention [2]. One of the most investigated SMMs is $TbPc_2$ ($Tb(C_{32}H_{16}N_8)_2{\cdot}CH_2Cl_2$ in bulk), whose chemical robustness enables thermal evaporation on surfaces [3]. As far as the magnetic properties are concerned, the ground spin state manifold, $\mathbf{J} = 6$, of $TbPc_2$ is split by a strong crystal field at the Tb^{3+} ion, which results in a separation between the ground state, $J_z = \pm 6$, and the first excited state, $J_z = \pm 5$, of the order of a few hundred Kelvin [4]. The exceptionally large anisotropy of $TbPc_2$, as well as the long correlation time of its molecular spin fluctuations, makes the system a promising candidate for applications in quantum computation [5]. In the crystalline phase, $TbPc_2$ is characterized by a low-temperature butterfly-shaped hysteresis, which opens at temperatures as high as 15 K. In contrast, submonolayers of $TbPc_2$ on Au(111) do not show a similarly high blocking temperature [3]. The weak hysteresis in submonolayers on various conducting surfaces may be due to the effects of the substrate on the magnetization dynamics, or possibly variation in the intermolecular interactions between neighbouring $TbPc_2$. However, the exact details of how and why the low-temperature dynamics are affected are still not clear. Therefore, a better understanding of the phenomenon is mandatory if these types of molecules are to be used in spintronic devices.

Here, we use the muon spin relaxation (μSR) technique to measure the local spin dynamics of bulk $TbPc_2$ and its depth dependence in thin films (a thick ~1 μm and a thin ~100 nm) evaporated onto an Au surface. In these experiments, fully spin-polarized muons are implanted into the sample and used as a local probe to detect dipolar fields from their neighbouring molecules (see Figure 1). Thus, they provide a direct observation of the spin dynamics of individual SMMs. This resolution, coupled with the unique sensitivity to fluctuation times in the range ~10^{-11} to 10^{-4} s, makes this technique very suitable for studies of SMMs, both in the bulk and at the nanoscale.

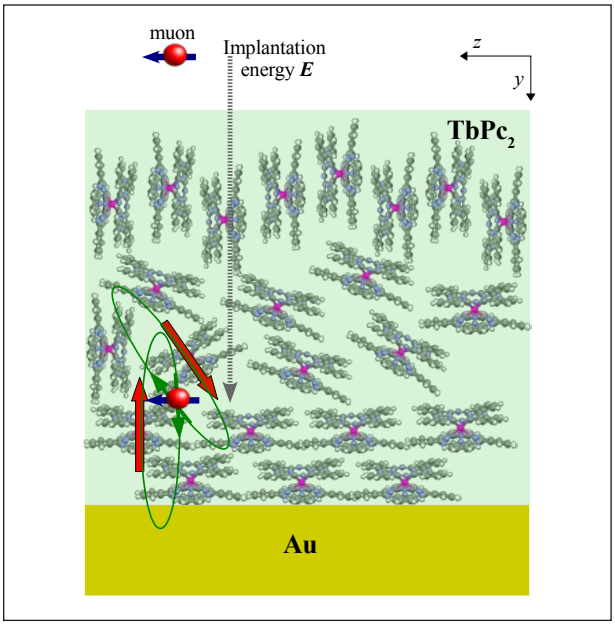

Figure 1: **Schematic of a typical LE-μSR experiment. Fully spin-polarized muons (along z) are implanted with energy E into a thin film of $TbPc_2$ and sense the dipolar magnetic fields from the moments of neighbouring SMMs. The muon mean implantation depth is proportional to E.**

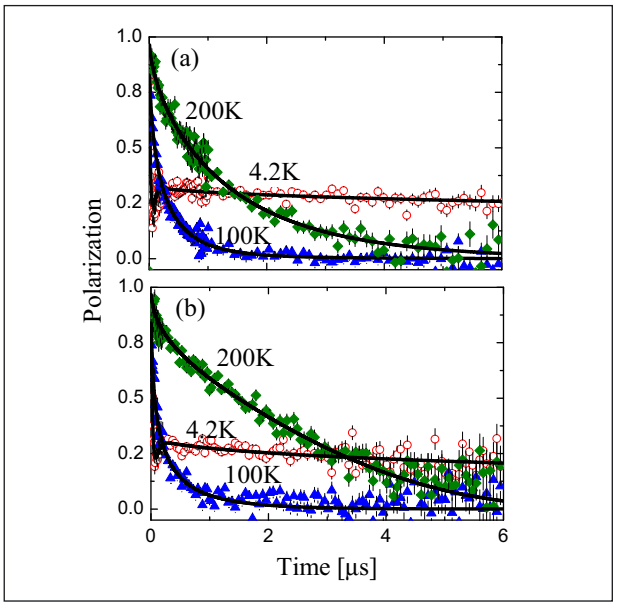

Figure 2: **Typical muon spin depolarization curves in the (a) bulk and (b) thick-film samples measured in ZF and at various temperatures. The lines are model fits.**

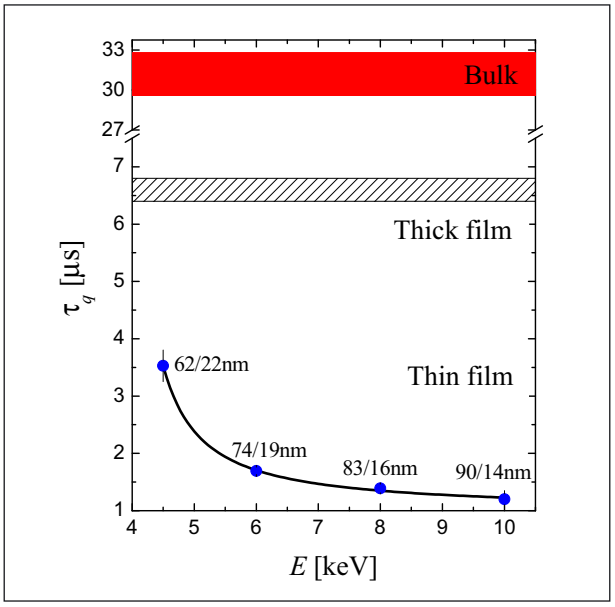

Figure 3: τ_q **as a function of E and corresponding mean/rms implantation depth. The shaded and hatched areas represent the values and uncertainty in the bulk and thick-film samples, respectively.**

Examples of muon spin depolarization curves measured in zero magnetic field (ZF) in the bulk and in thick-film samples are presented in Figure 2a and b, respectively. The measurements in both samples exhibit a striking qualitative similarity over the whole temperature range, indicating that the SMM properties of $TbPc_2$ are clearly maintained in thin films. However, we also find significant differences that point to different magnetic properties between bulk and films [6].

The muon spin depolarization measurements can be fitted to the expected behaviour to extract the size and time dependence of the $TbPc_2$ molecular spin. Detailed analysis of the results shows that the $TbPc_2$ relaxation of the magnetization in films is faster than in bulk crystalline powder. In particular, the molecular spin dynamics are significantly enhanced with proximity of the molecules to the $TbPc_2$/Au substrate interface. This is consistent with the disappearance of hysteresis in the monolayer observed with XMCD. As shown in Figure 3, at low temperature we find that the correlation time of the molecular spin dynamics, τ_q, increases gradually from 1.4 ± 0.1 μs near the interface to 6.6 ± 0.2 μs far from it (thick film). This unambiguously proves that other mechanisms than a possible direct interaction with the substrate are responsible for the disappearance of the hysteresis. It appears to be a characteristic effect of $TbPc_2$ SMMs and their strong sensitivity to their crystalline environment and magnetic dilution [7]. A possible explanation is that the depth-dependent packing alters the superexchange interaction between neighbouring Pc molecules and, in turn, the molecular spin dynamics. However, further experiments on isotropic or diamagnetic MPc_2 derivatives are necessary to characterize weak intermolecular interactions. We also find that the correlation time measured in films is much shorter than in the bulk, 31.2 ± 1.6 μs. Nevertheless, the time range of a few μs makes the $TbPc_2$ system a possible candidate for applications in quantum computation, even in thin films. Finally, these measurements provide an interesting possibility of controlling the spin dynamics of SMMs by controlling their packing, e.g. by a different choice of substrate or different deposition conditions. This may prove useful for tuning the correlation time of SMMs to match it with a specific potential application.

Full details of this study can be found in [6].

References

[1] D. Gatteschi et al., Angew. Chem., Int. Ed. **42** 268–297 (2003).
[2] A. Cornia et al., Chem. Soc. Rev. **40** 3076–3091 (2011).
[3] L. Margheriti et al., Adv. Mater. **22** 5488–5493 (2010).
[4] N. Ishikawa et al., J. Am. Chem. Soc. **125** 8694–8695 (2003).
[5] D.P. Di Vincenzo, Fortschr. Phys. **48** 771–783 (2000).
[6] A. Hofmann et al., ACS Nano **6** 8390–8396 (2012).
[7] L. Malavolti et al., J. Mat. Chem. C (2013) in press.

Links

[1] Laboratory for Muon Spin Spectroscopy (LMU): http://lmu.web.psi.ch/
[2] Laboratory for Molecular Magnetism (LAMM): http://www.unifi.it/LAMM/
[3] INSTM: http://www.instm.it/test_new_version/english_version/index.php

Directly-coupled ferromagnetism and ferroelectricity in Mn_2GeO_4

Jonathan White[1], Takashi Honda[2] and Tsuyoshi Kimura[2], Christof Niedermayer[1], Oksana Zaharko[1], Amy Poole[1], Bertrand Roessli[1], Michel Kenzelmann[3]

[1]*Laboratory for Neutron Scattering (LNS), PSI;* [2]*Osaka University, Japan;* [3]*Laboratory for Developments and Methods (LDM), PSI*

The coupling between magnetism and electricity is intrinsic to the fabric of our universe. A fascinating example of this interplay is found in magnetoelectric multiferroics, where spontaneous magnetic and electric-dipole orders can co-exist and be directly coupled. This remarkable behaviour is of great current interest since it may underpin future technologies. We have discovered a multiferroic state in a three-dimensional magnetic insulator that displays both coupled and spontaneous ferromagnetic and ferroelectric orders. This extremely rare state is an exciting manifestation of a new magnetoelectric coupling paradigm.

A ferroic material displays a spontaneous internal alignment of a property that may be switched by an appropriate conjugate field. Important examples here include ferromagnets, where aligned electron spins can be tuned by an applied magnetic field, and ferroelectrics, where electric-dipole order can be controlled using an electric field. Magnetoelectric multiferroics display simultaneous magnetic and ferroelectric orders that can each be controlled using either a single magnetic or electric field. This behaviour is not easy to find in solids, since the spontaneous alignment of both magnetic spins and electric dipoles below their ordering temperatures break different symmetries – in general, magnetic ordering breaks time reversal symmetry, while an electric-dipole ordering breaks space inversion symmetry. Magnetoelectric materials known to display a state with these simultaneously broken symmetries are rare and, in many of them, any coupling between the electric and magnetic properties is weak and indirect, because the magnetic and electric orders arise from chemically different parts of the host material [1].

Magnetic spirals generate ferroelectricity…

Nevertheless, over the last decade, a number of novel ideas have led to the discovery of strong magnetoelectric coupling effects in solids. One of the most successful has been the study of magnetic insulators that display complex magnetic interactions between localised moments, and which therefore display exotic ordered states such as magnetic spirals (Figure 1) [2–4]. These types of moment arrangements generate an electric polarisation because they break spatial inversion symmetry, i.e. there is no point in the crystal about which one can spatially invert the ordered moments and recover the same arrangement. So, since it is the spiral order that simultaneously breaks the necessary symmetries, there is an intrinsically strong and direct coupling between the magnetic and electric orders. This strong coupling is expected to underpin efficient future technologies in nanoscale switching, and data storage.

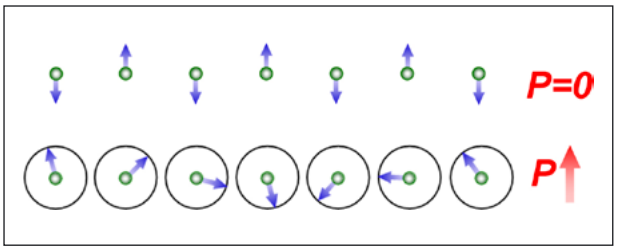

Figure 1: **Each chain of green atoms is symmetric around the central ion, and hence has spatial inversion symmetry. This is also true for a simple antiferromagnetic arrangement of localised magnetic moments (blue arrows) shown at the top. In contrast, the spiral moment arrangement (bottom) is *not* symmetric about any point in the crystal. Hence, a magnetoelectric coupling is permitted, and an electric polarisation, *P*, allowed.**

…though ferromagnetism is trickier…

At present, many solids have been discovered that display a symmetry-breaking magnetic transition into a spiral-ordered

state that directly generates the electric polarisation. However, their potential usefulness is limited since, on the macroscopic scale, spiral structures, such as that shown in Figure 1, display no net ferromagnetic component that may be used for switching.

…but finding them working together…

We have studied single crystals of the magnetic insulator Mn_2GeO_4 by both bulk method and neutron scattering techniques [5]. This material displays a three-dimensional arrangement of magnetic Mn^{2+} ions with many possible magnetic interactions, an observation that led to us to suspect that a symmetry-breaking spin arrangement, and hence multiferroic state, was waiting to be discovered. Indeed, on cooling below a magnetic transition at $T = 5.5$ K, bulk measurements (Figure 2) confirmed the onset of an electric polarisation along the crystal **c**-axis. Most surprisingly, within the same phase, we also discovered the existence of a ferromagnetic moment, also along the **c**-axis. These two macroscopic orders are both spontaneous and display similar coercive magnetic fields, implying that they originate from a singular underlying magnetic state. By neutron scattering experiments conducted at the Swiss Spallation Neutron Source, SINQ, at PSI, we discovered that the magnetism displays two co-existing components; an almost collinear order, which is canted and so causes the ferromagnetism, and an exotic spiral order, which generates the electric polarisation. What is remarkable in this material

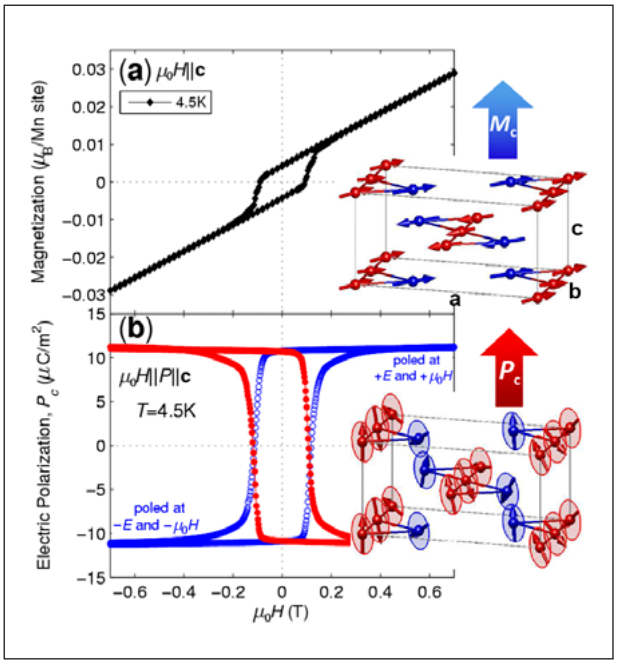

Figure 2: **(a) Measurement of ferromagnetic magnetisation along the c-axis, caused by collective moment canting of the collinear part of the magnetism (inset). (b) Measurement of ferroelectric polarisation along the c-axis, generated by an exotic spiral order.**

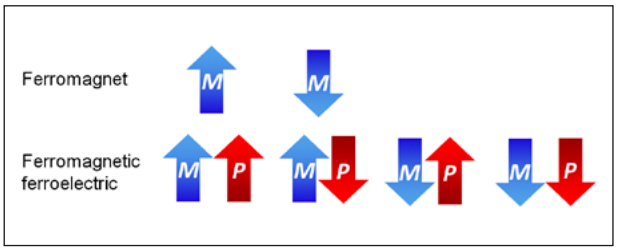

Figure 3: **Comparison between the functions of a simple 2-state ferromagnetic device (top) and those of a 4-state ferromagnetic ferroelectric device displaying the magnetoelectric coupling paradigm discovered in Mn_2GeO_4 (bottom).**

is that these two components superpose to form a single elaborate magnetic structure, which spontaneously breaks the necessary symmetries for magnetoelectric coupling. We speculate that weak spin-orbit interactions play a pivotal role by dictating how various domains of the collinear and spiral orders may superpose when forming a multiferroic domain state. It is these microscopic interactions that provide the new mechanism for the direct coupling of ferromagnetism and ferroelectricity observed for the first time in this material.

…may yield new technologies.

The magnetoelectric coupling in Mn_2GeO_4 is restricted to extremely low temperatures. However, the key result is the discovery of a functional paradigm in a real solid that may find use in efficient and high volume data storage applications. This is illustrated in Figure 3. Unlike a conventional ferromagnet, with typically two states, a single multiferroic sample of Mn_2GeO_4 contains four states, associated with the ferromagnetic and ferroelectric vectors that may each point up or down. Moreover, since these vectors are parallel in Mn_2GeO_4, it is much easier to engineer the reading and writing of such states in a device. The long-term goal is the discovery and synthesis of new materials that may display a similar magnetoelectric coupling paradigm as presented here, both with enhanced properties and at room temperature.

References

[1] N.A. Hill, J. Phys. Chem. B **104** 6694 (2000).
[2] S.-W. Cheong and M. Mostovoy, Nat. Mater. **6** 13 (2007).
[3] T. Kimura et al., Nature **426** 55–58 (2003).
[4] T. Arima, J. Phys. Soc. Jpn. **80** 052001 (2011).
[5] J.S. White et al., Phys. Rev. Lett. **108** 077204 (2012).

Link

[1] Laboratory for Neutron Scattering (LNS), PSI: http://www.psi.ch/lns/

Closing in on the Standard Model

Aldo Antognini, *Institute for Particle Physics (IPP), ETH Zurich;*
Urs Langenegger, Bernhard Lauss and Adrian Signer, *Laboratory for Particle Physics (LTP), PSI*

The discovery of a particle at CERN consistent with the long-sought Higgs boson is a major breakthrough in our understanding of fundamental particles and their interactions. However, the discovery of a Higgs candidate is just the beginning of an intensive programme to further test the Standard Model of particle physics and search for deviations to obtain clues as to what lies beyond. This is a worldwide programme that requires input from a large number of experiments, from the high-energy frontier covered at the Large Hadron Collider (LHC) to the high-intensity and high-precision frontier covered in low-energy measurements, where experiments at PSI play a vital role. Through international collaborations, PSI's Laboratory for Particle Physics (LTP) is involved in unique contributions in different parts of this programme and this article highlights three recent cases within this activity.

The Standard Model (SM) is arguably one of the most successful theories in physics. It explains and predicts a vast amount of experimental results and describes all non-gravitational interactions between fundamental particles, up to energy scales of several hundred GeV. However, despite its success, it is clear that the SM cannot be the ultimate theory. The SM can neither explain dark matter nor the dominance of matter over antimatter in the universe. It also fails to provide a solution to the so-called Strong CP problem, to mention just one of its shortcomings. Thus, particle physics faces the dilemma of having a theory that is, on the one hand, immensely successful, but on the other hand has obvious deficiencies.

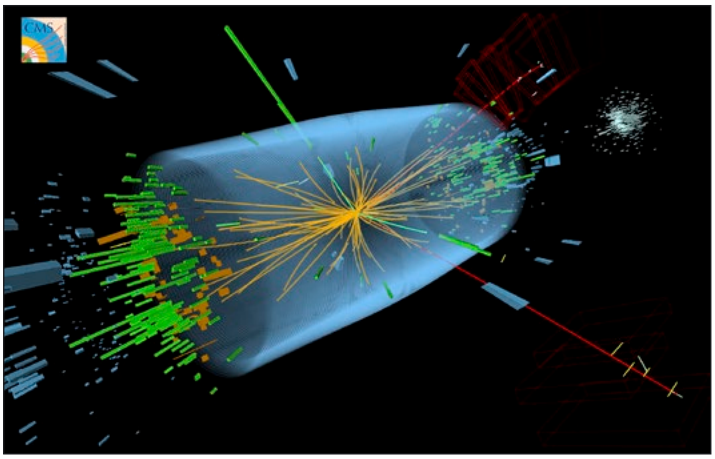

Figure 1: **3D display of the CMS experiment showing a proton-proton collision at a centre-of-mass energy of 8 TeV. The tracks of charged particles are shown as golden lines, and energy deposits in the calorimeters are illustrated as golden and green towers. The event is consistent with a Higgs decay into two Z bosons, with one Z decaying into a pair of electrons (green lines and green towers) and the other into a pair of muons (red lines).**

In order to obtain clues as to how to extend the SM to a more complete theory, there is an extensive worldwide programme underway whereby the SM is being investigated at an ever more detailed level. With the recent discovery at CERN of a Higgs candidate, these tests have entered a new era. The properties of this new particle have to be determined and compared with SM predictions. Of course, tests of this nature are not constrained to the Higgs particle, but are carried out for all parts of the SM. New physics can manifest itself directly, through the production of a new particle, or indirectly, by affecting low-energy observables through virtual contributions from quantum loops. Indirect effects are somewhat subtler, as they do not always provide unambiguous information about the nature of new physics. On the other hand, they are sensitive to energy scales well beyond the reach of any collider. Direct and indirect tests must not be considered as independent, as they go hand in hand and complement each other in the attempt to obtain maximal information.

This article describes three cases in more detail. In the first, a new particle (the Higgs candidate) has been produced and is now being investigated. In the second, a detailed test of the proton structure has found full agreement with the SM. Finally, in the third case, a careful study of muonic hydrogen has found some tension between the expected and measured results, leading to the question as to whether this is due to new physics.

The Higgs boson: Found at last?

High-energy physicists have spent nearly half a century searching for the final missing piece of the SM, the Higgs boson. In 2012, the ATLAS and CMS collaborations at the LHC at CERN discovered a particle that fits the description and could very well be the SM Higgs boson [1, 2]. This discovery is the result of the meticulous and persistent hard work of many thousands of people over more than 20 years. The CMS group at PSI has contributed key ingredients to this success from the formation of the CMS collaboration in the 1990s.

The Higgs boson is an unstable particle and decays into (quasi-)stable particles that can be measured. Several decay channels have contributed to the discovery – the best sensitivity is provided by the two decay modes with the best resolution: (1) the two-photon final state and (2) the decay into 2 Z bosons with two pairs of charged leptons (electrons or muons). For the measurement of the two-photon final state, the electromagnetic calorimeter is essential. The research and development of its innovative photon detectors at PSI is a crucial component in this successful measurement, and PSI physicists have designed, developed, and largely constructed the CMS pixel detector. The pixel detector is the innermost component of the CMS experiment and is used for the reconstruction of charged particle trajectories and for the precise determination of the proton-proton collision vertices. Over the past two years, the LHC has collided protons with protons at ever-increasing rates and centre-of-mass energies. On average, more than 20 proton-proton collisions ("pile-up") occur per bunch crossing. The very high granularity of the pixel detector is essential for efficiently finding charged particle trajectories in these high pile-up conditions. The CMS experiment and the pixel detector have coped very well with these challenging conditions, thanks to the relentless effort of PSI group members in pixel detector operation and calibration. The PSI group has directly contributed to the search for the Higgs boson through the primary vertex reconstruction. For the $H \rightarrow Z Z$ decay (decay mode (2)), the pixel data ensure that the four charged leptons emerge from the same space point and, therefore, suppress background events. Other analyses pursued at PSI include the search for the rare decay $B_s \rightarrow \mu^+ \mu^-$ [3] and the lifetime of the Λ_b baryon [4].

In February 2013, the LHC shut down for about two years, to undergo maintenance and improvements. This will allow the centre-of-mass energy of the proton-proton collisions to be raised to 13 TeV and the luminosity to be increased by a factor two, after it starts up again in 2015. Depending on the LHC settings, the pile-up may increase by a factor of two above the current level. Since this would be considerably above the original specifications, for the past two years the PSI group has been leading the effort to build a replacement detector [5]. This new detector will have an additional layer and an innermost layer even closer to the LHC beam pipe than the current one. At the same time, it will consist of less material. The new detector will provide better and more efficient measurements of charged particle trajectories. These improvements are essential for investigating whether the particle discovered is really the SM Higgs boson. To address this question, its production, decay characteristics, and self-coupling strength need to be measured precisely. There is a joint effort of PSI theoretical and experimental physicists to contribute to these investigations with phenomenological studies.

Muon capture on the proton confirms Standard Model calculation

The measurement of the negative muon capture rate on the proton, λ_c ($\mu^- + p \rightarrow \nu_\mu + n$) = (714.9 ± 5.4 ± 5.1) s^{-1}, by the MuCap Collaboration allowed the first precise and unambiguous determination of the proton's weak pseudo-scalar form factor, $g_p = 8.06 \pm 0.55$ [6]. This resolved a very unclear situation with conflicting experimental results and provides an excellent test of SM calculations of this process [7].

While weak processes among fundamental leptons are described via a vector–axial-vector (V-A) interaction, the impact of the weak force is modified in the presence of strong interactions. g_p parameterizes this modification of the weak axial proton current. Chiral perturbation theory allows us to calculate this fundamental proton property. The understanding of the weak axial current is closely connected to ideas of spontaneous breaking of chiral symmetry and the generation of

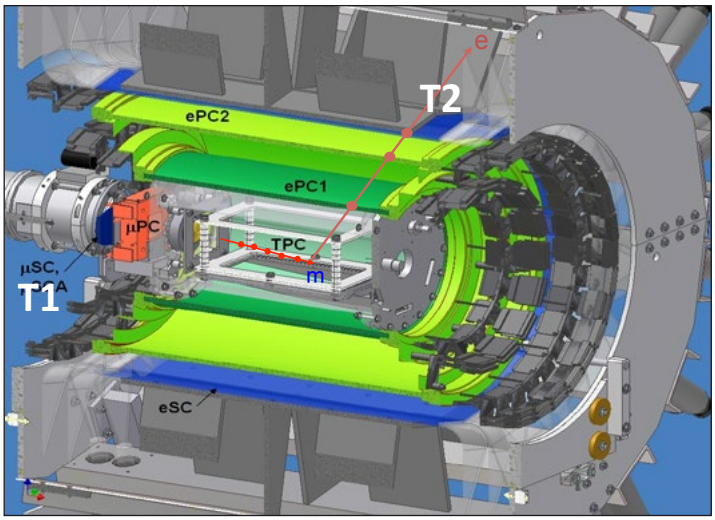

Figure 2: **3D sketch of the MuCap experiment showing the incoming muon stop in the central TPC detector and the decay electron being tracked in the surrounding barrel detectors. The lifetime of each muon is measured by the time difference between muon entrance (T1) and decay electron track (T2).**

Figure 3: **Assembly of the time projection chamber developed by the PSI Detector Group.**

hadron masses, ideas which led to the award of the 2008 Nobel Prize in Physics to Yoichiro Nambu.

As it is fundamental to weak interactions, the determination of g_p was one of the first experimental goals at PSI. The MuCap experiment now aims at comparing the lifetimes, τ, of μ^- and μ^+ in hydrogen. The capture rate follows from this as the difference of the inverted lifetimes, $(1/\tau_{\mu^+} - 1/\tau_{\mu^-}) = \lambda_c$, as the μ^+ do not interact with the surrounding atoms. However, the μ^- in hydrogen are subject to many competing atomic and molecular processes. To reduce their influence significantly, experimental conditions have to be carefully selected and controlled. Central to the experiment's apparatus (Figure 2) and its success was the Time Projection Chamber (TPC, Figure 3), which served to track the incoming muons and detect in three dimensions the positions where they stopped. Following pioneering studies by the Petersburg Nuclear Physics Institute (PNPI), this unique detector was developed at PSI. The exceptional feature of this TPC, which works as an active target, is that it operates in ultrapure hydrogen, as detector gas, at room temperature and 10 bar pressure. New detector construction materials and techniques were found in order to operate under ultraclean conditions, i.e. any other gas component than hydrogen was at the part-per-billion level. These ultraclean conditions were maintained over weeks, using a special continuous purification system developed by the collaborators from PNPI. The TPC defined an unambiguous muon stop in hydrogen, with the surrounding wire chambers tracking the decay electron back to its muon origin. The decay time was then determined in the outermost layer – a large scintillation detector constructed by the US collaborators.

The analysis of the more than 10^{10} observed muon decays involved much dedicated work on various systematic effects and led to PhD theses at the Universities of Washington, Illinois and Berkeley. Data were blinded, to prevent psychological bias during the analysis, and only after common agreement on the analysis and systematic errors was the envelope with the unknown blinding factor opened. The final MuCap result on g_p is so precise that the original calculation had to include radiative corrections for comparison and the new value will enter any new textbook on weak interactions.

The proton radius puzzle

There are three ways of determining the proton charge radius. The historical one is by electron-proton elastic scattering. The second method is from high-precision spectroscopy in hydrogen (H), i.e. by measuring atomic transition frequencies in H. A more precise determination of the radius can be achieved by a third method: laser spectroscopy of muonic hydrogen (μp), an atom formed by a negative muon and a proton. The extended nature of the proton, being a composite system of quarks and gluons, causes a shift of the energy levels in both H and μp. Thus, the measured transition frequencies in H and μp depend on the proton size. However, because the muon mass is about 200 times larger than the electron mass, the energy levels in μp are more strongly affected by the finite size (structure) of the proton than the H energy levels.

In 2010, the CREMA Collaboration measured a transition frequency between the 2S and 2P states in μp [8]. The resulting proton radius was an order of magnitude more precise, but with a 5σ variance from the values extracted from H spectroscopy and electron-proton scattering. This discrepancy triggered lively discussion concerning the accuracy of the various experiments, bound-state QED, the proton structure, the Rydberg constant, and even the possibilities of new physics. This year, the analysis of a second 2S-2P transition was completed [9]. The resulting proton radius is in perfect agreement with the previous μp value and thus reinforces the so-called 'proton radius puzzle'.

The principle of the μp Lamb-shift experiment is to form μp in the 2S state and then measure 2S-2P energy splitting by means of laser spectroscopy, using the set-up illustrated in Figure 4: Negative muons from the PSI proton accelerator are stopped in hydrogen. A 5 ns laser pulse with a wavelength tuneable from 5.5 to 6 μm illuminates the target. On-resonance light induces 2S$\rightarrow$2P transitions, which are immediately followed by 2P$\rightarrow$1S de-excitation via 1.9 keV X-ray emission, and a resonance curve is obtained by measuring the number of X-rays in time-coincidence with the laser pulse.

Two quantities are determined from the two measured transitions. Summing the two muonic measurements led to an assessment of the "pure" 2S-2P Lamb shift and, from that, an rms charge radius of 0.84087(39) fm was deduced. Subtracting the two transition frequencies gave the 2S-hyperfine splitting and, from that, a Zemach radius of 1.082(37) fm was

determined, in agreement with the values extracted from H and scattering experiments. These radii play a crucial role in the understanding of the atomic hydrogen spectrum (bound-state QED) and provide information to test non-perturbative aspects of quantum chromodynamics.

The new results fuel the debate as to whether the discrepancies observed can be explained by an incomplete understanding of the systematic errors that are inherent to all measurements, or whether they are due to new physics. The proton radius value from μp could deviate from the values from electron-proton scattering and H spectroscopy if the muon-proton interaction differed from the electron-proton interaction. There are models which could explain this discrepancy without conflicting with other experimental observations, but the window for such "new physics" is small.

These models also predict a significant deviation for muonic helium. Therefore, the next experiment proposed by the CREMA Collaboration is the measurement of 2S-2P energy splitting in muonic helium. In addition, a muon-proton scattering experiment is on-going at PSI (MUSE Collaboration) and new electron-proton and H spectroscopy experiments are underway.

References

[1] S. Chatrchyan et al., Phys. Lett. **716** 30–61 (2012).
[2] G. Aad et al., Phys. Lett. **716** 1–29 (2012).
[3] S. Chatrchyan et al., JHEP **1204** 033 (2012).
[4] S. Chatrchyan et al., CMS-BPH-11-013.
[5] S. Chatrchyan et al., CERN-LHCC-2012-016.
[6] V.A. Andreev et al., Phys. Rev. Lett. **110** 012504 (2013).
[7] P. Kammel and K. Kubodera, Annu. Rev. Nucl. Part. Sci. **60** 327–353 (2010).
[8] R. Pohl et al., Nature **466** 213–216 (2010).
[9] A. Antognini et al., Science **339** 417–420 (2013).

Links

[1] CMS: http://cms.web.cern.ch
[2] Muon Capture (MuCap): http://muon.npl.washington.edu/exp/MuCap/
[3] Proton radius (CREMA): https://muhy.web.psi.ch/wiki/index.php

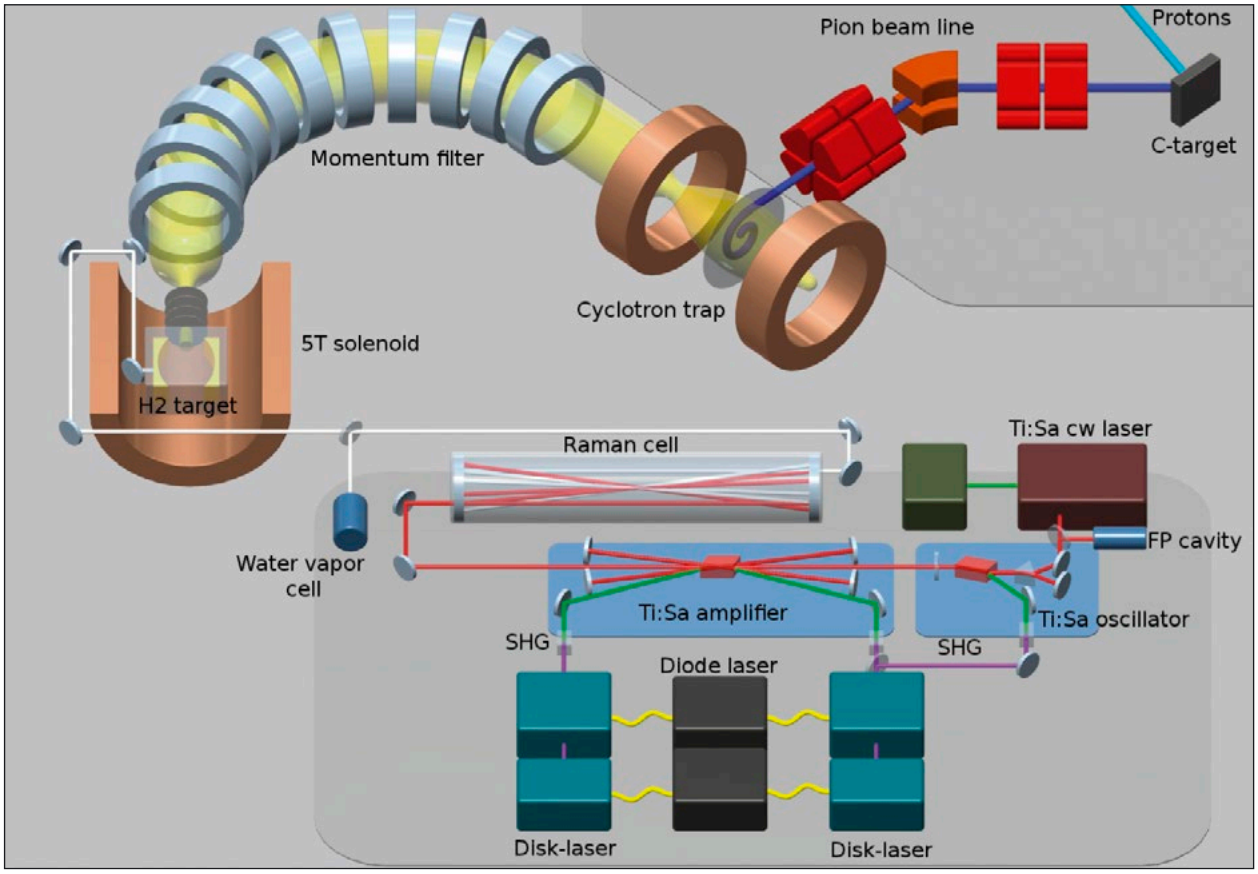

Figure 4: **Experimental apparatus: Negative pions are transported to the cyclotron trap, where they decay into MeV-energy muons, which are decelerated by a thin foil placed at the trap centre. The resulting keV-energy muons leave the trap and follow a toroidal magnetic field of 0.15 T (acting as a momentum filter) before entering a 5 T solenoid, where the hydrogen target is placed. A muon entrance detector provides a signal that triggers the laser system. About 0.9 μs later, the formed μp is irradiated by the laser pulse to induce the 2S-2P transition.**

Enhancing the infrared light excitation efficiency of metallic nanotips via surface-plasmon resonance

S. Tsujino, A. Mustonen, P. Helfenstein, V. A. Guzenko, C. Spreu and J. Gobrecht, *Laboratory for Micro- and Nanotechnology (LMN)*, P. Beaud *(FEMTO)* and H.-H. Braun *(SwissFEL), all PSI;* T. Feurer, *University of Bern, Switzerland;* H.-W. Fink, *University of Zürich, Switzerland*

Ultrafast electron bunches can be generated from metallic field emitter arrays by combining the near-infrared laser-induced field emission from millions of metallic nanotips. However, the small fraction of the tip area limits the maximum bunch charge. To beat this limit, a novel light-tip coupling method using surface-plasmon resonance was developed. In combination with stacked double-gate structures, the realization of a high-current and high-brightness cathode that can out-perform the state-of-the-art photocathode appears to be possible, which may improve the performance of X-ray free-electron lasers, such as SwissFEL, for shorter wavelength and higher X-ray power.

Can we produce a cathode that can out-perform the state-of-the-art photocathode based on the field emitter cathode? This is an important and urgent question that can have a large impact on future X-ray free-electron lasers, such as SwissFEL, that normally employ photocathodes. Although field emitters are the highest brightness cathodes that have been successfully applied in, for example, high-resolution microscopy, it has proven to be highly challenging to harness this property to create a high-current and high-brightness cathode.

Combining the high-brightness electron beamlets from thousands to millions of nanotips, field emitter arrays (FEAs, see Figure 1) generate high current. Ultrafast electron pulses can be generated by exciting the metallic nanotips by near-infrared ultrafast laser pulses with the help of optical electric field enhancement at the tip apexes [1]: Generation of short electron bunches with up to 5 pC bunch charge was demonstrated recently using an array of 1.2×10^5 metallic nanotips with ~5 nm apex radius of curvature and 50 fs near-infrared laser pulses. However, the array quantum efficiency was low, because of the small fraction of the emission area – of the order of 10^{-5}. An approach to further increase the bunch charge is to increase the tip density by reducing the array pitch. However, concomitant reduction of the gate-aperture diameters below the wavelength of the near-infrared excitation laser pulses is a critical limitation, as transmission through the holes becomes prohibitively small.

In work reported in [2], we developed a novel method to beat this limit and drastically enhance the light-tip coupling in sub-micron-pitch arrays by combining the surface-plasmon-polariton (SPP) resonance of the gate electrode (Figure 2).

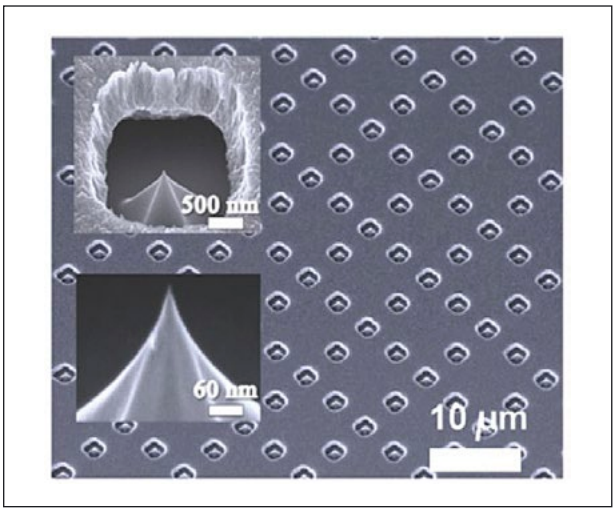

Figure 1: **SEM image of a single-gate molybdenum emitter array with ~5 µm apex radius of curvature and 5 µm array pitch [1].**

This demonstrated that the extraordinary optical transmission through the sub-wavelength size gate apertures is conserved in the presence of the molybdenum emitters and, at the same time, a large field enhancement at the emitter tip apex is achieved when the laser excitation is normal to the FEA, an important characteristic for accelerator applications. Analysis predicts that near-infrared laser pulses with a pulse energy of ~10^{-4} J, exciting a sub-micron-pitch FEA of 1 mm diameter, can generate 200 pC electron bunches with 10 ps duration, as the baseline cathode performance specification of the SwissFEL X-ray free-electron laser requires.

The estimated array quantum efficiency reaches a value of ~10^{-6}, although this is a factor of 60 lower than the quantum

efficiency of UV-laser-excited photocathodes (6×10^{-5} for copper). In contrast, the use of nanotip arrays here eliminates the necessity to generate UV harmonics of the driving laser, thereby simplifying the optical setup and increasing the overall efficiency by the reciprocal of the UV harmonic generation efficiency.

To realize a low intrinsic emittance and high beam brightness field emission cathode, it is crucial to reduce the beam divergence of the individual beamlet by orders of magnitude. Recently published experiments [3] showed that this is possible by a double-gate structure, as shown in Figure 3. With the addition of the on-chip beam collimation structure for an individual beamlet of a 4×10^4-tip FEA beam, it demonstrated the reduction of the transverse electron velocity spread down to ~2×10^{-4} c_0 (where c_0 is the speed of light) with a minimal reduction of the emission current; this corresponds to an intrinsic emittance below 0.1 mm-mrad for a 1 mm-diameter FEA, and more than a factor 2 improvement compared with state-of-the-art photocathodes.

Based on these results, researchers are now studying the SPP-enhanced laser-induced field emission from sub-micron array-pitch double-gate devices to produce a field emission cathode that can out-perform a state-of-the-art photocathode. In the coming years, we expect to see a number of novel applications of FEAs, ranging from THz-TWTs to compact FELs, taking advantage of recent advancements in these high-current and high-brightness beam generation technologies.

The authors gratefully acknowledge the technical help of B. Haas, J. Lehmann and A. Lücke during FEA fabrication. This work was performed as a part of the SwissFEL Project.

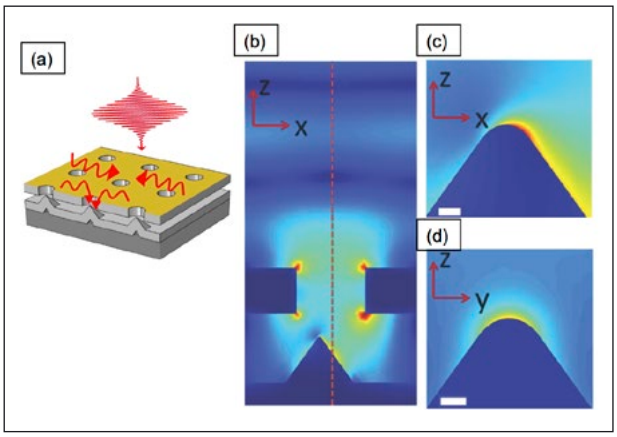

Figure 2: **(a) Excitation of the surface-plasmon-polariton (SPP) resonance of a 750 nm-pitch single-gate nanotip array by normal incidence near-infrared ultrafast laser pulses; (b) Optical electric field distribution in an emitter cavity. Resonant SPP excitation enhances the transmission of the 900 nm photons through the sub-wavelength gate aperture. Asymmetric light-tip coupling creates an enhanced field at the tip, as shown in (c) and (d), displaying close-ups of the field near the tip (scale bars are 10 nm) in the x-z and y-z planes, respectively [2].**

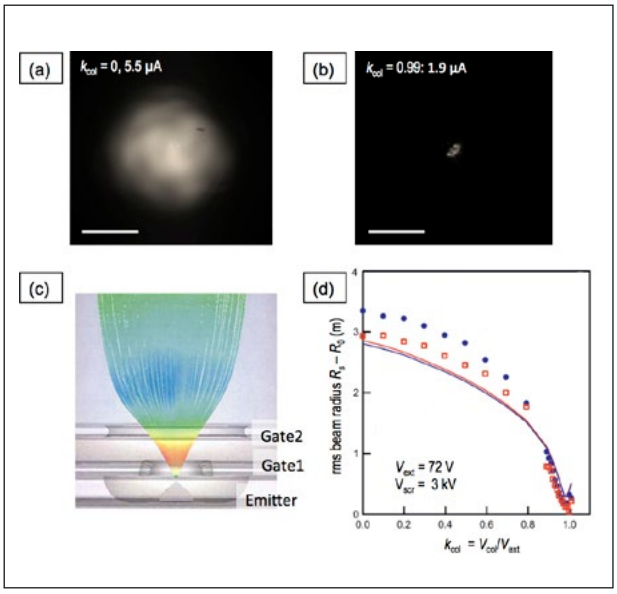

Figure 3: **Field emission beam image of a 4×10^4-tip double-gate FEA with an array diameter of 2.26 mm, measured with the electron extraction potential V_{ext} of 72 V: (a) No collimation potential with V_{col} and k_{col} (=V_{col}/V_{ext}) equal to zero, with a total emission current of 5.5 µA; (b) Maximally collimated beam at k_{col} of 0.99, with an emission current of 1.9 µA (the lines represent 20 mm on the screen); (c) Simulated electron emission; (d) Comparison of the measured rms beam radius R_s (blue and red points) subtracted by the rms radius R_0 of the FEA and the calculated rms single-emitter beam radius [3].**

References

[1] A. Mustonen, P. Beaud, E. Kirk, T. Feurer and S. Tsujino, *Five picocoulomb electron bunch generation by ultrafast laser-induced field emission from metallic nano-tip arrays*, Applied Physics Letters **99** 103504 (2011).

[2] A. Mustonen, P. Beaud, E. Kirk, T. Feurer and S. Tsujino, *Efficient light coupling for optically excited high-density metallic nanotip arrays*, Scientific Reports **2** 915 (2012).

[3] P. Helfenstein, V. A. Guzenko, H.-W. Fink and S. Tsujino, *Electron beam collimation with a 40,000 tip metallic double-gate field emitter array and in-situ control of nanotip sharpness distribution*, Journal of Applied Physics **113** 043306 (2013).

Links

1 Laboratory for Micro- and Nanotechnology (LMN): http://www.psi.ch/lmn/

2 Femtosecond X-Ray Group (FEMTO): http://femto.web.psi.ch

3 SwissFEL: http://www.psi.ch/swissfel/

Strained silicon nanowires making transitors faster

Renato A. Minamisawa and Hans Sigg, *Laboratory for Micro- and Nanotechnology (LMN), PSI*
Martin J. Süess, *Electron Microscopy (EMEZ) and Nanometallurgy, ETH Zurich, Switzerland*

Miniaturization of the transistors in the integrated circuits of microchips follows a given pattern which is called "scaling" and is the driving force behind ever more powerful electronics, which make our everyday lives more comfortable and labour more productive. But as we enter the nanometre regime, the continuous implementation of this powerful shrinking concept is impeded by physical constrains; new approaches are required, such as using stressed silicon and germanium with improved electronic properties. In this context, a research group composed of members of PSI's Laboratory for Micro- and Nanotechnology (LMN) and ETH Zurich has developed and demonstrated a promising method to maximally stress silicon nanowires compatible with scaling laws. This works on the nanometre, as well as on the micrometre, scale, where it offers new applications in photonics. On top of that, the method can be used as a platform for the investigation of strained materials.

By steadily downscaling the physical dimensions of complementary metal-oxide semiconductor (CMOS) field-effect transistors (FET) based on silicon (Si), the performance of state-of-the-art integrated circuits (IC), such as the central processor units (CPUs) in computers, has improved steadily. Nevertheless, intense research is going on to further improve the speed of processors and make them less power-hungry.

An alternative approach to improving device performance is mobility enhancement by imposing strain, which increases the speed and reduces the power consumption of FETs. This approach is particularly attractive because the gain obtained adds to any benefit provided by traditionally applied scaling [1]. This gain is achieved through strain-induced manipulation of the band structure, which modifies the effective masses and phonon scattering within the transport channel and thus the carriers' mobility.

Strain has also been proposed as a means of fabricating Si-integrable Ge lasers for high-performance optical interconnects [2]. The reported strain levels of 0.25%, corresponding to ca. 0.3 GPa, were, however, considerably below those required to make Ge a direct bandgap semiconductor. In such systems, lasing is very inefficient, as follows from experiments we have performed at the infrared beamline of the SLS [3].

Conventionally, strain is induced in state-of-the-art CMOS devices using stressor layers. This limits tensile stress to ~2 GPa and/or complicates integration in scaled devices when the required stressor thickness exceeds the lateral dimensions of the transistor gate. Stressor layers would also hinder fabrication of an efficient optical cavity, which on top of the insufficiently converted bandgap, obstructs the making of a suitable Ge-based laser.

In contrast, our new design concept enables record strain levels to be induced in semiconductor materials, such as Si and Ge, and is free of external actuators and stressor layers. The process is based on pure elastic deformation, is compatible with fabrication boundaries in microelectronics, is adaptable to different length scales, and enables precise control over the induced strain. Our PSI/ETH consortium has demonstrated uniform 7.6 GPa tensile stress in Si nanowires, which is the highest level reported to date, using an integrated top-down approach [4].

Method

Silicon-on-insulator (SOI) nanowires of 13 nm diameter were biaxially tensile stressed with 1.3 GPa and used as the starting substrate. Constricted structures were patterned using e-beam lithography and reactive ion etching (RIE) followed by wet chemical etching of the buried oxide (BOX), creating suspended and constricted structures in a uniaxial stress state (see Figure 1). As the layer thicknesses and the force in the structure remain constant, the stress is inversely proportional to the cross-sectional area, as shown in Figure 2(a), such that the stress accumulates at the constricted region. The stress/strain ratio in the constriction can, therefore, be finely tuned by varying the dimensions of the constriction and pads, as shown in Figure 2(b). As the strain concentration

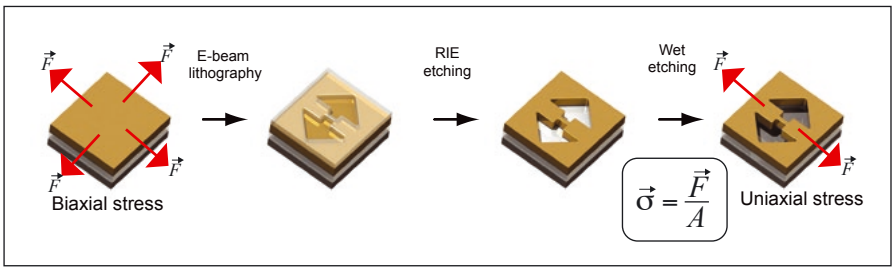

Figure1: **Schematics of the process flow used to fabricate strained nanostructures: After patterning and releasing, the suspended structures are in a uniaxial stress state. Since the stress is inversely proportional to the cross-sectional area of the film, the stress accumulates in the constriction.**

depends solely on relative dimensions, such as the ratio between the width of constriction and width of pad, the method can be scaled to micrometres or nanometres.

Demonstration

The strain enhancement obtained, relative to the strain in the starting substrate ($\varepsilon/\varepsilon_0$), versus the cross-section ratio for bridges with different 'a' and 'b' dimensions and with different length ratios is shown in Figure 2(c). Strain was measured using μ-Raman spectroscopy. The strain achieved was up to six times higher than the starting strain (ε_0) and was limited only by the fracture strain of the bridges at strain ~4.5 %. We found this limit to be independent of the nanowire diameter. The experimental data closely matches the prediction of constant force, as shown by the curved lines in Figure 2(c). The excellent match with finite-element calculations (FEM), using the known elastic constants of the materials involved, provides strong support for the generality of our approach.

Outlook

The investigations described above have demonstrated that our strain concept is scalable to different materials and length scales, and thus can be implemented for a vast number of applications. For example, besides the application of strained silicon nanowires in transistors, this approach could very well be applied to micrometre-thick strained Ge layers for photonic applications and will offer many options for investigation of the fundamental properties of strained materials, for example using PSI's large facilities. However, before we follow up these fundamental investigations, we are trying to find out if transistors with such ultra-strained nanowire-channels are indeed able to outperform state-of-the-art systems in speed and energy savings. This investigation is being performed in collaboration with other partners, including the Forschungszentrum Jülich, Germany.

References

[1] M. Ieong, B. Doris, J. Kedzierski, K. Rim and M. Yang, *Silicon device scaling to the sub-10 nm regime*, Science **306** 2057–2060 (2004).

[2] J. Liu et al, *Ge-on-Si laser operating at room temperature*, Optics Letters **35** 679–681 (2010).

[3] C. Lee et al., *Direct-Gap Gain and Optical Absorption in Germanium*, Phys. Rev. Lett. **109** 057402 (2012).

[4] R.A. Minamisawa, M.J. Süess et al., *Top-down fabricated silicon nanowires under tensile elastic strain up to 4.5%*, Nature Comm. **3** 1096 (2012).

Links

[1] Nanospectroscopy LMN PSI: http://www.psi.ch/lmn/silicon-nanowires

[2] Electron Microscopy ETH Zurich: http://www.emez.ethz.ch/

[3] Nanometallurgy ETH Zurich: http://www.met.mat.ethz.ch/research/index

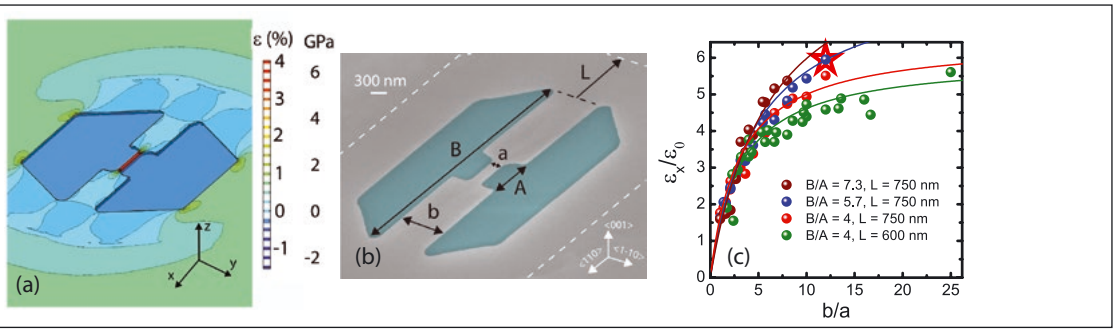

Figure 2: **Strain enhancement achieved in suspended and constricted bridges fabricated from 13 nm-thick strained Si layers on oxide (SOI): (a) FEM simulation of the strain in a structure similar to that shown in (b); (b) SEM micrograph of an under-etched bridge, annotated are the main parameters used to control the strain; (c) The length and width of constriction and pad controls the enhancement $\varepsilon/\varepsilon_0$. The star marks the highest achieved longitudinal stress of 7.6 GPa. This is equivalent to about 6× enhancement with respect to the initial stress, representing a world record in strain for top-down fabricated nanowires.**

G protein-coupled receptors (GPCRs): How are signals transmitted into a cell?

Xavier Deupi and Gebhard F.X. Schertler, *Laboratory of Biomolecular Research (LBR), PSI*

The Nobel Prize in Chemistry for 2012 was awarded to Robert J. Lefkowitz and Brian K. Kobilka for their groundbreaking discoveries that reveal the inner workings of G protein-coupled receptors (GPCRs), a family of cell-surface proteins of key importance in human physiology. Researchers at the Laboratory of Biomolecular Research use structural, molecular and cellular biology to study the molecular basis of the activation mechanisms of GPCRs and obtain a global picture of their function. This knowledge will allow the discovery of new and better drugs to treat, for instance, neurological disorders and cancer.

Relevance of G protein-coupled receptors

GPRCs are a large family of proteins embedded in the cell membrane that serve as the communication interface with the external environment. These receptors are able to detect a wide variety of sensory signals of external origin, such as photons, odours or pheromones, and endogenous signals including neurotransmitters and hormones. Once a GPCR binds its specific ligand, it becomes activated and transmits the information to the cell by activating specific cellular signaling pathways (Figure 1).

This way, GPCRs allow the coordinated activity between cells and tissues in higher organisms and, moreover, provide an important link to our environment as the principal receptors for our senses of vision, smell and taste. GPCRs are thus essential in cell physiology, and their malfunction is commonly translated into pathological outcomes, such as asthma, migraines, cardiac malfunction, neuropsychiatric conditions or cancer. As a result, GPCRs constitute one of the most important pharmaceutical targets, with around 30% of prescribed drugs acting through this family of proteins.

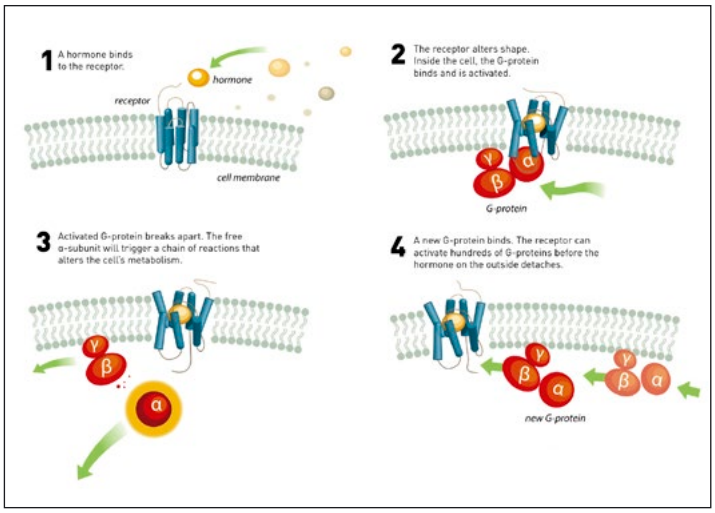

Figure 1: **When a ligand (e.g. a hormone, olfactory or taste molecule, or a pharmaceutical drug) couples with a GPCR on the cell surface, a chain of reactions inside the cell is triggered.**
(Figure adapted from, and courtesy of, http://www.nobelprize.org)

GPCR research at the Laboratory of Biomolecular Research

Despite the importance of GPCRs in human physiology, our understanding of the molecular mechanisms of GPCR activation is still hampered by the lack of enough structural information. Gebhard Schertler, Head of the Department of Biology and Chemistry at PSI and Prof. for Structural Biology at ETH, has made major contributions to this field. For instance, he deduced the first structural template for GPCRs from 3D electron microscopy data, and solved the first structure of a recombinant GPCR (rhodopsin), of the β2 adrenergic receptor (together with Brian Kobilka, at Stanford University), which was the first solved structure of a ligand-binding GPCR, and of the β1 adrenergic receptor (in collaboration with Chris Tate, at the MRC-LMB in Cambridge), where he obtained the first structures of the receptor bound to full and partial agonists. Together with Jörg Standfuss (Laboratory of Biomolecular Research, PSI), he has made major contributions to understanding the vision process at the molecular level by solving the structures of a mammalian rhodopsin in fully activated states [1].

The last six years have been a very exciting time in the field of GPCR structural biology, when more than 70 structures have

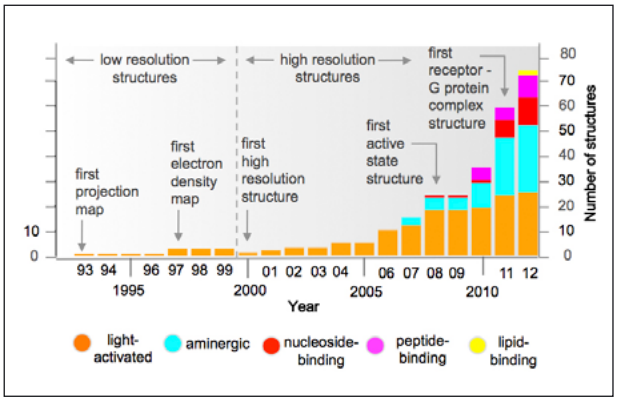

Figure 2: **The combination of a number of innovative protein engineering techniques and crystallography methods [2] has resulted in an almost exponential growth in the number of solved GPCR structures. As a result, more than 70 crystal structures of 15 different GPCRs from 5 major families have been determined during the past 12 years.**

been determined, providing unprecedented insights into the structural and functional diversity of this protein family (Figure 2).

The availability of this increasing amount of structural information has allowed us to perform a systematic bioinformatics analysis to analyze all known structures and reveal key similarities and differences among diverse GPCRs. In collaboration with researchers at the MRC-Laboratory of Molecular Biology in Cambridge, we have identified a structural scaffold that is present in all known GPCR structures [3] (Figure 3). While there is some degree of sequence variability in this scaffold, it forms a consensus network of interactions that "shapes" the protein, allowing diverse sequences to adopt a similar structure, thereby contributing to the evolutionary success of the GPCR fold. In addition to increasing our basic knowledge of GPCR structure and function, these findings will be valuable for engineering GPCRs with specific properties, e.g. increased stability, a key property for successful X-ray crystallography on GPCRs.

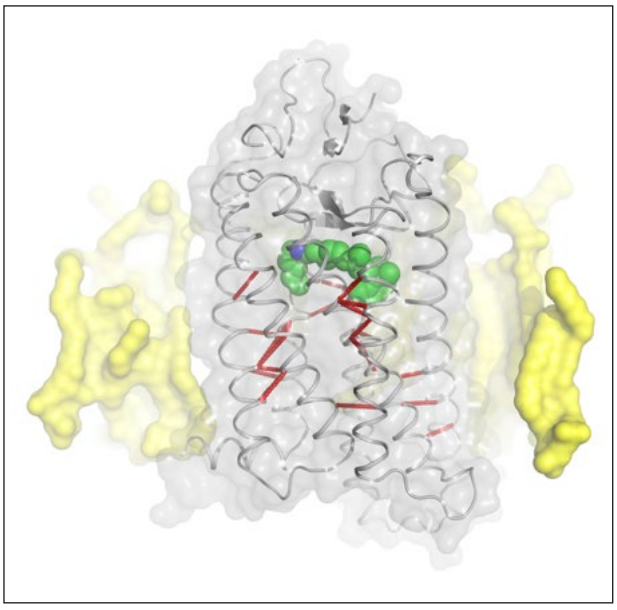

Figure 3: **We have identified a network of interactions (red lines) present in all known GPCR structures that is important for the structural stability of these proteins. The discovery of this conserved network allows a better understanding of the essential features of GPCRs. The network is represented here in the structure of rhodopsin, a GPCR present in our retinas that allows us to see in dim-light conditions.**

In addition, the analysis of the structures of the different receptor-ligand complexes has enabled us to identify a consensus "ligand-binding cradle", formed by non-conserved residues but present in nearly all GPCR structures. This information increases our understanding of the molecular basis of the affinity and selectivity of drugs to their receptors.

Given their relevance in human physiology and pathology, there is an enormous potential for the development of new drugs to treat neurological disorders, inflammatory diseases, cancer and metabolic imbalances. Thus, elucidating the structure of GPCRs and understanding the molecular mechanism of receptor activation is not only of fundamental biological interest, but also holds great potential for enhancing human health.

References

[1] X. Deupi, P.C. Edwards, A. Singhal, B. Nickle, D.D. Oprian, G.F.X. Schertler and J. Standfuss, *Stabilized G protein binding site in the structure of constitutively active metarhodopsin-II*, PNAS **109**(1) 119–124 (2012).

[2] F. Brueckner, C.L. Piscitelli, C.J. Tsai, J. Standfuss, X. Deupi and G.F.X. Schertler, *Structure of β-Adrenergic Receptors*, Methods Enzymol. **520** 117–151 (2013).

[3] A.J. Venkatakrishnan, X. Deupi, G. Lebon, C.G. Tate, G.F. Schertler and M.M. Babu, *Molecular signatures of G protein-coupled receptors*, Nature **494** 185–194 (2013).

Link

[1] Laboratory of Biomolecular Research (LBR): http://www.psi.ch/lbr/

Voltage-gated sodium channels visualized by cryo-electron microscopy

Ching-Ju Tsai, Gebhard Schertler and Xiao-Dan Li, *Laboratory of Biomolecular Research (LBR), PSI;*
Kazutoshi Tani, Katsumasa Irie and Yoshinori Fujiyoshi, *Cellular and Structural Physiology Institute (CeSPI), Nagoya University, Japan*

Voltage-gated sodium channels (Na_v channels) trigger electrical action potentials in neurons and cause many human diseases, such as periodic paralysis, cardiac arrhythmias and epilepsy associated with their dysfunction. Na_v channels require different structural states to carry out their precise function. To understand how Na_v channels operate at the molecular level, we have characterized two structures in the near-physiological state. We have observed two structures of a bacterial voltage-gated sodium channel simultaneously existing in one two-dimensional crystal, assigned as two inactivated states, at 9Å resolution using cryo electron microscopy. The structural information of the inactivation in voltage-gated sodium channels after activation provides structural insights into the gating mechanism and therefore sheds light on future drug design. Our structural model elucidates the inactivation mechanism of the voltage-gated sodium channel in general.

Our research focuses on the understanding of the structure-function relationship of voltage-gated sodium channels, whose proper function is closely related to human health [1]. There has been no structural information on voltage-gated ion channels under physiological conditions available until now, primarily due to the lack of well-diffracting 2D crystals. Using 2D crystals of a bacterial voltage-gated sodium channel, which is the ancestor of the human sodium channel [2]), produced in a lipid environment, combined with cryo-electron microscopy, we have obtained two inactivated structures of this channel with distinct features and their functional relevance has been tested by the electrophysiology technique.

Biomolecular photography: electron microscopy

There are three major methods for visualising membrane protein structures: (I) X-ray crystallography, (II) NMR spectroscopy, and (III) electron microscopy. Unlike X-ray crystallography and NMR spectroscopy, that need to retrieve structural information indirectly, electron microscopy is an imaging tool to directly visualize proteins in solution as well as in crystal form [3]. Similar to light microscopy, an electron microscope also contains a set of lenses to enlarge objects to high magnification. By using a high-energy (typically in 80-300 kV) electron beam to illuminate a thin sample, such as a 2D crystal, the atomic resolution of its protein structure can be achieved [4, 5].

Native crystallization for membrane proteins

Membrane proteins carry essential functions for energy conservation and cell-signal transduction in all living organisms and provide more than 50 % of current drug targets. Membrane proteins can only function in a cell membrane which is composed of a lipid bilayer, and it is therefore of great interest to visualize it in its native environment, or one very much like it. Unlike a water-soluble protein, which can be studied only in solid 3D crystal form or in solution, membrane proteins can form 2D crystals in a lipid bilayer at a high protein density [6]. A bacterial voltage-gated sodium channel (Na_vCt) protein was purified to high quality and reconstituted in a lipid bilayer to form well-ordered 2D crystals under controlled conditions (Figure 1A). By taking images of 2D crystals at various angles using cryo-electron microscopy, we retrieved the 3D information of the Na_vCt 2D crystals to 9Å resolution (Figures 1B & 1C). We could visualize the subunit and secondary structures arrangement associated with the channel's structure in a lipid environment.

Voltage-gating in sodium channels

Bacterial voltage-gated sodium channels are formed of four identical units creating an ion-selective pore between them and four voltage sensors around the pore (Figure 2A). From the Na_vCt 2D crystals, we have obtained two structures with

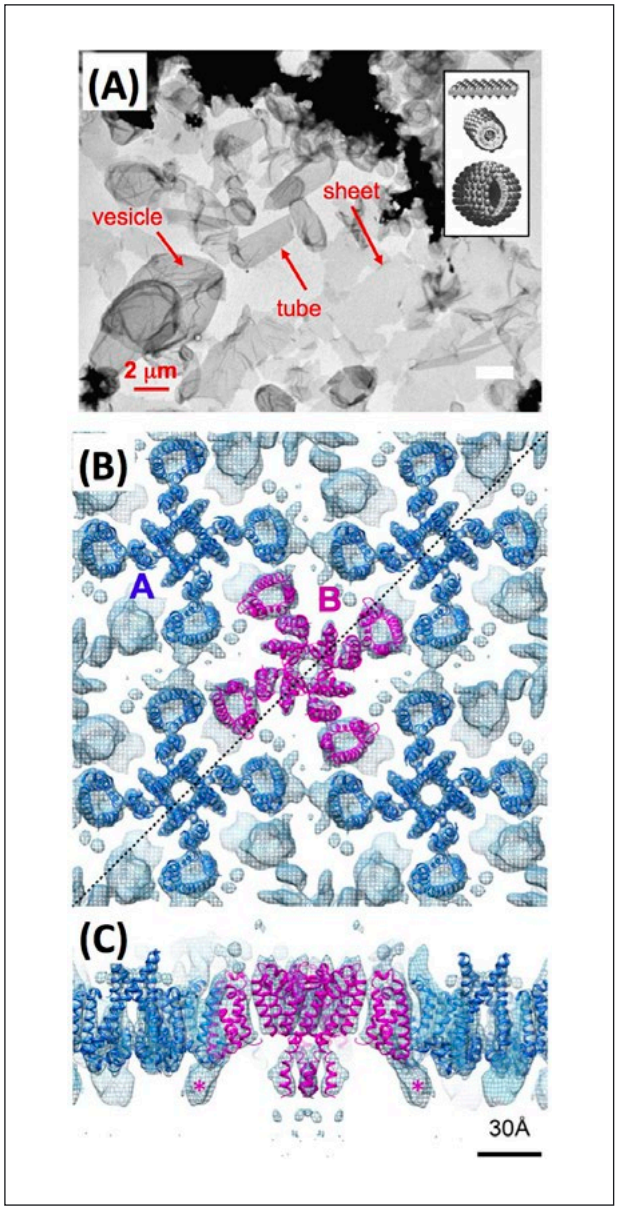

Figure 1: **Electron microscopy images of the voltage-gated sodium channel Na_vCt: (A) 2D crystals with representative shape (inset); (B) Top view, and (C) side view of the 9Å density map obtained from the Na_vCt 2D crystals. The dashed lines in (B) delineate the section in (C).**

the voltage sensor locked in the activated state (in comparison with the activated channel structures), while major differences have been found in the pore and linker region of the channel. We found three major differences between these two structures (Figure 2B) and these changes from one state to another show how Na_vCt returns from the activated state to the resting state during the inactivation cycle (Figure 2C). We are continuing to investigate the structures at different stages of the channel open-inactivation-close cycle. Once details of all possible states of such proteins are known and understood, then it will be feasible to create new medical drugs to combat disease.

References

[1] E. Savio-Galimberti, M.H. Gollob and D. Darbar, *Voltage-gated sodium channels: biophysics, pharmacology, and related channelopathies*, Front. Pharmacol. **3** 124 (2012).

[2] K. Charalambous and B.A. Wallace, *NaChBac: the long lost sodium channel ancestor*, Biochemistry-US **50** 6742–6752 (2011).

[3] Y. Fujiyoshi, *Structural physiology based on electron crystallography*, Protein Sci. **20** 806–817 (2011).

[4] S. Raunser and T. Walz, *Electron Crystallography as a Technique to Study the Structure on Membrane Proteins in a Lipidic Environment*, Ann. Rev. Biophys. **38** 89–105 (2009).

[5] T. Gonen, *The collection of high-resolution electron diffraction data*, Methods Mol. Biol. 955 153–169 (2013).

[6] T.M. Dreaden, M. Metcalfe, L.Y. Kim, M.C. Johnson, B.A. Barry and I. Schmidt-Krey, *Screening for two-dimensional crystals by transmission electron microscopy of negatively stained samples*, Methods Mol. Biol. **955** 73–101 (2013).

Links

[1] LBR: http://www.psi.ch/lbr/

[2] CeSPI: http://www.cespi.nagoya-u.ac.jp/Eng/

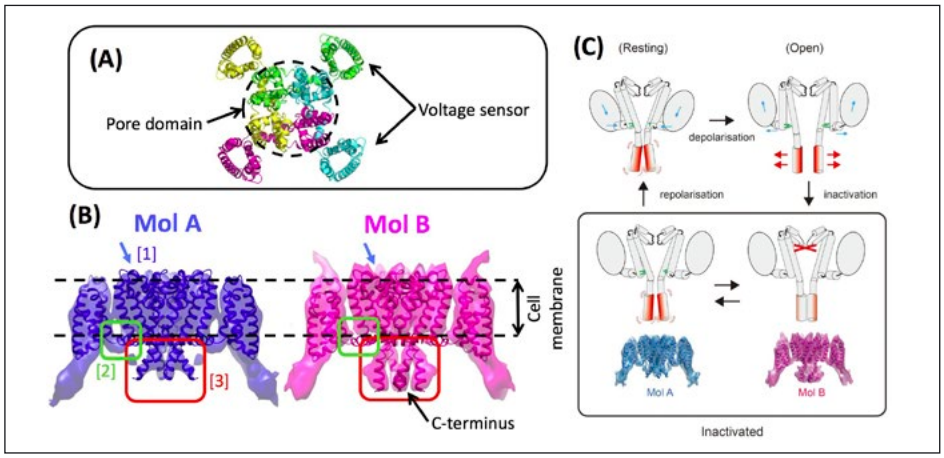

Figure 2: **Structures of Na_vCt: (A) Molecular model of Na_vCt; (B) Three highlighted differences between the two inactivated states; (C) Molecular rearrangement of Na_vCt during the inactivation cycle.**

Scandium-44: Production and preclinical evaluation of a novel PET isotope

Cristina Müller, Maruta Bunka, Josefine Reber, Andreas Türler and Roger Schibli,
Center for Radiopharmaceutical Sciences ETH-PSI-USZ, Laboratory of Radiochemistry and Environmental Chemistry (LCH), PSI, and Department of Chemistry and Applied Biosciences, ETH Zurich

In the last decade, PET (positron emission tomography) has become a widely used imaging technology in nuclear medicine and ^{68}Ga has emerged as an excellent radioisotope for clinical application when injected in conjunction with somatostatin-based peptides for the imaging of neuroendocrine tumours. However, its short half-life (~1 h) makes distribution logistics difficult. The positron-emitting ^{44}Sc has excellent decay characteristics (half-life: ~4 h), potentially allowing shipment of radiopharmaceuticals to more distant hospitals. Here, we report on the development of cyclotron-produced ^{44}Sc at PSI and its preclinical evaluation, including PET imaging with a DOTA-folate conjugate in tumour-bearing mice.

Background

In recent years, nuclear imaging has been revived by the excellent PET imaging quality which has been achieved in tumour patients injected with ^{68}Ga-labelled somatostatin analogues [1].
However, the short half-life of ^{68}Ga ($t_{1/2}$ = 68 min) is a drawback as it does not allow the distribution of ^{68}Ga radiopharmaceuticals to distant hospitals (Figure 1A). But ^{44}Sc is a PET isotope with an almost 4-fold longer half-life ($t_{1/2}$ = 3.97 h) and chemical properties that allow coordination by established chelator systems, and it may thus be an attractive alternative to ^{68}Ga (Figure 1B) [2].

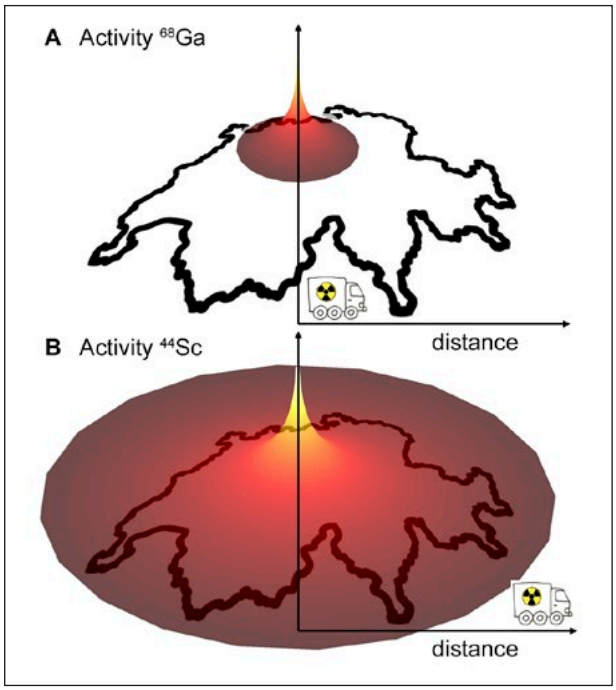

Figure 1: **Distribution logistics of the PET isotopes. A: ^{68}Ga ($t_{1/2}$ = 68 min); and B: ^{44}Sc ($t_{1/2}$ = 3.97 h).**

Aim of the study

The aim of this study was to produce ^{44}Sc via irradiation of enriched $^{44}CaCO_3$/graphite targets at the cyclotron at PSI. Furthermore, we wanted to develop a semi-automated separation process allowing the formulation of ^{44}Sc suitable for radiolabelling of biomolecules. To investigate ^{44}Sc in vitro and in vivo, we chose a novel folate conjugate (cm09), which had previously proved to have favourable pharmacokinetics, with high uptake in folate receptor (FR)-positive tumour xenografts in its ^{177}Lu-labelled version [3].

Production and purification of ^{44}Sc

Production of ^{44}Sc was performed via the ^{44}Ca(p,n)^{44}Sc nuclear reaction [4] (Figure 2). To prepare the targets, 150 mg of graphite powder were mixed with 5–7 mg of enriched $^{44}CaCO_3$, pressed and encapsulated in aluminium. Irradiation at the cyclotron was performed at ~17 MeV and lasted for 30–40 min at a beam current of 50 µA.
Purification of ^{44}Sc was carried out by a semi-automated process using a self-made separation system. Upon dissolution of the $^{44}CaCO_3$ in hydrochloric acid, ^{44}Sc(III) was sepa-

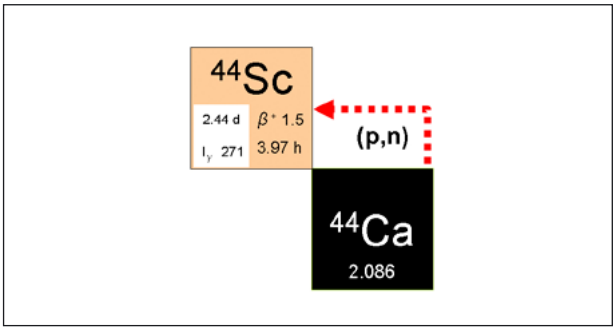

Figure 2: **Nuclear reaction for the production of ^{44}Sc via irradiation of ^{44}Ca targets at a cyclotron.**

rated from Ca(II) by extraction chromatography. In a second step, cation exchange chromatography was performed in order to allow the formulation of ^{44}Sc in a solution of ammonium acetate suitable for direct labelling procedures.

Radiolabelling of a DOTA-Folate Conjugate

For a proof-of-concept study, we employed a 1,4,7,10-tetraazacyclododecane-1,4,7,10-tetraacetate (DOTA)-folate conjugate (cm09) with a biological half-life of several hours. Radiolabelling of cm09 was performed by incubation of cm09 (~15 nmol) with the ^{44}Sc-solution (100-200 MBq) at 95°C for 10 min. Quality control was performed by HPLC. At a specific activity of ~7 MBq/nmol, ^{44}Sc-cm09 was obtained in a radiochemical yield of > 97 %.
The radiolabelled compound was stable in blood plasma over at least 4 h and showed FR-specific binding to KB tumour cells, a FR-positive human cervical cancer cell line.

PET imaging studies

PET imaging studies were performed with a small-animal PET/CT scanner (Vista eXplore, GE Healthcare) at the Animal Imaging Center of the CRS-ETH Zurich. Derenzo phantoms were fabricated, filled with either ^{44}Sc or ^{68}Ga (8-9 MBq) and scanned for 30 min. Excellent resolution of about 1 mm was obtained with ^{44}Sc, and the results were superior even to those achieved with ^{68}Ga (Figure 3A).
After preparation of ^{44}Sc-cm09 (100–200 MBq), the radiotracer was shipped to the ETH Zurich, where it was injected into KB tumour-bearing mice (~25 MBq/mouse). PET/CT scans of 30 min duration were performed 4 h after administration of ^{44}Sc-cm09. This provided excellent visualization of tumour xenografts in mice (Figure 3B). Besides accumulation in the tumours, radioactivity was also found in the kidneys as a consequence of renal excretion and binding to FRs, which are also expressed in the proximal tubule cells.

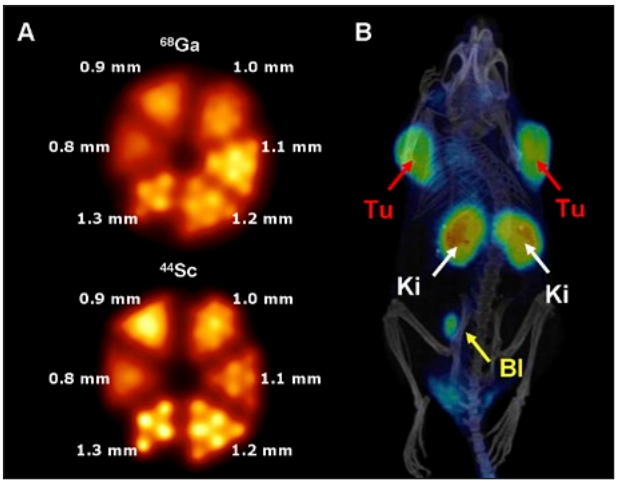

Figure 3: **A: Derenzo phantom of ^{68}Ga and ^{44}Sc (~ 9 MBq). B: In vivo PET/CT scan of a tumour-bearing mouse 4 h after injection of ^{44}Sc-cm09. (Tu = tumour xenograft, Ki = kidney, Bl = urinary bladder).**

Conclusion

In this study we were able to demonstrate that the production of ^{44}Sc is feasible at the cyclotron at PSI. Moreover, we have demonstrated the excellent features of this isotope for PET imaging. Due to its favourable half-life, ^{44}Sc could be distributed to hospitals located several hundred kilometres away from production facilities. Application of ^{44}Sc as a diagnostic match of clinically employed β$^-$-emitting radionuclides (^{177}Lu, ^{90}Y) would be attractive since equal alternatives for PET do not yet exist in routine clinical procedures.

Acknowledgements

We gratefully thank Walter Hirzel, Ernst Schaub, Yvonne Eichholzer, André Isenschmid, Nadja Romano, Cindy Fischer (ETH), Claudia Keller (ETH) and Martin Hungerbühler (ETH) for their technical assistance.

References

[1] M.U. Khan et al., Eur. J. Surg. Oncol. **35** 561–567 (2009).
[2] E. Koumarianou et al., Appl. Radiat. Isotopes. **70** 2669–2676 (2012).
[3] C. Müller at al., J. Nucl. Med. **54** 124–131 (2013).
[4] G.W. Severin et al., Appl. Radiat. Isotopes. **70** 1526–1530 (2012).

Link

[1] Radionuclide Production and maintenance, CRS: www.psi.ch/zrw/radionuclide-production-and-maintenance

Imaging and radioimmunotherapy of fibroblast activation protein (FAP)-expressing tumours

Eliane Fischer, Susan Cohrs, Kurt Zimmermann and Roger Schibli, *Center for Radiopharmaceutical Sciences ETH-PSI-USZ (operated jointly by ETH Zurich, Paul Scherrer Institute and University Hospital Zürich);*
Krishna Chaitanya and Christoph Renner, *University Hospital Zürich, Switzerland*

In recent years, targeting components of the tumour microenvironment has become a promising strategy in cancer therapy. Fibroblast activation protein (FAP) is highly expressed in the tumour microenvironment, but absent from healthy tissue. In our studies, we radiolabelled new FAP-specific antibodies (ESC11 and ESC14) for the diagnosis and radioimmunotherapy of FAP-expressing tumours in mice. Our results demonstrate the potential of ESC11 and ESC14 as powerful radioimmunoconjugates or antibody-drug conjugates for diagnostic and therapeutic use in patients with FAP-expressing tumours.

Introduction

Cancer-associated fibroblasts (CAFs) are a major component of the tumour microenvironment and contribute substantially to every stage of tumour development. Fibroblast activation protein (FAP) is a serine protease which is highly expressed on CAFs. FAP is a key mediator of tumour progression, extracellular matrix remodelling, and metastasis formation. Therefore, FAP has emerged as a potential target for cancer therapy, for example by specific eradication of FAP-expressing cells with cytotoxic immunoconjugates. Here, we developed FAP-specific radiolabelled antibodies for imaging and therapy of FAP-expressing tumours [1].

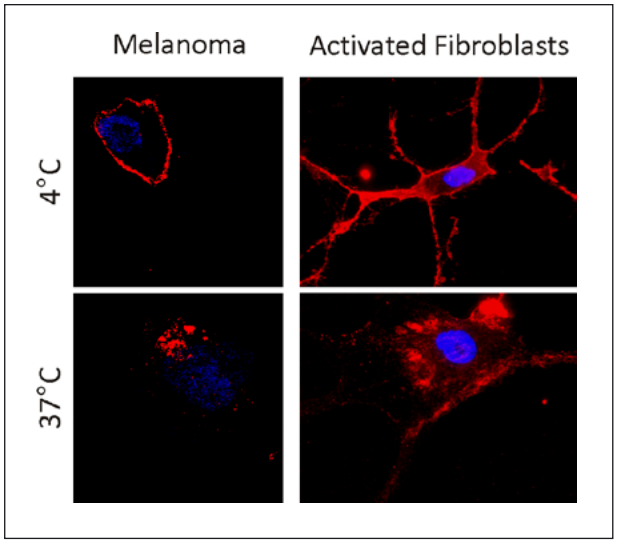

Figure 1: **After 30 minutes of incubation at 37°C, ESC11 internalised into melanoma cells (left) and activated fibroblasts (right). FAP staining is shown in red.**

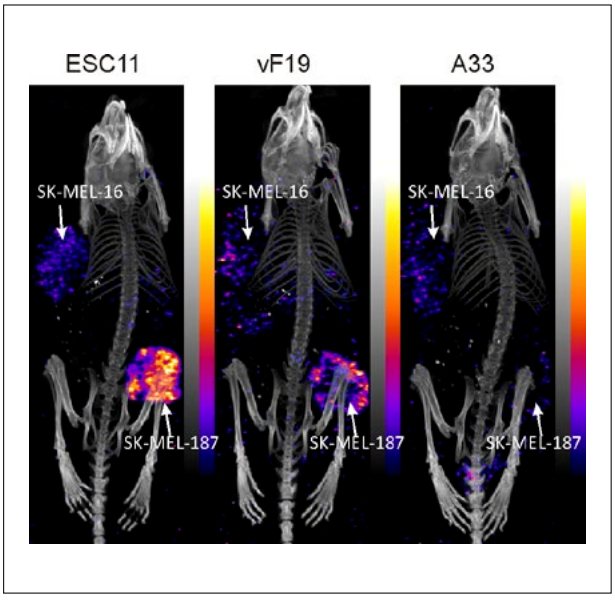

Figure 2: **Post mortem SPECT/CT images (maximum intensity projections) showing the distribution of ^{177}Lu-ESC11, ^{177}Lu-vF19, and ^{177}Lu-A33 in nude mice, 72 h post injection. SK-MEL-187: FAP-expressing tumour; SK-MEL-16: FAP-negative tumour.**

FAP-specific antibodies

For our studies, we used the two novel fully human FAP-specific antibodies ESC11 and ESC14, which we selected from a phage library [2]. These antibodies bind to both human and murine FAP. For preclinical evaluation of radioimmunoconjugates, human-mouse cross-reactive antibodies are preferentially used to detect possible accumulation in tissue expressing homologous FAP. In addition, for targeting of the tumour

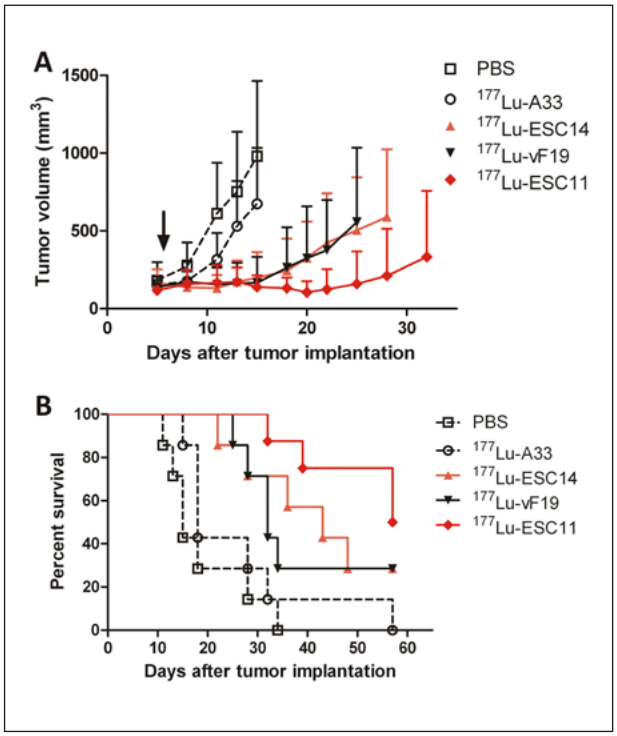

Figure 3: **A) Tumour growth curves showing mean tumour volumes +SD; B) Kaplan-Meier survival curves of treated and control groups.**

microenvironment in preclinical models, cross-reactivity with the homologous antigen of the model species is a prerequisite. Different from a previously described anti-FAP antibody (vF19), ESC11 and ESC14 internalise rapidly into FAP-expressing tumour cells or activated fibroblasts (Figure 1).

Imaging FAP-expressing tumours

ESC11 and ESC14 were labelled with the radiolanthanide ^{177}Lu. This radionuclide emits both γ photons and β$^-$particles, which are suitable for imaging and therapy, respectively. A previously described anti-FAP antibody (vF19) and a non-binding control antibody (A33) were included in the studies. We imaged a FAP-expressing human melanoma (SK-MEL-187) and a FAP-negative human melanoma (SK-MEL-16) in nude mice. Specific uptake in the FAP-expressing tumour was observed with all three anti-FAP antibodies. ESC11 achieved a higher tumour uptake than ESC11 and vF19, while uptake of the control antibody A33 was low (Figure 2).

Radioimmunotherapy

Radioimmunotherapy, the targeted delivery of therapeutic radioisotopes to the tumour site by monoclonal antibodies, is an attractive strategy for cancer treatment. Here, we performed radioimmunotherapy in nude mice bearing subcutaneous FAP-positive SK-MEL-187 tumours. Tumour-bearing mice were injected intravenously with 8 MBq (15 µg) ^{177}Lu-labelled antibodies or PBS 5 days after tumour implantation. Radioimmunotherapy with ^{177}Lu-labelled anti-FAP antibodies delayed growth of established melanoma tumours. All three FAP-specific antibodies prolonged median survival in these mice to >43 days, compared with 14 days in the control group, but the effect of ESC11 was still more pronounced (median survival = 58 days). The treated mice showed no signs of radiotoxicity.

Conclusions

The novel antibodies described in this study, ESC11 and ESC14, internalize into FAP-expressing cells and exhibit excellent in vivo targeting properties. They are therefore ideal scaffolds for the development of immunoconjugates with cytotoxic drugs or radiometals that are retained within the cells. Our preclinical studies using a melanoma model serve as a basis for the development of the ESC11 and ESC14 antibodies for targeting FAP-expressing tumour cells or CAFs. Since ESC11 and ESC14 cross-react with rodent FAP, these antibodies can be used to study CAF-targeting in syngeneic mouse models.

References

[1] W.N. Brennen, J.T. Isaacs and S.R. Denmeade, *Rationale Behind Targeting Fibroblast Activation Protein-Expressing Cancer-Associated Fibroblasts as a Novel Chemotherapeutic Strategy*, Mol. Cancer Ther. **11**(2) 257–266 (2012).

[2] E. Fischer, K. Chaitanya, T. Wüest, A. Wadle, A.M. Scott, M. van den Broek, R. Schibli, S. Bauer and C. Renner, *Radioimmunotherapy of Fibroblast Activation Protein Positive Tumors by Rapidly Internalizing Antibodies*, Clin. Cancer Res. **18**(22) 6208–6218 (2012).

Links

[1] Center for Radiopharmaceutical Sciences: http://www.psi.ch/zrw/

[2] Tumor Targeting Group: http://www.psi.ch/zrw/tumor-targeting

Intermetallic targets for superheavy element production

Robert Eichler and Ilya Usoltsev, *Laboratory for Radiochemistry and Environmental Chemistry (LCH), PSI*

Almost 150 years after Mendeleev's discovery of the ordering principle of elements depicted by the Periodic Table, the proof of its universal validity is still a hot topic of chemical research. Most investigations regarding the laws of periodicity amongst the elements are based upon examination of the chemical properties of superheavy elements (SHE) at the edge of the Periodic Table. Here, deviations of chemical properties are largest due to the influence of the high nuclear charge on the electronic structure of the atoms, which in turn determines their chemical properties. SHE are produced artificially at the rate of single atoms per week at large accelerators in the high-energy fusion of heavy ion beam atoms with actinide targets. We present here new-generation actinide target technology for SHE production. Theory predicts that SHE are produced in supernovae and may therefore appear in nature. Knowledge of the chemical properties of SHE is necessary for a proof of this prediction.

Highly intense heavy ion beams of calcium with atomic mass 48 are delivered for the production of SHE from the U-400 cyclotron at the Flerov Laboratory of Nuclear Reactions (FLNR) at the Joint Institute for Nuclear Research (JINR) in Dubna, Russian Federation. Recently, this work culminated in the discovery of six new elements heavier than copernicium (Cn, Z = 112) [1], see Figure 1.

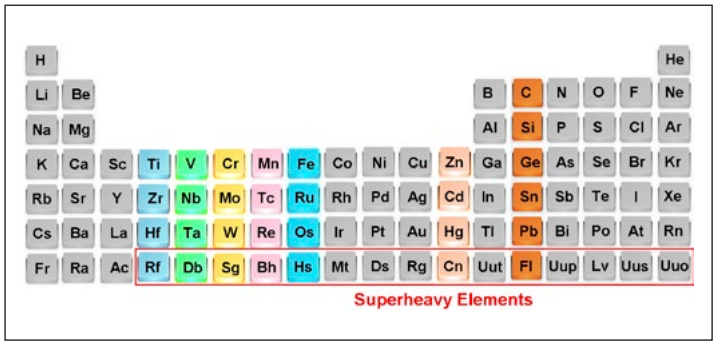

Figure 1: **The Periodic Table of the elements. Chemically investigated SHE and their groups are shown in colour.**

Targets of plutonium, with molecular mass numbers of 242 and 244, were irradiated for our latest chemistry experiments with Cn [2, 3] and flerovium (Fl, Z=114) [4]. During the irradiation, approximately 10^{13} ^{48}Ca ions pass per second through the thin actinide production target. Throughout a month-long experimental campaign, the integral beam yielded about $5 \cdot 10^{18}$ particles, corresponding to roughly twice the number of actinide atoms present in the target itself. Each beam ion had an average positive charge of 18 and lost about 20 MeV in passing through the target. Therefore, the conditions imposed on the materials used for the preparation of the targets were extreme: thermal stress (up to 1200 °C), mechanical stress (shock waves, atomic displacements), charging stress (18+ per ion), sputtering processes and chemical stress (chemical reactions of the target material and its backing). Until now, actinide targets have been prepared by the electrochemical deposition of 1–2 µm layers of actinide oxide on 2 µm titanium foils [5]. Such targets, if used in stationary mode, withstand the conditions described above for less than two weeks, until severely damaged by the beam (see Figure 2). The destruction is facilitated by the high-temperature reactions of the metallic titanium foil with the actinide material. For this reason, the described target preparation technology has to be improved, especially considering the enormous cost of the rare actinide isotopes, their chemical toxicity, and the radiation hazard.

We report here on the successful preparation and high-intensity irradiation tests of a completely new style of production targets for SHE, based on intermetallic actinide compounds with noble metals [6]. The production of such targets has two steps: In the first, a homogeneous oxide layer of the desired actinide is deposited on a noble metal foil, 3 µm thick, by exposing an actinide nitrate solution in isopropanol to a high voltage. In the second step, the foil and oxide layer are heated in a flow of pure hydrogen to temperatures up to 1300 °C, depending on the noble metal used.

The reduction of the highly stable actinide oxide with hydrogen, and therefore the formation of a purely metallic target, is feasible only due to the superimposed reaction between

the actinide (An) and the noble metal (e.g. palladium, Pd), leading to the intermetallic phase:

$$x\,AnO_2 + x\,H_2 + y\,Pd \leftrightarrow An_xPd_y + x\,H_2O$$

The formation of this intermetallic compound, which dissolves in the noble metal matrix, leads to a complete reduction of the target material and its even distribution over the whole thickness of the noble metal foil [6]. As a proof of principle, this method has been successfully applied to produce Pd-based intermetallic targets with ^{243}Am. Two stationary targets were prepared and irradiated at the U-400 cyclotron at FLNR Dubna using high-intensity beams of ^{48}Ca. Optical micrographs of the targets before and after irradiation (Figure 3), in conjunction with radioanalytical alpha spectroscopic measurement of the target layers, showed that intermetallic targets withstand high ^{48}Ca beam intensities and are stable and chemically inert under harsh irradiation conditions. Thus, such Pd-based intermetallic targets were found to be superior to widely-used Ti-based targets, due to higher thermal and electrical conductivity combined with enhanced chemical and mechanical stability.

Thus, we conclude that the proposed target preparation technology enables higher production yields of SHE to be obtained in future long-term experiments. Therefore, a considerable improvement in the precision of the data measured during chemical investigation of these heaviest elements is expected.

References

[1] Yu.Ts. Oganessian et al., Phys. Rev. Lett. **104** 142502 (2010).
[2] R. Eichler et al., Nature **447** 72–75 (2007).
[3] R. Eichler et al., Angew. Chem. Intl. Ed. **47** 3262 (2008).
[4] R. Eichler et al., Radiochim. Acta **98** 133 (2010).
[5] K. Eberhardt et al., Nucl. Instr. Meth. A **521** 208 (2004).
[6] I. Usoltsev et al., Nucl. Instr. Meth. A **691** 5 (2012).

Links

[1] Laboratory for Radiochemistry and Environmental Chemistry (LCH): http://www.psi.ch/lch/research-groups
[2] Flerov Laboratory for Nuclear Reactions: http://flerovlab.jinr.ru/flnr/

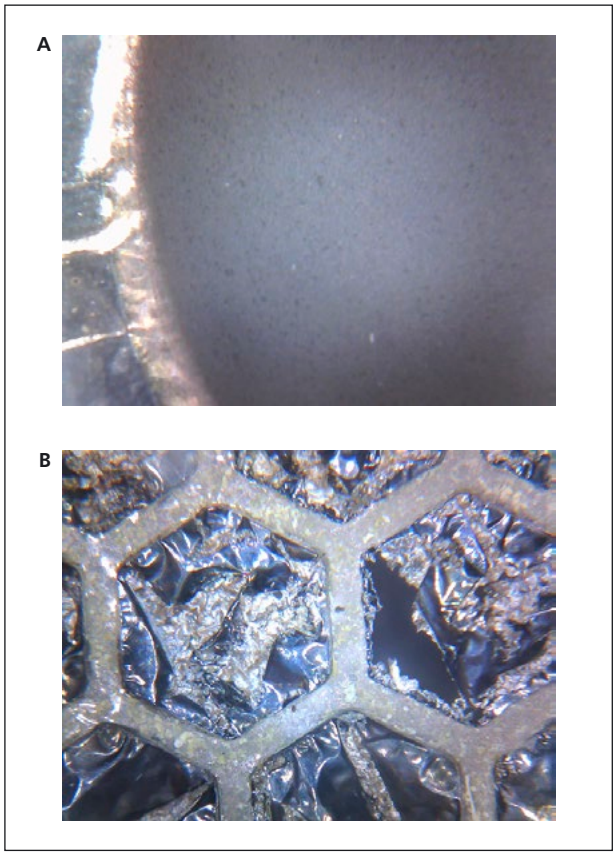

Figure 2: **Micrographs of a titanium-based target before (A) and after (B) irradiation with ^{48}Ca particles at intensities up to $7 \cdot 10^{12}$ ^{48}Ca per second for about 120 hours. The irradiated part is framed by a honeycomb with edges covered by the cooling grid and thus not irradiated.**

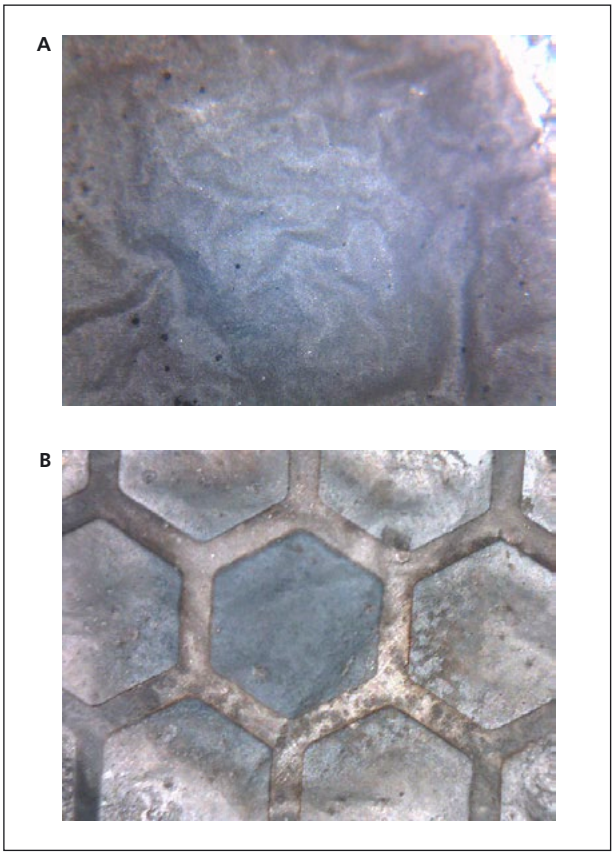

Figure 3: **Micrographs of a palladium-based target before (A) and after (B) irradiation with ^{48}Ca particles at almost twice the intensities of the titanium-based target – up to $1.2 \cdot 10^{13}$ ^{48}Ca per second for about 60 hours. The Pd foil and the actinide distribution remain unchanged.**

The new Control Systems Backbone

Timo Korhonen, Roger Kalt, Babak Kalantari, Damir Anicic, Ernst Johansen, Mario Jurcevic, Michael Laznovsky, Lionel Schebacher, Stefan Scherrer and Dirk Zimoch, *Large Research Facilities (GFA), PSI*

The operation of the PSI accelerators and beamline experiments relies on an efficient and reliable control system. Devices that steer the particle beams, collect data from the detectors and provide feedback to the users are all connected to the control system. The electronics to connect to those devices to handle this data needs to satisfy conflicting constraints of providing cutting-edge technology to serve the forefront science and, at the same time, be able to cater for the long lifetime of the large facilities – often several decades. We report here the development of an electronic board that brings us a required technology leap.

Introduction

The large facilities of PSI each comprise thousands of devices connected to the control system that deliver a large amount of measurement data or information about the status of an experiment. This data has to be transported, processed and visualized for operating the machine and steering some subsystems, and to provide scientists with experimental data to analyse. New facilities such as SwissFEL require the use of devices that often are orders of magnitude faster than what was the cutting edge 10 –15 years ago.

The existing control systems at PSI have been built mainly around the VME bus [Link 1] system. The VME standard was first introduced 30 years ago and, although it has evolved and withstood the test of time exceptionally well, the technology has reached its limits. On the other hand, it is still the optimal choice for many applications, and it would be very difficult to replace even a part of the existing infrastructure that still does its job extremely well. We need to find a way to bring in new technology, but avoid developing a second parallel infrastructure that would cost a lot of money and manpower and also require many changes in the surrounding infrastructure.

Goals and new possibilities

Evolution of the control system requires flexible ways to integrate new components and methods for processing and transporting the large data volumes the modern systems produce. Implementing the front-end electronic systems is cost and labour intensive. They also have a long lifetime, which makes it practically impossible to keep up with the continuously evolving computing equipment. A better strategy is to focus on data transfer infrastructure and connectivity.

However, several devices provide data too rapidly for even the fastest media available. The modern way to handle this is to use field programmable gate arrays (FPGA) to process the data stream right at the source and compress it to a level that the infrastructure can handle.

Introducing capabilities of fast front-end processing, data transport and industry-standard interfaces in our existing infrastructure would enable us to build new types of instruments and embed them in the computing infrastructure, to utilize the full possibilities of modern data processing.

Developing something like this with only our internal resources would have been difficult. We were thus happy to find an industrial partner to help us do this. In close collaboration with the company IOxOS SA [1], we have been able to develop a board that brings us all the things listed above: connectivity, data transport capability, processing power at the front end and the possibility to integrate it into our existing environment.

The new board and its architecture

The co-development started with discussions about our requirements. A series of design and review meetings resulted in the single-board computer called IFC_1210.

This board is built to the industry standard PCI Express [2], found in practically any modern computer. The PCIe switch of the board has a total maximum capacity of 32 gigabytes/second. It also allows us to connect the board directly to a powerful remote computing server as if it were an internal

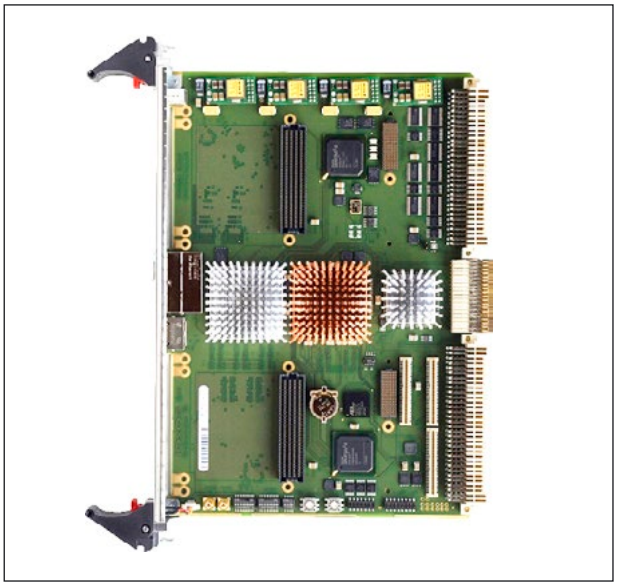

Figure 1: **The IFC_1210 Board: In the middle, from left to right, can be seen the CPU, FPGA, PCI Express Switch and UHM connector.**

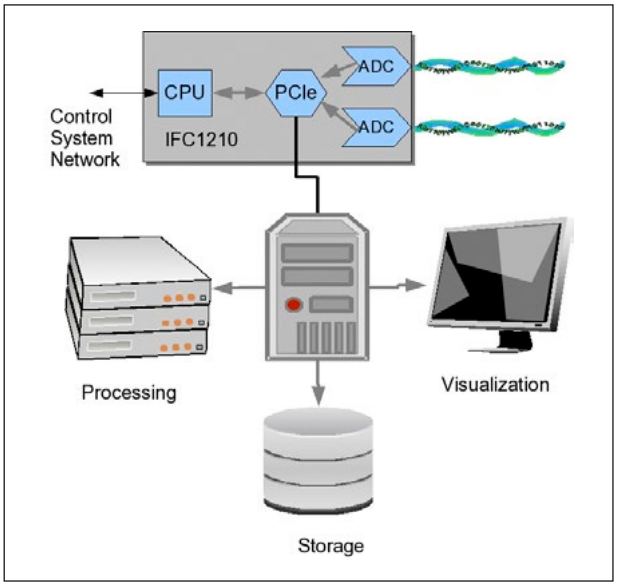

Figure 2: **Possibilities of embedding the IFC_1210 into computing infrastructure.**

peripheral, and this way build effective parallel processing solutions.

A small, but very important, technical detail is the use of a special connector (UHM, Ultra-Hard Metric) that allows high-speed links such as the PCI express to be routed through the existing VME backplane. This allows us to use this new technology in all our existing facilities, old and new, and take full advantage of the existing infrastructure.

A powerful FPGA is attached to the PCI infrastructure, to serve two major purposes. Firstly, it connects to the VME bus and to two FMC (FPGA Mezzanine Card) interface slots [3]. FMC is an industry standard for input/output cards that can be directly attached to an FPGA. Different types of I/O cards can be used by reprogramming the FPGA, without the need to modify the hardware. Secondly, the FPGA is used for fast processing of the data directly at the source.

For running an operating system such as Linux and the control system software EPICS [4], a Freescale [5] dual-core QorIQ P2020 CPU is included on the board. This way, the board can be used both as a master controller on the VME bus and as a standalone computer. A regular CPU is accessible for a wider range of programmers and the availability of many software tools make it very flexible. Much effort has been invested in software support for the board, to make it easy to embed in the control system environment.

Conclusions

With the IFC_1210, we now have a building block for applications that need the high data rates of today. With this architecture, embedded devices can become integral parts of modern computing infrastructure. The use of standard interfaces makes it possible to benefit from what is available on the market and to insert new technology where it is needed.

Several people from different groups within PSI's Large Research Facilities Department (GFA) [Link 2] have contributed to the development of the board and the infrastructure around it. Of course, the know-how and the design and implementation work of the company IOxOS was the crucial point of this development.

References

[1] IOxOS SA: http://www.ioxos.ch
[2] PCI-SIG: http://www.pcisig.com
[3] ANSI/VITA 57.1-2008 FMC:
FPGA Mezzanine Card Base Specification
[4] EPICS: http://www.aps.anl.gov/epics/
[5] Freescale Corporation: http://www.freescale.com

Links

[1] VME bus: http://en.wikipedia.org/wiki/VMEbus
[2] Large Research Facilities (GFA): http://www.psi.ch/gfa

Strategy and Highlights of General Energy Research

Alexander Wokaun, *General Energy Research Department (ENE), PSI*

PSI's General Energy Department is progressing towards its two main goals – the harvesting of renewable energies and their efficient conversion. In preparation for the "Action plan for coordinated energy research" of the Swiss Federation, we are advancing our plans for a Research and Technology Transfer Platform that will demonstrate the processes of sustainable biomass conversion and the storage of electricity in the form of hydrogen, both combined with the production of renewable methane (substitute natural gas). The results of 2012, as summarized here and highlighted in the following sections, form an excellent basis for this.

The harvesting of renewable energies, transformation to energy carriers for flexible use, and efficient conversion of final energy into energy services have remained at the focus of activities at PSI's General Energy Department in 2012.

As a first energy chain, biomass resources that are not competing with higher value-added exploitation are transformed into methane, which can then be converted efficiently to electricity, heat, and motive power in near-zero emission combustion devices.

The second value chain targets harvesting solar energy, which is transformed into either electricity or hydrogen produced by high-temperature solar chemistry. The envisaged area of application is transportation, based on either electrochemical storage in advanced batteries or on fuel cell propulsion trains.

These efforts are framed by experimental studies of environmental consequences of the energy-related activities for the atmosphere, by life cycle analysis, and by studying scenarios for the future development of the energy system.

Bioenergy, Catalysis, and Sustainable Chemistry

Two Laboratories, headed by Oliver Kröcher (Bioenergy and Catalysis) and Jeroen van Bokhoven (Catalysis and Sustainable Chemistry), have joined forces to advance catalytic processes for the conversion of biomass. They share the vision that advanced characterization methods available at PSI's large research facilities are powerful tools for elucidating catalytic reaction mechanisms, as illustrated in the contribution by Szlachetko et al. (pp. 56–57).

Combustion Research

Based on its experience in the low-NO_x combustion of natural gas under gas turbine relevant conditions, the Laboratory for Combustion Research focuses on efforts on reducing the CO_2 footprint of electricity generation. Besides the use of biogenic methane, pre-combustion reforming followed by CO_2 sequestration is an important option. In this context, particular attention must be paid to flame stability in order to avoid undesired flashback phenomena of the hydrogen-rich gases, as illustrated on pp. 60–61.

High temperature Solar Chemistry

The Laboratory for Solar Technology has advanced the realization of its vision of a two-step solar-driven thermochemical cycle that splits water into its elements – hydrogen and oxygen. A 100 kW reactor was tested at the Odeillo solar tower facility, providing insights into the challenges that must be overcome during the steps that are necessary for scaling up the process to an industrially relevant power level (pp. 58–59).

Electrochemistry

In its first year under the leadership of Thomas J. Schmidt, the Laboratory for Electrochemistry strengthened its focus on the development of functional materials for electrochemical energy storage and conversion. Graphene-based papers for supercapacitors, electrode materials for next generation lithium-sulphur batteries, and membranes for polymer electrolyte fuel cells were advanced, as shown in the contribution on pp. 62–63.

Atmospheric Chemistry

The Laboratory for Atmospheric Chemistry has contributed importantly to the international CLOUD project at CERN, in which the influence of galactic cosmic rays on climate-relevant cloud formation processes is being studied. The importance of secondary organic aerosol particles formed in the atmosphere from gaseous precursors, and its attribution to sources as varied as traffic, wood burning, cooking and natural biogenic emissions, represent the second focus (pp. 80–81).

Energy Systems Analysis

The Laboratory for Energy Systems Analysis, operated jointly by PSI's two Energy Departments, profited from the advice and positive recommendations of an audit in 2012. Scenarios for the future electricity and energy supply of our country, a crucial element of the present societal and political debate, have been developed and demonstrate the high sensitivity to the underlying assumptions on the development of electricity demand.

Competence Center Energy and Mobility

In its seventh year of operation, this Center of the ETH Domain has continued its successful track record (pp. 64–65) under the new leadership of Urs Elber. The efforts of Novatlantis, the outreach activity of CCEM towards cities and communities, received particular attention, to secure the next phase for realizing Lighthouse Projects and to extend to new partner regions. For its future development, CCEM has contributed towards the conception of the Competence Centers to be created as an element of the Federal energy strategy, as described below.

New opportunities in the framework of the Energy Strategy 2050

After announcing its Energy Strategy 2050, the Swiss Federal Council communicated an "Action plan for coordinated energy research", to which PSI and CCEM have actively contributed. It was delivered to the parliament as a special dispatch in October 2012, and was debated and approved in the spring session of 2013.

The action plan aims at bringing together the research capacities of the Swiss academic institutions to address the grand challenges lying ahead for our country when implementing the goals of the Energy Strategy. Research capacity will be expanded in order to contribute options and solutions from the natural, engineering and social sciences. The latter are important because, ultimately, industry has to bring these results and products to the marketplace, but society decides on accepting and investing into the pillars of the new energy system.

Reinforcing existing research competence is a first element of the "Action plan". Here, PSI would like to advance and strengthen the Catalysis Center, joining the activities of laboratories in the General Energy and Synchrotron Research Departments.

A second important element of the action plan is the creation of "Swiss Competence Centers for Energy Research" (SCCERs). Seven topics have been defined that relate to the Federal action fields of energy efficiency, electricity grids and energy systems, storage of electricity and heat, renewable energy provision, and the implications for the economy, the environment, regulations and societal behaviour.

The institutions of the ETH Domain and the seven regions of the Universities of Applied Sciences have started to prepare for the associated calls for proposals, and decided to coordinate their efforts, both naming a coordinating institution for each particular topic.

Energy storage will be among the most crucial challenges associated with the systemic integration of decentralized renewables. PSI and Empa will therefore apply to spearhead the coordinated research effort on this topic. The Electrochemistry Laboratory of PSI is strengthening its recently launched effort in electrolysis, which profits from our long-standing experience in fuel cell technology, as electrolysis represents one of the most promising options for the chemical storage of electricity in the form of hydrogen.

The second SCCER to be coordinated by PSI is devoted to the topic of biomass. We envisage creating a centre of biomass conversion, addressing all kinds of sustainably available biomass feedstocks. In this context, we particularly welcome the foundation (as of January 2013) of a joint institute with the University of Applied Sciences and Arts Northwestern Switzerland (FHNW) – the "Institute for Biomass Conversion and Resource Efficiency" (IBRE). We congratulate Frédéric Vogel, head of the Catalytic Process Engineering group, who was elected as professor at FHNW in this institute. Associated with the "Biomass" SCCER is the realization of a Research and Technology Transfer Platform, to be erected at PSI West. This will be centred around a 1.3 MW biomass gasifier, to be operated as a combined heat and power plant by industrial partners. Research at this platform will advance the methane-from-wood process developed by PSI, and will be extended to the power-to-gas process (producing additional methane by CO_2 hydrogenation, using electrolytically produced hydrogen), the hydrothermal gasification of wet biomass, and the production of biomass-derived chemicals and liquid fuels.

We are looking forward to seeing the plans for these two Competence Centers and the associated platform being further developed during 2013.

High energy-resolution off-resonant spectroscopy

Jakub Szlachetko, Maarten Nachtegaal, Evgeny Kleymenov, Olga Safonova and Christian König, *Bioenergy and Catalysis Laboratory (LBK), PSI;* Jacinto Sá, Markus Janousch and Jeroen van Bokhoven, *Laboratory for Catalysis and Sustainable Chemistry (LSK), PSI;* Jean-Claude Dousse and Joanna Hoszowska, *University of Fribourg, Switzerland*

To obtain insight into fast chemical processes, such as decomposition and synthesis, the spectroscopic technique of choice must have high penetration depth, high chemical sensitivity and a high time resolution. We have developed a technique, called high energy-resolution off-resonant spectroscopy (HEROS), which combines these properties. HEROS was applied to follow the structural changes of platinum acetylacetonate ($Pt(acac)_2$), a catalyst precursor, during decomposition in hydrogen with sub-second time resolution. This revealed that the decomposition of $Pt(acac)_2$ is a two-step process. We envisage that HEROS will be the technique of choice to follow dynamic structural changes of catalytic active sites, and that HEROS might turn out to be a valuable spectroscopic tool at X-ray free-electron lasers.

Introduction

Studying chemical processes under reaction conditions is a challenging task due to the reaction complexity, reaction time scales and low concentration of the element of interest. X-ray techniques are an ideal tool for in situ studies because of their penetration properties, chemical specificity and sensitivity. In particular, X-ray absorption and emission spectroscopy (XAS and XES) allow the in situ measurement of local electronic and geometric structures of an element of interest.

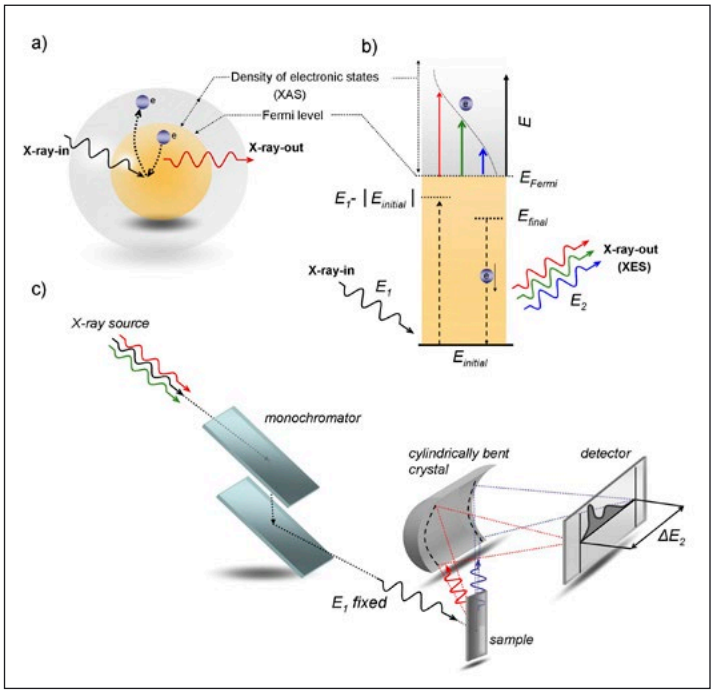

Figure 1: **(a) Schematic representation and (b) energy level drawing for an off-resonant scattering process; (c) The scanning-free von Hamos arrangement used in the HEROS experiment.**

To obtain a complete picture of dynamic chemical processes, recent developments of XAS have been focused on improving the energy and time resolutions. Energy resolution is obtained by the application of wavelength dispersive spectrometers at synchrotrons. Detecting X-ray emission lines with eV resolution enables high energy-resolved XAS spectra to be recorded [1, 2]. Since the X-ray absorption edge reflects the empty density of states, detailed information is obtained about the electronic and geometric structures of the central absorber. However, the necessity of scanning the incident X-ray beam energy across the absorption edge of interest limits the application of high energy-resolution XAS to move beyond the minute regime.

We report on the application of high energy-resolution off-resonant spectroscopy (HEROS) to follow changes in the structure of metal compounds with sub-second time resolution. In HEROS, a XES spectrum is recorded at a single incident energy that lies well below the absorption edge of interest. A schematic diagram and energy level drawing of the off-resonant scattering process in an atom is presented in Figures 1a and 1b, respectively.

The energy of the incoming X-ray, E_1, is smaller than the absolute value of the binding energy of the initial state, $E_{initial}$. The

electron (denoted by e) can be nonetheless excited into an unoccupied state above the Fermi level by taking energy from the emitted photon. The energy of the emitted photon, E_2, will thus be reduced by the amount of energy needed to promote the core-electron into the unoccupied density of states. Consequently, the energy distribution of emitted photons will provide information about the XAS of an atom at fixed excitation energy, E_1. To obtain a high time resolution, HEROS spectra were collected with a wavelength-dispersive spectrometer in the von Hamos geometry (Figure 1c) [3]. In this geometry, the emitted X-rays are diffracted by a cylindrically bent crystal and recorded by a micro-strip (PSI's Mythen) detector. Therefore the time resolution for acquisition is only limited by the overall experimental efficiency and not by the speed of scanning the incident energy axis.

Decomposition of $Pt(acac)_2$

As an example, the decomposition of platinum (II) acetylacetonate ($Pt(acac)_2$) in hydrogen was followed by in-situ HEROS [4]. β-Diketonate metal complexes are widely used as catalysts and metal precursors. Understanding of the decomposition under realistic conditions is highly desirable since it can help unravel the reaction mechanism. The metal complex was flash heated to 150 °C and HEROS spectra were collected every 500 ms. The measured HEROS-XES and reconstructed HEROS-XAS spectra are shown in Figure 2, left and right, respectively. As schematically shown, three zones can be detected in the HEROS spectra (marked by A, B and C). Selected HEROS-XES and HEROS-XAS spectra from these three zones are plotted in Figure 2, bottom. The spectra collected in zones A and B differ in the white-line intensity, which corresponds to the population of the 5d unoccupied density of states. The spectra in zone C, as compared with zones A and B, show an edge energy shift, which can be interpreted as a change in the Pt oxidation state.

The spectra displayed in the initial zone A (0–30 s) are characteristic of $Pt(acac)_2$, whereas those in the final zone (70–100 s) relate to metallic Pt particles. The spectra in the intermediary zone (40–65 s) correspond to an intermediate species. Part of the platinum may have been reduced, forming Pt particles that are partially covered with products of acac decomposition.

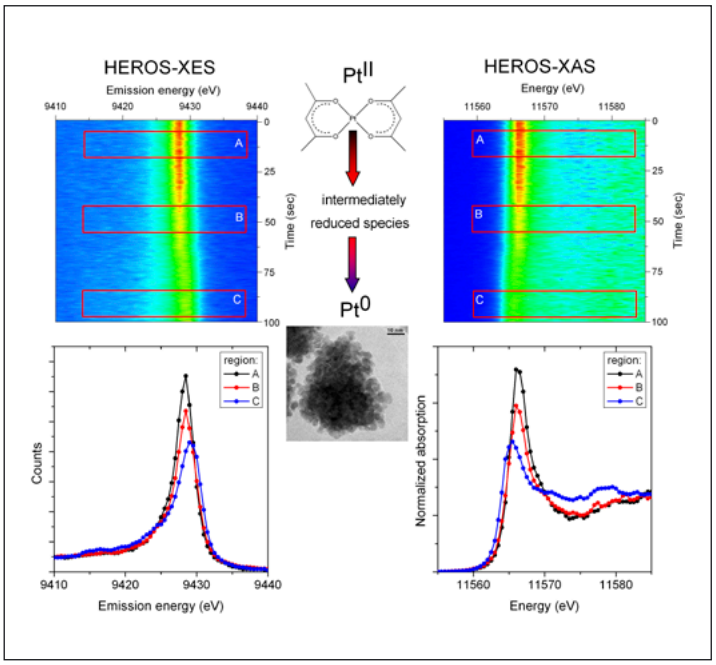

Figure 2: **In situ decomposition of $Pt(acac)_2$ under 5 % H_2 in He at 150 °C followed by HEROS. The HEROS XES and XAS spectra versus the experimental time are plotted at top left and right. The corresponding 1D spectra from zones A, B and C are plotted in the lower panels. The suggested reaction path is drawn in the middle.**

Outlook

We have developed high energy-resolution off-resonant spectroscopy to follow in situ chemical processes with unprecedented time and energy resolutions. The experimental and theoretical approach allows detailed information about unoccupied electronic states to be obtained at sub-second time scales. HEROS will play a prominent role in understanding chemical processes and might turn out to be a valuable spectroscopic tool at X ray free-electron lasers.

References

[1] E. Kleymenov, M. Nachtegaal et al., Rev. Sci. Instr. **82** 065107 (2011).
[2] J. Szlachetko, M. Nachtegaal et al., J. Electron Spectrosc. Relat. Phenom. (Available online 21 November 2012), DOI:10.1016/j.elspec.2012.11.002
[3] J. Szlachetko, M. Nachtegaal et al., Rev. Sci. Instr. **83** 103105–103107 (2012).
[4] J. Szlachetko, M. Nachtegaal et al., Chem. Commun. **48** 10898–10900 (2012).

Link

[1] SuperXAS beamline (Laboratory for Bioenergy and Catalysis): http://www.psi.ch/sls/superxas

A 100 kW solar pilot plant for the thermochemical dissociation of zinc oxide

Willy Villasmil, Yvonne Bäuerle, Rahul Bhosale, Majk Brkic, Alwin Frei, Peter Schaller, Daniel Wuillemin and Anton Meier, *Solar Technology Laboratory (LST), PSI;* Aldo Steinfeld, *Solar Technology Laboratory (LST), PSI, and Department of Mechanical and Process Engineering, ETH Zurich*

The solar two-step Zn/ZnO redox cycle for splitting H_2O and/or CO_2 inherently operates at high temperatures and utilizes the entire solar spectrum, and as such provides a thermodynamically favourable path to efficient solar fuel production. Following the technical demonstration with a 10 kW solar reactor prototype, a 100 kW solar pilot plant has been designed, fabricated, and experimentally tested at the large-scale solar concentrating facility of PROMES-CNRS in Odeillo, France. This operational experience has pointed out further R&D needs and is guiding the development of an industrial solar chemical plant for the production of H_2 and syngas - a precursor for liquid hydrocarbon fuels.

The solar two-step Zn/ZnO redox cycle [1, 2] consists of: (1) the endothermic dissociation of ZnO to Zn and O_2 at 2000 K using concentrated solar energy; and (2) the exothermic reaction of Zn with H_2O/CO_2 to H_2/CO (a mixture known as *syngas*, the precursor of liquid hydrocarbon fuels) and the initial ZnO. The latter is then recycled to the first step, thus closing the material cycle. A 100 kW solar pilot plant for performing the first step has been designed, fabricated, and experimentally tested at PROMES-CNRS in Odeillo, France. A description of the pilot plant layout, including the solar reactor technology, operational experience, and results from work in progress, are presented below.

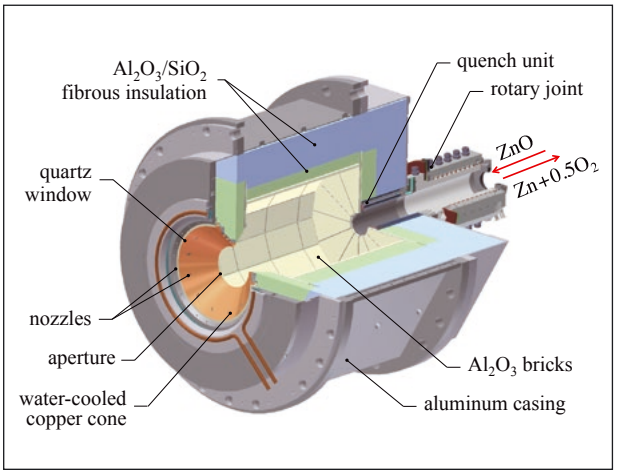

Figure 1: **Schematic of the 100 kW solar reactor.**

Solar reactor design

The design of the 100 kW solar reactor was based upon its predecessor – a 10 kW reactor prototype [1] which has been experimentally demonstrated at PSI's High Flux Solar Simulator [3]. The scaled-up reactor, schematically shown in Figure 1, consists of a rotating cylindrical cavity receiver with a 600 mm-dia. transparent quartz window and a 190 mm-dia. aperture for the access of concentrated solar radiation at an average solar concentration ratio of 3500 suns (1 sun = 1000 W/m^2). The cavity wall is composed of self-supporting refractory Al_2O_3 bricks packed by vacuum-formed Al_2O_3/SiO_2 thermal insulation. A layer of ZnO particles lining the inner cavity wall is directly exposed to the incoming concentrated solar radiation. With this arrangement, ZnO serves simultaneously the functions of radiant absorber, chemical reactant, and thermal insulator. A dynamic screw feeder that extends and retracts within the cavity enables the batch addition of ZnO particles during operation. Recombination of product gases, Zn(g) and O_2, is minimized by rapidly cooling with an inert gas (Ar) stream injected in a water-cooled quench unit directly incorporated in the reactor exit.

Experimental setup

The experimental campaign was conducted at the large-scale solar furnace (MWSF) of PROMES-CNRS in Odeillo, France. This solar concentrating research facility, shown in Figure 2, comprises a field of 63 heliostats that track the sun and direct the solar radiation onto a parabolic concentrator, which in turn

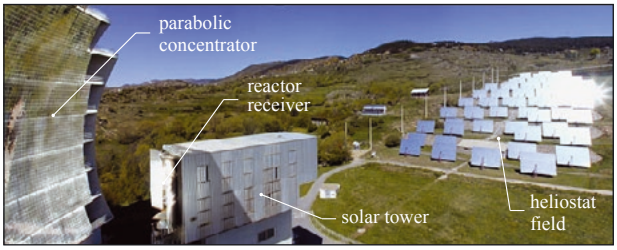

Figure 2: **Large solar furnace in Odeillo, France [4].**

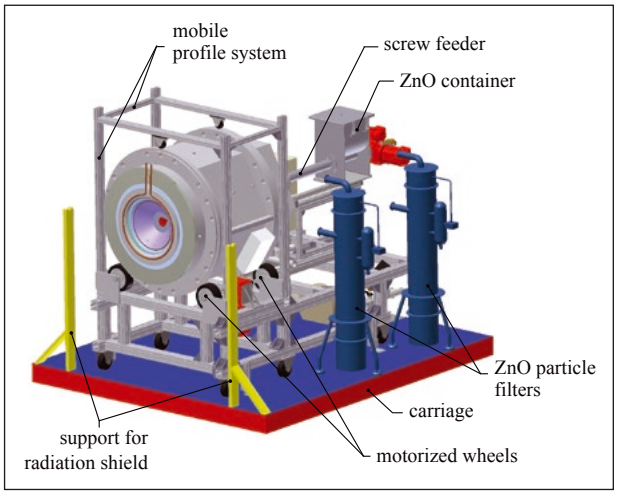

Figure 3: **3D layout of the 100 kW solar pilot plant.**

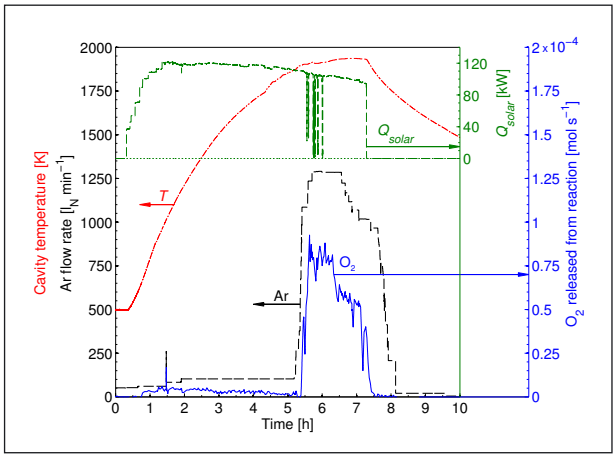

Figure 4: **Solar power input, Q_{solar}, cavity temperature, T, Ar quench flow rate, and O_2 release from the reaction measured during a typical experimental run.**

focuses the sun's rays onto its focal plane, located in the solar tower.

The solar reactor and peripheral components are shown schematically in Figure 3. Data acquisition and process control systems were used to continuously monitor and control temperatures and pressure inside the reactor, cooling water supply (spillage radiation shield, screw feeder, front shield, and quench unit), and inert gas supply (quench and purge gases). The product gas composition was analysed by gas chromatography and an O_2 detector. Two mechanical filters (mean pore size 0.3 µm) allowed the Zn and ZnO particles produced to be collected downstream. The solar flux distribution over the aperture was measured for each heliostat using a set of thermogauges.

Solar experimentation

Figure 4 shows the solar power input, Q_{solar}, cavity temperature, T, Ar quench flow rate, and O_2 release from the reaction during a representative experimental run with batch feeding. The peak operating temperature was 1943 K, measured approx. 15 mm behind the inner surface of the Al_2O_3 bricks forming the cavity wall. Thermal dissociation of ZnO was monitored by online measurement of O_2 in the product stream. Additional chemical species, such as N_2, H_2, CO_2, CO, and CH_4, were also monitored, to detect and quantify side reactions and/or possible air leakages. For the set of experimental runs performed, the weight of the solid products collected downstream was up to 573 g and their Zn content – determined via chemical analysis – was in the range 13–63 mol%.

During the experimentation campaign, more than 60 hours of on-sun testing at the MWSF were achieved, with each experiment lasting between 3 and 9 hours. The reactor cavity lining exhibited good mechanical and thermal stability and did not show any visible degradation at the end of the experimental campaign.

References

[1] P. Loutzenhiser et al., Materials **3** 4922–4938 (2010).
[2] M. Romero and A. Steinfeld, Energy Environ. Sci. **5** 9234–9245 (2012).
[3] J. Petrasch et al., J. Solar Energy Eng. **129**(4) 405–411 (2007).
[4] MWSF, PROMES-CNRS, 11 December 2012.

Links

[1] Solar Technology Laboratory, PSI: http://solar.web.psi.ch/
[2] Professorship of Renewable Energy Carriers, ETH Zurich: http://www.pre.ethz.ch/

Safe and low-emission combustion of hydrogen-rich fuel mixtures

P. Jansohn, Y.-C. Lin, M. Schultze, I. Mantzaras and R. Bombach, *Combustion Research Laboratory (CRL), PSI*

A promising technology for reducing greenhouse gas emissions in power generation systems is the combustion of syngas or hydrogen-rich fuels (> 80 % vol. H_2) in gas turbine cycles, with integrated solid fuel gasification combined with pre-combustion carbon capture. The significantly higher flame speed and drastically reduced auto-ignition delay times of hydrogen-containing fuel mixtures increase the risk of flame flashback, i.e. anchoring of the flame close to the fuel injection point. Hybrid combustion approaches, such as the catalytic-rich/homogeneous-lean combustion concept, can very effectively mitigate the associated risks (over-heating of burner components) and the NO_x emissions.

In order to mitigate the CO_2 emissions from power generation systems, various technologies of carbon capture and sequestration (CCS) have been proposed. One of such options is the integrated gasification combined cycle (IGCC) combined with pre-combustion capture of CO_2. Here, the H_2 content in the fuel gas may reach over 70 vol. %, which causes operability issues for the gas turbine combustor, such as the higher risk of flashback. Accordingly, understanding the combustion characteristics and flashback phenomena of H_2-rich fuel gases is essential. The term "flashback" is generally defined as the phenomenon when a flame propagates back into the burner, i.e. upstream of the location in the combustor where it is supposed to anchor and burn steadily. Generally, three mechanisms of flashback relevant for non-swirl continuous flow combustors are discussed: turbulent flame propagation in the core flow, flashback due to combustion instabilities, and flashback in the boundary layer, near walls.

Prediction of flashback based on turbulent flame speed

In our recent work [1], we propose the turbulent flame speed (S_T) to be an indicator of flashback propensity. For turbulent, lean-premixed, non-swirled, confined jet flames of H_2-rich fuel gases, we could experimentally show that flashback occurs at a certain fuel/air ratio (e.g. $\Phi = 0.4$) in our specific burner configuration and that the flame propagation at flashback occurs exclusively within the boundary layer (of the premixing pipe connected to the axial-dump combustor). The criterion for turbulent boundary layer flashback was thus defined based on critical velocity gradients either imposed by the fluid flow structure (g_f) or the chemical kinetic properties of the flame propagation (g_c). For the occurrence of flashback, the velocity gradient, represented by the flame propagation, must exceed that prescribed by the near-wall flow conditions in the fuel supply pipe. If this condition ($g_c > g_f$) is met, the flame is able to penetrate upstream within a thin layer close to the wall.

The velocity gradient representing the flame front characteristics (g_c) is defined as $S_T/(\mathrm{Le} \times \delta_{L0})$, where Le is the Lewis number and δ_{L0} is the laminar flame front thickness. The Lewis number is incorporated in the denominator to reveal the observed trend from the literature that the critical velocity gradient increases as the Lewis number decreases. The velocity gradient prescribed by the flow (g_f) is taken from CFD results or analytical equations (e.g. the Blasius correlation for fully-developed turbulent pipe flow). Phenomenologically, the relevance of the proposed criterion can be pictured such that, the higher the g_c, the more resistant the flame front is to the strain rate induced by the flow. Or equivalently: with higher g_c, the flame can more easily survive within a thin flow

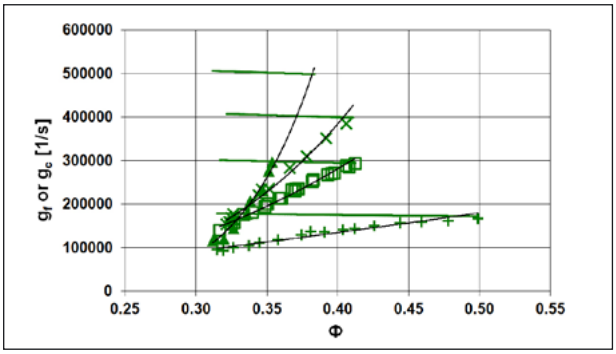

Figure 1: **Velocity gradients (g_f and g_c) for an H_2/N_2 fuel mixture as a function of the equivalence ratio (i.e. fuel to air ratio).**

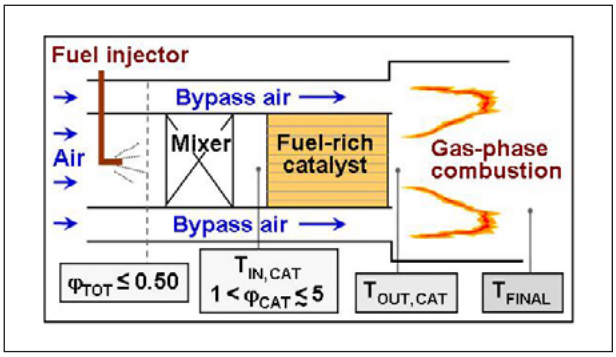

Figure 2: **Catalytic-rich/gaseous-lean combustion concept.**

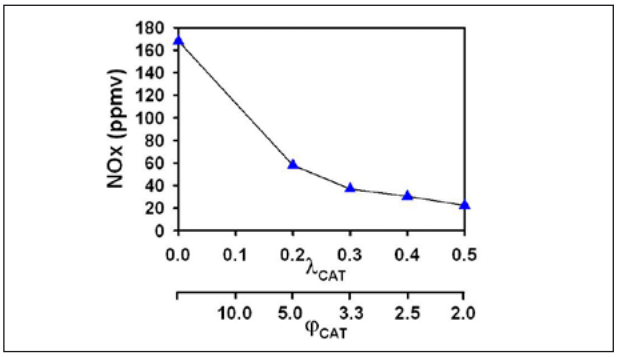

Figure 4: **NO_x emissions, at a pressure of 8 bar, as a function of the rich equivalence ratio (φ_{CAT}) in the catalytic module (air excess ratio $\lambda_{CAT} = 1/\varphi_{CAT}$).**

sheet at high shear stress without being extinguished, and hence the flashback propensity is higher. The predicted flashback limits (Φ_{FB}) are determined by the crossover points at which the regression curves (for g_c and g_f) intersect. The data show (Figure 1) that the present approach provides reasonable estimations on the flashback limits for various fuel compositions (H_2-rich, syngas, methane). The reduced operational range at high pressure and the reduced flashback propensity caused by decreasing the preheat temperature are both well reproduced. The experimental finding that flashback occurs at much leaner conditions for H_2-rich fuels, even when compared with syngas, is also well captured.

Staged catalytic combustion of hydrogen/air mixtures

In the catalytic-rich/gaseous-lean hybrid combustion concept of Figure 2, part of the air and all of the fuel are driven in a catalytic reactor at fuel-rich stoichiometries ($\varphi_{CAT} > 1$). Hot combustion products and unconverted fuel are subsequently mixed with the bypass air, forming a fuel-lean homogeneous (gas-phase) combustion zone. This approach is suitable for a wide range of fuels, which includes low calorific value biofuels, whereby flame stability is an issue, and also for hydrogen-rich fuels for which conventional lean-premixed gaseous combustion entails the risk of flame flashback.

Fundamental kinetic studies have been carried out at PSI's optically accessible, high-pressure channel flow catalytic reactor with H_2/air mixtures and platinum as catalyst. Planar Laser Induced Fluorescence (LIF) of the OH radical monitored homogeneous combustion. Comparisons between measured and predicted 2D maps of the OH radical are shown in Figure 3 for five cases [2].

The observed good agreement between the measured and predicted homogeneous ignition positions (demarcated by the vertical arrows in Figure 3) attests to the aptness of the employed gas-phase H_2/O_2 chemical reaction mechanism.

In addition to basic kinetic studies, a lab scale reactor model based on the concept in Figure 2 has been built and tested, together with a group from University of Applied Sciences and Arts Northwestern Switzerland FHNW, Windisch, Switzerland (Institute for Thermo- and Fluid-Engineering, Prof. T. Griffin). The results achieved (Figure 4) indicate that, by decreasing the equivalence ratio in the catalytic module to $\varphi_{CAT} = 2$ (i.e. by increasing the hydrogen conversion in the catalytic stage), the NO_x emissions at the end of the gaseous combustion zone drop by a factor of about eight [3].

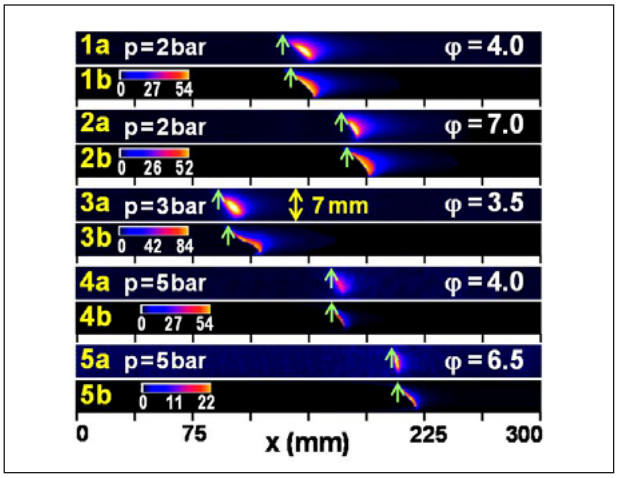

Figure 3: **OH distributions in rich H_2/air combustion: (a) LIF measurements, (b) predictions. Colour bars provide the predicted OH (ppmv) and vertical arrows mark the homogeneous ignition positions.**

References

[1] Y.-C. Lin, S. Daniele, P. Jansohn, K. Boulouchos, Proc. ASME Turbo Expo 2013, Paper GT2013–95518.

[2] M. Schultze, J. Mantzaras, R. Bombach, K. Boulouchos, Proc. Combustion Institute **34** 2269–2277 (2013).

[3] F. Bolanos, D. Winkler, F. Piringer, T. Griffin, R. Bombach and J. Mantzaras, Proc. ASME Turbo Expo 2013, Paper GT2013-94420.

Link

[1] Combustion Research Laboratory (CRL), PSI: http://crl.web.psi.ch/

Electrochemical energy research – A key factor in addressing future energy challenges

Thomas J. Schmidt, Felix N. Büchi, Lorenz Gubler, Rüdiger Kötz and Petr Novák,
Electrochemistry Laboratory (LEC), PSI

Electrochemical energy research becomes an increasingly important field for addressing the challenges of a future energy system consisting largely of intermittent renewable energy supplies. Electrochemical energy storage and conversion are considered to play significant roles and have both been areas of focus in PSI's Electrochemistry Laboratory for more than two decades. Our integrated approach to electrochemical materials science, the R&D of components, systems and devices, as well as the development of important diagnostic tools in the field of secondary batteries, supercapacitors, polymer electrolyte fuel cells and water electrolysis, allows us to significantly contribute to the challenges of future energy systems.

The future of the Swiss energy supply, after the phase-out of nuclear energy, will heavily rely on intermittent renewable energy sources, such as solar or wind. To guarantee the continuous (both temporal and regional), reliable, and cost-efficient supply of power, heat, and fuels derived from these energy sources for Switzerland, in a European context, it is critical to develop the science and technology of energy storage and conversion devices for both stationary and mobile applications. While electrochemical energy conversion and storage will play a significant role in this future, to cope with energy supply intermittency, the Electrochemistry Laboratory, with its over twenty years of experience in these fields, will contribute to shaping the future of the overall energy system. Our multidisciplinary and internationally renowned research team, combined with an integrated R&D approach on both the fundamentals and applications of secondary batteries, supercapacitors, polymer electrolyte fuel cells, and water electrolysis, is the basis of our present and prospective research and development.

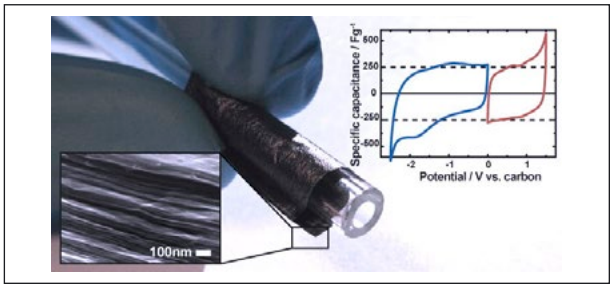

Figure 1: **Electrochemical behaviour of 25 µm partially reduced graphite oxide paper electrode, alongside an electron micrograph, enabling the creation of both high-energy and high-power supercapacitors.**

Materials development

Electrochemical materials science is one of the key components in the development of advanced devices. One of our continuous efforts around the preparation and in-depth understanding of electrodes for supercapacitors resulted in the successful development of 25 µm graphite paper based on partially reduced graphite oxide (a graphene-type material) as self-supporting, binder-free and flexible electrode, enabling the creation of high-energy, high-power supercapacitors (Figure 1 [1]).

Alongside energy storage in supercapacitors, our research focus is also on next-generation high-energy batteries, e.g. the Li-S system. In this context, we have successfully demonstrated a composite positive-electrode material based on graphitized carbon fibres and sulphur with a significantly improved cycle life (Figure 2).

For several years, we have been developing a low-cost proton-conducting membrane for polymer electrolyte fuel cells. Within our ongoing successful collaboration with Belenos CPH, we have leap-frogged several steps in this development in order to achieve technologically important results. Figure 3 illustrates the performance of a fuel cell operated with our GEN2 radiation-grafted membrane compared with that of cells using DuPont's state-of-the-art Nafion membrane.

At the same time, in situ aging of membrane electrode assemblies (MEA) using potential cycling (strongly oxidizing conditions) resulted in their clear outperforming of stabilized Nafion membranes, with MEAs consisting of our GEN2 membrane still operational long after the Nafion-based MEAs had all failed in accelerating aging tests.

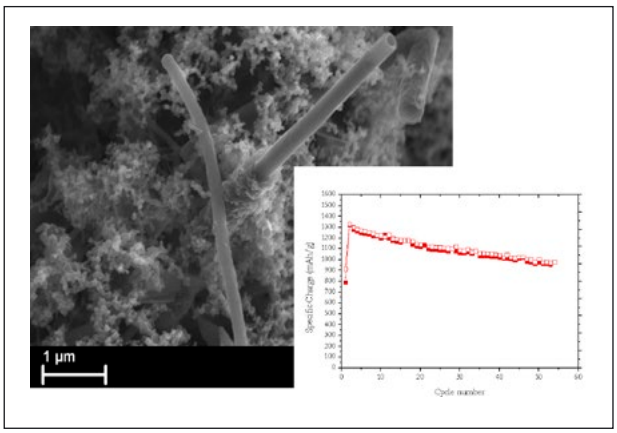

Figure 2: **Cycle stability of our proprietary composite electrode shown for Li-S batteries in the micrograph.**

In situ diagnostics

Understanding modern materials and developing them further are only possible with the use of advanced diagnostics tools helping not only to improve materials but also to provide insights into relevant failure modes. As an example, Figure 4 demonstrates, for the first time, the mechanistic elucidation of an important membrane and MEA failure mode in technical devices upon membrane pinhole formation during fuel cell operation, obtained using a combination of X-ray tomographic and infrared microscopy at the Swiss Light Source (SLS) [2].

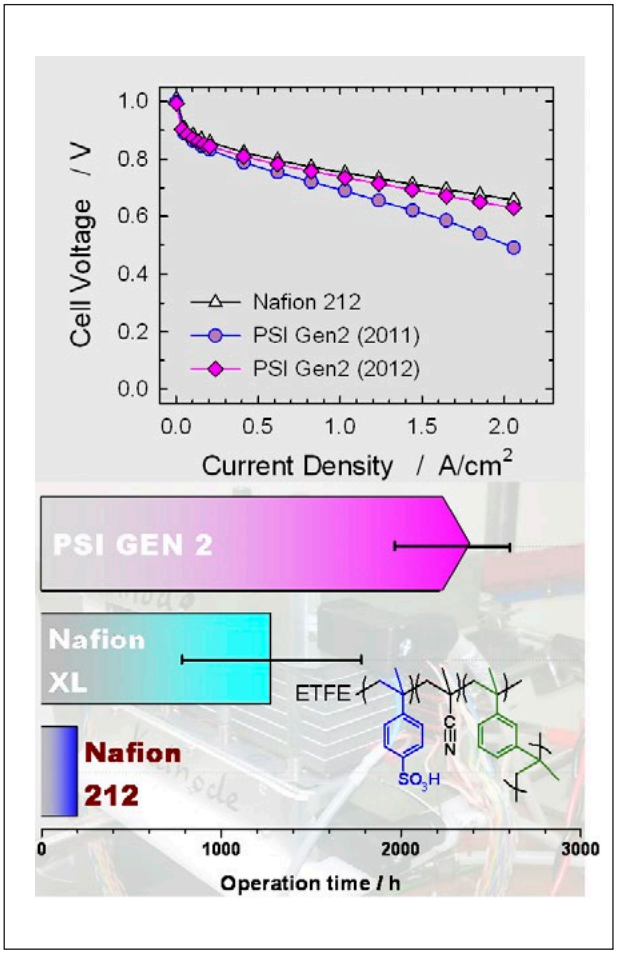

Figure 3: **Performance of our GEN2 radiation-grafted membrane inside a fuel cell, as well as its high in situ stability, compared with state-of-the-art Nafion membranes in accelerated-aging tests.**

Conclusion

PSI's Electrochemistry Laboratory is well set up to take on the challenge of future R&D for energy conversion and storage, not only with the accumulated experience and know-how of its personnel, but also based on its strategic position within the General Energy Department and within PSI, with its high-level large-scale facilities.

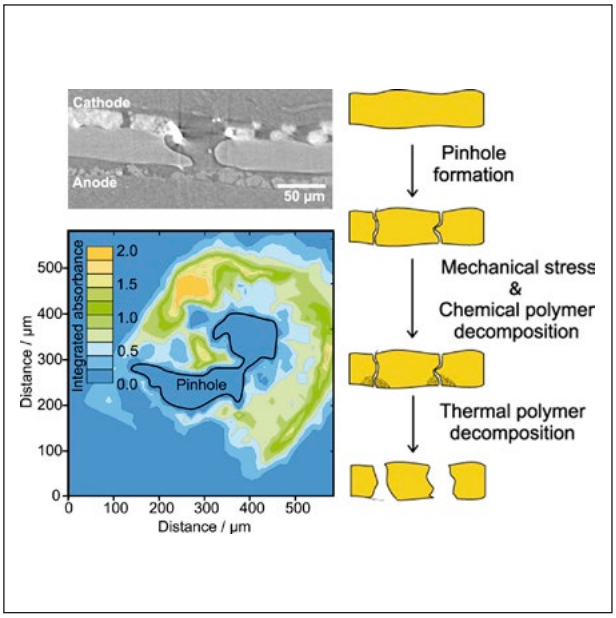

Figure 4: **Elucidation of membrane pinhole formation inside a fuel cell using a combination of X-ray tomographic and infrared microscopy at the SLS.**

References

[1] PSI Electrochemistry Laboratory – Annual Report 2011, p. 53.

[2] S. Kreitmeier, M. Michiardi, A. Wokaun and F.N. Büchi, *Factors determining the gas crossover through pinholes in polymer electrolyte fuel cell membranes*, Electrochim. Acta **80** 240–247 (2012).

Link

[1] Electrochemistry Laboratory (LEC): http://www.psi.ch/lec/

Transdisciplinary challenges – Networked research

Urs Elber and Alexander Wokaun, *Competence Center Energy and Mobility (CCEM)*

The Swiss Government has decided to implement a new energy policy, based on more renewable energy, the phasing out of nuclear power plants and, most importantly, the more efficient use of energy. To support this, it is planning to establish the relevant framework conditions: Laws and regulations, environmental taxes, and the funding of renewable energies and efficiencies. While many measures aim to establish a more conscious use of energy, others help to commercialize new technologies and concepts. But which technologies will be available in 30 years? How are we going to store energy in the most efficient way over time? How will our mobility needs be met? How do these questions relate to one another? These questions are transdisciplinary and the answers can be found in networked research. In order to address these questions, the ETH Domain founded the CCEM in 2006 as an institution to coordinate and finance energy research activities within the Domain, together with industrial partners, Universities and Universities of Applied Sciences.

CCEM – Part of the value chain

To create new products out of innovative research, many steps and actors are necessary, as illustrated by the value chain of research:

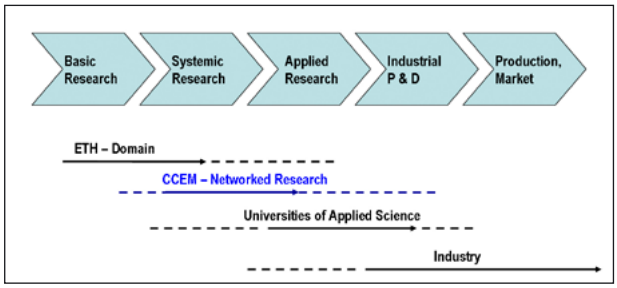

Figure 1: **The value chain of innovation from fundamental research to market introduction.**

The goal of the Competence Center for Energy and Mobility CCEM – with PSI as Leading House – is to decrease the gap between basic research and further developments, as well as connecting research partners, industries and governmental stakeholders. It does so by providing financial and organizational support to projects in this field. The CCEM was founded by the ETH Domain, but today in most of the projects, Universities of Applied Science and industries are contributing relevant tasks.

In 2012, CCEM issued its 8th call. Eight new proposals were submitted by ETH Domain institutions and their partners for joint projects.

As Figure 2 shows, CCEM is funding the projects with an average of 17 % of the total project costs, representing the "glue money" character of this approach. The direct industrial contribution of 19 % demonstrates the closeness of projects to today's industrial needs, and 23 % of competitive governmental funds indicate that the projects address important societal needs. According to the rules, CCEM funding cannot exceed the competitive governmental funding and the direct industrial contributions. Not more than a maximum of one-third of total projects costs are financed by CCEM. As this impact analysis is demonstrating, CCEM funds are well invested and have a multiplying effect.

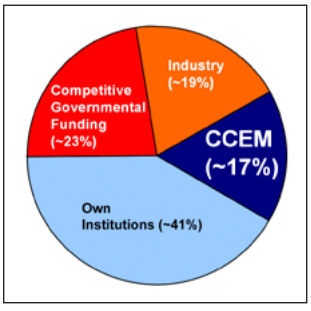

Figure 2: **Fractional share of CCEM seed funding and first-, second- and third-party contributions.**

New projects started in 2012

The Competence Center for Energy and Mobility extended its activities in 2012 with the following new projects emerging out of the 7th call:

- NO_x Reduction: In-cylinder emission reduction in large diesel engines
- UMEM: Sustainable cities and urban energy systems of the future – Urban Multiscale Energy Modelling
- HITTEC: Integration of a high-temperature thermoelectric converter for electricity generation in a solid-oxide fuel cell system

- DuraCAT: Highly durable oxide-based catalysts for polymer electrolyte fuel cells
- SOLAR FUELS: Solar thermochemical production of fuels from CO_2 and H_2O using ceria redox reactions
- SOLAR-HTG: Solar assisted hydrothermal gasification process
- CatPor: Catalysis in Porous media for automotive Applications
- MeAWT: Methods of Advanced Waste Treatment

In addition, the following projects have been approved and will start in 2013:

- ARRMATplus: Development of attrition resistant fluidised-bed methanation catalysts
- TeKaF: Temperaturabhängige Kapazitätsausnutzung für Freileitungsnetze

Together with CCES (Competence Center for Environment and Sustainability), two further projects have also been approved and initiated:

- OPTIWARES: OPTImization of the use of Wood As a Renewable Energy Source
- GEOTHERM-2: Geothermal Reservoir Processes: Towards the implementation of research into the creation and sustainable use of Enhanced Geo-thermal Systems

The evaluation process of the proposals submitted at the 8th call is still on-going.

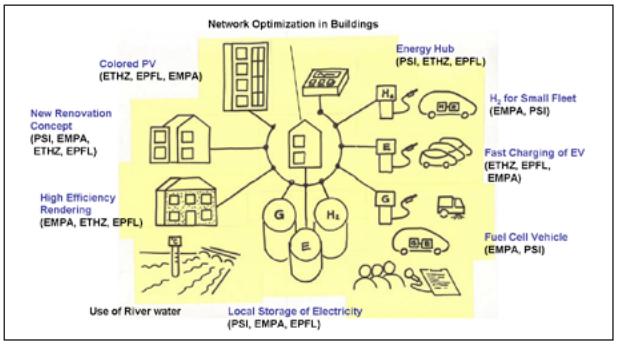

Figure 3: **Portfolio of projects for the next phase of the "Pilotregion Basel".**

Novatlantis – Sustainability in the ETH Domain

While CCEM focuses on technology and natural sciences projects, the transfer organization Novatlantis focuses on implementing these CCEM projects as P&D as well as "Lighthouse" projects in practice, supported mainly by cities, cantons and governmental agencies.

With the decided change in the energy politics of Switzerland, there is more need for new technologies supporting the necessary efforts. Long before the tragic events leading to this decision, CCEM had been facilitating and supporting institutional research in its core competence fields, i.e. energy and mobility. The actuality of many projects has thus become higher than ever.

As these projects have a systemic approach, many are developed to the point that the results can be put in place as P&D and Lighthouse projects. As the results are made visible, this supports decision makers in creating new framework conditions to enable the going-to-market process.

Novatlantis has a broad network and track record of enabling the implementation of Lighthouse projects. It creates and supports concepts for cities, cantons and national organizations to transfer new knowledge from science to the public. Impact is achieved on both sides: While the public then understands the new possibilities, industrial partners and researchers have an additional test environment and motivation. Altogether, Lighthouse projects are an indispensable part of the commercialization of new technologies.

Ten years of our contributions to the "Pilotregion Basel" have resulted in numerous activities and pilot facilities. A four-year prolongation of the partnership between the government and administration of the Canton Basel-Stadt, the ETH Domain, and local implementing agencies has been approved, with the goal of achieving concrete results (Figure 3).

In this context, the "Bauforum" in Basel and Zurich was a good opportunity to pass on the gained know-how to a wide audience of architects, planners, building owners, city officials and decision makers.

Receiving very positive resonance, the "Mobility Forum" has illustrated new opportunities, technologies and studies to fleet managers, mobility planners, and traffic and energy experts.

Further efforts have started to involve other regions of Switzerland in establishing Lighthouse projects and concepts developed by Novatlantis.

In most of the areas of current concern, ETH Institutions and CCEM are contributing to the development of the solutions needed for new energy and mobility demands.

CCEM and the future

In 2013, another Call for Proposals will be launched. More systemic research is needed, connecting researchers and research fields to new solutions.

Networked research is one answer to the inter- and transdisciplinary challenges present in the field of energy and the Swiss Government will be supporting Swiss Competence Centers for Energy in the future with its "Aktionsplan koordinierte Energieforschung". In the coming years, the activities of CCEM will be extended into these new Competence Centers to ensure that the experience gained is used as the basis for further progress.

Links

[1] Competence Center Energy and Mobility (CCEM): http://www.ccem.ch
[2] Novatlantis: http://www.novatlantis.ch

Basic and applied research, the motor for nuclear competence

J.-M. Cavedon, *Nuclear Energy and Safety Department (NES), PSI*

Although opinion on the role of nuclear production of electricity in the long-term Swiss energy mix is still divided, one clear statement has emerged: the need for keeping nuclear competence is undisputed. It has been the historical role of PSI's Nuclear Energy and Safety Department (NES), and will remain its duty, to keep this competence at the highest international level. We see our basic and applied research as the motor that powers our nuclear competence. Whether improving the accuracy of existing knowledge, extending it on rare, safety-relevant events, reaching ultimate atomic-level description of how radionuclides interact with matter, or exploring material under harsh irradiation conditions, the goal is the same: more and better knowledge to be applied to the safe and efficient operation of nuclear plants in Switzerland and in the world.

The future role of nuclear electricity supply in the energy mix of Switzerland is, two years after the enormous tsunami in Japan that crippled the Fukushima-Daiichi nuclear plant, still under political debate. Legally binding decisions are yet to be taken, but a ban on new nuclear plants on Swiss soil is likely. All stakeholders agree on one thing, however: whatever the decision on phase-out, and whatever its implementation speed may be, keeping nuclear competence is a must. We have demonstrated over the years at PSI that nuclear research at the international forefront is the motor that powers nuclear competence and keeps it at the highest level.

The worldwide renowned highest level of reliability, efficiency and safety of the Swiss nuclear power plants has been explicitly confirmed by the European Stress Test exercises, and we are proud to be at the root of the competence chain that enables such achievements to be made. We have selected this year's scientific and technical highlights of PSI's Nuclear Energy and Safety Department (NES) in order to illustrate how we have developed, and have maintained, our high nuclear competence level in 2012.

We have, for instance, increased the accuracy of existing software for the simulation of processes inside reactors, enriched software simulating severe accidents with additional physico-chemical phenomena, explored nuclear materials under extreme irradiation conditions and understood down to the atomic layer structure how a radionuclide is retained in a nuclear repository.

Computational simulation

Despite the exponential growth of computing power in the past five decades, we have not yet reached the computing capability that would allow true and full high-fidelity calculation of coupled neutronic and thermal-hydraulic events over very long time periods. However, needed developments are underway on new coupling schemes that simultaneously improve accuracy and reduce computational needs. Zerkak et al. report on such progress to the benefit of our STARS code platform (the NES LRS project **S**teady-State and **T**ransient **A**nalysis **R**esearch for the **S**wiss reactors). Benchmarking is carried out against two well-known postulated reference accident cases: the ejection of a control rod and a turbine trip. Birchley et al. report on a qualitative improvement of the MELCOR-based severe accident code platform. The evolution towards core meltdown may undergo acceleration in accidental situations where spent fuel is exposed to air. The standard saturating oxidation process may then be overrun by "breakaway", i.e. accelerated kinetics, where the nitrogen in the air is suspected of acting as a catalyst. In full international collaboration, the PSI breakaway oxidation model has been benchmarked against experimental data obtained in Europe (the QUENCH experiment at the Karlsruhe Institute of Technology, Germany) and in the USA (spent-fuel cladding oxidation and fire experiment at the Sandia National Laboratories). The breakaway phenomenon is now captured and introduced in the severe accident codes. Detailed understanding and modelling of the exothermal reactions leading to zirconium oxide and zirconium nitride is the next issue to be tackled.

MEGAPIE liquid-metal spallation target

A novel exploration, made in 2006 and possible only at PSI, was the 4-month-long irradiation of a liquid lead-bismuth eutectic (LBE) target by the most powerful proton beam in the world, delivered by our 2 mA high-intensity proton accelerator (HIPA). The MEGAPIE experiment is instrumental in testing the concept of accelerator-driven nuclear transmutation at the megawatt power level. After due target cooling and disassembly, time has now come for detailed post-irradiation examination. Dai et al. report this year on the first series of examinations, the non-destructive ones on the target window for the proton beam. After an irradiation time during which each atom of the T91 steel window was displaced as much as seven times (up to 7.1 displacements per atom), no crack or crack initiation was to be seen. Neither had a change in the wall thickness been detected. The proton beam fluence was deduced from the transmutation pattern of the safety window and had the expected, almost Gaussian, distribution profile. More detailed information on the MEGAPIE target calls for destructive analysis. Thanks to the availability of our Hot Laboratory and to our long years of expertise in handling highly radioactive components, Kuster et al. have initiated the extraction of more than 700 samples from the target. The LBE was removed in a careful low-temperature melting process, and the steel housing cut by blade and wire, under conditions that minimized the use of machining liquids and the associated waste volume. The successful operations of the reporting year will allow sample delivery to the international partners of the MEGAPIE experiment in 2013.
The expertise acquired over decades on proton accelerators, target technology and radioactive sample extraction, all present at PSI, were essential to the success of this experiment. The richest scientific fruits will be reaped in 2013, and beyond, by all international partners.

Radionuclides

Ultimate understanding of why and how a radionuclide is retained in a natural or a man-made material is the scientific foundation of the safety of a nuclear waste repository. We highlight this year the work of Tits et al., who have explained how the radioactive element neptunium is retained (sorbed) in the cementitious structures in which it will be contained within the future Swiss nuclear waste repository. By a combination of wet chemistry experiments and X-ray absorption spectroscopy at PSI's synchrotron X-ray beams and elsewhere, the authors have made clear that Np is well sorbed in all its valence states and for all pH conditions. The non-trivial behaviour of Np at valence 5 has also been satisfactorily explained.

Educational activities

Another essential activity for keeping nuclear competence is education. The Master's course in Nuclear Engineering, jointly offered by ETH Zurich and EPF Lausanne, also relies on PSI's collaboration as application laboratory for block courses, such as the Nuclear Computational Lab. We have also been able this year to secure the further common operation of our research Laboratory for Reactor Systems with its academically oriented sister structure, the Laboratory for Reactor Systems at EPFL, by the double appointment of Prof. Pautz as head of both, which re-establishes the historical leadership of Prof. Chawla over both the research and education units on reactor systems.

Looking forward

Many countries, including some in our neighbourhood, will continue their development and use of the nuclear energy source, most certainly making the necessary improvements to raise their measures against extreme events to levels reached long ago in Switzerland. The nuclear phase-out under discussion in Switzerland will therefore not improve the global nuclear safety in Europe. The last years of operation of nuclear plants may rather turn into a safety challenge, if the economic drive and the political will are not well matched during phase-out and post-operational periods. A weakening of the national scientific and technical competence on nuclear reactors and the nuclear fuel cycle, including the indispensable storage of nuclear waste, is something the country should not let happen in this context.
We hope the following examples of our activities will convince you that the whole personnel of the Nuclear Energy and Safety Department is fully engaged in basic and applied science that powers the maintenance of our competence and our educational efforts. We are devoted to the peaceful, safe and efficient use of nuclear fission as a sustainable source of energy, as long as it will be needed.

Improved temporal coupling schemes for thermal-hydraulic/neutronic analysis of LWR transients

Omar Zerkak, Damar Wicaksono, Konstantin Nikitin, Hakim Ferroukhi and Andreas Pautz,
Laboratory for Reactor Physics and Systems Behaviour (LRS), PSI

The high-fidelity computational simulation of Light Water Reactor accident-scenario transients allows ultimately for a better evaluation of the performance and safety margins of these reactors. This requires the use of complex calculation methodologies based on the intricate space-time coupling of different computational models that were originally designed for standalone usage. In this context, the temporal coupling scheme of the thermal-hydraulic analysis code TRACE with the core simulator SIMULATE-3K has been revised for higher numerical accuracy and reduced CPU time. The improvements obtained with the coupling schemes have been verified on the basis of the analysis of a control rod ejection accident and a turbine trip event.

The STARS Project [Link 1] – **S**teady-state and **T**ransient **A**nalysis **R**esearch for the **S**wiss reactors – is an international effort, whose main partner is the Swiss Nuclear Inspectorate, ENSI. One central goal of the project is to improve space-time resolution in the simulation of accidental transients of the Swiss Light Water Reactors (LWRs), in order to more accurately evaluate how safe the reactors are. This requires the development of complex multi-physics computational methodologies that operate an intricate space-time coupling of different simulation codes. The particular intention is to establish coupling schemes that provide more accurate and more efficient simulations when large detailed core models or very long transients are to be analysed.

In 2012, emphasis was given to assessing enhanced temporal coupling schemes for the TS3K coupled code, originally developed by Studsvik Scandpower and maintained by PSI. TS3K implements space-time coupling of the thermal-hydraulics (T-H) plant system code TRACE with the core transient simulation code SIMULATE-3K (S3K) [1]. The temporal coupling employs a conventional operator-splitting (OS) method, where the T-H solver (TRACE) uses power densities evaluated in the core at the end of the previous time-step. The neutronics solver (S3K) is provided afterwards with the new T-H feedback quantities needed to compute the nuclear reactions cross-sections, thus completing the time-step integration of the coupled problem. This results in a nearly fully explicit scheme that exhibits poor numerical accuracy and a stability conditioned by the time-step size.

To overcome these limitations and following the experience gathered from participation in the EU Nuclear Reactor Integrated Simulation Project (NURISP) [2], different possible

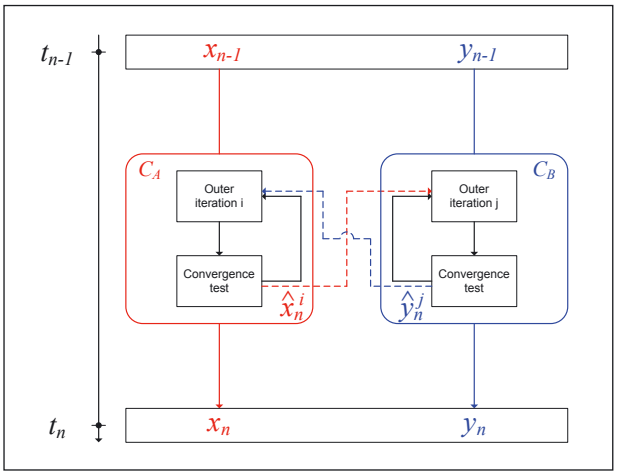

Figure 1: **Temporal coupling of two codes, C_A and C_B, based on a Fixed Point Iteration method.**

enhancements were devised to improve the temporal coupling in TS3K, with the objective of achieving a given target accuracy using larger time-step sizes than with the conventional OS method. Semi-implicit methods are one option, but these can lead to a deeper footprint in the source codes and result in a heavy maintenance overhead, as the TRACE and S3K codes are often modified by the developers. This prevents the use of the most accurate schemes, such as Approximate Block Newton methods. Thus, for practical reasons, the focus on semi-implicit schemes had to be limited to the more workable Fixed Point Iteration (FPI) methods, such as the one illustrated in Figure 1, which shows an FPI coupling scheme at the level of the solver outer-iterations of two codes, C_A and C_B.

Two temporal coupling schemes have been studied, namely:

a) The application to the conventional OS of a weighted time-

projection of the power (OS-WTP), which can theoretically bring about 2nd-order accurate prediction of the power variable; b) The semi-implicit predictor-corrector (PC) to advance the T-H solution. Also, an adaptive time-stepping algorithm (ATS) applicable to all the investigated coupling schemes has been implemented. The ATS consists of adapting the time-step size by tracking the fastest dynamical scales of the main physical variables exchanged by the two codes (here the power and the T-H feedback quantities) and to thereby optimise the trade-off between accuracy and CPU time.

Evaluation of the coupling schemes

To assess the developed schemes, two examples of LWR reactivity insertion transients were analysed – a neutronics-driven transient, such as the PWR Rod Ejection Accident (REA), and a T-H driven transient such as the BWR Turbine Trip (TT) [3]. Very tight convergence criteria were used in TS3K to ensure the consistent evaluation of the schemes. Some of the results obtained for the PWR REA are shown in Figure 2.

Here, the power peak error as a function of the time-step size is compared between the OS-WTP approach (using two variants of the weighting γ applied to the temporal projection of the power), the PC scheme and the conventional OS method. The error is calculated relative to the solution obtained with a time-step of 10^{-4} s – the recommended minimum in S3K. One can observe that the time-step needed by the OS-WTP (with $\gamma = 1$) and the PC to achieve a convergence error lower than 1% is more than 3 times larger than in the conventional OS.

Analogous results were obtained for the BWR TT transient and Figure 3 shows the results obtained with the various schemes applying the ATS algorithm.

Here, the relation between power peak error and CPU time speed-up (achieved by varying a "safety factor" in the ATS algorithm that limits the maximum fractional change of any state variable between two consecutive time-steps) is shown, along with the 1% error and 20 times speed-up lines, noting that the lower right quadrant constitutes an optimal trade-off between CPU time and accuracy. Thus, even with the slowest speed-up, the conventional OS method fails in reducing the error below 1%. In contrast, with the ATS applied to the OS-WTP or PC schemes, a speed-up factor of 20 can be achieved while maintaining high accuracy.

Thus, the OS-WTP and PC schemes, combined together with the ATS algorithm, allow the error to be reduced to levels where numerical diffusion becomes non-negligible, if not predominant. Further studies will be needed to determine an optimal safety-factor for the ATS algorithm. Also, the possibility of parallelizing the implementation of the coupling will be investigated, to further reduce CPU usage and enable coupling strategies at a deeper level of the solvers' iteration loops.

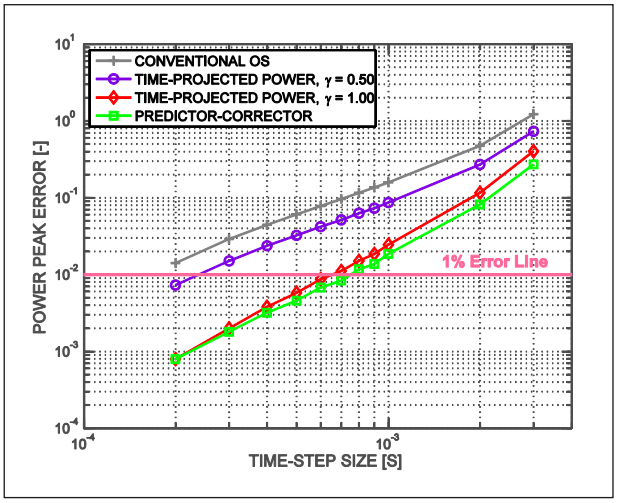

Figure 2: **PWR REA - Power peak error as a function of the time-step size for different coupling schemes.**

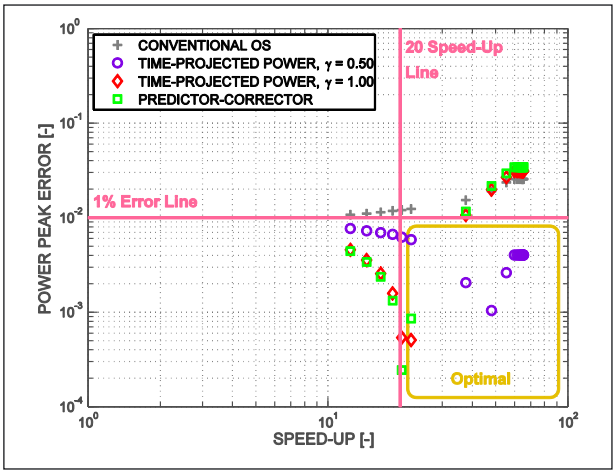

Figure 3: **BWR TT - Power peak error as a function of the CPU time speed-up using adaptive time-stepping with different coupling schemes.**

References

[1] J. Judd and G. Grandi, *Simulate-3K linkage with reactor system codes*, NURETH-14, Toronto (CA), 25–30 September 2011.

[2] O. Zerkak, M. Zimmermann, I. Gajev and T. Kozlowski, *Specifications for advanced temporal coupling schemes in the NURESIM platform*, NUclear Reactor Integrated Simulation Project, NURISP, D.3.2.1.2 (2011).

[3] D. Wicaksono, O. Zerkak, K. Nikitin, H. Ferroukhi and R. Chawla, *Application of power time-projection on the operator-splitting coupling scheme of the TRACE/S3K coupled code*, Submitted to M&C 2013, Sun Valley (USA), 5–9 May 2013.

Link

[1] STARS Project: http://stars.web.psi.ch/

Modelling of the accelerated oxidation of nuclear fuel rod cladding during air ingress sequences

J. Birchley, L. Fernandez Moguel and B. Jäckel, *Laboratory for Thermal-Hydraulics (LTH), PSI*

The MELCOR and SCDAPSim codes are used in tandem in Switzerland to analyse different aspects of severe accident transients in light water reactors. In order to improve the simulation of air ingress, a new oxidation model has been developed at PSI which captures the accelerated oxidation that is observed to occur in an air environment. Such situations are important in connection with spent fuel accident scenarios and are receiving considerable attention from regulators following the accident at Fukushima. The model had already been assessed against data from separate-effects experiments, and has now been successfully implemented into special versions of SCDAPSim and MELCOR 1.8.6. It has been shown to reproduce the intended oxidation behaviour and gives similar results when used in both codes. Initial assessment studies have shown good agreement with recently obtained experimental data.

Background

Air ingress scenarios can arise in connection with spent fuel loss of coolant accidents and certain reactor sequences [1]. The presence of air can lead to accelerated oxidation of the Zircaloy cladding where the chemical kinetics switches from parabolic (the rate decreases as the oxide layer builds up) to linear (the rate stays constant). Air ingress is typically associated with poor heat transfer, while the 85% higher heat of reaction drives the heating and core degradation processes further. Furthermore, the exposure of uranium dioxide to air at high temperatures can lead to increased release of some fission products [2]. Correct modelling of the air oxidation is necessary to capture the core damage escalation and provide the boundary conditions for nuclide release.

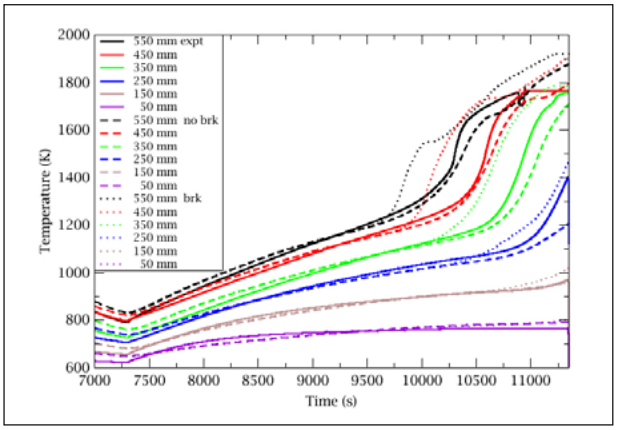

Figure 1: **Bundle temperatures in QUENCH-16 air phase. Solid=data; dashed=breakaway disabled; dotted=breakaway enabled.**

A new oxidation model developed at PSI captures the accelerated oxidation in air, using separate-effects data obtained under uniform isothermal conditions. The key feature of the model is the accelerated (breakaway) kinetics. Data available at the time indicated that nitrogen acts as a catalyst, but not as an important active species. Since there are remaining uncertainties in the breakaway process, this feature can optionally be disabled to reproduce the standard parabolic oxidation. The main phase of assessment was simulation of integral transient data using the reactor analysis codes SCDAPSim and MELCOR containing the new model [Link 1]. It was first necessary to implement the model in local code versions, which was achieved with the help of significant support from the respective code development teams.

Recent air ingress experiments in the QUENCH facility at Karlsruhe Institute of Technology (KIT) [3] and spent fuel experiments at Sandia National Laboratories (SNL) have yielded important new data with which to assess the model under representative accident conditions, and verify its correct implementation in the codes.

Simulation of QUENCH air ingress tests

The QUENCH-10 and -16 tests each comprised oxidation in steam followed by air ingress and subsequent reflood, thus simulating a severe accident involving reactor vessel breach. QUENCH-16 included a long period in which all the oxygen was consumed in order to study the interaction between a partially oxidised cladding and nitrogen. Code-data comparisons

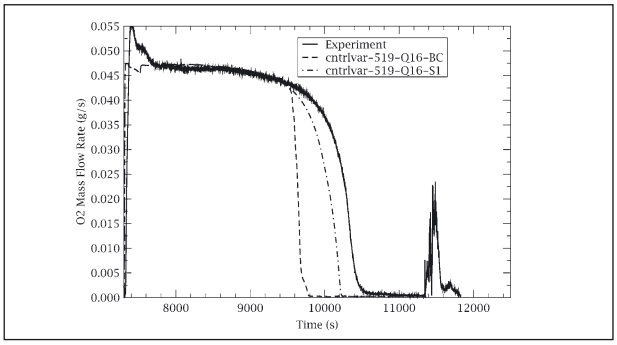

Figure 2: **Oxygen consumption in QUENCH-16. Solid=data; dashed=breakaway enabled; dot-dashed=breakaway disabled.**

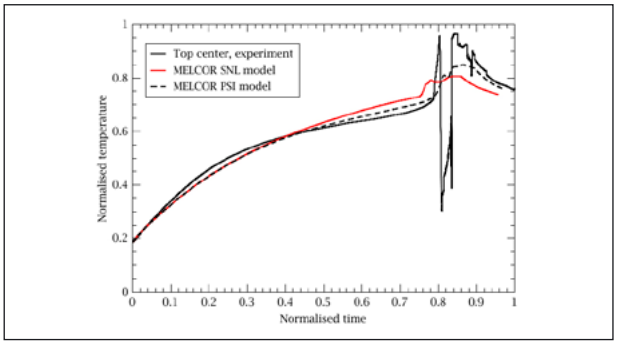

Figure 3: **Thermal response during spent fuel test 2. Solid=data; dotted=SNL model, dashed=PSI model.**

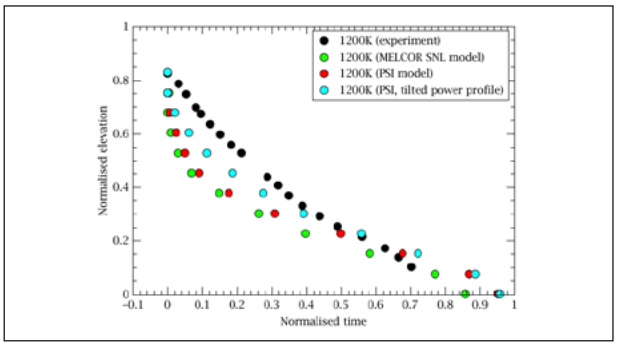

Figure 4: **Downward propagation of fire in spent fuel test 2. Black=data; green SNL model; red=PSI model; cyan=PSI model with modified power profile.**

for the thermal response and oxygen consumption during the air ingress are shown in Figures 1 and 2, respectively.
The results for oxygen consumption using both codes agree with each other when breakaway is enabled, and are identical with the classical parabolic model when it is disabled. Good agreement with the data is achieved, bearing in mind the above-mentioned uncertainties.

Simulation of spent fuel tests

An experimental project was performed by SNL on cladding oxidation, ignition and fire propagation in full-scale PWR fuel assemblies in dry air, in two phases. Phase 1 was performed with a single assembly and Phase 2 with a cruciform arrangement of five assemblies. In both cases, ignition was first observed near the top of the central region, and the fire spread downward and outward. We are currently analysing the data using MELCOR with the new model.
Figure 3 compares the measured and calculated thermal response near the top of the fuel assembly in Phase 1. The classical parabolic kinetics showed a slower thermal escalation and delayed ignition compared with the data.
Figure 4 compares the fire propagation and the occurrence of breakaway at the different locations. The results show that first ignition was triggered by breakaway, but the mechanism for propagation was thermal radiation to the cooler region ahead of the flame. Highly encouraging is the agreement with the data-tuned SNL model. Discrepancies in the propagation are due to uncertainties in the experimental power profile.

Conclusions and outlook

The PSI oxidation model has been implemented into the SCDAPSim and MELCOR codes used for reactor accident analysis. Code and model comparisons for integral transient conditions verify the correct implementation.
Comparison with data for the oxygen consumption reveals some differences, as may be expected due to the currently limited knowledge of the breakaway process.
The data showed unexpectedly high formation of zirconium nitride under oxygen-starved conditions, followed by re-oxidation of the nitride during reflood in the QUENCH-16 test and in the later stages of the spent fuel experiments. Both reactions are exothermic and have a strong impact on the fuel damage. The experiments reveal a need to model those reactions.

References

[1] D.A. Powers et al., *A Review of Technical Issues of Air Ingression during Severe Reactor Accidents*, USNRC NUREG/CR-6218, SAND94-0731, Sandia National Laboratories, September 1994.
[2] A. Auvinen et al., *Progress on Ruthenium Release and Transport under Air Ingress Conditions*, Nucl. Eng. and Design **238**(12) 3418–3428 (2008).
[3] J. Birchley et al., *Conduct and Analytical Support to Air Ingress Experiment QUENCH-16*, 5th European Review Meeting on Severe Accident Research (ERMSAR-2012), Cologne, Germany, 21–23 March 2012.

Link

[1] Severe Accident System codes at PSI: https://sacre.web.psi.ch/codes/index.htm

Sample extraction on the MEGAPIE liquid lead-bismuth spallation neutron target

Daniel Kuster, Viktor Boutellier, Sandro Hahl, Rudolf Schwarz, Andreas Spahr, Hans Leu, Herbert Schweikert, Yong Dai, Michael Wohlmuther, Didier Gavillet and Andreas Lagotzki, *Hot Laboratory (AHL), PSI*

MEGAPIE is an experiment aiming at demonstrating the safe operation of a liquid-metal spallation target at a beam power level of 1 MW in the SINQ target station at PSI. It is an international collaboration of ten partners and is of relevance for accelerator-driven reactor systems, in which an accelerator and target provide the neutrons necessary to maintain a fission reaction. The MEGAPIE experiment will be an important ingredient in defining and initiating the next step towards building a target for the accelerator of a dedicated accelerator-driven reactor system (ADS). These reactor systems would use nuclear waste to produce energy, at the same time reducing the overall amount of radioactive waste or transmuting long-lived radioactive nuclides into short-lived ones. Sample extraction on parts of the target, including all preparations and handling in the PSI hot cells, began in 2011 and has continued in 2012.

After the four-month period of operation of the MEGAPIE target in the PSI Swiss Spallation Neutron Source (SINQ) in 2006 [Link 1], the target was cut into pieces at the Swiss interim storage facility for radioactive waste – the "Zwischenlager Wuerenlingen AG" (ZWILAG) – adjacent to PSI.

Target preparation

Ten cylindrical segments (maximum diameter 400 mm, maximum height 300 mm), filled with PbBi, arrived at the Hot Laboratory in the spring of 2011, when first inspection was made and PbBi samples taken [1]. After inactive test operation for melting and cutting, the active part of the procedure followed in 2012 in the hot cell, with the melting of all the PbBi out of the segments using our oven, which was designed in-house, and cutting and cleaning the samples from the steel housing rings. To avoid changing the sample structure, the maximum temperature in the melting process was kept below 200 °C. To avoid the escape of polonium and tritium, the oven was kept under low pressure during the melting process. After melting, the oven was opened and vented with argon through a filter system consisting of 2 HEPA and 2 activated carbon filters, as well as 3 water columns (tritium filter). In the exhaust, several filter papers showed no contamination of the exhaust air after flooding three times with argon.

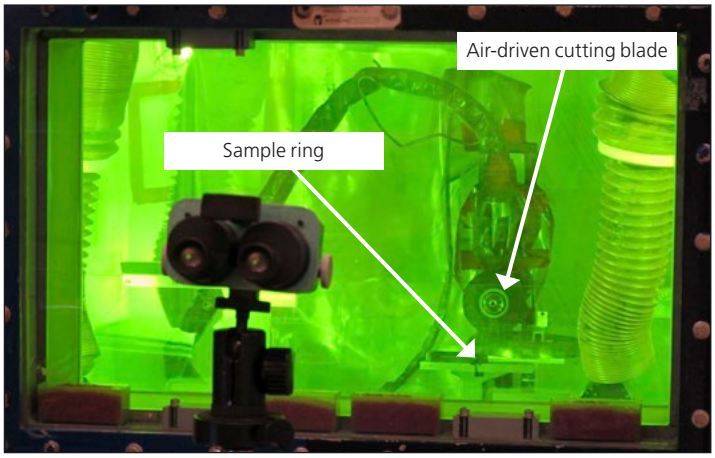

Figure 1: **First cutting with CNC milling machine in the hot cell.**

Target sectioning

The first sectioning in the hot cell was followed by numerically controlled milling, using a machine of type "OPTIMUM BF 20 Vario", with an air-driven rotating cutting blade.
This sectioning was performed without using any cooling fluid. To keep the temperature of the samples below 200 °C, control of the blade feed was very sensitive. Also, the cutting blade was changed quite frequently.
To avoid high contamination in the hot cell, the milling machine was encased in an additional alpha box (see Figure 1) and an exhaust tube was connected from the machine housing directly to the hot-cell exhaust filter.
Before final wire cutting, the samples were cleaned in a hot oil bath, followed by wiping off the rest of the PbBi and cleaning them finally in an HNO_3 acid bath for some minutes.

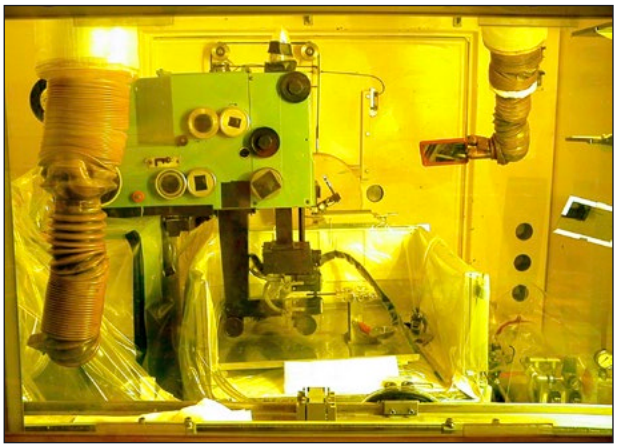

Figure 2: **EDM cutting in the hot cell.**

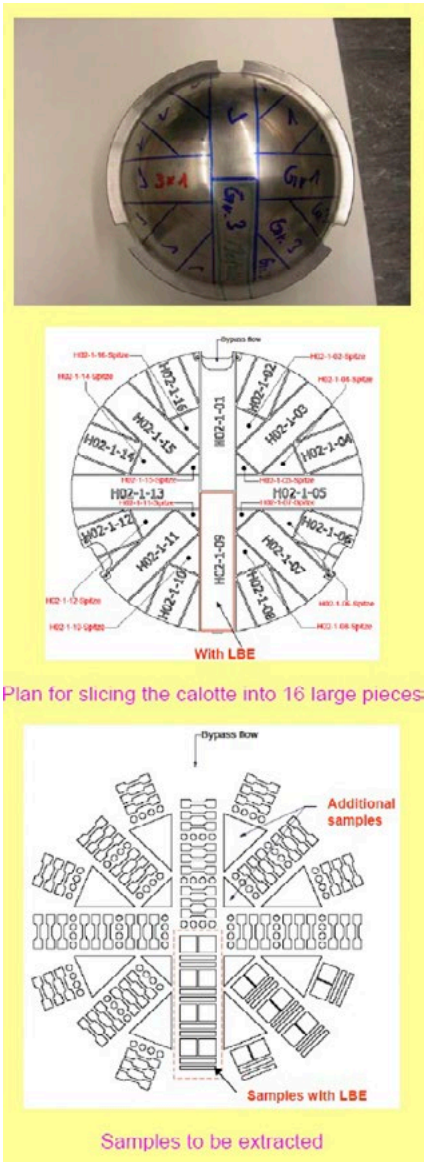

Figure 3: **How samples were taken from the beam window of the MEGAPIE target.**

Final wire cutting started in November 2012 and is planned to be completed by the middle of March 2013. For this, we used an EDM machine of type "AGIE EDM 250". The advantage of this EDM type of device is that the control unit is completely separated from the machine. This allows the electronic control unit to be positioned outside the hot cell, thus making sure that the radiation within the cell has no influence on the numerical control of the machine. During cutting, a water jet between the wire and the samples replaced the usual water tank. This allows cutting to be carried out with only 20 litres of water in the hot cell and, after the cutting process, this water evaporates within a few hours.

Contamination

The maximum removable surface hot-cell contamination measured was 12 Bq/cm^2 alpha and <15,000 Bq/cm^2 beta/gamma. After every process step, the hot cell was cleaned, first with manipulaters, then followed by direct cleaning by staff wearing forced-air ventilated suits.

By the beginning of April 2013, more than 700 samples should be ready for testing at PSI and the MEGAPIE partner hot laboratories, after shipping in special transport containers.

After sample preparation, all waste will be packed into special KCT-12 waste containers. The waste that is expected includes the milling machine, the oven, the filter units from the oven and from the EDM machine, the rest of the MEGAPIE segments, tools and decontamination materials. The total volume of the expected waste is about 2 m^3. Finally, the container will be filled with concrete and prepared for end storage.

Two hot cells (2.5 m × 2.5 m each) were used for 1 year when analysing the MEGAPIE segments in the hot cells, for PbBi sample extraction, thickness measurements of the beam window, melting out of the PbBi, sample cutting with the milling and EDM machines, sample cleaning and waste disposal.

Conclusions

The results of this sample testing will provide an important material indication for further liquid metal targets following the MEGAPIE project.

Reference

[1] M. Wohlmuther and W. Wagner, *PIE preparation of the MEGAPIE target*, Journal of Nuclear Materials **431** 10–15 (2012).

Link

[1] The MEGAPIE project: http://megapie.web.psi.ch/

Non-destructive testing and proton distribution profile determination of the MEGAPIE target

Yong Dai, *Laboratory for Nuclear Materials (LNM);* Michael Wohlmuther, *High Intensity Proton Accelerators (ABE);* Viktor Boutellier, Didier Gavillet, Sandro Hahl, Daniel Kuster, Hans-Peter Linder, Andreas Lagotzki, Rudolf Schwarz and Holger Wiese, *Hot Laboratory Division (AHL);* Kurt Geissmann, Knud Thomson and Werner Wagner, *Spallation Neutron Source Division (ASQ);* Patrick Suter, Rudolf Thermer and Charles Zumbach, *Mechanical Engineering Sciences (AMI), all PSI*

The MEGAPIE test, performed at the SINQ facility at PSI in 2006, was the first time a liquid lead-bismuth eutectic (LBE) spallation target had ever been operated in the 1 MW regime. The container window, through which the proton beam passed into the target, is now being visually inspected and non-destructively tested ultrasonically. No visible failure and no detectable change in thickness in the beam window area have been detected. Gamma mapping was also performed and the results were used to evaluate the accumulated proton fluence distribution profile – the input data for determining irradiation parameters. The results of these investigations will provide important information for the R&D of future accelerator-driven systems (ADS) for nuclear waste transmutation.

MEGAPIE [Link 1] was the unique experiment, performed at the SINQ facility at PSI in 2006, in which a liquid lead-bismuth eutectic (LBE) target was operated in the 1 MW regime. The post-irradiation examination (PIE) of the target components exposed to high fluxes of high-energy protons and spallation neutrons in a flowing LBE environment is one of most important tasks of the MEGAPIE project. The PIE of MEGAPIE will provide important information for the R&D of future accelerator-driven systems (ADS) for nuclear waste transmutation. Non-destructive testing (NDT), including visual inspection and ultrasonic measurement, is an important part of the PIE, and can detect relatively large failures and changes in the proton beam window area of the so-called T91 calotte, the most intensively irradiated part of the LBE container, made of ferritic/martensitic T91 steel. Gamma mapping on the T91 calotte is necessary for evaluating the accumulated proton fluence distribution profile, which is needed for determining the irradiation parameters of the target.

Non-destructive testing on the T91 calotte

After operation, the MEGAPIE target cooled down without the liquid LBE being removed. The target was sawed into large pieces at ZWILAG (the interim storage facility for radioactive waste, adjacent to PSI [Link 2]), with solidified LBE inside it [1]. Visual inspection was performed on some selected pieces in PSI's hot cells. It was observed at ZWILAG that some foreign material had been deposited on the beam window [1]. This was sticking to the calotte and was difficult to remove. Figure 1a shows the appearance of the T91 calotte after irradiation and Figure 1b its appearance after removal of the deposited material. Observation using a high-resolution video camera installed in the hot-cell showed no visible failure in the proton beam window area.

The LBE in the selected pieces was removed by melting in a specially designed oven. This melting was performed in an argon atmosphere at below 180°C. After melting of the LBE, the selected pieces were again inspected. Figure 2 shows the appearance of the inner surface of the T91 calotte after LBE removal. It can be seen that the inner surface of the calotte was only partially covered with LBE. The same is true for the other pieces. This means that the surfaces of components were not well wetted by LBE during irradiation. Again, no evidence of failure was found.

The material deposited on the T91 calotte is black within its bulk, but with a thin white surface layer on some parts. Analysis using energy-dispersive X-ray spectroscopy (EDX) indicated that the black material contained mainly carbon (~80 at.%) and oxygen (~20 at.%), while the white material in the surface layer was mainly silicon oxide with some carbon content. The deposited material was most likely produced from oil leaked out of the secondary oil-cooling loop.

Ultrasonic measurements were conducted on the proton beam window of the T91 calotte before and after irradiation. Before irradiation, the measurement was conducted before filling the calotte with LBE. After irradiation, the measurement was

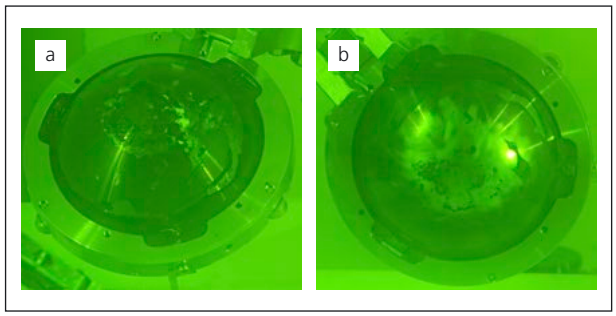

Figure 1: **Photos taken through the glass window of a hot-cell showing: (a) the T91 calotte after irradiation, (b) the T91 calotte after removal of the deposited material.**

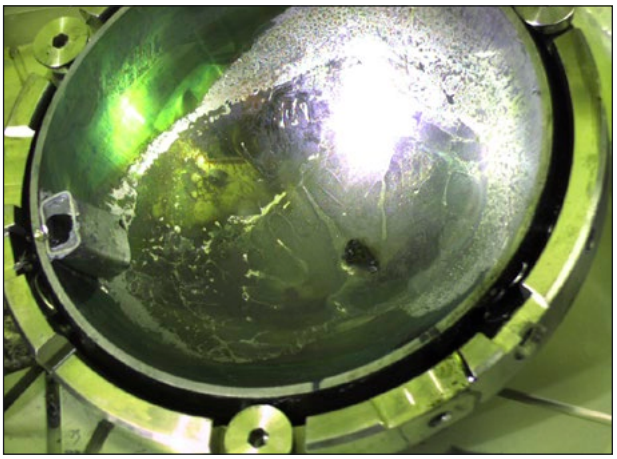

Figure 2: **The inner surface of the T91 calotte after melting and removing the LBE.**

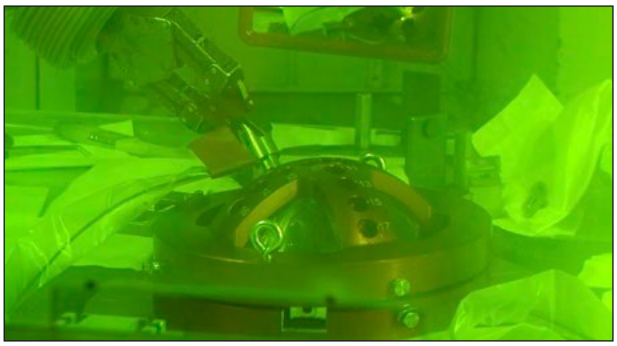

Figure 3: **Ultrasonic measurement being made of the T91 calotte wall thickness in a hot-cell.**

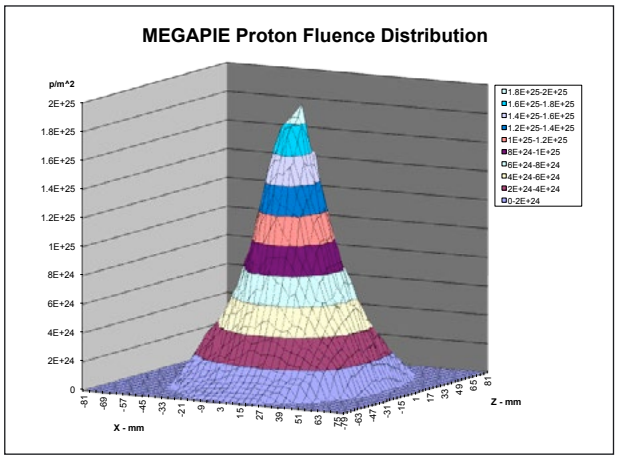

Figure 4: **3D view of proton fluence distribution.**

done on the calotte when it was fully filled with solidified LBE. In order to repeat the measurement made before irradiation, a special fixture was constructed for hot-cell application (see Figure 3). The thickness measured at 102 positions in the proton beam window area demonstrated that, within the precision of the measurement of about 5 µm, no change in the wall thickness in the proton beam window was produced by LBE corrosion after 4 months of operation.

Gamma mapping on the $AlMg_3$ calotte of the safety container

As in the case of STIP (SINQ Target Irradiation Program) irradiation [2], gamma mapping of the $AlMg_3$ proton beam window of the safety-container was necessary for evaluating the distribution profile of the accumulated proton fluence after operation. Gamma-mapping, i.e. conducting gamma spectrometry measurements point by point over an area, was conducted in steps of 4 mm over a projection area of 160×160 mm^2, and a full gamma spectrum obtained at each measuring position. ^{22}Na was the dominant isotope detected. Since the $^{27}_{13}Al \rightarrow {}^{22}_{11}Na$ reaction has a threshold energy of about 30 MeV, ^{22}Na was essentially produced by high-energy protons. Therefore, the distribution of the proton fluence can be deduced from the distribution of ^{22}Na after geometrical corrections. Figure 4 presents a 3D view of the accumulated proton fluence distribution and shows that the maximum proton fluence of the MEGAPIE target was $1.9\times10^{+25}$ p/m^2. The proton fluence distribution was used as the input data of further neutronics calculations of irradiation parameters. The results indicate that the maximum irradiation dose was 7.1 dpa (displacements per atom). Detailed analysis of surface, microstructure, and mechanical properties will be conducted in 2013.

References

[1] M. Wohlmuther and W. Wagner, *PIE preparation of the MEGAPIE target*, Journal of Nuclear Materials **431** 10–15 (2012).

[2] Y. Dai, R. Brun, W. Gao, K. Geissmann, S. Hahl, H. Hou, Y. Huang, H.P. Linder, B. Long, A. Spahr, P. Vontobel, W. Wagner, H.L. Wang and L. Zanini, *The fourth SINQ Target Irradiation Program, STIP-IV*, Journal of Nuclear Materials **431** 2–9 (2012).

Links

[1] The MEGAPIE project: http://megapie.web.psi.ch/

[2] ZWILAG: http://www.zwilag.ch/en/

Immobilization of redox-sensitive actinides in cementitious materials: The case of neptunium

Jan Tits, Xavi Gaona, Rainer Dähn and Erich Wieland, *Laboratory for Waste Management (LES), PSI*

Calcium silicate hydrate (C-S-H) phases are major components of cementitious materials planned to be used in low- and intermediate-level radioactive waste (L/ILW) disposal, due to their sorption properties and long-term stability. The present study shows that the sorption behaviour of the different redox states of neptunium (Np^{IV}, Np^{V} and Np^{VI}) on C-S-H phases strongly depends on differences in their hydrolysis behaviour at high pH. Variations in the chemical composition of the solids only have a minor influence on uptake processes. The results will help in assessing the safety of the L/ILW repositories that Switzerland needs to build.

It is planned to use cementitious materials in deep geological repositories for low- and intermediate-level radioactive waste (L/ILW) in many countries, for conditioning of the waste and as a backfill material in waste containers and tunnels. L/ILW contains redox-sensitive actinides such as neptunium (Np), which may exist in the oxidation states +IV, +V and +VI in a cementitious environment under reducing or oxidizing conditions.

The uptake of radionuclides by cemenitious materials is an important factor influencing their release from the repository into the surrounding host rock. A profound understanding of the mechanisms controlling this uptake is essential to enable a detailed assessment of the long-term safety of cement-based repositories to be made.

Calcium silicate hydrate phases (C-S-H phases) are major constituents of cementitious materials. They may control the retardation of radionuclides in the cementitious near field due to their favourable sorption properties and their long-term stability during cement degradation. C-S-H phases have a layered structure built up of Ca octahedral sheets linked on each side to chains of Si tetrahedra and interlayers containing H_2O and Ca cations. Metal cations can sorb either on the silanol sites (≡Si-OH) at the edges of the C-S-H structures or by exchanging for Ca in the C-S-H interlayer.

Wet chemistry experiments

Actinides such as Np are classified as hard Lewis acids [1] and thus exhibit a strong affinity for oxygen-containing hard bases, such as the surface hydroxyl groups of C-S-H phases. The strength of the resulting ionic bond is influenced by the effective charge of the actinides; i.e. sorption becomes stronger with increasing effective charge (e.g. [1]). Thus, in the case of Np, uptake by C-S-H phases is expected to decrease in the order: $Np^{IV}(4) > Np^{VI}O_2^{2+}(3.3) > Np^{V}O_2^{+}(2.2)$, where the numbers in brackets represent the effective charge of the respective Np species.

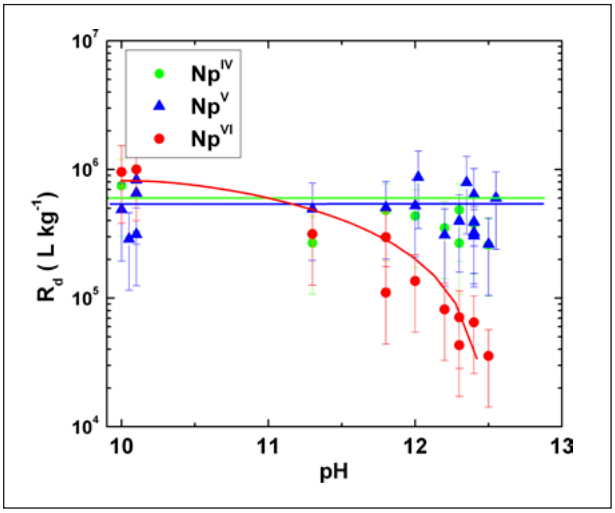

Figure 1: **Np^{IV}, Np^{V} and Np^{VI} uptake by C-S-H phases.**

Batch sorption experiments were carried out on C-S-H phases with ^{239}Np under reducing conditions (Np^{IV}), slightly oxidizing conditions (Np^{V}) and strongly oxidizing conditions (Np^{VI}). The different redox conditions were established by applying either reducing (Na-dithionite) or oxidizing (Na-hypochlorite) agents. Uptake of the radionuclides was quantified in terms of the distribution ratio $R_d = C_{sorb}/C_{sol}$, with C_{sorb} being the moles of radionuclide sorbed per kg sorbent and C_{sol} the aqueous radionuclide concentration at equilibrium (Figure 1).

Under reducing conditions, very strong, pH independent, uptake of Np^{IV} by C-S-H phases was observed in the pH range $10 < pH < 13.3$, as expected from its high effective charge of

+4. Similarly high, and nearly pH independent, R_d values were obtained for Np^{V} taken up by C-S-H phases, notwithstanding the much lower effective charge (+2.2) of the $Np^{V}O_2^{+}$ cation. R_d values for Np^{VI} were found to be similar in value to those determined for Np^{IV} and Np^{V} at pH = 10. With increasing pH, a significant decrease in R_d values was observed compared with Np^{IV} and Np^{V}. The unexpectedly strong uptake of Np^{V} is partially explained by its weak hydrolysis behaviour compared with the other Np redox states: In the pH range 10<pH<13.3, Np^{IV} and Np^{VI} form hydrolysed species $Np^{IV}(OH)_4$, $Np^{VI}O_2(OH)_3^{-}$ and $Np^{VI}(OH)_4^{2-}$, whereas the dominating Np^{V} species in this pH range are $Np^{V}O_2^{+}$ and $Np^{V}O_2OH$. The presence of several negatively charged hydroxyl groups in the coordination sphere of the Np^{IV} and Np^{VI} aqueous species hinders their binding to surface OH groups of the C-S-H phases because the resulting increased electrostatic repulsion between the OH ligands destabilises the Np-surface bond [2]. The uptake of Np^{V} species is less hindered due to the lower number of OH ligands. In the case of Np^{VI}, electrostatic ligand repulsion allows a maximum of 4 OH groups around the Np^{VI} cation [2], meaning that the $Np^{VI}O_2(OH)_4^{2-}$ species, dominant above pH = 12, cannot sorb (addition of a surface OH group), resulting in decreasing R_d values.

EXAFS investigations

Extended X-ray Absorption Fine Structure Spectroscopy (EXAFS) was employed to determine the local coordination environment of the sorbed Np in its different oxidation states. Experiments were conducted at beamline BM20 of the European Synchrotron Radiation Facility, Grenoble, France (ESRF), with EXAFS spectra recorded on C-S-H samples loaded with Np^{IV}, Np^{V} and Np^{VI} (~0.04 mol kg^{-1}) and equilibrated for 2 months [3, 4]. In the case of Np^{IV} sorbed on C-S-H phases, this technique allowed the type of neighbouring atoms, the coordination number and the distances between Np an its neighbouring atoms to be determined. Data analysis showed that the coordination environment of the sorbed Np^{IV} species consists of ~8 O atoms at ~2.3 Å, 3–5 Si atoms at ~3.6 Å and 8–12 Ca atoms at ~4 Å. The large number of neighbouring Si and Ca atoms indicates that the sorbed Np^{IV} species are predominantly incorporated in the C-S-H interlayers (Figure 2).
In the case of the C-S-H samples doped with Np^{V} and Np^{VI}, data interpretation was less straightforward. Significantly longer distances to the axial O atoms and shorter distances to the equatorial O atoms for the Np^{V} sorbed species compared with the aqueous species, however, suggest that most of the H_2O molecules are detached from the Np^{V} coordination sphere upon uptake by C-S-H phases. This indicates incorporation in the C-S-H structure rather than surface sorption of Np^{V}. In the case of C-S-H phases loaded with Np^{VI}, the EXAFS data did not allow a distinction to be made between surface adsorption and incorporation into the C-S-H structure.

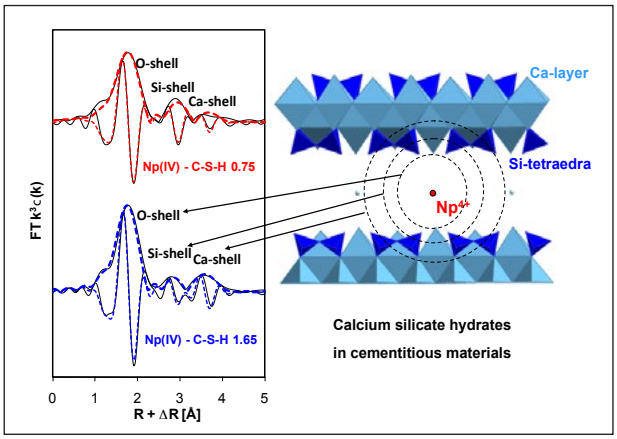

Figure 2: **Fourier transforms for Np(IV) taken up by C-S-H phases (left) and the corresponding structural interpretation (right).**

The study suggests that the specific local environment of the C-S-H interlayer may significantly contribute to the stabilisation of sorbed Np species, thus reducing the importance of the effective charge of the Np species on the sorption bond strength.

Conclusions

The present study provides clear evidence that the uptake of Np^{IV}, Np^{V} and Np^{VI} by C-S-H phases under high pH conditions is not solely controlled by their effective charge, as expected for hard Lewis acids. The similar R_d values observed for the uptake of the different Np redox species is explained partially by their different hydrolysis behaviour and the electrostatic repulsion effects between the OH groups of the hydrolysed species, and partially by the specific local coordination environment in the C-S-H interlayers shown by EXAFS to be the preferred Np sorption sites. Thus, uptake in the C-S-H interlayers is an important mechanism controlling the long-term immobilisation of Np in a cement-based repository.

References

[1] G.R. Choppin, Radiochim. Acta **32** 43 (1983).
[2] V. Neck et al., Radiochim. Acta **88** 815 (2000).
[3] X. Gaona et al., Environ. Sci. Technol. **45** 8765 (2011).
[4] X. Gaona et al., Appl. Geochem. **28** 109 (2013).

Link

[1] Laboratory for Waste Management: http://les.web.psi.ch/

Reconstruction of atmospheric lead concentrations in Russia since AD 1680

Anja Eichler, Leonhard Tobler, Gabriela Gramlich and Margit Schwikowski, *Laboratory of Radiochemistry and Environmental Chemistry (LCH), PSI, and Oeschger Centre for Climate Change Research, Bern University;*
Stella Eyrikh, Natalia Malygina and Tatyana Papina, *Institute for Water and Environmental Problems, Barnaul, Russia*

Lead (Pb) is a potentially toxic trace element, and thus harmful to humans and the environment. Although the share of Russian Pb emissions to the total European emissions is estimated to be up to 50%, no long-term atmospheric Pb measurements are available for Russia. Here, we provide a first high-resolution Pb ice-core record from a Siberian Altai glacier, representing past atmospheric Pb concentrations in Russia. Major findings are that, during AD 1680–1935, Pb was mainly emitted into the atmosphere from mining in the Altai for the production of Russian coins, whereas Russian leaded gasoline has been the major Pb source since the 1930s.

Introduction

The atmospheric lead (Pb) cycle introduced by human activities is much more extended than the natural Pb cycle and has caused Pb pollution to be a worldwide issue for humans and the environment. While historical Pb emissions from Western Europe, North America, and Asia are well documented, there is no equivalent data for Eastern Europe. Here, we present ice-core Pb concentrations from the Belukha glacier in the Siberian Altai for the period AD 1680–1995, assumed to be representative for emissions in Eastern Europe and the Altai.

Figure 1: **View of the Belukha mountain. The ice core was drilled at the saddle located between the two summits.**
(Photo courtesy of Alexey Nagaev)

Ice-core archive

Samples analysed in this study originate from a 139 m ice core drilled at the Belukha glacier (49° 48' 26"N, 86° 34' 43"E, 4062 m.a.s.l.) in July 2001. The drilling site is located on the saddle between the two summits of Belukha, the highest mountain in the Altai (Figure 1). The Altai region, forming the border between Russia, Kazakhstan, Mongolia, and China, is mainly affected by westerly air streams and thus by air pollution from Eastern Europe. The ice core was extracted from a cold glacier and thus the composition of the atmosphere in the past is well archived. Concentrations of Pb were determined by inductively coupled plasma sector-field mass spectrometry (ICP-SF-MS) [1].

Lead in the pre-industrial period

Pb concentrations in the pre-industrial period AD 1680–1935 were, on average, one order of magnitude lower compared with the period AD 1935–1995. However, even in the pre-industrial period, before the introduction of leaded gasoline, Pb concentrations were not constant with time. They already began to increase during the 18th century and revealed elevated values from the beginning of the 19th century on (Figure 2). This was due to intensified mining and related metallurgical processing in the area of the Rudny Altai (Russian for "ore Altai") for the production of Russian coins. Since the time of Catherine the Great, in the 1770s, all Russian coins were produced in the Altai Mountains, near the drilling site.

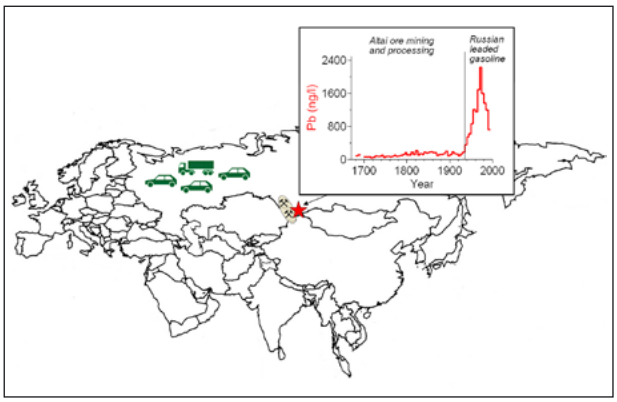

Figure 2: **Atmospheric lead concentrations in the period AD 1680–1995 reconstructed using an ice core from the Belukha glacier in the Siberian Altai (drilling site: red star). While lead was mainly emitted into the atmosphere from mining in the Altai (grey ellipse) for the production of Russian coins in the period AD 1680–1935, Russian leaded gasoline has been the major lead source since the 1930s.**

Pb from leaded gasoline: AD 1935–1995

After 1935, Pb concentrations increased noticeably due to rapid industrialization in the Soviet Union (SU) after the introduction of the five-year plans. The largest Pb-emission source in Russia in the last 55 years has been road traffic [2]. In 1995, for instance, leaded gasoline accounted for about 80 % of all Pb emissions. Maximum atmospheric Pb values between 1970 and 1975 are in phase with the economic output during that time. The decrease in Pb concentrations at the end of the 1970s and in the 1980s is in phase with economic difficulties caused by the oil crisis, and secondary factors such as the continuing growth of defence expenditures [3]. The collapse of the SU economy at the end of the 1980s, ending with its dissolution in 1991, caused further decrease in total gasoline production [4]. Thus, we assume that the decline in atmospheric Pb concentrations from the end of the 1970s was caused by the economic crisis in the SU, but was not due to a widespread phase-out of leaded gasoline. Although the sale of leaded gasoline had already been banned in the SU on a regional level in the 1950s (e.g. in Moscow, Leningrad, Kiev) [4], the Russian Federal Government had taken less action to phase out leaded gasoline. Nowadays, Russia is still the largest Pb emitter in Europe [2].

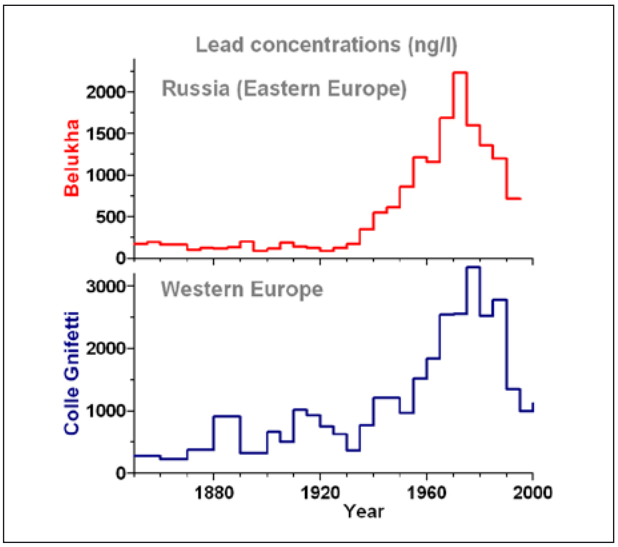

Figure 3: **Comparison of the historical atmospheric lead concentrations between Eastern and Western Europe in the period AD 1850–1995. The Western European record is from a Colle Gnifetti ice core drilled in the Swiss Alps [5].**

Comparison with Western Europe

The share of SU/Russian Pb emissions to total Eastern European emissions is estimated to be 70–80 % [1]. Therefore we consider the established Pb record for Russia to be representative for the emission history in Eastern Europe. An ice core from the Colle Gnifetti in the Swiss Alps had already been used in an earlier study to reconstruct the history of Pb pollution in Western Europe [5]. Interestingly, Western European Pb concentrations had already increased from the mid-19th century onwards, indicating earlier industrialization (Figure 3). Comparable to Eastern Europe, Western European Pb emissions peaked in the 1970s due to traffic emissions. However, the subsequent downward trend in Western Europe has been mainly caused by the introduction of unleaded gasoline.

Acknowledgements

We gratefully acknowledge the help of Patrick Ginot, Beat Rufibach, Susanne Olivier, Martin Lüthi, Henrik Rhyn, Dimitrii N. Kozlov, Sergej Derewstschikow, Vladimir Vashenzev, Andrej Jerjomin, Veronica Morozova, Alexander Chebotkin, and Igor Karakulko during the ice core drilling expedition in the Altai.

References

[1] A. Eichler et al., Env. Sci. Tech. **46** 4323 (2012).
[2] H. von Storch et al., Sci. Tot. Environ. **311** 151 (2003).
[3] V.G Treml, RFE-RL Res. Rep. **2** 53 (1993).
[4] V.M. Thomas et al., Ambio **30** 104 (2001).
[5] M. Schwikowski et al., Env. Sci. Tech. **38** 957 (2004).

Links

[1] Laboratory of Radiochemistry and Environmental Chemistry (LCH): http://www.psi.ch/lch/analytical-chemistry
[2] Oeschger Centre for Climate Research: http://www.oeschger.unibe.ch/

Particulate matter concentrations in Paris are surprisingly low and mostly due to regional emissions

André S.H. Prévôt, Monica Crippa, Peter Zotter, Jay G. Slowik, Imad El Haddad and Urs Baltensperger,
Laboratory of Atmospheric Chemistry (LAC) PSI, and the MEGAPOLI Team

Particulate matter is detrimental to human health when inhaled and is also important concerning its influence on solar radiation and thus on climate. The study of air quality in Paris (France), a megacity of more than 10 million inhabitants, revealed surprisingly low particulate matter (PM) levels. Furthermore, about 70 % of the fine PM mass is transported into the megacity from surrounding areas and is not due to emissions of the megacity. Traffic contributes little to the organic fine PM. Instead, a large fraction of the carbonaceous aerosol is of secondary biogenic and marine origin. Cooking activities and, during winter, residential wood burning are the major primary organic PM sources. Other megacities around the world, in Asia, Africa and South America, suffer from much higher pollution levels that need investigation and abatement strategies.

More and more people around the world live in megacities (urban areas with more than 10 million inhabitants). Within the European MEGAPOLI project (Megacities: Emissions, urban, regional and Global Atmospheric POLlution and climate effects, and Integrated tools for assessment and mitigation), the Paris Metropolitan area was studied in detail concerning its air pollution levels and its impact on the surroundings, with a focus on fine particulate matter (PM2.5: particles with an aerodynamic diameter smaller than 2.5 µm). Particulate matter is toxic when inhaled and influences the radiation balance of the earth, thereby affecting the climate. A summer and winter campaign, including three ground measurement stations, several mobile laboratories and an aircraft, were used to characterize PM in unprecedented detail in Europe.

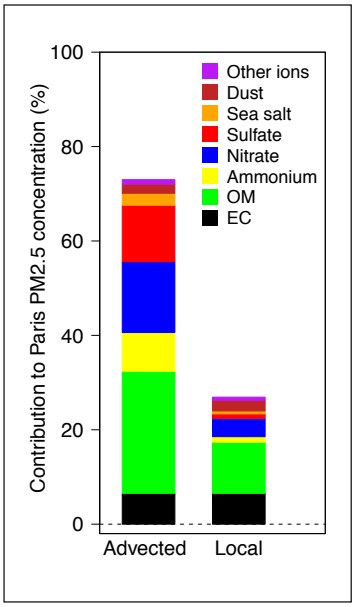

Figure 1: **Imported fine particulate matter (PM2.5) versus particulate matter from emissions in Paris (OM: Organic mass; EC: Elemental carbon) [1]).**

Low contribution of local emissions

An analysis of the campaign data and long-term observations revealed that, on average, around 70 % of PM is not due to emissions from Paris but is imported from outside the city (Figure 1). At high PM concentrations, the local contribution drops to below 20 %. During the winter campaign, the concentrations of most PM components showed basically the same time trends in the city centre (LHVP), 20 kilometres southwest (SIRTA) and 20 kilometres northwest (GOLF) (Figure 2). Differences indicating local contributions were found for black carbon and, to a lower extent, for the organic mass.

Source apportionment of organics

The use of aerosol mass spectrometry allows the separation of different sources of the organic particulate mass. This fraction is significant at all seasons and is regarded to be more toxic than the inorganic components and therefore of special interest. One can distinguish primary, i.e. directly emitted, organic aerosol (e.g. from traffic, wood burning, cooking and other sources) and secondary organic aerosol (formed in the atmosphere due to atmospheric oxidation of carbon containing gases). In both summer and winter, the regional secondary organic aerosol contributes more than 50 % to the or-

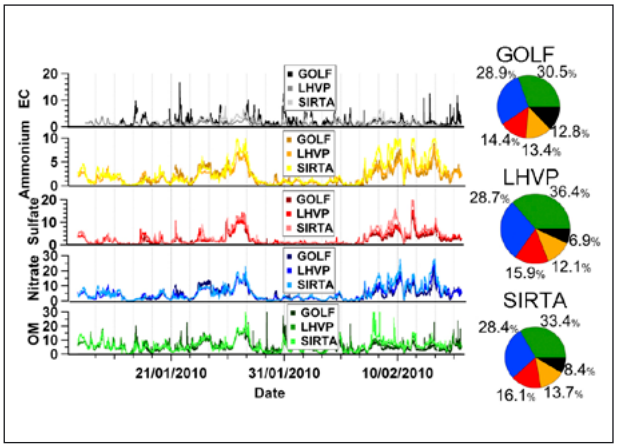

Figure 2: **Time trends of the main components of fine particulate matter (elemental carbon, ammonium, sulfate, nitrate, and organic mass (OM) in µg m^{-3}) [2].**

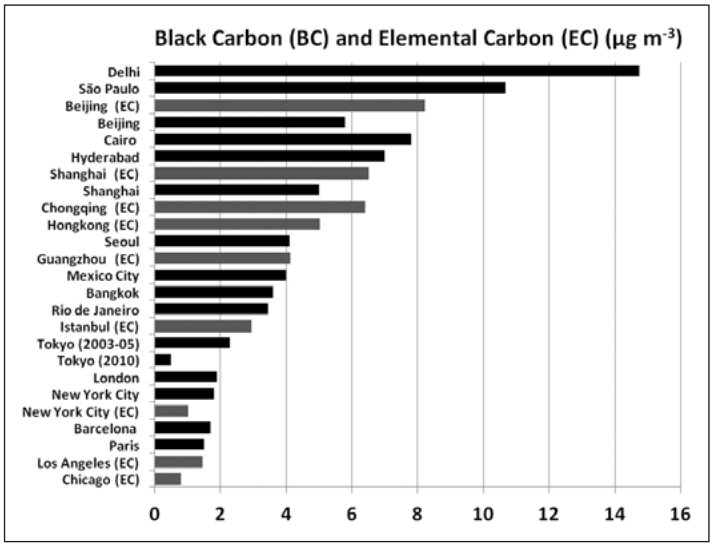

Figure 4: **Black carbon or elemental carbon measurements in different megacities around the world [1].**

ganic mass. Concerning the primary organic aerosol, the most surprising fact was the very high contribution of cooking. One observes peak concentrations of cooking organic aerosol during lunch and dinner periods (Figure 3). Both cooking and wood burning contribute more than traffic to the organic mass. The low contribution of traffic could be confirmed by ^{14}C measurements, indicating average fossil contributions to total carbon of less than 40 % in summer and less than 25 % in winter on average.

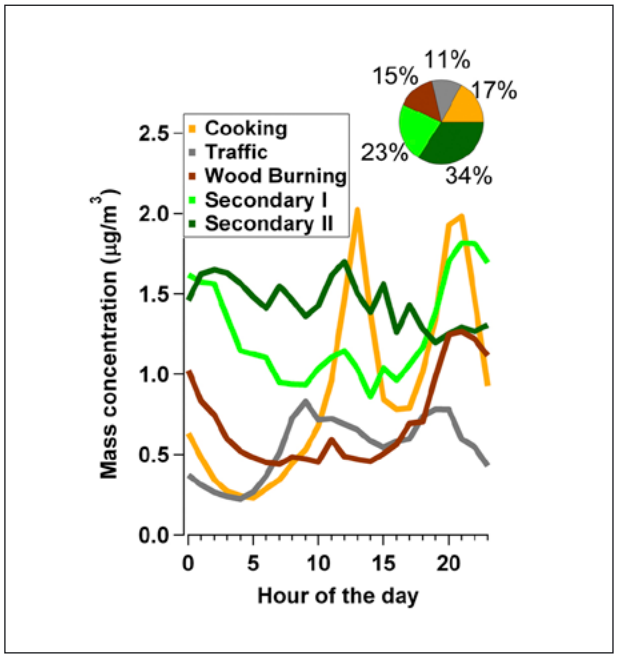

Figure 3: **Average diurnal variations of the particulate organic mass components in the centre of Paris during winter [2]. The secondary organic aerosol could be divided into low-volatility (34 %) and semi-volatile components (23 %).**

Concentration levels in Paris are generally rather low

The fine PM concentrations were roughly 10 µg/m^3 in summer and 20 µg/m^3 in winter, on average, with episodes with continental pollution of around 50 µg/m^3 [2, 3]. In comparison, the pollution episode in Beijing in mid-January 2013 reached up to 1000 µg/m^3. The difference between Paris and, in general, European/US cities in comparison with megacities in Asia, South America or Africa can be seen in Figure 4. Black carbon (or elemental carbon) is generally generated by combustion. The much lower concentrations in Europe and the US are, to a large extent, due to the very modern vehicle fleet.

Acknowledgements

This work was financed by the European Commission as part of the MEGAPOLI project, as well as by the Swiss National Science Foundation.

References

[1] M. Beekmann et al., submitted (2013).
[2] M. Crippa et al., Atmos. Chem. Phys. **13** 961-981 (2013).
[3] M. Crippa et al., J. Geophys. Res. **118** 1–19 (2013).

Links

[1] MEGAPOLI Project: http://megapoli.dmi.dk/index.html
[2] Laboratory of Atmospheric Chemistry (LAC): http://www.psi.ch/lac

Interactive tool for the analysis and comparison of advanced vehicle technologies

Andrew Simons and Johannes Hofer
Technology Assessment Group, Laboratory for Energy Systems Analysis (LEA), PSI

Passenger vehicles of the future must have significantly reduced energy demand and emissions as well as a far more efficient use of natural resources. Ideally there will be a transition to the use of domestic renewable fuels and to almost CO_2-free electricity supplies. For each technology or fuel there are disadvantages as well as advantages, and making a comparison therefore means considering a complex and interlinked problem. In order to do this, we have developed a model which links vehicle size, performance and operational interdependencies (i.e. energy sources) to the resulting life-cycle costs, burdens and potential impacts.

The THELMA project [Link 1] is currently assessing the potential role and consequences of electrified vehicle technologies in Switzerland. The final assessment will be based on a range of development scenarios extending to 2050 and requires the advanced modelling of battery electric (BEV), fuel cell (FCV), hybrid electric (HEV) and plug-in hybrid electric (PHEV) vehicle configurations. Reference technologies in the form of advanced internal combustion engine (ICEV) technologies must also be analysed to enable comparisons to be made. As contribution to THELMA, the authors combine vehicle modelling with life-cycle assessment to analyze the interdependence of vehicle performance criteria, energy use, costs, and environmental impacts of the various technologies. An interactive analysis tool is under development.

Vehicle modelling

Vehicle modelling aims to understand the influence of technology and performance criteria on the resulting vehicle mass, energy use and costs. Integrated into this is the analysis of the energy and power densities of components, powertrain efficiencies, recuperative braking and auxiliary energy demands. The model therefore sizes the components to meet the specified range and performance requirements. Energy demand per km is determined by modelling the use of the vehicle over a driving cycle consisting of urban and/or extra-urban stages. This provides a consistent and representative basis for vehicle comparison. Knowledge of energy use and component sizes is then used to calculate manufacturing and running costs, and total cost of ownership.

Scenario			Low	High
Performance	Acceleration	sec.	15	10
	Top speed	km/h	80	140
Range	BEV	km	80	250
	PHEV	km	20	80
	FCV	km	200	800
Energy source	Electricity	Mix	CH	EU

Table 1: **Performance and usage criteria values.**

Life cycle assessment (LCA)

Here, the aim is to analyse the various technologies with a focus on their production, use and end-of-life, and to thereby quantify the resource intensities, energy demands and emissions associated with the complete life cycle of each vehicle. The foreground inventory data used is currently in the process of publication [1, 2].

Initial results

The results given in Figures 1 & 2 represent vehicle technologies confined by the "Low" and "High" scenario bounds defined in Table 1. These are representative of the state-of-the-art in 2012 and relevant to midsize vehicles. In all cases, the vehicles follow a mixed driving cycle. The ICEV and HEV are petrol-fuelled. The electricity mixes used for charging and hydrogen production via electrolysis have been selected due to their consistently different LCA results for the indicators used.

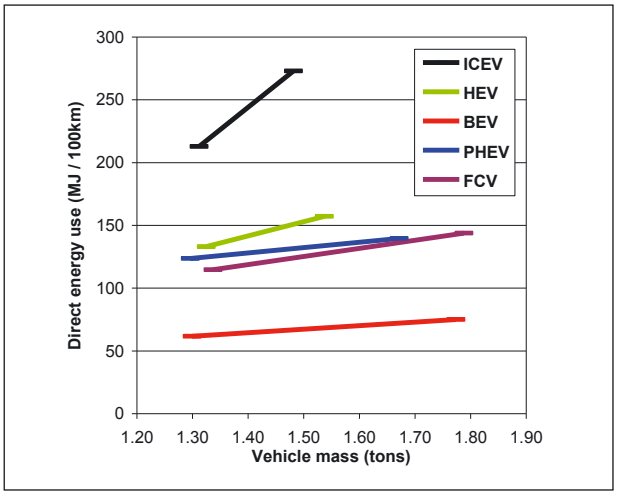

Figure 1: **Energy use and vehicle mass.**

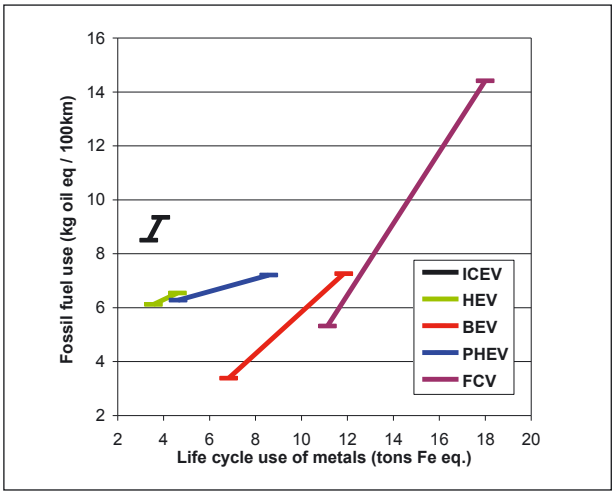

Figure 2: **Life cycle use of metals and fossil fuels.**

In Figure 1, results from our vehicle modelling highlight possible improvements in powertrain efficiency. They show that vehicle weight is by no means an overarching indication of energy demand and that increasing the performance (acceleration and top-speed) of alternative vehicles comes with lower weight penalties than doing the same for ICEV.

Although vehicle mass and energy use are important quantifications, they provide only a very superficial means for assessment. In order to understand the possible consequences of each technology, it is necessary to look at what is contained within the mass and what contributes to the final energy used. Figure 2 demonstrates aspects of this by showing characterised results for critical and limited material and energy resources. Results reflect the total equivalent demand for metals and fossil fuels over the complete life cycle, i.e. those also used in the processes and infrastructures for producing fuels and roads. The use of metals is quantified according to the equivalent scarcity of each element relative to that of iron (Fe), whereas for fossil fuels it is relevant to the lower heating value of crude oil. With increasing electrification of the drivetrain, the demand for metals having specific electrochemical, electromagnetic or catalytic properties also increases. Increasing vehicle performance again means increased motor, battery or fuel-cell size and thus a further increase in the use of scarce metals. What the results for metals do not, however, take fully into account is the potential for recycling. With such significant demands for relatively scarce resources and potentially very high numbers of vehicles (as well as other products using the same resources), it is quite likely that valuable materials will be almost fully regained at the end-of-life of the vehicle or component.

The results for fossil fuel use underpin the necessity of understanding the primary resource intensities of the processes contributing to the final energy carrier in the vehicle. Fossil fuel use also mirrors very closely the results for greenhouse gas emissions (not shown).

The interactive tool

An interactive tool for use by a broader range of users is under development. The interface to this tool will allow users to apply values to a range of vehicle-specific criteria and to select from a range of outcome indicators. For LCA results, the overall amounts are differentiated between the different life cycle aspects. Results change when the criteria change.

Outlook

Data and results have been finalised for current technologies and the focus is now on generating data for future technology scenarios, up to the year 2050. This new methodological framework is potentially very useful as an aspect of a broader scoping Multi-Criteria Decision Analysis (MCDA) tool for passenger vehicles.

References

[1] A. Simons, *Road transport: New life cycle inventories for fossil fuelled passenger cars and non-exhaust emissions in ecoinvent v3*, Submitted to: Int. J. LCA.

[2] A. Prasanna and C. Bauer, *Environmental Evaluation of future passenger vehicle technologies focusing on electric drivetrains*, Submitted to: Environ. Sci. Technol.

Links

[1] Technology-Centered Electric Mobility Assessment: http://www.thelma-emobility.net/

[2] Laboratory for Energy Systems Analysis (LEA) @ PSI: http://lea.web.psi.ch/

[3] Technology Assessment (TA): http://www.psi.ch/gabe

User facilities 85

The Paul Scherrer Institute develops, builds and operates Switzerland's complex, large-scale research facilities, serving users from the national and international scientific communities. The research topics under investigation include materials and life sciences, energy and the environment. The facilities available are the SINQ spallation neutron source, the SμS muon source and the SLS synchrotron light source. These provide beams of neutrons, muons and photons, respectively, making PSI one of only two research centres in the world with these three types of complementary research probes on one site.

In elementary particle physics, high beam-intensity experiments that require large numbers of muons are being performed, and experiments at PSI's Ultracold Neutron Source (UCN) are contributing to our knowledge of the fundamental forces of nature by helping determine the properties of the neutron.

All of these facilities are powered by one of the two major accelerators at PSI: the neutron and muon sources by the proton cyclotron, and the synchrotron light source by an electron storage ring. An additional, smaller, proton accelerator is used for the proton therapy facilities. A large number of scientists and technicians work at the accelerators for the benefit of the users, to ensure smooth operation and continuous improvement in performance.

The next large accelerator-based project, SwissFEL, will provide ultrashort, highly intense X-ray pulses for the investigation of fast processes and the determination of molecular structures. It is planned to begin operation of this facility in 2016. All required approvals for the construction of SwissFEL have now been obtained and construction work began in April 2013.

◀ **PSI scientist Rustem Khasanov preparing an experiment at PSI's Swiss Muon Source, SμS.** (Photo: Scanderbeg Sauer Photography)

Operation of the PSI Accelerator Facilities in 2012

Markus Kostezer, Andreas Lüdeke, Anton C. Mezger, Marco Schippers and Mike Seidel
Department of Large Research Facilities (GFA), PSI

The three accelerator facilities at PSI are operated by the Department of Large Research Facilities. These are: the High-Intensity Proton Facility, the Swiss Light Source and the Proscan medical accelerator. This article covers operational aspects of these facilities during 2012, as well as performance highlights and new developments achieved in them.

High-intensity proton accelerator (HIPA)

The experience from previous years showed that many technical problems occur during the first two weeks of operation following start-up. Therefore, almost two weeks of beam development were scheduled to diagnose and eliminate such start-up problems at the beginning of the 2012 operational period. As a result of this investment, the first week of user operation already showed a high availability of 85%, which increased to over 90% during the second week with the nominal production beam current of 2.2 mA. Figure 1 shows that just a few severe technical problems led to significantly reduced availabilities in Weeks 21, 28 and 47. The first reduced availability of 76% in Week 21 was caused by a vacuum leak in the Ring Cyclotron due to a broken RF pickup. The other incidents, in Weeks 28 (59%) and 47 (81%), were caused by failures of the targets M and E. In these cases, the rotation mechanism of the targets showed increased torque that later resulted in failure of rotation. Target M stopped rotating on a Friday evening and could not be repaired during the weekend. The service block scheduled for the following week was used to repair the target, and user operation could be resumed two days earlier than scheduled. In this way, part of the lost beam time was given back to the users. Target E showed torque problems during Week 47 and the decision was taken to replace it on Friday, before the weekend. Thanks to the commitment of the technical groups, the interruption could be kept down to only 24 hours and production was resumed on Friday evening.

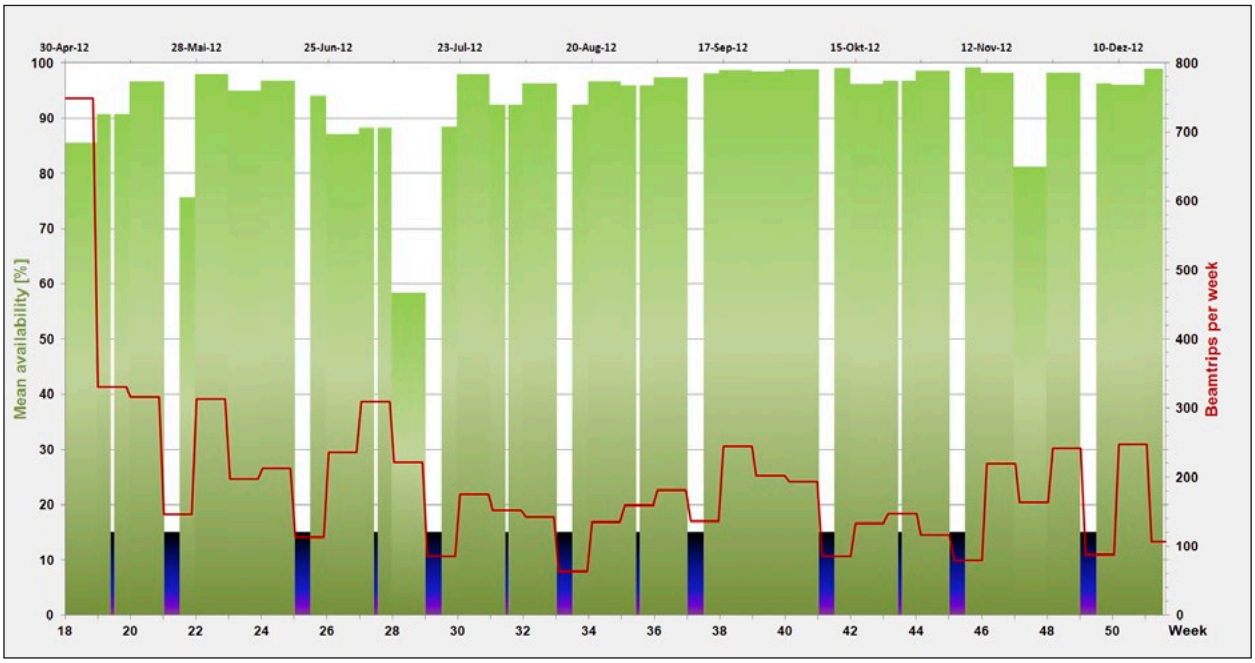

Figure 1: **Operation of the Proton Facility in 2012 showing availability and beam trips per week. Service blocks are indicated in blue.**

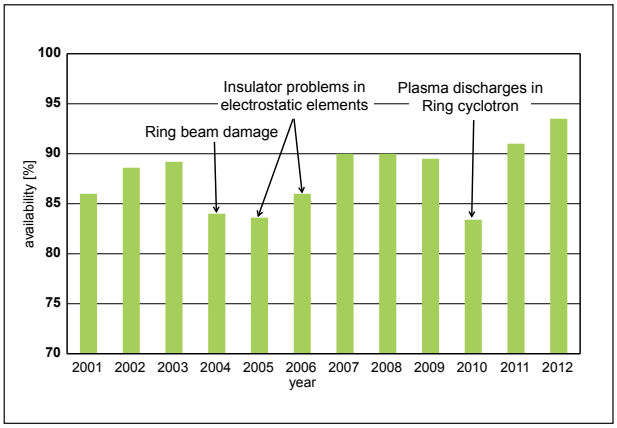

Figure 2: **HIPA availability over the last 11 years.**

Beam-time statistics for HIPA	2012
Total beam time	
To meson production targets	4936 h
To SINQ	≈ 4885 h
Beam current integral	
To meson production targets	10.4 Ah
To SINQ	7.1 Ah
To UCN	0.06 Ah
Outages	
Unscheduled outages > 5 min	205 h
Total outages (current < 1 mA)	321 h
Availability	**93.5 %**

Table 1: **Operational statistics for the proton facility.**

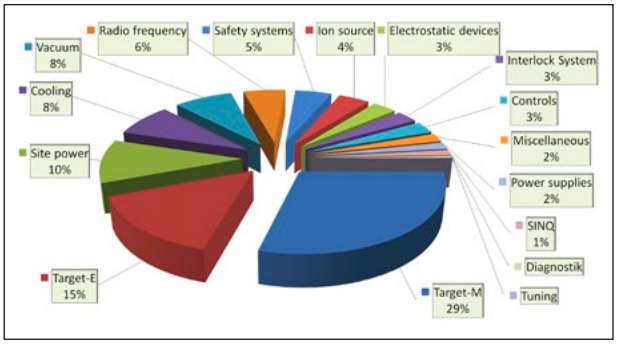

Figure 3: **Downtime characterization for HIPA outages exceeding 5 minutes (total 205 hours).**

Figure 1 shows the facility availability in blocks of four weeks together throughout 2012, as well as the number of short beam trips. The number of beam trips is sensitive to the optimization of beam losses in the facility. The value of ≈200 trips per week represents good performance in comparison with other years. The overall availability of the facility amounted to 93.5%, without considering compensation time. The integrated charge was 10.4 Ah on target E and 7.1 Ah on the SINQ spallation target (Table 1). Both figures represent all-time highs in the performance of the HIPA facility. The statistics over the last 11 years are shown in Figure 2.

The relative contributions by the various technical systems to the downtimes are shown in Figure 3. These downtimes were dominated by target failures, which represented 45% of the registered downtime. Another significant contribution was from site power failures, often due to the effect of lightning on the grid, that caused the main field circuits of the cyclotrons to trip.

PROSCAN

In the year 2012, it was possible to continue operation of the medical accelerator facility on a high level. Similar to 2011, the sum total of operational hours was 7020 hours, and overall availability reached 97.4 %. For the treatment of patients at Gantry-1 and Optis-2, the centre for proton therapy used 3023 hours of operation time, and 660 hours were used for irradiation of material samples in the PIF facility. The number of unplanned interruptions longer than 2.5 hours was 13.

The chimney of the ion source in the cyclotron contains a slit for injecting the initial proton beam. At low injection energy levels, the beam orbit is susceptible to small changes of the geometry and the electromagnetic field. Thus the maximum achievable beam intensity depends critically on the angular orientation of this slit. It occurred twice, in February and June, that the high intensity required for OPTIS-2 operation could not be achieved. The chimney had to be realigned in a time-consuming procedure. A new laser-based survey system is being developed with the help of the PSI workshop to improve the reproducibility of chimney orientation.

As another improvement, a new degassing unit for reducing the amount of oxygen and CO_2 in the cooling circuit of the beamlines and the cyclotron was installed and successfully commissioned in December. The free oxygen in the circuit

Figure 4: **Degassing unit for the cooling circuits of the COMET cyclotron.**

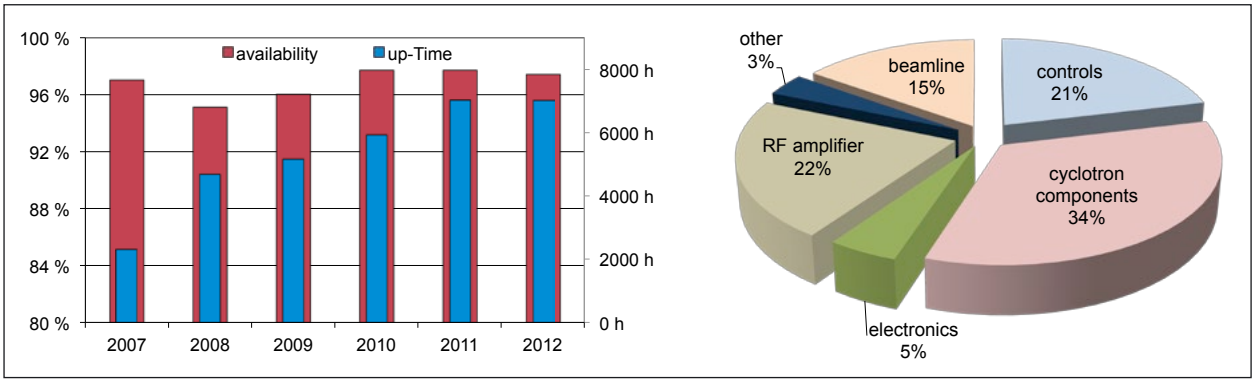

Figure 5: **Operating hours per year; availability of PROSCAN (left) and unscheduled downtime by causes.**

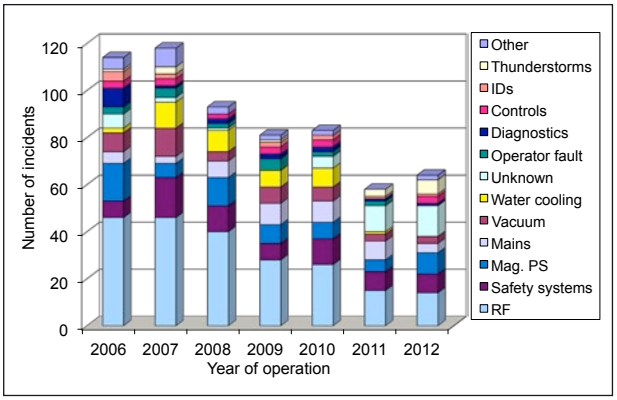

Figure 6: **Beam outage count per failure category.**

leads to oxidation and the abrasion of copper from the cooling pipes. Deposition of the copper oxide produced may lead to a reduction of the cross-sections.

According to the experience at other PSI accelerators, these effects can ultimately lead to malfunction of components and costly repairs.

In the case of an unplanned loss of grid power, the power supply of the superconducting coil is automatically bypassed, resulting in a very slow exponential decay of the coil current. In order to quickly resume operation after the event, it is necessary to reconnect power supply and coil, although the current has not yet vanished. On 16 November, this situation occurred and resulted in several failures and the damage of a capacitor. To avoid such problems in the future, a special discharge unit for the coil was designed, in collaboration with the company Bruker. This unit allows the current to be ramped down quickly and thus the circuit to be safely restarted.

Development and Operation of the SLS

The Swiss Light Source succeeded in 2012 in repeating the excellent operational statistics of 2011. The beam availability in 2012 again reached 98.7% and the mean time between failures was three and a half days. The number of beam outages was almost as low as in 2011, when an all-time low was achieved. Figure 6 shows beam outage count per failure type over the past 7 years. It is clearly visible that the improvements made to the RF interlock system over this period have created an enduring improvement.

Figure 6 shows only the effect of beam outages, but in fact users may also suffer from other types of unfavourable beam conditions. For example, the quality of experimental data can already deteriorate if the beam current drops due to an outage of the injector, or if the orbit feedback fails and the beam positions therefore drift. Figure 7 shows the mean time between any of these beam distortions over the past 6 years. We have succeeded over the past six years in significantly improving this figure and are now routinely reaching an average of more than one and a half days between any of these beam distortions.

Although the excellent yearly availability statistics do not suggest it, the year 2012 actually started with serious operational problems. In the first eight weeks of user operation we had to run with a reduced beam current of 350 mA. The problem originated from coupled bunch modes, causing beam instabilities and sudden beam losses. Several unsuccessful attempts were made to tune the higher order modes of the cavities, which were the likely cause of the coupled bunch modes, but the problem was eventually resolved by changing the RF frequency slightly. To achieve this, we had to increase the temperature of the SLS building by 1°C. Together with the

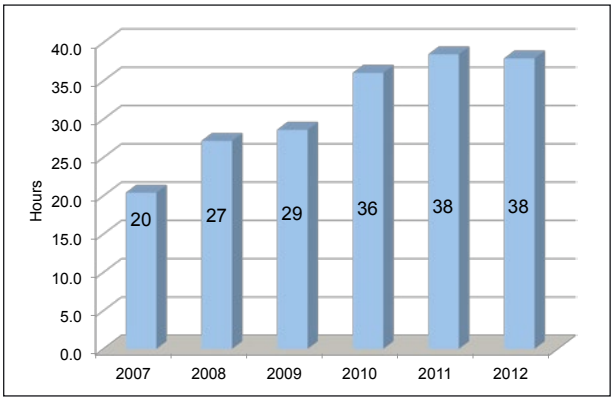

Figure 7: **Mean time between beam distortions.**

seasonal increase of the outside temperature, this measure expanded the concrete floor and resulted in an increase of the circumference of the storage ring. The RF frequency was reduced by about 300 Hz and this was sufficient to reliably suppress the coupled bunch modes and recover stable conditions for 400 mA top-up operation.

The RF group used the shutdowns extensively for preventive maintenance. Six water leaks in the cavity cooling system were found and sealed during 2012 shutdowns. Some leaks that had been sealed with glue several years ago had reopened as

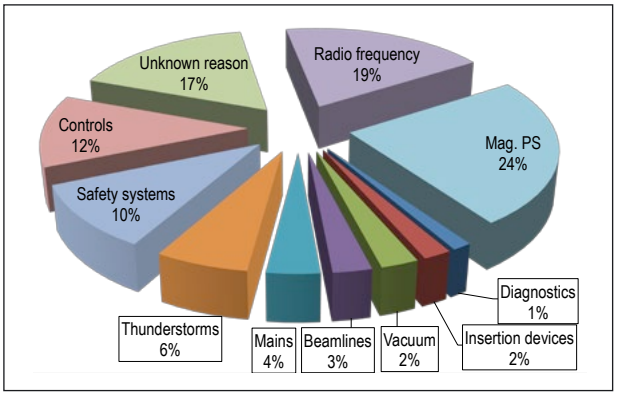

Figure 8: **Beam outages per failure category in 2012.**

the glue became brittle with time. In order to fix these leaks, the first step necessary was to remove the old glue completely and a dental burr turned out to be the perfect instrument for performing this task. One water leak showed up just after a shutdown. The 48 hours needed to seal this leak were spent during machine development time and therefore do not show up in the downtime statistics. It is probable that long beam outages would have occurred without this preventive maintenance. In 2008, such interruptions caused a total of 98 hours of downtime.

The only beam downtime in 2012 that was longer than five hours was caused by a water leak in the main dipole power supply of the storage ring. A water hose broke in the power supply and the water loss caused the whole cooling water circuit to trip. Within five hours and twenty minutes the power supply was repaired and dried, the cooling circuit was refilled, all tripped systems were restarted and the beam was recovered. Figure 8 shows the fractional durations of the beam outage events in 2012, assigned to the different failure categories.

The magnet power supplies were responsible for about a quarter, and the RF for about a fifth, of beam downtime. The statistical increase in the number of beam losses by unknown sources was most likely the result of an upgrade of the RF interlock systems, which now avoids the false assignment of certain failures to the RF systems. Previously, beam losses had caused some RF trips that were recognized as the cause

Beam Time Statistics	2012		2011	
Total beam time	6928 h	78.9%	6824 h	77.9%
• User operation	4968 h	56.6%	5000 h	57.1%
- incl. compensation time	160 h	1.8%	160 h	1.8%
• Beamline commissioning	968 h	11.0%	976 h	11.1%
• Setup + beam development	992 h	11.3%	848 h	9.7%
Shutdown	1864 h	21.2%	1944 h	22.2%
User operation downtimes	59		53	
• Unscheduled outage duration	63 h	1.3%	65 h	1.3%
• Injector outage (non top-up)	23 h	0.5%	22 h	0.4%
Total beam integral	2369 Ah		2506 Ah	
Availability	98.7%		98.7%	
Availability after Compensation	102.0%		101.9%	
MTBF (mean time btw. failures)	84.2 h		94.3 h	
MTTR (mean time to recover)	1.1 h		1.2 h	

Table 2: **SLS Operation Statistics.**

of the interruption. However, the real causes, for example a small dip in a magnet power supply current or a transient fluctuation in the RF phase, were not recognized by any diagnostics. To diagnose and eliminate these triggers for beam trips will be the challenge for the future. Operational data is summarized in Table 2.

In order to achieve a permanent solution for the problem of recurring water leaks in the RF cavities, it is planned to replace all cavities. The replacement of the first RF cavity has been postponed by a year, since an RF test facility is first of all needed to condition the cavity to full RF power. External conditioning of the new cavities has been rejected on financial grounds. The increased occurrence of water leaks underlines the importance of the timely replacement of the cavities.

We have continued our efforts to reduce betatron coupling in the storage ring to reach ultra-low vertical beam emittance [1]. This has now led to an international collaboration to use the SLS as a test bed for future accelerators. In particular, the damping rings of future linear colliders will require extremely low coupling. Research on this type of damping ring will now be performed at the SLS as part of collaboration within the EU project "Test Infrastructure and Accelerator Research Area (TIARA)" [2].

References

[1] M. Aiba et al, *Ultra low vertical emittance at SLS through systematic and random optimization*, Nuclear Inst. and Methods in Physics Research A **694** 133–139 (2012).

[2] TIARA WP6 : SVET R&D Infrastructure: http://www.eu-tiara.eu/rtd/index.php?id=42

Link

[1] Department of Large Research Facilities (GFA): http://www.psi.ch/gfa

The Swiss Light Source in 2012 – A well-established, but dynamic, facility

Stefan Müller, Jeroen van Bokhoven, Oliver Bunk, Christoph Quitmann and J. Friso van der Veen,
Synchrotron Radiation and Nanotechnology Department (SYN), PSI

Over the last decade, the Swiss Light Source has been developed into a world-class science and research facility. Its advanced beamlines offer unique opportunities for materials characterisation. In 2012, the SLS staff provided high-class services to more than 1500 users, from academia and the private sector, and performed cutting-edge research with regional and international groups. As a result, there has been an impressive growth in high-impact publications, the number of new proposals, instrumentation developments and scientific collaborations. The research at SLS contributes to, for example, the understanding of structure-function relationships in proteins, the tailoring of materials' properties, the development of catalysts and the cleaning of our environment. In 2012, the development of the next generation of pixel detectors was vigorously continued, novel diffractive X-ray optics for free-electron laser applications were tested, collaboration with industry was increased and educational and outreach activities intensified.

User operation – high community loyalty

The key figures on facility use, such as numbers of submitted proposals, user visits, experimental days and experiments all show a slight increase (Table 1). The competition among users for access is strong and only the best research is supported by SLS. On average, the overbooking of the beamlines has been approximately a factor of two, though at some beamlines it was between three and four.

Among SLS users, PhD students and early-career researchers form the majority (60%). This underlines the important role of SLS in supporting national and international early-career users in their effort to become the next generation of scientific leaders.

The geographic distribution of SLS users remained the same as in the previous year, with 60% coming from abroad. In 2012, the share of user visits between the three protein crystallography (PX) beamlines and the other fourteen non-PX beamlines was approx. 50:50.

	2012	2011	2010
Submitted proposals	808	778	668
User visits	3825	3338	3221
Experimental days	1855	1787	1884
Number of experiments	1187	1058	1085

Table 1: **SLS key figures for user operation 2010–2012.**

The excellence of our user community and in-house scientists is illustrated by a remarkably high number of refereed user publications in 2012. A total of 532 publications were generated, of which 118 were in journals having an impact factor ≥ 7.1 (Phys. Rev. Letters).

Proprietary research – strong connections to the pharmaceutical industry

The Swiss Light Source is number one in PDB (Protein Data Bank) depositions among European national facilities: During the past eleven years, 2476 protein structures have been deposited with data collected at SLS and many pharmaceutical companies have called on the expertise of SLS to analyze the structure of complex biomolecules.

Review committees

The Scientific Advisory Committee and two Proposal Review Committees (PRCs) delivered outstanding work for the facility. The role of the Photon Science Advisory Committee (Photon-SAC), headed by Prof. Dr. Gerhard Materlik (Diamond Light Source, Harwell, UK), is to advise PSI on the strategy for SLS and SwissFEL. The two PRCs evaluated a total of 808 proposals. These PRCs – one for macromolecular crystallography and one for all other activities – are chaired by

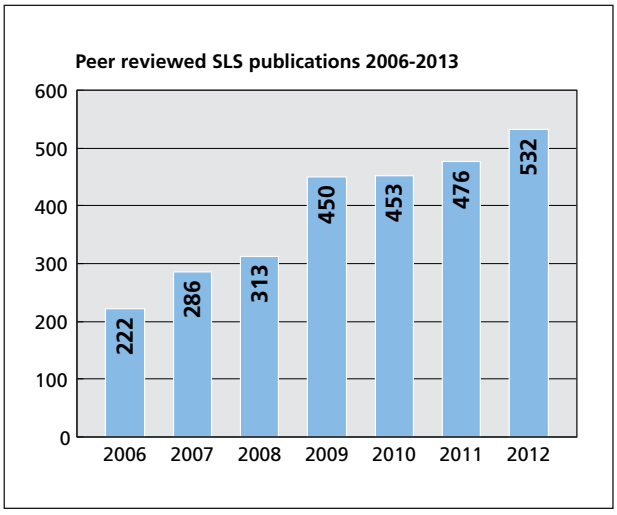

Figure 1: **Number of peer reviewed SLS publications in the years 2006–2012.**

Prof. Dr. Ph. Aebi (University of Fribourg) and Prof. Dr. Nenad Ban (ETH Zurich), respectively.
We would like to thank the chairs and members of these committees for their advice and their thorough evaluations of the proposals.

Investments in new instruments – new opportunities

OMNY (tOMography Nano crYo stage) is an ongoing instrumentation project at SLS, implementing an endstation for tomographic nano-imaging at 10 nm resolution in 3D using ptychography. A test setup operating at room temperature and atmospheric pressure has been built and first measurements demonstrate a resolution of 8 nm in 2D and ~50 nm in 3D (limited by sample issues). This test setup is now in user operation at the cSAXS beamline.
A new type of multi-axis goniometer, called **PRIGo** (Parallel Robotics Inspired Goniometer), has been developed for macromolecular crystallography applications at SLS, enabling the precise orientation of the crystal and the collection of Bijvoet pairs. With its compact design, it offers the highest degree of freedom in a crowded sample environment. Combined with the single-photon-counting PILATUS 2M-Fast detector, the beamline X06DA now offers new data collection opportunities, taking full advantages of crystal geometry and detector properties.
X-ray photoelectron spectroscopy (XPS) performed at pressures up to 20 mbar (here referred to as Near-Ambient Pressure Photoemission, **NAPP**) is an emerging tool that allows the examination of the chemistry of surfaces that are relevant to catalysis and the environment under nearly realistic reactant and pressure conditions. The SLS-NAPP instrument has been set up as a mobile end-station, prepared for different beamlines, e.g. the Phoenix beamline. For environmental surface chemistry, the long-term focus is to establish a molecular-level description of, for example, the impact of atmospheric particles on air pollution. In the field of catalysis, the ultimate aim is to measure industrially relevant catalyst structures under catalytic conditions with realistic flow dynamics.
The new beamline X-Treme started to receive regular users in 2012. X-Treme is a beamline for dichroic X-ray absorption spectroscopy, focusing on magnetic phenomena in high magnetic fields and at low temperature.
PEARL (Photo-Emission and Atomic Resolution Laboratory) is a new soft X-ray beamline dedicated to surface science. This beamline is co-financed by four Swiss institutions and received its first light in December 2011. Commissioning of the optics and installation of the end-station were accomplished in 2012.

Outreach activities – imparting knowledge and raising awareness

The EU-funded 'PSI Fellow' programme will enable 11 postdocs to start their work in 2013 at SLS. Selection of candidates was based not only on their excellence but also on achieving a close match between the candidates' and the facility's interests. We expect much from this unique recruitment tool.
The PSI Summer School in Condensed Matter Research, designed to stimulate interest at PhD and postdoctoral level in condensed matter physics, materials science and related fields at large facilities, was held in Zug from 11–17 August, followed by practical training at PSI. It provided PhD students and postdocs with expert training in the use of large-scale facilities, which is not available within the traditional system of graduate and post-graduate education. We would like to acknowledge the financial support of the school by the EU-FP7 Programme. Other outreach activities include hosting international conferences and workshops and the quarterly publication of the PSI Facility Newsletter [Link 2].

Our users make the difference

We thank all of our users for their loyalty, for the excellent science they brought to the SLS and, last but not least, for their friendly cooperation.

Links

[1] SLS: http://www.psi.ch/sls/
[2] PSI Facility Newsletter: http://www.psi.ch/info/facility-news

The Swiss Spallation Neutron Source: SINQ 2012

Stefan Janssen, Christian Rüegg, Eberhard Lehmann and Kurt N. Clausen
NUM Department – Research with Neutrons and Muons, PSI

Thanks to the outstanding performance of the proton accelerator HIPA in 2012, the SINQ target received a total charge of 7.1 Ah, a value never achieved before. This enabled an efficient and successful user programme to be carried out, with more than 450 experiments and – for the first time – more than 1000 visits by scientists from all over the world. By the end of the year, the new thermal triple-axis spectrometer EIGER could be taken into operation. This instrument is now fully available to the user community.

SINQ target and user operation: All-time records

Once again, SINQ has broken several records: In 2012, the meanwhile 8th target received a total charge of 7.1 Ah, a value that had never been reached before. This value is the result of two causes: Firstly, the PSI proton accelerator HIPA performed extraordinarily well, with 2.2 mA in standard operation, an all-time availability record of 93.5 % and many long periods without interruption. Secondly, the SINQ facility itself again performed extremely reliably, with an availability of 99 % with respect to proton availability.

Thanks to these excellent conditions, a large number of scientific experiments could be performed: 474 with an average duration of 4½ days. Twelve instruments were in full user operation in 2012: three spectrometers, three diffractometers, two facilities for small angle scattering, a reflectometer, a strain scanner and two facilities for neutron imaging. For the first time, these instruments welcomed more than 1000 visits of users in a single year – performed by more than 500 different scientists – which impressively documents the high demand for SINQ beam time from the national and international neutron user community (Figure 1).

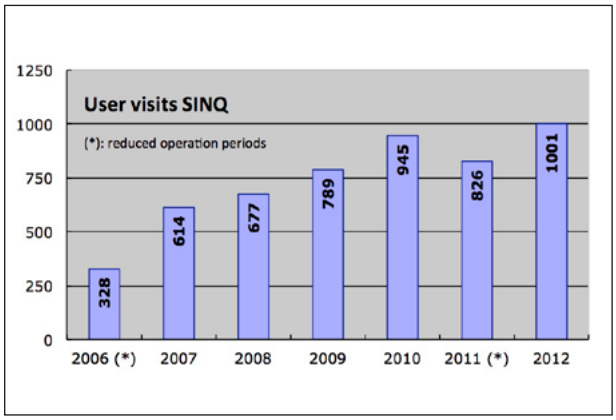

Figure 1: **Development of annual user visits to SINQ since 2006.**

Most users again came from Swiss groups, who used 54% of the beam time in 2012, followed by groups from Germany (11%), Denmark and the United Kingdom (both 6%), and France, Japan, USA (all 3 %). In total, scientists from 31 different countries made use of SINQ beam time during the last year.

Apart from those users affiliated to PSI, most of the Swiss user groups came from ETH Zurich (16 %), EPF Lausanne (5 %), EMPA and the University of Bern (both 3 %).

Future requests for SINQ beam time also remain at a very high level. For the second time in a row, the User Office received almost 400 new proposals in the year.

Instrumentation and highlights

The latest addition to the family of neutron spectrometers at SINQ, the EIGER spectrometer, turned out to be a big success in half a dozen commissioning experiments that were performed in late 2012. When normalized by the source flux, its performance is among that of the best spectrometers of this type in the world. Efficiency gains for experiments at SINQ in the energy range 2–10 meV is now significant and new science is being carried out on materials with excitations at energies above that range, which were previously inaccessible. Among the first experiments made were studies of magnetic excitations and phonons in quantum and frustrated magnets, magnetic semiconductors and novel superconductors. EIGER has already received nine proposals in these areas of research in its first submission round. The unique combination of

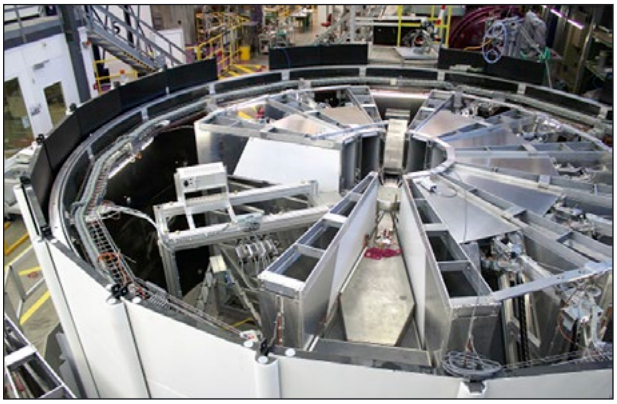

Figure 2: **A prototype for an Extreme Environment Spectrometer at the ESS being tested on the MARS spectrometer at SINQ.**

neutron and photon spectroscopy at PSI, and their complementarity, now enables studies of the dynamics in solids from 0 to several eV on samples that are as diverse as single atomic layers of model two-dimensional insulators and large single crystals of superconductors.

Further investment in the suite of spectrometers at SINQ is already underway. In collaboration with the Laboratory for Quantum Magnetism at EPF Lausanne and jointly funded by EPFL, the Swiss National Science Foundation (SNSF) and PSI, a new multi-analyser system for the RITA-II spectrometer is currently being developed.

The European Spallation Source ESS is a vital project for the future of neutron scattering in Europe. Supported by the State Secretariat for Education, Research and Innovation, a large programme started in 2012 at PSI and at a number of Swiss universities in preparation for the construction of the ESS in Lund, Sweden. Instrument concepts and key technologies for neutron scattering are being developed and tested, with the aim of contributing local Swiss expertise to the design and anticipated construction of this next-generation neutron source. Figure 2 shows prototype analyser segments being tested on the MARS spectrometer at SINQ.

The ESS instrumentation design work packages are an example of the strong national and international partners that were involved in many collaborative activities at SINQ during 2012. These include, most importantly, science projects such as the new initiative on Mott physics beyond the Heisenberg model, launched as the SNSF Sinergia project between seven groups at EPF Lausanne and PSI, and the education of students from all Swiss universities. The strong links to the Swiss universities were further strengthened by the appointment of a joint professorship with the Department of Condensed Matter Physics at the University of Geneva.

Use of the test beamline BOA for neutron imaging purposes was continued. A much higher contrast for hydrogen could be verified experimentally, which might have a strong influence on several future studies. Further important potential at BOA could be identified for imaging with polarized neutrons and high-resolution options.

In a specific COST-supported project for in-situ studies of heat-treated wood, essential data were obtained on the change in water uptake behaviour. The simultaneous observation of the diffracted signal and the transmission image using two separate image detectors was found to be very promising, in particular for energy-selective imaging.

Finally, a project for optimizing the spatial resolution in neutron imaging ("neutron microscope") was initiated and is partly funded by SNSF.

Among the scientific highlights in 2012 from experiments at SINQ are many studies of the fundamental structural, and electronic and magnetic properties of materials. There is a clear trend towards the control of these using experimentally challenging combinations of parameters such as electric and magnetic fields, ultra-low temperatures, pressure and in-situ chemical conditions, which requires further developments and investment in the advanced sample environment for neutron scattering experiments. Beautiful examples of this are the use of electric fields to control fascinating spin structures called skyrmions [1] and their detection by small-angle neutron scattering, quantum criticality in dipolar-coupled model antiferromagnets controlled by a magnetic field [2], and using the same parameter studies of vortex lattices in several families of superconductors [3, 4].

References

[1] J.S. White et al., J. Phys. Condens. Matter **24** 432201 (2012).
[2] C. Kraemer et al., Science **336** 1416 (2012).
[3] P. Das et al., PRL **108** 087002 (2012).
[4] P.K. Biswas et al., PRL **108** 077001 (2012).

Links

[1] SINQ: The Swiss Spallation Neutron Source: http://www.psi.ch/sinq
[2] Laboratory for Neutron Scattering (LNS): http://www.psi.ch/lns
[3] NIAG – Neutron Imaging and Activation Group: http://www.psi.ch/niag
[4] Scientific Highlights from the NUM Department – Research with Neutrons and Muons: http://www.psi.ch/num/scientific-highlights

Ultracold neutrons for the world's most sensitive search for a neutron electric dipole moment

Bertrand Blau, Klaus Kirch, Bernhard Lauss, Philipp Schmidt-Wellenburg and Geza Zsigmond,
on behalf of the PSI UCN project team and the nEDM Collaboration, NUM Department, ASQ and LTP, PSI

Ultracold neutrons (UCN) are powerful probes in studies of fundamental physics. PSI's new high-intensity UCN source is used to search for the neutron electric dipole moment (nEDM). The results will influence particle physics and cosmology, and our understanding of the matter-antimatter asymmetry observed in our Universe today. In 2012, the UCN source regularly delivered ultracold neutrons to the nEDM experiment and, in parallel, for source characterization measurements. The performance achieved makes it the world's most sensitive nEDM search. Further improvements of the source and the nEDM apparatus are being pursued. The international nEDM collaboration is also preparing a new setup for the next-generation "n2EDM" experiment, which will increase the measurement sensitivity by one additional order of magnitude

The PSI ultracold neutron (UCN) source [Link 1] was designed and built in order to improve experimental sensitivity in the search for the electric dipole moment of the neutron (nEDM), discussed further below and in [Link 2]. In its second year of operation, the UCN source reliably delivered UCN to the experiments 24 hours a day over many weeks. The intensity of UCN available to experiments has increased by a factor of about 90 since the first beam arrived on target. In 2012, typically every 360s a 3s proton pulse produced spallation neutrons which were subsequently moderated and down-scattered to become ultracold. The final down-scattering step occurs at the centre of the UCN source, in solid deuterium (sD_2) at 5K. The UCN output critically depends on the quality of this large crystal (that is up to 30 litres in volume), which depends on many parameters. The UCN yield produced in 2012 from different D_2 crystals is shown in Figure 1, with considerable improvement obtained after initial tests.

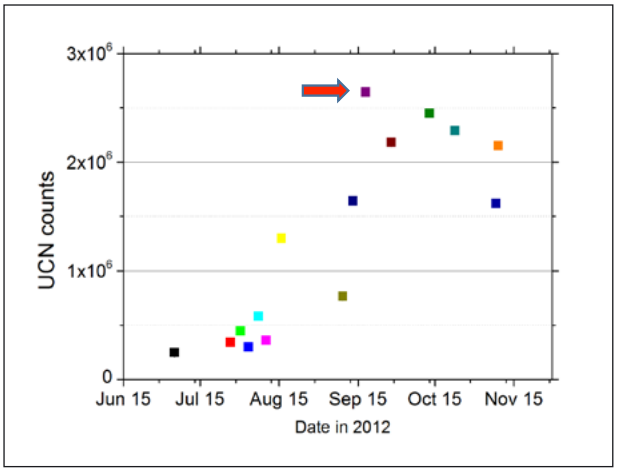

Figure 1: **UCN yield from different sD_2 crystals in 2012, observed with 2s proton pulses, all shutters open and thus no mechanical movement. The arrow indicates the highest UCN yield obtained so far.**

Many different measurements were performed in 2012 in order to improve the UCN yield and to better understand the performance of various parts of the setup.

A height profile of the thermal neutron flux along the UCN source's vacuum tank was determined for the first time, using gold foil activation, together with PSI's Radioanalytics Group. Figure 2 shows the dependence of the measured Au activation on position. Detailed simulation of these measurements is under way, using a full model of the source, in collaboration with the Target Development Group at PSI's Large Research Facilities Department. Another dedicated measurement showed that UCN transport through the installed guides, windows and source storage volume is behaving as expected.

Search for a neutron electric dipole moment (nEDM)

Although the neutron is electrically neutral, it could possess an electric dipole moment (EDM) along its spin. The unit of an EDM is elementary electric charge, e, times distance in cm: $e \cdot$ cm. An nEDM is predicted by many theories which go beyond the present Standard Model of particle physics. A measured nEDM would be a strong hint towards a specific solution for two of the most urgent open questions in particle physics: the origin of the matter–anti-matter imbalance in our Universe, and the strong CP problem of Quantum Chromodynamics.

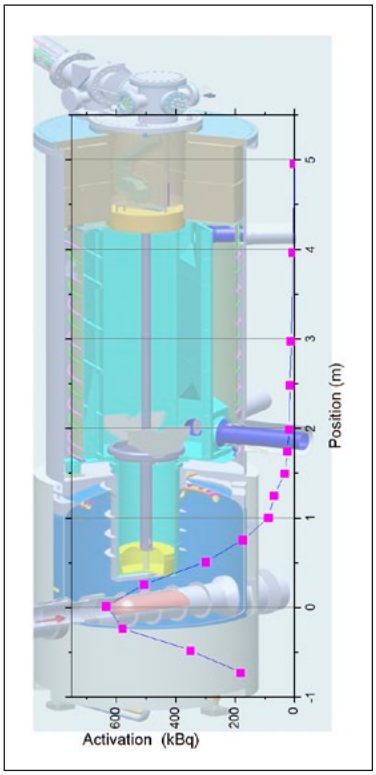

Figure 2: **Measured gold activation as a function of position along the UCN source vacuum tank.**

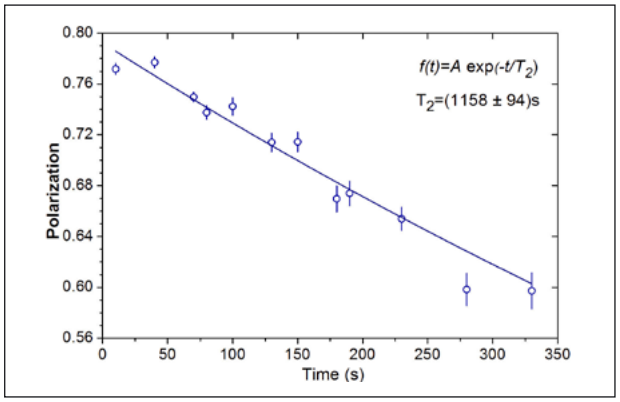

Figure 3: **T_2 time dependence of the transverse polarization of UCN during Ramsey measurements.**

Figure 4: **View of the entrance to the new n2EDM staging area in the WWHA hall, with the copper RF shielding already partially installed.**

The nEDM measurement uses the so-called Ramsey method of separated oscillatory fields. The Larmor precession frequency of spin-polarized neutrons in a magnetic field is compared for parallel and anti-parallel electric fields.

A European collaboration of 14 institutions has set up and started the world's most sensitive search for an nEDM at PSI's UCN source. The collaboration is using the apparatus which has set the presently most stringent limit on the nEDM: $d_n < 2.9 \times 10^{-26}$ e·cm [1]. This apparatus has been greatly improved, most importantly in its magnetic field monitoring capabilities. A very sensitive B-field gradiometer, using optically pumped cesium magnetometers, was installed and the performance of the mercury cohabiting magnetometer improved.

The sensitivity of one 200s measurement cycle is inversely proportional to the polarization at the end of the cycle times the square root of the number of neutrons in the chamber. This polarization is described by an exponential decay parametrized by a time constant T_2. Figure 3 shows the measured neutron polarisation product α with T_2=1158(94)s, exceeding former values by about 300s. At 200s, the best measured polarisation was α=0.69(1), which has to be compared with the best value of [1], α=0.43(1) after 130s. In autumn 2012, the average nEDM sensitivity in a single measurement cycle exceeded, for the first time, the single-cycle sensitivity of any other experiment in the world, and is being further improved. In the overall performance of the system, the collaboration has achieved a milestone in its goal to improve the current nEDM limit below $d_n < 5 \times 10^{-27}$ e·cm, or to discover it. To achieve the necessary statistical sensitivity, measurement cycles must be repeated many thousands of times in 2013 and 2014.

At the same time, the collaboration is preparing a completely new apparatus at PSI, dubbed "n2EDM", with the capability to increase the sensitivity by another factor of ten; by further increase of the UCN yield and adaption of the apparatus, and by further reduction of systematic effects. In 2012, construction work for n2EDM started by setting up a thermally insulated hall to stabilize the temperature around the experiment to about ±0.1°C. Several components of the new apparatus will be set up and tested in the staging area, with the final goal of commissioning the entire apparatus before installation at the UCN source.

Reference

[1] C.A. Baker et al., Phys.Rev.Lett. **97** 131801 (2006).

Links

[1] Ultracold neutron source at PSI: http://ucn.web.psi.ch/

[2] Search for the neutron electric dipole moment: http://nedm.web.psi.ch/

The Swiss Muon Source SμS 2012

Elvezio Morenzoni, *Laboratory for Muon Spin Spectroscopy (LMU)*;
Stefan Janssen and Kurt N. Clausen, *NUM Department – Research with Neutrons and Muons, all PSI*

The Swiss Muon Source continues to strengthen its leading role in the use of muons for condensed matter research, to the benefit of the national and international user communities. With a new record of 207 submitted proposals for beam time in 2012, the strong and steadily rising interest in our facilities has continued. With a new and unique High-Field (9.5T) instrument entering user operation in 2013, and the refurbishing of the DOLLY spectrometer, the PSI SμS facility can look forward to a busy and bright future.

User Laboratory SμS: new proposal record

The Swiss Muon Source SμS is one of PSI's highly attractive and successful user laboratories. In 2012, the facility received more applications for beam-time (proposals) than ever before: 207. That number even exceeds the previous all-time record from 2010 (Figure 1) and, for the third time in a row, the SμS received approximately 200 new proposals per year.
Thanks to the excellent performance of the PSI proton accelerator in 2012 and of the SμS instruments, the muon users could perform a total of 214 experiments on the four instruments in user operation: GPS, GPD, LTF and LEM. These experiments were performed during almost 360 user visits by 167 different scientists from all over the world.
Naturally, groups from PSI and the Swiss universities took a large share of the beam-time. The largest foreign SμS user community came from the United Kingdom (12%), followed by Germany (8%), Italy (4%), and Japan, the USA and France (all 3%). In total, users from 19 different countries performed their experiments at SμS in 2012.
The User Office regularly asks visiting scientists for feedback about their experiments and their stay at PSI. The feedback for SμS experiments in 2012 was again extraordinarily positive. In nine out of ten categories, more than 90% of users gave one of the two highest ratings for their SμS experiment. In particular, the scientific and technical support as well as the instrument hard- and software were rated extremely highly by the user community.
In 2013, the SμS user community can look forward to the new high-field SμS station and to the restart of the DOLLY facility.

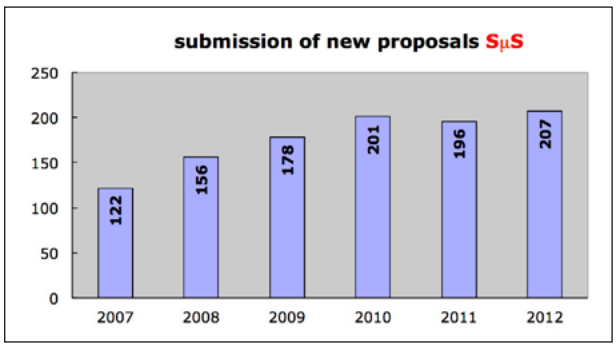

Figure 1: **Submitted SμS proposals since 2007.**

Research

The papers published in 2012 reflect the scientific relevance and wide range of subjects which can be addressed by muons in condensed matter research. Many publications appeared in journals with high impact factors. Among the highlights were studies of the subtle interplay between different types of magnetic and superconducting order in novel iron-based superconductors, which may lead to nano-scale layering of phases or to the avoidance of quantum critical points [1]. Heavy fermion systems were also at the focus of interest in systems where a quantum critical point scenario can be probed using pressure as tuning parameter. The unique depth-dependent magnetic information obtained by low-energy muons has been exploited not only to study the dynamics of molecular magnets (see separate scientific contribution on pp. 30–31) but also to search for a more effective source of thermal muonium production [2]. This result, obtained in collaboration with the Laboratory of Particle Physics at PSI, has implications in the particle physics research, where the muon as an elementary particle is used as a test bench of fundamental interactions. The positive effect of synergy between facilities available at SμS and SLS is also shown in work on the magnetic properties

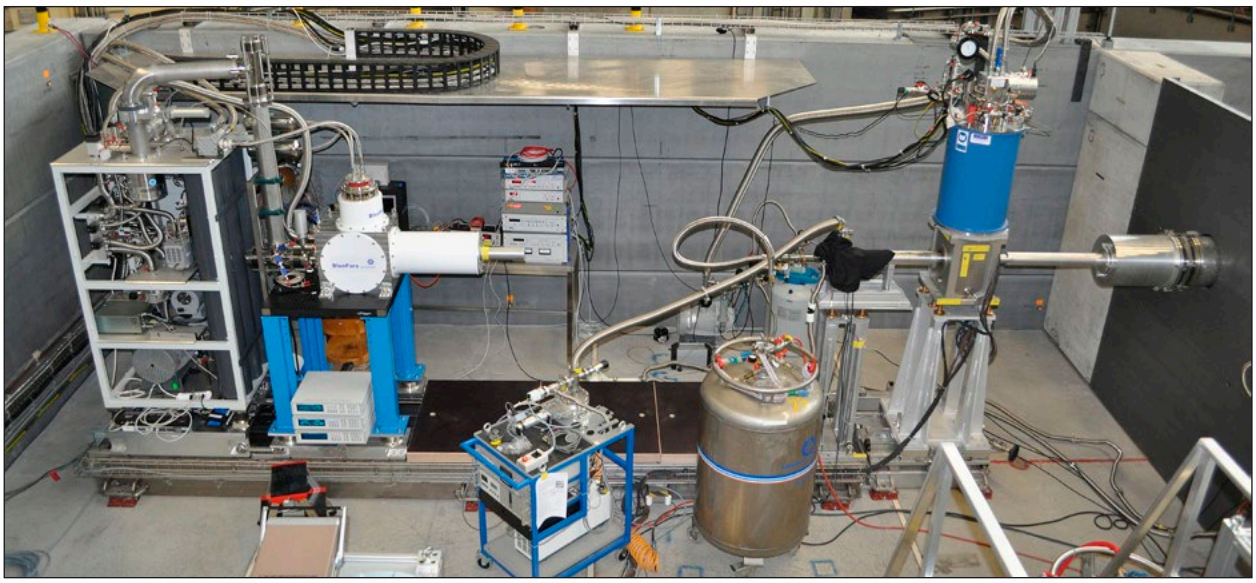

Figure 2: **High-field μSR instrument in the experimental area. On the right-hand side is the 9.5 T magnet and on the left-hand side can be seen the dilution refrigerator, which can cool samples down to temperatures below 20 mK.**

of atomically thin layers of the parent compound of a high-temperature superconductor [3].

Developments

Important improvements have been implemented in several instruments. A spin rotator for the low energy muon facility has been installed and put into operation. It provides the option to perform so-called longitudinal field measurements, and is thus an important tool for gaining detailed insights into time scales in spin dynamics.

The central project of the Laboratory for Muon Spin Spectroscopy in 2012 remained the development of the new instrument for high fields and low temperatures. This project is in its final stage. The horizontal dilution refrigerator has been delivered and put into operation, and commissioning of the beamline and of the instrument, including a full-size spectrometer, has been performed. In 2013, besides this new instrument, which will allow a previously inaccessible range in the B-T phase diagram of materials up to 9.5 T and down to ~20 mK to be investigated, the newly refurbished Dolly beamline will again be available.

A major reconstruction and extension of the πE1 area has allowed the DOLLY spectrometer and a particle physics experiment to be permanently accommodated at the same time. The modified beamline will allow muons to be sent to either of the two instruments. Besides the obvious advantages of a permanent installation for instrument performance, this solution will drastically reduce setup times and therefore increase the number of available experimental days to be distributed to the μSR user community. The new setup was commissioned in autumn 2012. It is expected to greatly enhance the capabilities of this instrument, which we plan to further extend with the availability of a ^{3}He cryostat.

Figure 3: **DOLLY instrument permanently installed in the πE1 area. The spin rotator is visible in the bottom left part of the picture. The large platform allows easy access to the cryostats and for changing samples.**

References

[1] A. Jesche et al., Physical Review B **86** 020501(R) (2012).
[2] A. Antognini et al., Physical Review Letters **108** 143401 (2012).
[3] M.P.M. Dean et al., Nature Materials **11** 850 (2012).

Links

[1] Laboratory for Muon Spectroscopy: http://lmu.web.psi.ch
[2] Scientific highlights from the NUM Department: http://www.psi.ch/num/scientific-highlights
[3] PSI User Office: http://www.psi.ch/useroffice

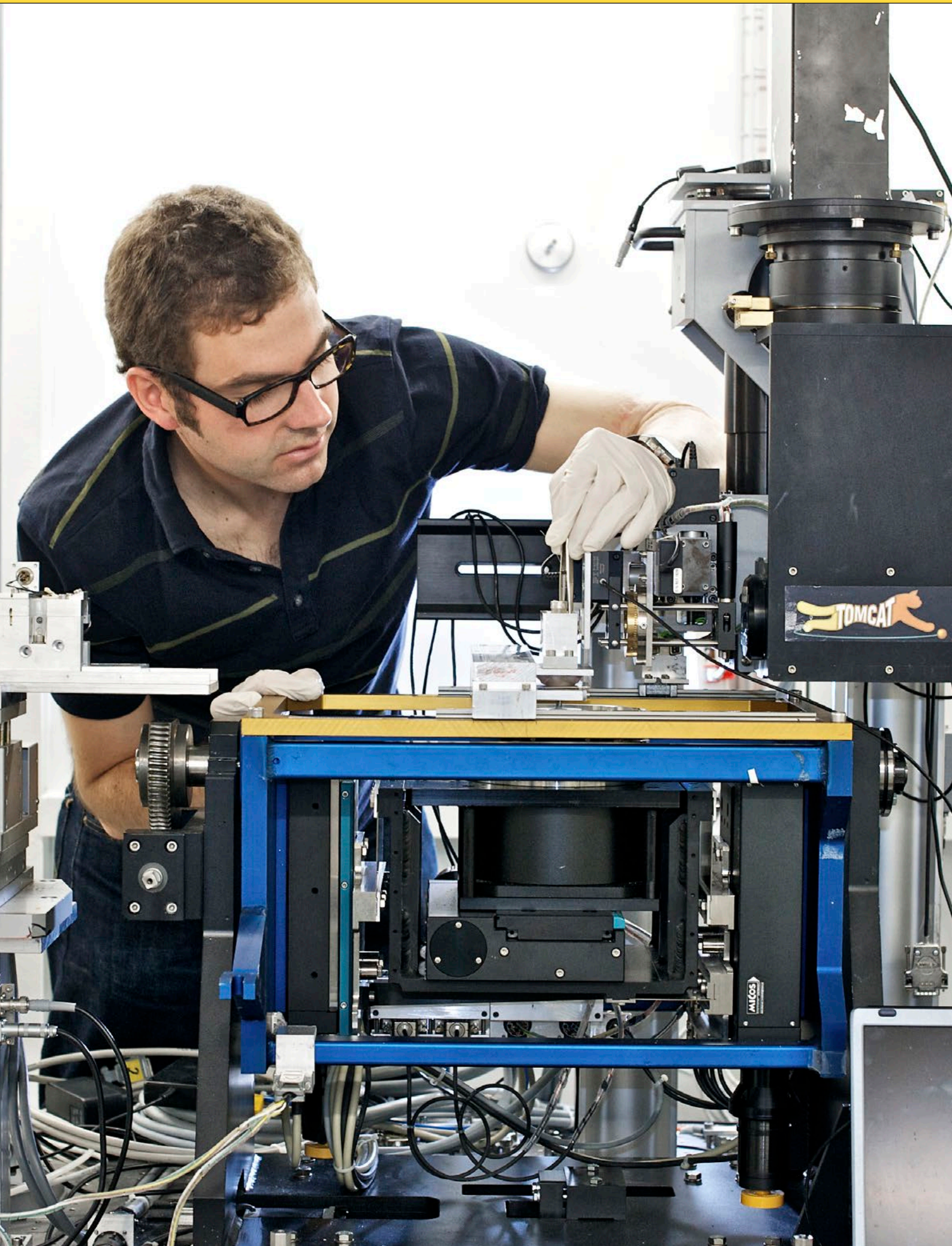
TOMCAT
MICOS

Technology Transfer (TT) is not an end in itself. In Switzerland, it is an important tool for the universities and the Institutions of the ETH Domain, to which PSI belongs, for contributing to the economic development and wealth creation of the country through innovation. In some ways, TT contributes to a "Return On Investment" (ROI) in the economy, which, in turn, through taxes, provides the government with funds to reinvest in research, thus completing a virtuous circle. To improve the transfer process especially with Swiss companies and in particular with SMEs, new marketing instruments have been created which will be of great help to industrial scouting networks, constituted nationally of CTI Innovation Mentors and regionally by Industrial Coaches from several local bodies, for directing SMEs to PSI.

To this end, as examples of successful collaborations between PSI and Swiss companies, in the next pages are highlighted the witnesses of the following two enterprises: Basilea Pharmaceutica International Ltd. (based in Basel, Switzerland) is a fully integrated research and development company, focusing on the development of innovative pharmaceutical products for the treatment of bacterial and fungal infections, and cancer; Tofwerk AG is located in Thun and develops time-of-flight mass and ion mobility spectrometers for industrial and scientific research.

In addition, examples are given where technologies developed within PSI's own research projects are being spun-off into industrial usage: The first is a licensed technology in the field of medical diagnostics, "Differential Phase Contrast", and the second is the "Neutron Imaging for Nuclear Energy" process and the "Fast Neutron Imaging Detector", developed for nuclear energy research but also applicable in many other fields.

◀ **PSI scientist Bernd Pinzer preparing an experiment at the TOMCAT beamline at SLS on the origins of Alzheimer's disease.**
(Photo: Markus Fischer/PSI)

Technology Transfer: A tool for "Return On Investment" in the economy and in research

Giorgio Travaglini, Markus Frei-Hardt, Christine Huber-Musahl, Peter Hardegger and Andrea Foglia, *Technology Transfer Office (TT), PSI;* Robert Zboray, *Laboratory for Thermal-Hydraulics (LTH), PSI*

"Generating knowledge out of money" is the process followed by an economy investing an important part of its GDP in research and development. In return, the economy is expecting an inverse process which would "make money out of knowledge" or, in other words, a "Return On Investment". This process also occurs through the Technology Transfer of public research institutions that push their research results and the arising technologies towards industry, thus fostering innovation, industrial competitiveness and, subsequently, the welfare of the country, as discussed here from PSI's perspective.

Technology Transfer (TT) is not an end in itself. In Switzerland, it is an important tool for the universities and the Institutions of the ETH Domain, to which PSI belongs, for contributing to the economic development and wealth creation of the country through innovation. In some ways, TT contributes to a "Return On Investment" (ROI) in the economy, which, in turn, through taxes, provides the government with funds to reinvest in research, thus completing a virtuous circle.

The creation of wealth

How can PSI contribute to the creation of wealth in Switzerland? There are essentially four main mechanisms for doing this:

1) Business with, and for, companies

PSI is renowned worldwide for its outstanding level of research and for the combination of its unique large research facilities. PSI also has a long tradition of collaboration with key industrial players. In the case of scientific services, companies pay the full cost of obtaining access to results without the need to publish the findings. In the case of collaboration, however, the know-how developed with international partners will be available internationally. Where is, then, the ROI for Switzerland? Such collaboration opens up the opportunity to train young people and sometimes this generates revenue from the intellectual propriety rights created and transferred. The income from PSI's licenses and from third-party co-financing of collaboration projects is subsequently internally reinvested in the research activities of PSI, and thus in Switzerland.

Through the funding mechanisms of the Commission for Technology and Innovation (CTI), PSI can offer research collaboration to Swiss companies by transferring cutting-edge technologies to small and medium-sized companies (SMEs), or developing new solutions tailored to their innovation needs. Specific rules apply in these cases on how to use the Intellectual Property Rights (IPR) generated. Within this framework, the ROI of the TT is mainly provided by the advantages generated through innovation that preserve and create new jobs in Switzerland. To overcome potential barriers for SMEs in approaching PSI with their needs and ideas, the TT team has improved its internet portal for companies [Link 1] with the addition of two features. On the one hand, the new topic on 'Expertise' [Link 2] shows expert knowledge as well as the qualified laboratories available at PSI to support companies' research and development. On the other hand, the category 'Companies' [Link 3] has been created, where various types of collaboration opportunities for companies with PSI are highlighted in twenty reference examples, each followed by a company representative's personal statement. The focus has been put on SMEs, presenting different kinds of collaboration, such as CTI projects, know-how transfer, joint technology development, the licensing of intellectual property, and analysis and development by means of PSI's large R&D facilities. In addition to that, the TT team has recently published a new brochure [Link 4] with the aim of showing to SMEs the various ways in which they could collaborate with PSI. These new marketing instruments will be of great help to industrial scouting networks, constituted nationally of CTI Innovation Mentors and regionally by Industrial Coaches from several local bodies, for directing SMEs to PSI.

2) Large research facilities for the competitiveness of Swiss companies

SwissFEL is the next large research facility project planned and being realized at PSI with the support of industry. To obtain the maximum from this project, PSI has given the highest priority to collaboration with Swiss industrial partners, in order to develop cutting-edge technologies together with our own scientists. In this way, part of the considerable investment for SwissFEL will return to Swiss companies. The much sought-after knowledge acquired will increase a company's competitiveness worldwide when tendering for projects where similar FEL infrastructures are planned or the same technologies can be exploited for other industrial applications and market segments (e.g. as spin-off product).

3) PSI's technologies as business for spin-off

Of course, the foundation of spin-off companies which start their business based on PSI's technologies and support represents a potential for strengthening competitiveness in a specific field or occupying a new market niche.

4) The High-Tech Zone (HTZ) for strengthening the "Location Switzerland"

Together with a private investor, PSI has initiated the planning of a modern building complex in the area adjacent to its site, to attract and host companies willing to benefit from the unique combination of the large research facilities and the expertise available at the Institute. In this context, the ROI of the HTZ mainly results from very efficient technology, knowledge and personnel transfer *in situ*, targeting the creation of new jobs and hence increasing tax income from related new businesses and people. To maximize the impact of this initiative, PSI and Canton Aargau intend to convert the HTZ into the nucleus of a Swiss Innovation Park, according to the objectives of the Research and Innovation Promotion Act (FIFG). The aims of the Swiss Innovation Park are to contribute towards strengthening the attractiveness of the "Location Switzerland" for high-tech companies worldwide, by making available innovation locations where internationally renowned research centres and industrial key players come together, thus leading to the whole value chain under one "roof".

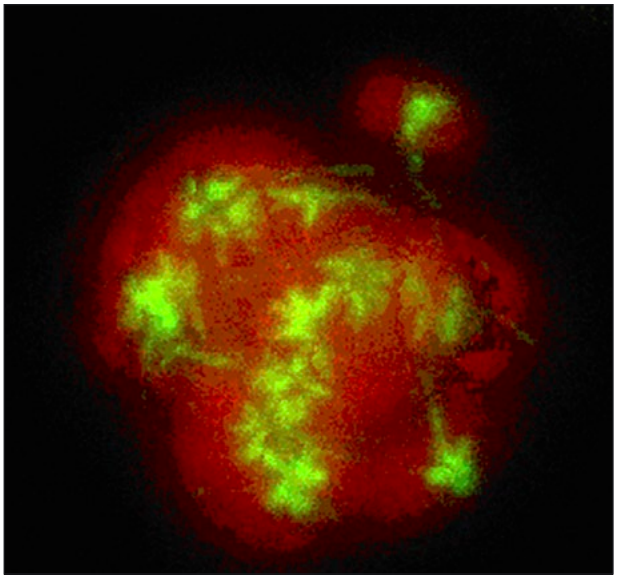

Figure 1: **BAL27862-treated mitotic tumour cell (Green: microtubules; Red: DNA).**

The first of the above points is highlighted below by two statements from successful collaborations between SMEs and PSI, followed by two examples of technologies developed at PSI that are leading, or could lead, to ROI in terms of industrial applications and/or knowledge transfer.

SMEs at PSI: Welcome

Basilea Pharmaceutica International Ltd. (based in Basel, Switzerland) is a fully-integrated research and development company, focusing on the development of innovative pharmaceutical products for the treatment of bacterial and fungal infections, and cancer. Basilea targets the increasing medical challenge of resistance and non-response to current treatment options, and has been collaborating with PSI since 2010. Using the microtubule cytoskeleton as a model system, structure-phenotype relationship analyses are being performed with novel microtubule-targeting drugs, including Basilea's anti-cancer compound BAL27862 (Figure1).
A prodrug of BAL27862 (BAL101553) entered clinical evaluation in advanced cancer patients in 2011.

«Thanks to the expertise of the group of Michel Steinmetz at PSI, high-resolution microtubule structural information has been obtained. Together with detailed phenotypic analysis, this has aided our understanding of the mechanism of action of BAL27862, a novel anticancer compound with a broad potential in drug refractory cancer patients. We really appreciate the reliable and successful cooperation with PSI.»
Dr. Heidi Lane, Basilea Pharmaceutica International Ltd., Basel

Tofwerk AG is located in Thun and develops time-of-flight mass and ion mobility spectrometers for industrial and scientific research. The time-of-flight mass spectrometers of Tofwerk are among the fastest in the world. They can record up to 100,000 complete mass spectra per second in order to monitor fast processes. Tofwerk collaborates with PSI on the development of a new mass spectrometer for the analysis of aerosol particles. While Tofwerk is responsible for the hard-

ware and software development, PSI provides its know-how in the field of atmospheric chemistry and its infrastructure for testing and performance evaluation. The project is supported by CTI.

«The collaboration with PSI is essential for the development and marketing of this mass spectrometer. We thereby can profit from the unique infrastructure at PSI as well as from the expertise of PSI scientists and graduate/PhD students for evaluating the performance of the instruments. This will significantly contribute to the further success of the project. PSI also supports us by presenting their findings at conferences – which is essential for the worldwide marketing of our product.»
Mike Cubison, Project Manager; Marc Gonin, CEO, Tofwerk AG, Thun

As far as technologies are concerned, the basic research performed at PSI can lead not only to scientific excellence but also to highly advanced technologies, according to our mission statement: "We create knowledge – today for tomorrow". In order to generate ROI, one of the major tasks of TT is to assess the application potential of new technologies developed at PSI.
Two examples showcase the working principles followed at PSI: The first is a licensed technology in the field of medical diagnostics, "Differential Phase Contrast", which is also very promising for application in other fields, such as material analysis.
The second example of transfer is in the field of nuclear energy. Anachronistic? Not strategic, in view of the phasing out of nuclear power? Not at all! Now, more than ever, PSI has the mission to keep research in this branch active in order to attract, hire and educate new, young talent. It is a matter not only of technology transfer but also of knowledge transfer that will ensure the correct management, optimal functioning and effective maintenance of nuclear power plants, as well as their proper shut down and decommissioning in the future. The "Neutron Imaging for Nuclear Energy" process and the "Fast Neutron Imaging Detector" developed at PSI prove to the coming generation how research in this field is still very active and also has the potential to create opportunities for TT outside the nuclear energy field.

A Different View: Differential Phase Contrast – Licensed to BrukerMicroCT

A new method forms the basis for the widespread use of an X-ray technique which distinguishes types of tissue that normally appear the same in conventional X-ray images.

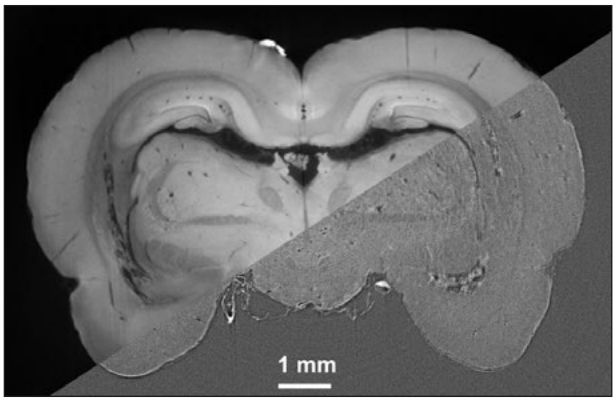

Figure 2: **Image of a rat's brain, generated at the TOMCAT tomography beamline at SLS research group at PSI using the phase-contrast method (left part) and a conventional method (lower-right). The major anatomical structures are clearly visible, down to the order of 10 thousandths of a millimetre.**

Traditional X-ray images can clearly distinguish between bone and soft tissue, with muscles, cartilage, tendons and soft-tissue tumours all looking virtually identical. The phase-contrast technique developed a few years ago at PSI enables X-ray images to be produced that clearly distinguish between these tissue types (Figure 2).
In short, the phase-contrast method makes use of the fact that light that passes through matter is not only attenuated, but also travels more slowly. Two waves that start off "in phase" (meaning that the peaks of both waves are adjacent) and then pass through different materials are subsequently phase-shifted. This difference in phase contains important information about the structure of the object being examined, which can be visualized using the phase-contrast method.
Phase-contrast and darkfield images often give a better contrast for studies of soft tissues biological materials or small animals as a whole than X-ray absorption images. The Belgian Company Skyskan, renamed Bruker-microCT after its acquisition by Bruker in April 2012, has developed a first prototype of a laboratory system dedicated to biological objects and small-animal studies that allows the visualization and 3D reconstruction of traditional attenuation information with simultaneous extraction of phase-contrast and darkfield images during a single tomographic scan. The system is based on a grating interferometer and uses a phase-stepping procedure to separate phase, absorption and darkfield information for following tomographic reconstruction. In order to develop and subsequently market these instruments, Skyscan and PSI successfully negotiated and signed a license on the core patents in January 2012.
This licence will not only allow the commercial use of this important technology, revenues generated through the related sales of instruments will also be a partial refund of the significant investment that has been made for the development of this new and promising technology over the years.

Neutron imaging for nuclear energy technology and fuel bundle development

Neutron imaging is a non-intrusive, contactless technique and can be very helpful in examining processes of high interest in nuclear energy technology. It offers excellent contrast for aqueous processes inside metal containers, such as two-phase flow in a nuclear fuel assembly, which would be opaque to other radiation-based techniques, such as X-ray or gamma radiography. Two-phase flow in boiling water reactor fuel rod bundles is responsible for the efficient transfer of the heat produced in the reactor core and should be maintained to guarantee the integrity of the fuel assemblies. Especially in the upper part of the bundle, where the liquid phase is in the form of a thin film on the fuel rod surfaces, the loss of this film (dry out) represents a severe safety issue and, from another perspective, limits the efficiency of such reactors. The use of functional spacer grids with mixing vanes in the fuel bundle, as illustrated in Figure 3, can be very beneficial in increasing the margin to dry out.

The Laboratory for Thermal Hydraulics (LTH), in the Nuclear Energy and Safety Department (NES) at PSI, has carried out extensive investigations on different fuel bundle models and prototypical spacers at the ICON beamline, in cooperation with the Neutron Imaging Group at SINQ. High-resolution neutron tomography enabled the performance of the spacers to be examined in detail, to find out how efficient they were in separating the two phases and in enhancing the liquid film thickness. The visualization in Figure 4 shows a prototypical spacer with two vanes and the liquid film on the vanes as it detaches from their tips.

Although many patents exist on spacers, they are developed and tested based on industrial engineering practice, and judgment lacks insight into their basic functioning mechanisms and the ability to optimize them. This is where this technique can be an attractive option for nuclear fuel vendors, for testing and developing new spacer types.

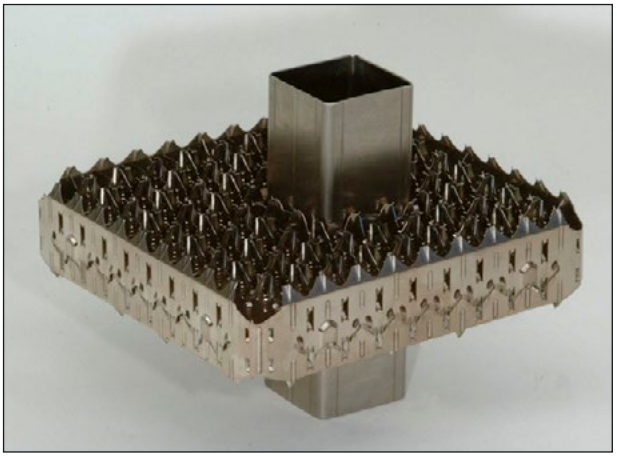

Figure 3: **The ULTRAFLOW spacer grid of the ATRIUM10 XM, the newest boiling water reactor fuel assembly from AREVA (Source: Glück, NED 238, 2008).**

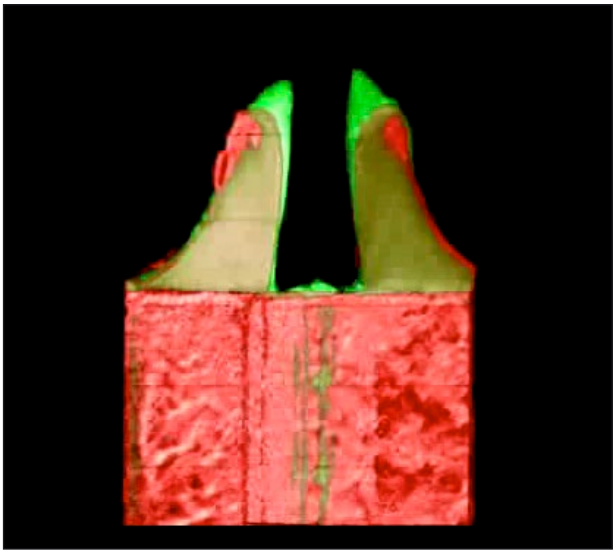

Figure 4: **3D rendering of the section of a prototypical spacer with two vanes, similar to those of ULTRAFLOW, and of the water film on them, obtained by cold neutron imaging at the ICON beamline at SINQ.**

Along the same lines, LTH has started the development of an imaging system using fast neutrons and the establishment of a corresponding laboratory. Fast neutrons possess high penetrating power and can extend the range of applicability of the above-mentioned imaging technique for fuel bundles. Furthermore, other applications areas are also conceivable, such as a molten-core–water interaction (steam explosion) for severe accident studies or liquid-metal two-phase flow problems related to Generation IV reactors. The system under development consists of a compact, deuterium-deuterium fusion-based fast-neutron generator and fast-neutron detector prototypes, all tailored for imaging purposes. Several potential applications of spin-off activities from the fast-neutron laboratory can extend beyond nuclear thermal hydraulics. One of these, which has already resulted in a patent application, is the development of an energy-sensitive, fast-neutron imaging detector. Such a detector could find both commercial applications, e.g. in detection of special nuclear materials or hidden explosives, in nuclear safety, as well as application in pure science, such as in a neutron beam monitor or in fusion research.

Links

[1] Industry and the Economy: www.psi.ch/industry
[2] Expertise and Services: http://www.psi.ch/industry/expertise
[3] Collaborating Companies: http://www.psi.ch/industry/companies
[4] Brochure: http://www.psi.ch/industry/unternehmen


BLUE
STARS
PYREX
250ml
Latex-FREE

Facts and figures 105

In order for a large research institute such as PSI to perform the many scientific studies that it does, which are much more numerous and cover an even broader spectrum than it is possible to mention in this short review report, a large staff of administrators, computing specialists and technologists is required to support the scientists at the front-end of the research. The former are as essential as the latter, especially in the design, construction and operation of such large-scale facilities as are available at PSI.

The distributions of the Institute's financing, its staffing and its educational involvement in 2012 are given in the following pages, together with the User Service statistics covering the usage of the large-scale facilities. As in the previous year, government funding provided over two-thirds of the total used to run the Institute, with the remainder being provided by third-parties, as well as almost 6% supplied by the Federal government specifically to support the construction of the new SwissFEL large-scale facility. Staffing levels remained essentially as they were in 2011.

Educational involvement remained at about the same level as in 2011, but the User Service recorded a significant increase in overall User Visits and an increase in every other aspect as well. This follows the steady trend observed over recent years.

The composition and distribution of the advisory boards and scientific commissions, whose task it is to guide the Institute in its current scientific endeavours and in its future goals, also remained essentially the same as in the previous year, with very few changes in membership. This gives continuity to the long-term goals of PSI while allowing for regular change, as necessary, to keep the quality and achievement of scientific research at the highest possible level.

◀ **At the "Lehrberufe à la carte" event, young people were able to learn about opportunities for vocational training at PSI.** (Photo: Frank Reiser/PSI)

PSI in 2012 – an overview

Finances

Total PSI expenditure in 2012 was CHF 337.2 million, of which the Swiss government provided 75.8%, i.e. CHF 248.9 million, not including the financing of building works and the maintenance of real estate. Out of this, 68.2% (CHF 229.9 million) was allocated to basic financing and 5.6% (CHF 19.0 million) specifically provided for the SwissFEL project. External second- and third-party funding added up to CHF 88.3 million (26.2% of total expenditure). Third-party revenue totalled CHF 106.4 million, with 53.8% coming from private industry, 26.8% from Swiss federal research programmes, 9.6% from EU programmes and 9.9% from other sources. This breakdown is listed in Table 1 and the budget distribution across the Research Departments is given in Figure 1.

PSI Financial Statement (in CHF millions)		
	2012	
Expenditure		
Operations*	304.2	90.2%
Investments*	33.0	9.8%
Total	**337.2**	**100.0%**
Expenditure according to source of income		
Federal funding (basic)	229.9	68.2%
Federal funding for SwissFEL	19.0	5.6%
Second- and third-party funds	88.3	26.2%
Total	**337.2**	**100.0%**
Third-party revenue		
Private industry	57.2	53.8%
Federal research funding	28.5	26.8%
EU programmes	10.2	9.6%
Other (incl. Scientific Services)	10.5	9.9%
Total	**106.4**	**100.0%**
* Including personnel costs. Total personnel costs of CHF 218.6 million corresponded to 64.8% of total expenditure.		

Table 1: **PSI finances in 2012.**

Staffing

At the end of 2012, slightly more than 1500 full-time equivalent staff positions were occupied at PSI. The distribution of staffing according to fields of activity can be seen in Figure 2. Of the total PSI staff, 25.2% were women and 47% were non-Swiss citizens.

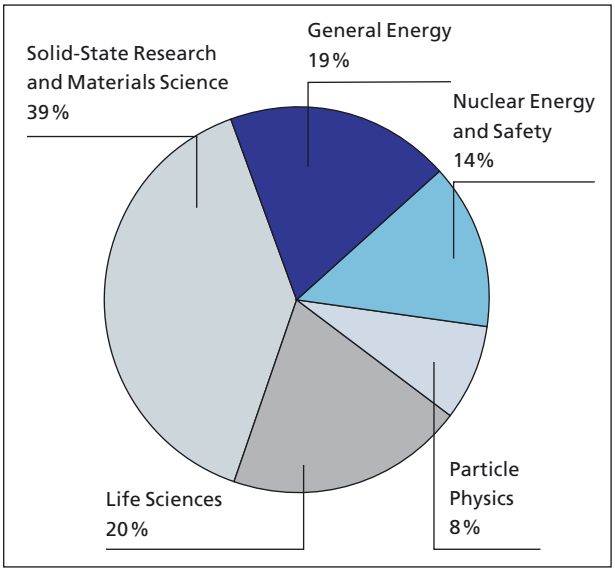

Figure 1: **Total budget distribution for 2012 across PSI Research Departments. Research facilities are allocated to the appropriate Departments.**

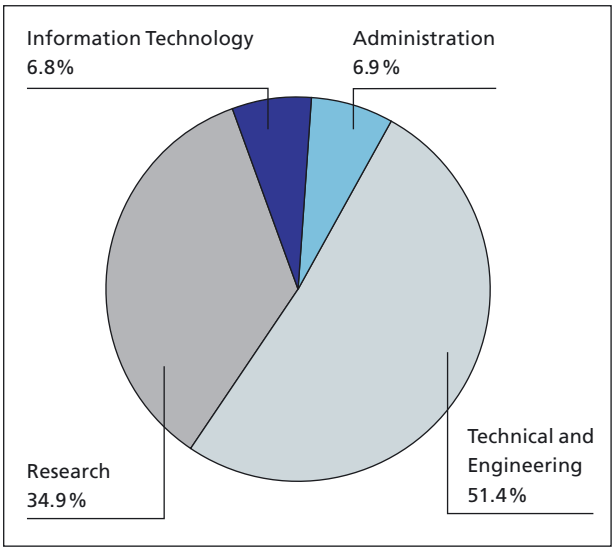

Figure 2: **The staffing structure of the Paul Scherrer Institute reflects the importance of technical staff for running the institute's complex experimental facilities.**

Education

In addition to research, education at various levels is also a central priority for the Institute. Research opportunities are provided for students preparing their Masters or PhD theses, with more than 300 PhD students currently at PSI, including more than 200 actually employed by the Institute. The remainder are financed by other institutions or universities, but perform a substantial part of their experimental work at PSI's laboratories or large-scale facilities. The opportunity to work at PSI as trainees for a shorter period of time, and to gather work experience in scientific research as well as in administrative or organizational tasks, was taken by 100 other young people – secondary-school graduates and university students. More than 90 young people were doing an apprenticeship in 13 different professions. In addition, PSI offered courses in radiation protection and reactor technology, for internal staff as well as for external groups handling radioactive materials, such as medical doctors or fire-fighters.

The school lab (iLAB) provided pupils undergoing secondary education with the opportunity to perform various physics experiments and thus obtain a first-hand impression of scientific research. The iLAB was visited during 2012 by 189 classes, from different schools – compared with the 192 classes which visited in 2011 and the 180 classes coming in 2010.

PSI scientists were also active as educators outside the Institute, with about 100 staff giving lecture courses at universities and universities of applied science.

User Service

In 2012, PSI maintained its position as an attractive User Lab for scientists from all over the world (see Table 2). More than 2700 users visited the Institute and performed almost 1900 experiments at the 39 beamlines available at the large-scale facilities. The continually increasing interest in performing experiments at PSI is reflected in the growing number of proposals submitted to the user service, which reached an all-time high of 1415 in 2012. The total number of users who came to participate in experiments also reached its highest value ever – 2749 – as did the number of user visits to the SLS, SINQ and SμS large-scale facilities, that exceeded 5000 for the first time (see Figure 3), and the overall number of peer-reviewed publications based on research performed at the SLS, SINQ and SμS facilities reached 730.

The User Service at PSI's large-scale facilities also makes an important contribution to the education of future generations of scientists, which can be seen from the large number of young scientists among the users and their success in applying for beam time at international large-scale facilities.

User Lab 2012						
	SLS	SINQ	SμS	Particle Physics	PSI total	
					2012	2011
Number of beamlines/ instruments	18	12	4	5	**39**	**38**
Number of experiments	1187	474	214	5	**1880**	**1727**
Number of user visits	3825	1001	359	597	**5782**	**5077**
Number of individual users	1793	519	167	270	**2749**	**2336**
Number of new proposals	808	397	207	3	**1415**	**1378**

Table 2: **PSI user service in numbers.**

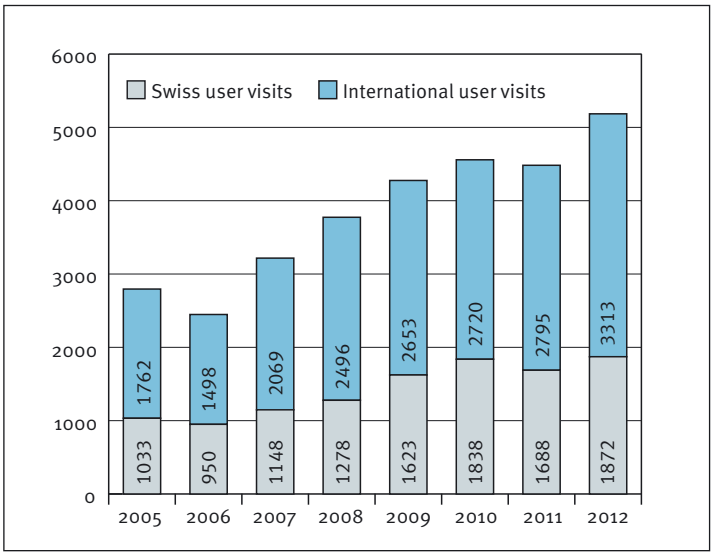

Figure 3: **The total number of user visits to SLS, SINQ and SμS reached an all-time high in 2012, exceeding 5000 for the first time.**

Advisory Board and Research Committees

The Advisory Board's main task is to advise the Directorate on the development of long-term research strategies and to evaluate the quality of past and planned research activities. The Board meets once or twice a year and consists of 11 scientists of high scientific standing, from Switzerland and abroad. The Research Committee of the Paul Scherrer Institute consists of 13 members selected from the various PSI Departments and evaluates proposed new projects and applications for financial support from external agencies, assesses ongoing projects and helps define appropriate new research topics for the Institute. An additional 8 Committees, with members from Switzerland and abroad, assess and advise the various large-scale facilities and the Research Departments on their past, present and future research activities and programmes.

Advisory Board and Research Committees

Advisory Board

Prof. Dr. Ø. Fischer, President	Department of Condensed Matter, University of Geneva, CH
Prof. Dr. G. Aeppli	London Centre for Nanotechnology, University College, London, GB
Prof. Dr. F. Carré	CEA, Saclay, Gif-sur-Yvette, FR
Prof. Dr. H.H. Coenen	Institute for Nuclear Chemistry, Forschungszentrum Jülich, DE
Prof. Dr. R.W. Falcone	ALS, Lawrence Berkeley National Laboratory, Berkeley, US
Prof. Dr. R. Klanner	Institute for Experimental Physics, University of Hamburg, DE
Prof. Dr. S. Larsen	Dept. of Chemistry, University of Copenhagen, DK
Prof. Dr. T. Mason	Oak Ridge National Laboratory, US
Prof. Dr. J. Rossbach	Institute for Experimental Physics, University of Hamburg, DE
Prof. Dr. Th. Sattelmayer	Chair of Thermodynamics, TU München, Garching, DE
Prof. Dr. E. Umbach	Karlsruhe Institute of Technology (KIT), DE

Research Committee

Prof. Dr. R. Horisberger, President	Research with Neutrons and Muons (NUM)
Dr. M. Ammann	Biology and Chemistry (BIO)
Dr. B. Delley	Research with Neutrons and Muons (NUM)
Dr. R. Eichler	Biology and Chemistry (BIO)
Dr. L. Heyderman	Synchrotron Radiation and Nanotechnology (SYN)
Dr. I. Mantzaras	General Energy (ENE)
Dr. W. Pfingsten	Nuclear Energy and Safety (NES)
Dr. T. Schietinger	Large Research Facilities (GFA)
Dr. M. Steinmetz	Biology and Chemistry (BIO)
Prof. Dr. H. Van Swygenhoven	Research with Neutrons and Muons (NUM)
Dr. F. Vogel	General Energy (ENE)
Prof. Dr. P. Willmott,	Synchrotron Radiation and Nanotechnology (SYN)
Dr. P. Hasler, Secretary	Biology and Chemistry (BIO)

Research Committees for specific research areas

SwissFEL
SwissFEL Free-electron Laser Advisory Committee (FLAC)

Prof. Dr. J. Rossbach, Chair
DESY, Hamburg, DE

Dr. J. Bahrdt
HZB, Berlin, DE

Dr. P. Emma
Lawrence Berkeley National Laboratory, Berkeley, US

Prof. Dr. M. Ferrario
INFN-LNF, Rome, IT

Dr. O. Groening
EMPA, Dübendorf, CH

Dr. A. Grudiev
CERN, Geneva, CH

Dr. H. Schlarb
DESY, Hamburg, DE

Dr. M. Svandrlik
ELETTRA, Trieste, IT

Dr. M. Yabashi
RIKEN-SPring-8, Hyogo, JP

Synchrotron Radiation SYN
Scientific Advisory Committee (SAC)

Prof. Dr. G. Materlik, Chair
Diamond Light Source, Didcot, GB

Prof. Dr. G.-L. Bona
EMPA, Dübendorf, CH

Prof. Dr. H. Brune
EPFL, Lausanne, CH

Prof. Dr. R. Claessen
University of Würzburg, DE

Prof. Dr. K. Diederichs
University of Konstanz, DE

Prof. Dr. J. Evans
University of Southampton, GB

Dr. J. Feldhaus
DESY, Hamburg, DE

Prof. Dr. J. Hastings
Stanford Linear Accelerator Center, Menlo Park, CA, US

Prof. Dr. C.-C. Kao,
Stanford Linear Accelerator Center, Menlo Park, CA, US

Dr. P. Lagarde
Synchrotron Soleil, Gif-sur-Yvette, FR

Prof. Dr. J. Marangos
Imperial College, London, GB

Prof. Dr. G. Margaritondo
EPFL, Lausanne, CH

Prof. F. Parmigiani
Free Electron Laser project-FERMI@Elettra, Trieste, IT

Prof. Dr. E. Rühl
Freie Universität Berlin, DE

Research with Neutrons and Muons NUM
SINQ Scientific Advisory Committee

Prof. Dr. A.T. Boothroyd, Chairman
University of Oxford, GB

Dr. L. Arleth
University of Copenhagen, DK

Dr. Th.J. Bücherl
TU München, DE

Dr. N.B. Christensen
Risø National Laboratory, DK

Dr. A. Evans
Rolls Royce Group, Bristol, GB

Dr. T. Keller
TU München, DE

Dr. K. Krämer
University of Bern, CH

Dr. M. Meven
TU München, DE

Prof. Dr. U. Olsson
University of Lund, SE

Prof. Dr. C. Pfleiderer
TU München, DE

Dr. A. Remhof
EMPA, Dübendorf, CH

Dr. M. Strobl
European Spallation Source, Lund, SE

Prof. Dr. W. Treimer
Beuth University of Applied Sciences, DE

Dr. M. Wörle
Swiss National Museum, Zurich, CH

SμS Scientific Advisory Committee

Prof. Dr. C. Bernhard, President
University of Fribourg, CH

Prof. Dr. E. Bauer
Vienna University of Technology, AT

Prof. Dr. S.J. Blundell
University of Oxford, GB

Prof. Dr. J.M. de Sá Campos Gil
University of Coimbra, PT

Prof. Dr. K. Chow
University of Alberta, CA

Prof. Dr. R. De Renzi
University of Parma, IT

Prof. Dr. A. de Visser
University of Amsterdam, NL

Prof. Dr. Ph. Mendels
University of Paris XI, FR

Prof. Dr. D. Pavuna
EPFL Lausanne, CH

Particle Physics at the Ring Cyclotron

Dr. C. Hoffman, President
LAMPF, Los Alamos, US

Prof. Dr. A.B. Blondel
University of Geneva, CH

Dr. D. Bryman
TRIUMF, Vancouver, CA

Dr. A. Ceccucci
CERN, Geneva, CH

Prof. Dr. G. Colangelo
University of Bern, CH

Prof. Dr. B.W. Filippone
California Institute of Technology, US

Prof. St. Passaggio
INFN Genoa, IT

Prof. Dr. M. Pendlebury
University of Sussex, Brighton, GB

Prof. Dr. M. Pohl
University of Geneva, CH

Prof. Dr. M. Ramsey-Musolf
University of Wisconsin-Madison, US

Dr. M. Spira, committee secretary
PSI, CH

Prof. Dr. U. Straumann
University of Zurich, CH

Biology and Chemistry BIO

Prof. Dr. D. Neri, President
ETH Zurich, CH

Prof. Dr. M. Grütter
University of Zurich, CH

Prof. Dr. Ch.W. Müller
EMBL, Heidelberg, DE

Prof. Dr. P. Nordlund
Karolinska Institute, Stockholm, SE

Prof. Dr. S. Werner
ETH Zurich, CH

Nuclear Energy and Safety NES

Dr. H. Forsström, President
Bromma, SE

Dr. F. Altorfer
ENSI, Brugg, CH

Prof. Dr. M. Giot
Université Catholique de Louvin, BE

Dr. P. Miazza
Nuclear Power Plant Mühleberg, CH

Dr. M. Plaschy
Alpiq, Olten, CH

Dr. J.-B. Thomas
CEA Saclay, Gif-sur-Yvette, FR

Prof. Dr. S. Virtanen
University of Erlangen-Nürnberg, DE

Dr. P. Zuidema
Nagra, Wettingen, CH

General Energy ENE

Prof. Dr. T. Peter, President
ETH Zurich, CH

Prof. Dr. G.-L. Bona
Empa, Dübendorf, CH

Dr. T. Kaiser
Consenec AG, Baden-Dättwil, CH

Prof. Dr. R. Pitz-Paal
DLR, Cologne, DE

Dr. R. Schmitz
Swiss Federal Office of Energy, Bern, CH

Prof. Dr. Ph.R. von Rohr
ETH Zurich, CH

Prof. Dr. A. Voss
University of Stuttgart, DE

Organizational Structure (as of January 2013)

Research Committee
Prof. Dr. Roland Horisberger

Large Project SwissFEL
Dr. Hans-Heinrich Braun/Dr. Rafael Abela

Center for Proton Therapy
Gudrun Goitein a.i.

Director:
Prof. Dr. Joël Mesot

Members of the board of directors:
Dr. Kurt N. Clausen
Prof. Dr. J. Friso van der Veen*
Prof. Dr. Alexander Wokaun*
Dr. Jean-Marc Cavedon
Prof. Dr. Gebhard Schertler
Prof. Dr. Leonid Rivkin
Dr. Peter Allenspach

Directorate Support
Dr. Thierry Strässle

Human Resources
Karsten Bugmann

Safety
Dr. Werner Roser

Industry, Financing and Operations
Dr. Philipp Dietrich

Science
Dr. Thierry Strässle

Communications
Dagmar Baroke

Technology Transfer
Dr. Giorgio Travaglini

Research Department	Particle Physics	Prof. Dr. Klaus Kirch
Research with Neutrons and Muons (NUM)	Neutron Scattering	Dr. Christian Rüegg
Dr. Kurt N. Clausen	Spallation Neutron Source Division	Dr. Werner Wagner
	Muon Spin Spectroscopy	Prof. Dr. Elvezio Morenzoni
	Development and Methods	Dr. Michel Kenzelmann
Research Department	Macromolecules and Bioimaging	Dr. Oliver Bunk
Synchrotron Radiation and Nanotechnology (SYN)	Condensed Matter and Materials Science	Dr. Frithjof Nolting
Prof. Dr. J. Friso van der Veen	Micro- and Nanotechnology	Prof. Dr. Jens Gobrecht
Research Department	Bioenergy and Catalysis	Dr. Oliver Kröcher
General Energy (ENE)	Solar Technology	Prof. Dr. Aldo Steinfeld
Prof. Dr. Alexander Wokaun	Combustion Research	Dr. Peter Jansohn
	Electrochemistry	Prof. Dr. Thomas J. Schmidt
	Atmospheric Chemistry	Prof. Dr. Urs Baltensperger
Competence Center for Energy and Mobility (CCEM)		Urs Elber
Research Department	Reactor Physics and Systems Behaviour	Prof. Dr. Andreas Pautz
Nuclear Energy and Safety (NES)	Thermal Hydraulics	Prof. Dr. Horst-Michael Prasser
Dr. Jean-Marc Cavedon	Hot Laboratory	Dr. Didier Gavillet
	Waste Management	Dr. Michael Bradbury
	Nuclear Materials	Hans-Peter Seifert a.i.
Research Department	Center for Radiopharmaceutical Sciences	Prof. Dr. Roger Schibli
Biology and Chemistry (BIO)	Biomolecular Research	Prof. Dr. Kurt Ballmer
Prof. Dr. Gebhard Schertler	Radiochemistry and Environmental Chemistry	Prof. Dr. Andreas Türler
Department	Accelerator/Concepts and Development	Dr. Terence Garvey
Large Research Facilities (GFA)	Accelerator/Operation and Development	Dr. Mike Seidel
Prof. Dr. Leonid Rivkin	Technical Support, Co-ordination and Operation	Jürgen Duppich
Department	Finance and Administrative Services	Karlheinz Falk
Logistics (LOG)	Buildings and Services	Lilian Jakob
Dr. Peter Allenspach	Infrastructure and Electrical Engineering	Max Huser
	Mechanical Engineering Sciences	Dr. Urs Ellenberger
	Information Technology	Dr. Stephan Egli
	Radiation Safety and Security	Dr. Sabine Mayer
	Communications	Dagmar Baroke

Catalysis and Sustainable Chemistry
Prof. Dr. Jeroen van Bokhoven

Energy Systems Analysis
Dr. Stefan Hirschberg

* Executive Committee / Deputy Directors

Additional information 111

Where to find what

Additional information on the Paul Scherrer Institute and its research is available online:

PSI homepage: http://www.psi.ch

Information on PSI's research facilities and laboratories, including an overview of its scientific activities, recent results and contact information: http://www.psi.ch/science/scientists-and-users

A popular presentation of PSI's recent results, in English, German and French: http://www.psi.ch/media/

Keep up-to-date on the latest news from PSI by following us on Twitter: http://twitter.com/psich_en

◀ **A ball track installed at the psi forum – PSI's visitors' centre. Small metal balls are transported upwards using electrical energy produced by a fuel cell and then allowed to roll down along a winding track under the influence of gravity.**
(Photo: Frank Reiser/PSI)

Paul Scherrer Institut, 5232 Villigen PSI, Switzerland
Tel. +41 56 310 21 11, Fax +41 56 310 21 99
www.psi.ch